

An Investigation of Higher Capacity Urban Freight Vehicles



Chris Eddy

Department of Engineering
University of Cambridge

This dissertation is submitted for the degree of
Doctor of Philosophy

St Catharine's College

November 2019

For Beth, whether she reads it or not.

Declaration

I hereby declare that except where specific reference is made to the work of others, the contents of this dissertation are original and have not been submitted in whole or in part for consideration for any other degree or qualification in this, or any other university. This dissertation is my own work and contains nothing which is the outcome of work done in collaboration with others, except as specified in the text and Acknowledgements. This dissertation contains fewer than 65,000 words including appendices, bibliography, footnotes, tables and equations and has fewer than 150 figures.

Chris Eddy
November 2019

Acknowledgements

I would like to acknowledge the following individuals and organisations:

- Professor David Cebon, for four years of expert guidance, boundless knowledge, and startlingly accurate predictions.
- The UK Engineering and Physical Sciences Research Council (EPSRC) for funding this work.
- Member organisations of the Cambridge Vehicle Dynamics Consortium (CVDC), for funding the Transport Research Group, and for their insightful criticism and advice. Particular thanks go to Mark Starosolsky of Laing O'Rourke for providing the test vehicle described in Chapter 2, and to Dr Yanbo Jia for his expertise in cyclist detection systems.
- Member organisations of the Centre for Sustainable Road Freight (SRF), particularly the two anonymised supermarkets described in Chapter 3 for allowing me to collect data, and to their drivers for allowing me to join them on their routes.
- St Catharine's College, for assisting with conference funding, and for providing an incredibly supportive environment over the last four years. Special mention goes to my friends and crewmates at SCCBC for helping create some of my very best memories of my time at Cambridge.
- My colleagues at the Transport Research Group, past and present—Rich, Xiaoxiang, Ayelet, Albert, Francesco, Ke Yan, Robert, Josh, Anil, Carl and Virginia—for their advice and support. Special thanks go to Leon and Graeme for teaching me everything about trucks, and to Chris for teaching me everything about everything else. Also to Julien for distracting me when I needed it, and to Daniel for distracting Julien when I didn't.
- Finally, the biggest thanks go to my family, who now know far more about trucks than they ever wanted to.

Abstract

Studies have shown that increasing the capacity of Heavy Goods Vehicles is one of the most effective ways of reducing fuel consumption per tonne-kilometre of freight moved, with consequent reductions in greenhouse and noxious emissions. Some of the disadvantages of larger vehicles are more pronounced in urban environments, including safety of other road users, and reduced manoeuvrability. This thesis discusses technologies for improving safety of vulnerable road users, and frameworks for assessing the maximum size of urban freight vehicles.

An overview of the freight industry is provided in Chapter 1, with a focus on maximising capacity as a method for reducing emissions. Chapter 2 focusses on the safety of vulnerable road users, through development of a camera-based detection system for cyclists, which is essential for a predictive collision avoidance system. The proposed system is accurate to within 10 cm at distances of greater than 1 m from the vehicle, but suffers from loss of accuracy at close range, and in poor lighting conditions.

The logistics of urban freight operations are analysed in Chapter 3, including a comparison between two supermarket home delivery operations, and an analysis of refuse collection schedules. A framework is proposed for selecting an optimum vehicle size for a multi-drop operation, given reductions in driving distance and time spent on other procedures. A potential capacity increase of 80% is demonstrated, requiring a 50% reduction in driving distance, and automation of certain procedures.

Chapters 4 to 6 propose a novel framework for assessing the optimum size of Heavy Goods Vehicles, according to the limits of their manoeuvrability. This method is based on simulation of vehicles attempting a library of real-world manoeuvres. Simulation models are described in Chapter 4, and path planning algorithms in Chapter 5. The framework is evaluated on three case studies: a 4.25 t grocery delivery vehicle, a 44 t articulated refuse collection vehicle, and a 44 t general urban vehicle with rear axle steering. A range of potential higher capacity vehicles are proposed in Chapter 6 for those applications

The impact of rear axle steering on manoeuvrability is also considered in detail in Chapter 6. It is shown that the use of rear axle steering does not always allow the use of a longer vehicle, because a rear axle steered vehicle cannot compromise between cut-in and

tailswing in the way a conventional vehicle can. However, the use of rear axle steering allows reduction in both tyre wear and rear axle load limits, which permits greater vehicle fill before rear axle loads are exceeded.

These results are compared, in Chapter 7, to an alternative method for modelling manoeuvrability (Performance-Based Standards). Finally, Chapter 8 presents some concluding remarks and recommendations for future work, including investigation of an improved cyclist detection system fusing cameras and ultrasonic sensors, and increased development of the manoeuvrability models to more accurately reflect real driving.

Table of contents

List of figures	xvii
List of tables	xxiii
Nomenclature	xxv
1 Introduction	1
1.1 Project Overview	1
1.1.1 Overview of the Road Freight Industry	1
1.1.2 Interventions for Reducing Road Freight Emissions	2
1.1.3 Overview of the Urban Freight Sector	10
1.1.4 Project Motivation	13
1.2 Case studies	14
1.2.1 Case Study A: Home Delivery of Groceries	15
1.2.2 Case Study B: Refuse Collection	17
1.2.3 Case Study C: Convenience Store Restocking	19
1.3 Thesis Outline	20
1.4 Summary	21
2 Cyclist Detection	23
2.1 Introduction and Literature Review	23
2.1.1 Motivation	23
2.1.2 Overview of Existing Cyclist Detection Systems	24
2.1.3 Vision Technologies for Vehicle and Cyclist Detection	25
2.2 System Outline	26
2.3 Test Program	28
2.4 Image Processing	29
2.4.1 Strategy	29
2.4.2 Calibration	30

2.4.3	Wheel Detection	34
2.4.4	Contact Point Location	36
2.4.5	Coordinate Conversion	38
2.4.6	Cyclist Tracking	38
2.4.7	Error Analysis	39
2.5	Results	41
2.6	Discussion	45
2.7	Conclusions	45
3	Analysis of Urban Delivery Systems	47
3.1	Introduction	47
3.2	Case Study A: Grocery Delivery Vehicle	47
3.2.1	Data Collection Methods	48
3.2.2	Comparison between Supermarkets	50
3.2.3	Analysis of Shift Length	60
3.2.4	Results and analysis	66
3.2.5	Summary	73
3.3	Case Study B: Refuse Collection Vehicle	74
3.4	Case Study C: Urban Store Vehicle	76
4	Manoeuvrability Modelling: Methodology	77
4.1	Introduction	77
4.1.1	Overview	77
4.1.2	Conventional Approach	78
4.1.3	Alternative Approach	80
4.2	Literature Review	83
4.2.1	Vehicle Models	83
4.2.2	Manoeuvrability Interventions	84
4.3	Manoeuvrability Models	87
4.3.1	Rigid Vehicle	87
4.3.2	Articulated Vehicle	90
4.4	Rear-axle Steering Systems	92
4.4.1	Rear Unsteered	93
4.4.2	Command-Steer	93
4.4.3	Partial Command-Steer	94
4.4.4	Path-Following Steering	94
4.5	Mass Distribution Models	95

4.5.1	Rigid Vehicle	96
4.5.2	Articulated Vehicle	98
4.5.3	Mass Distribution Model Calibration	100
4.6	Example Plot Construction	103
4.6.1	Vehicle Feasibility Constraint	103
4.6.2	Manoeuvrability Constraint	103
4.6.3	Axle Load Constraint	106
4.6.4	Gross Vehicle Weight Constraint	107
4.6.5	Discussion	110
4.7	Conclusions	112
5	Manoeuvrability Modelling: Algorithm Selection	115
5.1	Method and Limitations	115
5.1.1	Method Overview	115
5.1.2	Limitations	117
5.1.3	Algorithm Assessment Criteria	117
5.2	Literature Review	119
5.2.1	Rapidly-exploring Random Trees	119
5.2.2	Model Predictive Control	120
5.2.3	Spline-Based Methods	120
5.2.4	Geometric Proofs	120
5.3	Coordinate Conversion	121
5.4	Rapidly-exploring Random Trees (RRT)	121
5.4.1	Method	122
5.4.2	Results	124
5.5	Model Predictive Control (MPC)	126
5.5.1	Method	126
5.5.2	Results	128
5.6	Single- and Multi-segment Splines (SMSS)	130
5.6.1	Single-segment Splines	131
5.6.2	Multi-segment Splines	135
5.7	N Control Point Splines (NCPS)	139
5.7.1	Method	139
5.7.2	Results	140
5.8	Algorithm Selection	143
5.8.1	Quantitative Evaluation	143
5.8.2	Qualitative Evaluation	144

5.9	Conclusions	144
6	Manoeuvrability Modelling: Case Studies	147
6.1	Introduction	147
6.2	Comparison of Steering Strategies	148
6.2.1	Expected Results	152
6.2.2	Command Steer: Analysis	152
6.2.3	Path Following: Analysis	157
6.2.4	Summary	159
6.3	Case Study A	160
6.3.1	Current Vehicle	160
6.3.2	Rear Axle Steering: Command Steer	164
6.3.3	Rear Axle Steering: Path Following	167
6.3.4	Comparison of Potential Designs	168
6.3.5	Summary	169
6.4	Case Study B	170
6.4.1	Current Vehicle	170
6.4.2	Rear Axle Steering: Command-Steer	172
6.4.3	Rear Axle Steering: Partial Command-Steer	173
6.4.4	Rear Axle Steering: Path-Following	174
6.4.5	Articulation	174
6.4.6	Articulation and Rear Axle Steering	175
6.4.7	Comparison of Potential Designs	176
6.4.8	Summary	178
6.5	Case Study C	178
6.5.1	Rigid Vehicle	180
6.5.2	Articulated Vehicle	182
6.5.3	Summary	187
6.6	Overview	187
6.7	Conclusions	189
7	Performance-Based Standards Approach to Manoeuvrability	191
7.1	Introduction	191
7.1.1	Overview	191
7.1.2	Urban Performance-Based Standards	192
7.1.3	Motivation	192
7.2	Urban PBS Proposal	193

7.2.1	Proposed Framework	193
7.2.2	High Speed Analysis	194
7.2.3	Proposed Manoeuvres	194
7.2.4	Proposed Metrics	194
7.3	Simulation Results and Analysis	198
7.3.1	Case Study A: Grocery Delivery Vehicle	198
7.3.2	Case Study B: Refuse Collection Vehicle	198
7.3.3	Case Study C: Urban Store Vehicle	202
7.4	Conclusions	203
7.4.1	Effectiveness of Rear Axle Steering	203
7.4.2	Comparison of Methods	204
8	Conclusions and Further Work	207
8.1	Introduction (Chapter 1)	207
8.2	Cyclist Detection (Chapter 2)	207
8.3	Analysis of Urban Delivery Systems (Chapter 3)	208
8.4	Manoeuvrability Modelling: Methodology (Chapter 4)	209
8.5	Manoeuvrability Modelling: Algorithm Selection (Chapter 5)	210
8.6	Manoeuvrability Modelling: Case Studies (Chapter 6)	210
8.6.1	Case Study A: Grocery Delivery Vehicle	211
8.6.2	Case Study B: Refuse Collection Vehicle	211
8.6.3	Case Study C: Urban Store Vehicle	211
8.7	Performance-Based Standards Approach to Manoeuvrability (Chapter 7) . .	212
8.8	Further Work	212
	References	215

List of figures

1.1	Graphic showing contributions to emissions by sector [1]	2
1.2	Breakdown of transport emissions by vehicle type [2]	3
1.3	Interior layout of home delivery vehicles from two supermarkets (Photo Credit: Alamy)	17
1.4	Example Refuse Collection Vehicle (Photo Credit: Veolia)	18
1.5	Two vehicles commonly used for delivery to city centre stores (Photo Credit: Workhorse)	20
2.1	Breakdown of cyclist-HGV collisions by configuration. Data from Robinson and Chislett [3], graphic adapted from Jia [4]	24
2.2	Camera and ultrasonic setup	26
2.3	Camera configuration and field-of-view, shown approximately to scale with a cyclist at 1 m from the HGV	27
2.4	Sample images at various lateral separations and lighting intensities	29
2.5	Instrumentation schematic for image acquisition	30
2.6	Calibration grid processed to cover the entire image	31
2.7	General illustration of coordinate mapping	32
2.8	Examples of positive training images	35
2.9	Examples of (a) correctly and (b) wrongly detected features	36
2.10	Stages in the extraction of the ground contact point. (a) Cropping (b) Thresholding (c) Normalisation (d) Edge Detection (e) Selection of the lowest pixel	37
2.11	Comparison of calculated and measured longitudinal velocities	41
2.12	Output of camera-based detection system over three different lateral distances from the side of the HGV	42
2.13	Comparison between camera measurements and manually-extracted data points for a single run at (a) 1.5 m separation (b) 1 m separation (c) 0.75 m separation	43

3.1	GPS traces of supermarket vehicles	52
3.2	Box and whisker plot and probability density function for distances travelled between deliveries by each supermarket	53
3.3	Histograms of distance travelled between deliveries for each supermarket, showing fitted Gamma probability distributions	53
3.4	Box and whisker plots and probability density functions of time spent travelling per leg for each supermarket	54
3.5	Box and whisker plot and probability distribution function for average speed of travel between deliveries by each supermarket	55
3.6	Box and whisker plot and probability distribution function for total fuel consumption per delivery by each supermarket	55
3.7	Box and whisker plot and probability distribution function for average fuel consumption per 100 km by each supermarket	56
3.8	Example drive cycles for Supermarkets A and B	56
3.9	Time taken to complete delivery tasks for each supermarket	58
3.10	Function to convert from driving distance to driving time	62
3.11	Probability density function showing time spent on each delivery for each supermarket	63
3.12	Effect of multiplying the measured data by a factor of 2 or 0.5 before fitting Probability Density Function	65
3.13	Effect of truncating the measured data above a threshold of 3 km before fitting Probability Density Function	66
3.14	Effect on probability density function of different kerb time reduction scenarios compared to the measured data	67
3.15	Likelihood of shift length exceeding eight hours for varying number of deliveries, assuming no change to drop density	67
3.16	Likelihood of shift length exceeding eight hours with varying number of stops and distance between stops for Supermarket A	68
3.17	Likelihood of shift length exceeding eight hours with varying number of stops and distance between stops for Supermarket B	69
3.18	Likelihood of shift length exceeding eight hours with varying number of stops and maximum distance between stops for Supermarket A	69
3.19	Likelihood of shift length exceeding eight hours with varying number of stops and maximum distance between stops for Supermarket B	70
3.20	Effect of kerb time reduction scenario 1 (removing paperwork) on the 25% chance contour of the shift length exceeding 8 hours	71

3.21	Effect of kerb time reduction scenario 2 (automating material handling) on the 25% chance contour of the shift length exceeding 8 hours	72
3.22	Effect of kerb time reduction scenario 3 (removing paperwork and automating material handling) on the 25% chance contour of the shift length exceeding 8 hours	72
3.23	Box and whisker plots showing the duration of refuse collection trip for different collection patterns	75
4.1	Standard turning circle analysis of manoeuvrability for a rigid vehicle . . .	79
4.2	Standard turning circle analysis of manoeuvrability for an articulated vehicle	80
4.3	Configuration of a rigid vehicle under certain design assumptions	88
4.4	Calculation of Heading Angle for a Rigid Vehicle	89
4.5	Kinematic model of a rigid vehicle	89
4.6	Configuration of an articulated vehicle under certain design assumptions . .	91
4.7	Mass distribution model of a rigid vehicle	97
4.8	Mass distribution model of a rigid refuse collection vehicle	98
4.9	Multi-body model of an articulated vehicle	99
4.10	Multi-body model of an articulated refuse vehicle	100
4.11	Feasibility constraints	104
4.12	Manoeuvrability constraint by geometric arguments for a rigid vehicle . . .	105
4.13	Manoeuvrability constraint by geometric arguments for an articulated vehicle	107
4.14	Contours of constant rear axle load for a rigid vehicle with known payload density	108
4.15	Contours of constant trailer axle load for an articulated vehicle with known payload density	108
4.16	Contours of constant Gross Vehicle Weight for a rigid vehicle	109
4.17	Contours of constant total combination length for an articulated vehicle . .	110
4.18	Response of a rigid, unsteered vehicle to a steady-state roundabout manoeuvre, including load limits	111
4.19	Response of an articulated, unsteered vehicle to a steady-state roundabout manoeuvre, including load limits	112
5.1	Performance envelopes for the representative manoeuvres	116
5.2	Representative manoeuvres used for assessing path-planning algorithms . .	118
5.3	Illustration of the RRT algorithm	122
5.4	Illustration of parameters required to calculate H_i	123
5.5	Success boundaries as found by RRT algorithm	125

5.6	Illustration of the challenges associated with the RRT algorithm	126
5.7	Illustration of parameters used to evaluate the MPC cost function	128
5.8	Success boundaries as found by MPC algorithm	129
5.9	Parameters required to define a single-segment spline	131
5.10	Success boundaries as found by Single-segment Spline algorithm	134
5.11	Parameters required to define a spline composed of two segments	136
5.12	Success boundaries as found by Two-segment Spline algorithm	137
5.13	Success boundaries as found by Three-segment Spline algorithm	138
5.14	Definition of a spline with many segments using few parameters	139
5.15	Variation of the algorithm score for each manoeuvre with the number of control points used to define the spline	140
5.16	Success boundaries as found by Multiple Control Point Spline algorithm with 20 control points	142
5.17	Success boundaries found by the combination of the MPC and NCPS algorithms	145
6.1	Subset of manoeuvres from the ‘residential’ library	149
6.2	Comparison between success boundaries for vehicles with and without rear axle steering for a selection of manoeuvres	150
6.3	Annotated results for Manoeuvre 2 from the residential library	151
6.4	Comparison of tailswing (positive values) and cut-in (negative values) be- tween different steering strategies for an example manoeuvre. The vehicle had $L = 10.40$ m and $(a + b) = 4.72$ m	154
6.5	Comparison of Swept Path Width between different steering strategies for an example manoeuvre. The vehicle had $L = 10.40$ m and $(a + b) = 4.72$ m . .	154
6.6	Measurements of clearances around critical obstacles for example manoeuvre. The vehicle had $L = 9.75$ m and $(a + b) = 4.70$ m	156
6.7	Comparison of tailswing (positive values) and cut-in (negative values) be- tween different steering strategies for an example manoeuvre. The vehicle had $L = 10.40$ m and $(a + b) = 4.72$ m	157
6.8	Comparison of Swept Path Width between different steering strategies for an example manoeuvre. The vehicle had $L = 10.40$ m and $(a + b) = 4.72$ m . .	158
6.9	Measurements of clearances around critical obstacles for example manoeuvre. The vehicle had $L = 9.50$ m and $(a + b) = 4.70$ m	159
6.10	Arrangement of totes in the baseline vehicle	162
6.11	Baseline grocery delivery vehicle. Contours show constant success rate across all residential manoeuvres for a rigid vehicle with fixed rear axle . .	163

6.12	Axle load and GVW constraints for a home grocery delivery vehicle. Contours show constant success rate across all residential manoeuvres for a rigid vehicle with fixed rear axle	163
6.13	Proposed Command-Steered alternative to the baseline grocery delivery vehicle. Contours show constant success rate across all residential manoeuvres for a rigid vehicle with Command-Steer strategy	165
6.14	Contours of constant tailswing for different rear axle steering strategies. Solid blue contours represent an unsteered vehicle, dashed black contours represent a Command-Steered vehicle	166
6.15	Proposed Path-Following alternative to the baseline home delivery vehicle. Contours show constant success rate across all residential manoeuvres for a rigid vehicle with Path-Following strategy	167
6.16	Proposed design options for increasing capacity of a home grocery delivery vehicle	168
6.17	Baseline refuse collection vehicle. Contours show constant success rate across all residential manoeuvres for a rigid vehicle with fixed rear axle	171
6.18	Proposed Command-Steered alternative to the baseline refuse collection vehicle. Contours show constant success rate across all residential manoeuvres for a rigid vehicle with Command-Steer strategy	172
6.19	Proposed Partial Command-Steered alternative to the baseline refuse collection vehicle. Contours show constant success rate across all residential manoeuvres for a rigid vehicle with fixed rear axle, and the 30% success rate contour for a rigid vehicle with Partial Command-Steer strategy	173
6.20	Proposed Path-Following alternative to the baseline refuse collection vehicle. Contours show constant success rate across all residential manoeuvres for a rigid vehicle with Path-Following strategy	174
6.21	Proposed articulated alternative to the baseline refuse collection vehicle. Contours show constant success rate across all residential manoeuvres for an articulated vehicle with fixed rear axle	175
6.22	Proposed Path-Following articulated alternative to the baseline refuse collection vehicle. Contours show constant success rate across all residential manoeuvres for an articulated vehicle with Path-Following strategy	176
6.23	Baseline 10 t and 18 t rigid vehicles. Contours show constant success rate across all urban manoeuvres for a rigid vehicle with fixed rear axle	180

6.24	Proposed higher capacity alternatives to the 10 t and 18 t rigid vehicles. Contours show constant success rate across all urban manoeuvres for a rigid vehicle with fixed rear axle	181
6.25	Proposed Path-Following alternatives to the 10 t and 18 t rigid vehicles. Contours show constant success rate across all urban manoeuvres for a rigid vehicle with Path-Following strategy	183
6.26	Proposed articulated alternatives to the 10 t and 18 t rigid vehicles. Contours show constant success rate across all urban manoeuvres for an articulated vehicle with fixed rear axle	184
6.27	Baseline articulated vehicles and proposed articulated alternatives to the baseline rigid vehicles. Contours show constant success rate across all urban manoeuvres for an articulated vehicle with fixed rear axle	185
6.28	Path-following alternatives to baseline and proposed articulated vehicles from Figure 6.27. Contours show constant success rate across all urban manoeuvres for an articulated vehicle with Path-Following strategy	186
6.29	Summary of all vehicles considered as part of Case Study C (*Some vehicles with apparently unrealistic axle loads are included as they may be applicable for some specific load cases)	188
7.1	Measurement of Tail Swing	195
7.2	Measurement of Front Swing	196
7.3	Measurement of Swept Path Width	197
7.4	Measurement of Required Track Width	197

List of tables

1.1	Constraints on choice of vehicle for freight task	14
2.1	Average detection errors across all tests.	44
3.1	Data channels captured by the SRF logger	49
3.2	Mean time taken to complete delivery tasks	59
3.3	Effect of single-use plastic bags on the mean time to complete delivery . . .	60
3.4	Model parameters for statistical model of driver activities	61
3.5	Increase in number of deliveries which can be completed in 8 hours for different kerb time reduction scenarios, using the baseline driving distance and a reduced driving distance (50% reduction from the baseline)	73
4.1	Vehicle configurations to be considered	82
5.1	Evaluation of path-planning algorithms	143
6.1	Comparison between potential designs of Grocery Delivery Vehicle	169
6.2	Comparison between potential designs of Refuse Collection Vehicles	177
6.3	Example vehicles typically used in city centres	179
7.1	Recommendations for an Urban PBS framework by Isted et al. [5]	193
7.2	Simulation results for vehicles proposed in Case Study A	199
7.3	Simulation results for vehicles proposed in Case Study B	199
7.4	Simulation results for vehicles proposed in Case Study C	201
7.5	Approximate equivalence between PBS pass levels and real-world pass levels	204

Nomenclature

Chapter 2

μ_{ij}	Mean error between the measurements i and j [m]
σ_{ij}	Standard deviation of the uncertainty between the measurements i and j [m]
\mathbf{u}	Vector of u_i coordinates [-]
\mathbf{v}	Vector of v_i coordinates [-]
ε_{ij}	Uncertainty between the measurements i and j [m]
A	Transformation matrix [-]
C	Camera system measured cyclist position [m]
c_i	i_{th} coefficient of mapping polynomial in the u direction [-]
d	Nominal lateral distance from the side of the vehicle [m]
d_i	i_{th} coefficient of mapping polynomial in the v direction [-]
M	Manually measured cyclist position [m]
T	True cyclist position [m]
X	Longitudinal position relative to the vehicle [m]
Y	Lateral position relative to the vehicle [m]
(u, v)	Image coordinate system [px]
(x, y)	World coordinate system [m]
$\hat{\mathbf{X}}$	Vector of prior estimates of the states [-]

c	Vector of c_i coefficients [-]
d	Vector of d_i coefficients [-]
K	Vector of state Kalman gains [-]
P	Vector of state estimation errors [-]
p	Vector of prior estimates of the state errors [-]
Q	Vector of state process covariances [-]
R	Vector of state model covariances [-]
X	Vector of bicycle states [-]
z	Vector of state observations [-]

Chapter 3

$\Gamma(k)$	Gamma function [-]
θ	Gamma distribution scale parameter [-]
d_D	Leg driving distance [km]
E	Power series model first parameter [-]
F	Power series model second parameter [-]
k	Gamma distribution shape parameter [-]
M	Number of simulation repeats [-]
N	Number of deliveries per shift [-]
t_D	Leg driving time [min]
x	Gamma distribution input variable [-]

Chapter 4

$(a + b)$	Vehicle wheelbase [m]
(x, y)	Position in world coordinates [m]
Δs	Distance moved by the lead point in one time step [m]

Δt	Simulation time step [s]
δ	Steering angle [rad]
$\Delta\psi$	Vehicle yaw increment [rad/sec]
$\delta_{f,max}$	Front steering lock angle [rad]
$\delta_{r,max}$	Rear steering lock angle [rad]
Γ	Articulation angle [rad]
γ	Heading angle of the lead point [rad]
ψ	Vehicle yaw angle [rad]
ρ_i	Steady-state inner turn radius [m]
ρ_o	Steady-state outer turn radius [m]
ρ_p	Payload density [kg m^{-3}]
$\square n$	Simulation step index [-]
\square^{CS}	Superscript denoting Command-Steering system
\square_1	Subscript denoting tractor unit
\square_2	Subscript denoting trailer unit
\square_f	Subscript denoting front axle
\square_r	Subscript denoting rear axle
\square_{FW}	Subscript denoting Fifth Wheel
\square_{LP}	Subscript denoting Lead Point
a	Distance from centre of mass to front axle [m]
b	Distance from centre of mass to rear axle [m]
c	Rear overhang from the rear axle to the rear bumper [m]
d	Front overhang from the front axle to the front bumper [m]
e	Distance from tractor rear axle to fifth wheel [m]

g	Acceleration due to gravity [m s^{-1}]
h	Estimated height of payload [m]
K	Steering strategy gain [-]
L	Total vehicle length [m]
L_{cab}	Length of cab section of vehicle [m]
L_{equip}	Length of bin lifting equipment [m]
L_{pl}	Length of payload section of vehicle [m]
M	Vehicle mass [kg]
m_a	Mass of axle unit model element [kg]
m_c	Mass of chassis model element [kg]
m_e	Mass of engine and gearbox model element [kg]
m_p	Mass of payload model element [kg]
M_T	Mass of tractor unit [kg]
m_{equip}	Mass of bin lifting equipment [kg]
p_e	Position of engine and gearbox model element relative to front bumper [m]
q_c	Mass per unit length of chassis model element [kg m^{-1}]
R	Axle load [kg]
U	Vehicle speed [m s^{-1}]
w	Vehicle half-width [m]

Chapter 5

$(a + b)$	Vehicle wheelbase [m]
(r_i, θ_i)	Polar coordinates of the end point of the tangent to the path at the i_{th} control point relative to the control point [(m, rad)]
(u, v)	Position in image coordinates [px]

(x'_i, y'_i)	Coordinates of the endpoint of the tangent to the path at the i_{th} control point [m]
(x, y)	Position in world coordinates [m]
(x_i, y_i)	Coordinates of the i_{th} control point [m]
ΔJ	Cost function increment [-]
δ	Steering angle [rad]
$\delta_{f,i}$	Steering angle at the start of a motion primitive [rad]
$\delta_{f,lock}$	Front steering lock angle [rad]
$\dot{\delta}$	Steering rate [rad s^{-1}]
ε	Yaw angle error [rad]
λ	Scale factor from pixels to meters [-]
C	Spline coefficient matrix [-]
Q	Spline coordinates [m]
T	Spline parameter matrix [-]
ψ	Yaw angle [rad]
\square_f	Subscript denoting front axle
\square_g	Subscript denoting goal configuration
\square_i	Subscript denoting the i_{th} node
\square_n	Subscript denoting newly created node
\square_r	Subscript denoting rear axle
\square_s	Subscript denoting start configuration
\square_{rand}	Subscript denoting random configuration
$a_x - d_x, a_y - d_y$	Spline definition coefficients [-]
C_i	Spline control point [-]

d_F	Perpendicular distance from the centre of the front of the vehicle to the nearest boundary [m] [-]
d_L	Perpendicular distance from the front left corner of the vehicle to the nearest boundary [m]
d_P	Perpendicular distance from the centre of the front axle of the vehicle to the target path [m]
d_R	Perpendicular distance from the front right corner of the vehicle to the nearest boundary [m]
H	Node score [-]
h	Image height [px]
J	Cost function total [-]
k	Simulation step index [-]
K_ψ	Yaw angle gain [-]
K_e	Exponential term gain [-]
K_F	Front term gain [-]
K_L	Left side term gain [-]
K_P	Path following term gain [-]
K_R	Right side term gain [-]
L	Total vehicle length [m]
n	Number of spline segments [-]
t	Parametric position along a spline [-]

Chapter 1

Introduction

1.1 Project Overview

1.1.1 Overview of the Road Freight Industry

As part of an international effort to tackle climate change, the UK government has committed to reducing carbon emissions to net-zero by 2050 [6]. This figure is expected to limit global average temperature increases to less than 1.5 °C, which is the predicted threshold for dangerous levels of climate change. Achieving this ambitious target will require deep and far-reaching emissions cuts across all sectors.

In the UK, according to 2017 data, the transport sector was responsible for 27% of emissions, making it the largest emitting sector [1]. Figure 1.1 shows this information in a graphic from the Department for Business, Energy and Industrial Strategy. Crucially, this percentage is increasing. This is because other sectors are decarbonising faster. For example, emissions from the energy sector, which comprised 24% of UK emissions in 2017 have fallen by 60% relative to 1990 levels, whereas emissions from the freight sector have fallen by just 2% over the same period. Attempts to decarbonise the sector are also hampered by increased demand. Under the ‘business as usual’ assumption, international freight volumes are expected to triple by 2050 [7].

Within the transport sector, 58% of emissions in 2014 came from cars and taxis [2]. However, the road freight system contributes much of the remainder, with 16% from Heavy Goods Vehicles, and 15% from Vans (although some of these are service vehicles or personal transport vehicles and therefore do not carry freight). This data is shown in Figure 1.2.

The following sections identify a number of interventions for reducing the emissions of road freight vehicles.

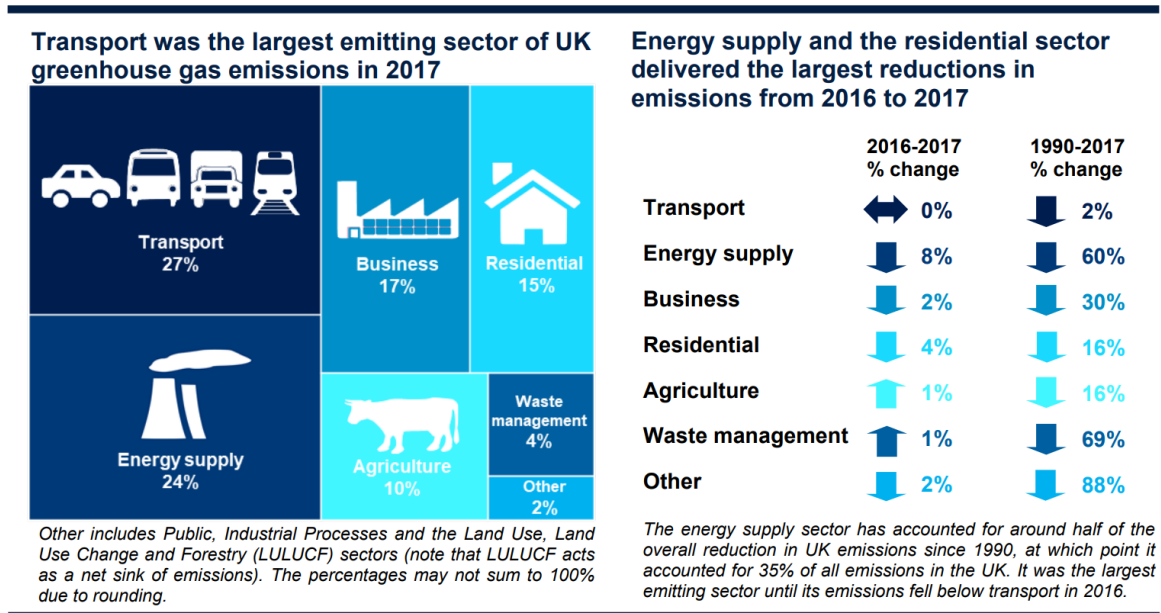


Fig. 1.1 Graphic showing contributions to emissions by sector [1]

1.1.2 Interventions for Reducing Road Freight Emissions

1.1.2.1 Alternative Energy Sources

Moving away from diesel powered vehicles is arguably the most efficient way to cut emissions. However, the barriers to any alternative fuel are high. Several summaries of potential fuel technologies exist [8, 9].

Gas-fuelled vehicles A variety of gas or dual-fuel (gas and diesel) vehicles are being trialled. Overviews of gas-fuelled vehicle technology are provided by Khan et al., and Stettler et al. noting significant barriers [10, 11]. The cost of the infrastructure required to supply large quantities of gas at low temperatures and high pressures is significant, particularly due to the inherent safety considerations which must be managed.

A popular option is the use of bio-gas, produced from anaerobic digestion of plant matter (either specially grown or waste material). Bio-gas vehicles can reduce CO₂ emissions by 60 to 90% compared to the equivalent diesel vehicle, depending on the gas-production technology used [8]. However, the quantity of bio-gas available in the UK is expected to be insufficient for it to be the primary fuel source for the transport industry in the future, due to the quantity of land required to grow source biomass, and the available quantities of agricultural and food waste [12].

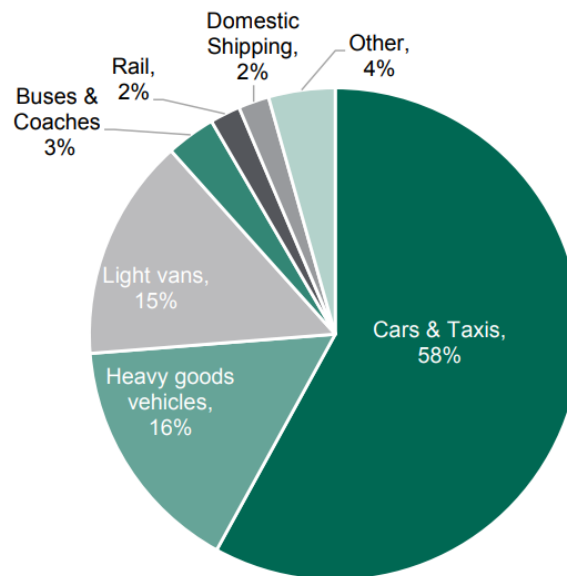


Fig. 1.2 Breakdown of transport emissions by vehicle type [2]

Finally, although the CO₂ emissions are lower than those of diesel vehicles, there are concerns that gas-fuelled vehicles can suffer from methane-slip due to incomplete combustion [13]. Additionally, methane, which contributes 30 times more to the greenhouse effect than CO₂ [14], can be vented to the atmosphere to avoid pressure build-up in storage tanks, or can leak during handling and refuelling [11].

For these reasons, it is expected that gas-fuelled vehicles will provide a ‘bridging technology’ while other technologies and infrastructures are developed [8].

Electrification A key method for reducing emissions is conversion of freight vehicles to electricity. The significant argument against this is that generating electricity still produces CO₂ so electric vehicles are no ‘greener’ than those with diesel or petrol engines. However, decarbonisation of the electricity grid is happening rapidly (in the UK at least) with a 90% drop in carbon emissions from the electricity sector by 2050 required to meet UK targets [15]. Nicolaides, Cebon and Miles analysed a number of options for electrification of road freight and predicted that electric freight vehicles would generate approximately the same well-to-wheel greenhouse gas emissions as an equivalent diesel vehicle in 2016 [16]. By 2030 however, decarbonisation of the electricity grid will result in a 25% drop in the greenhouse gas emissions generated by electric vehicles.

In addition, diesel fuel burnt in city centres contributes to lower air quality—Transport for London reports that London is in breach of legal limits for NO₂, attributing 4,300 deaths

per year in London to poor air quality [17]. The London Ultra Low Emission Zone is a policy similar to the congestion charge and covering the same area, to charge any vehicles which do not meet strict noxious and greenhouse gas emissions standards. Electric freight vehicles would naturally pass these restrictions, saving money for operators. Although the production of electricity from fossil fuels still generates noxious emissions, this occurs at power stations outside city centres, thus limiting impact on urban air quality and therefore public health.

The noise reduction due to electrification allows for the possibility of out of hours operation. During the London 2012 Olympic games, companies were encouraged to move deliveries outside of normal hours to reduce traffic congestion during the day [18]. Removing heavy vehicles from the roads during the daytime also reduced accidents as there were fewer people around which goods vehicles were operating. This policy was considered successful enough to be continued after the games.

The main technological barrier to electric vehicles is the prohibitive weight of batteries. Using smaller batteries reduces weight, but limits the range of the vehicles. Attempting to increase the payload of the vehicle increases the required battery size, which means the increase in load capacity is small. Electrification is most suited to small vans and trucks which have a small operating range and an urban drive cycle (low speed, with lots of starts and stops) [19]. Electrification has the significant added advantages for urban operations of zero noxious ‘tailpipe’ emissions and very low noise.

Possibilities for the electrification of long-haul, heavy trucks are being investigated [16]. Until battery capacity improves, the most promising solution is a ‘charge-on-the-move’ system, such as overhead cables to draw electricity from, inductive pads under the road for wireless charging, or an electrified track in the middle of the road [20–23]. Such a system requires significant investment in infrastructure, and a strong business case to encourage investment in specialised vehicles by fleet operators.

There have been numerous trials of electric vehicles in city centres [24–27], but none have used purely electric heavy trucks (10 t or more) for the reasons described above.

1.1.2.2 Vehicle Interventions

At the other end of the scale sit a group of interventions for which the barriers to adoption are much smaller, but the benefits in terms of carbon savings are correspondingly smaller.

Retro-fit Technologies Many solutions can be retro-fitted to existing vehicles. Examples include low rolling resistance tyres, aerodynamics packages for the front, rear, side or underbody of the vehicle, lower viscosity engine lubricants, and light-weighting. Odhams et al. summarise the fuel consumption benefits of some of these interventions, estimating

benefits of 6% from low rolling resistance tyres, 8% from aerodynamics at highway speeds, and 5% from improved transmission efficiency [28]. Galos et al. suggested that reducing trailer weight by 30% could reduce the mass energy consumption per tonne km by 13% [29].

Driver Training One often overlooked intervention is ‘eco-driver’ training. It is estimated that improving driver behaviour could reduce fuel use by as much as 6% according to Beusen et al. [30]. It was acknowledged however, that 40% of participants in this study had already been working to improve their driving style before taking the course.

This reduction comes at very low cost. Training drivers to spend more time in cruise control, minimise harsh acceleration and braking, and travel at lower speed where applicable, if successful, will reduce fuel consumption. However, it is necessary to ensure that training is effective, and the effects long-lasting. Beusen et al. monitored results for four months after a training course and found that some drivers had already returned to their original driving style, despite initial benefits [30]. Research programs are now attempting to understand driver behaviour and investigating effective training and long-term feedback methods for drivers [31–33].

Autonomous Vehicles Autonomous vehicles are a popular topic for discussion in the road transport sector. The benefits in terms of operating costs are substantial, since the driver can constitute 27–42% of a vehicle’s operating costs (data from Germany, the UK, and the US) [34]. There are also societal benefits such as the potential for reduced accidents [35]. The benefit of autonomous driving for emissions is only partly due to the autonomous functionality. Emissions savings from applying autonomy are comparable to the emissions savings from encouraging ‘perfect eco-driver’ behaviour, plus the possibility of carrying a greater payload due to the absence of cab and driver. Additional benefits could arise from additional logistical flexibility available in autonomous operations, and from the ability to create connected systems of vehicles (particularly in urban areas) which can collaborate to reduce congestion, thus reducing emissions [35]. The technical and legislative barriers to this technology are high, therefore autonomous systems are unlikely to be a practical solution in the time-frame required to meet emissions objectives.

Platooning Similarly, while platooning—controlling the speed of HGVs to follow each other closely enough to provide aerodynamic benefits—yields some benefits for fuel economy (5–7% at 70 km h⁻¹) [36], the barriers are equally high [37]. In this case, an additional barrier is the business case for such systems, specifically that the driver is still needed when the

vehicle leaves the platoon, so the benefits are small compared to the additional costs of developing and implementing the technology.

1.1.2.3 Logistics Interventions

The goal of the above vehicle interventions is to reduce the fuel consumption per tonne-km of freight moved, but it is also important to consider means for reducing the total distance travelled to transport a given amount of freight. These methods are broadly labelled logistics interventions, and fall loosely into two categories—measures with low barriers to adoption but relatively limited benefits, and major projects which completely redefine the logistics network, and could reduce fuel consumption significantly, but require large initial investment or some form of legislative assistance [38].

Reduce Demand The most effective approach is to reduce demand. However this is difficult due to current consumer attitudes and the reluctance of operators to risk market share by upsetting those consumers [39]. For example most online clothing retailers offer a free returns service, which can encourage consumers to buy in large quantities with the intention of returning the majority.

Additionally, demand for high-speed delivery from both end-users and manufacturers forces distributors to compromise on efficiency in favour of service. Vehicles are required to run half full in order to meet their delivery time slots. If customer service time requirements could be reduced, fewer vehicles with greater fill could be used instead.

Simple Interventions McKinnon et al. provide an overview of logistics interventions for reducing carbon emissions and many of the other negative externalities associated with road freight [38]. Simple interventions include better routing, and increasing vehicle fill. The first of these is intended to limit unnecessary distance travelled, and the second to make sure that the fuel cost per tonne-km is minimised.

For urban delivery vehicles, one suggested solution is to increase the size of delivery windows. It has been shown that even a small relaxation in delivery time can have a large impact on fuel saving due to increased efficiency of the route (i.e. the number of times the vehicle has to return to an area it visited previously is reduced). Campbell and Savelsbergh found that the expansion of one-hour time windows to two hours increases profits by more than 6% [40]. In the extreme, completely flexible, unattended deliveries could reduce costs by up to 33% compared to 2-hour delivery windows [41].

Collaboration Collaboration between carriers can help them keep pace with increasing demand for variety of product, delivered in a short time frame [42]. Research by Palmer et al. has shown that collaboration can reduce empty running and reduce carbon emissions per delivery by as much as 46% [43]. One reason this is not more common is the reluctance of operators to share data with competitors which would allow them to collaborate. Additionally the structures required to allow operators to share costs fairly are often not in place [44].

Consolidation Centres A possible solution to the reluctance to collaborate is the idea of consolidation centres, which are typically used at the edge of urban areas to combine incoming shipments into as few deliveries as possible. Users can pay a fee giving them access to inventory space and vehicles. Final delivery into the city centre is provided as a service by a single operator with optimised vehicles. A more detailed description is given by Allen et al. [45]. The primary barrier to these centres is the high up-front cost, and making the business case for users [46]. It has been recommended that city councils or other funding bodies could provided the initial investment to encourage such projects, which could then become financially self-sustained [47].

An example is the Bristol-Bath consolidation centre, which was largely funded by EU grants [48]. Because of the high capital cost of the centre, a high participation rate of locally operating companies is required—quoted as 70% uptake by Lewis et al. in a report for the Department for Transport [49]. Ways for local government to incentivise companies were discussed by Marcucci et al. [50], including fully funding the consolidation centres, increasing delivery permit costs in the city, and increasing delivery windows offered by the centre. Marcucci et al. estimate the maximum achievable market share, with incentives, to be 50%, without direct regulatory intervention.

Two examples of urban consolidation centres can be found in Monaco and London. In Monaco, large trucks are banned from the city centre, and all goods must pass through the city consolidation centre [51]. A trial of a consolidation centre in central London used light electric vehicles for last-mile delivery, reducing CO₂ emissions per parcel by up to 50% [24, 25].

An additional benefit of consolidation centres is to consumers, who can receive all their deliveries together instead of multiple deliveries from different couriers.

Third-Party Logistics Freight consolidation can be applied in a variety of different ways, allowing operators to effectively benefit from increased economies of scale. However, consolidation of a single operator's freight is often impractical, and consolidation between multiple operators can be limited by the reluctance of operators to communicate effectively

with their competitors. A solution to these limitations is the use of third-party logistics solutions, whereby logistics are provided by an external company to one or more fleet operators. This solution leads to increased quantities of freight making any given journey, thus permitting larger vehicles and thus reduced fleet emissions. The use of a third party eliminates the perceived risk to companies of communicating with their competitors.

This approach is particularly relevant to parcel deliveries, since the quantities of parcels carried on one vehicle are typically high (sometimes more than 100). This means that in order to fill a larger vehicle it often requires the parcels of more than one company. Additionally, current parcel delivery windows are often wide (either a day or half-day) such that less careful route planning is required.

In contrast, grocery delivery systems rarely use third-party logistics providers. Because a typical home grocery delivery is much larger in terms of mass and volume than a typical parcel delivery, the benefits are reduced. Also, grocery delivery services usually offer very narrow delivery windows (within one hour) which would require a complex route plan to be implemented by the logistics provider.

Physical Internet An extension of the consolidation concept is the ‘physical internet’, through which all freight travels in modular containers, allowing almost perfect consolidation into larger units [52]. Freight travels from its destination to the trunk network in small units, then is consolidated into larger units for the long-haul portion of the journey and back to small units for the last mile. This ensures that any given unit of freight makes as much of its journey as possible in the largest, most efficient vehicle possible. An overview of the concept of the physical internet is given by Montreuil, including a description of the implications of this system and the research requirements for future development . In particular, the difficulties of the transition from conventional logistics systems to the centralised physical internet are discussed, and suitable intermediate strategies are proposed [52].

Last Mile Solutions A common research focus is the optimum mode of transport for the ‘last mile’. The use of bicycles to transport goods in urban areas is becoming more widespread as operators look to reduce costs compared to standard goods vehicles. The obvious disadvantage of this is the lack of load capacity. This makes them suitable for small parcel deliveries, but irrelevant for large deliveries such as construction material, and of limited use for home delivery of groceries. It is estimated that in European cities, around 25% of city centre freight could be transported by bicycle [53]. Gruber et al. analysed the potential barriers to cargo cyclist use and found that suitable cyclist infrastructure (such as drop-kerbs) was vital [54].

Transporting freight by bicycle has the effect of reducing noise and emissions effectively to zero. However, there are social concerns, including the safety of riders. The effect of increasing the number of cyclists (often carrying wide cargo boxes) on congestion is unclear. It is not necessarily the case that this mode shift would reduce congestion (although it seems likely) and no research has been found in this area. The advantages and disadvantages of cycle freight are reviewed in more detail by the CycleLogistics consortium [55]. The CycleLogistics report also includes details of a project intended to persuade consumers to do their own shopping by bicycle.

An article by Schliwa et al. reviewed a number of studies on the use of cycles (including some on electric powered cycles) which in general found that cargo cycles could be a ‘viable solution’ for goods transport in urban centres (provided drop density is high) [56].

Some operators have attempted to combine bicycles and larger vehicles in their fleets, including ‘Hub and Spoke Models’, where larger vehicles act as ‘micro-hubs’ for cargo bike deliveries to operate from [57]. A number of successful delivery companies have been formed based purely around bicycle delivery. A successful case study is Outspoken [58], operating in Cambridge, a city which has an ‘established cycle culture’ [56]. This may have contributed to lower entry barriers. Outspoken, along with two other case studies described by Schliwa et al., services one major client in the parcel delivery sector [56].

Light electric trucks provide a potential means to transport goods too large for bicycle delivery. However, the cost structure for these vehicles is often poorly understood, since the initial purchase cost tends to be higher than conventional diesel vehicles, but operating costs are often lower [59]. Lebeau et al. showed that while electric vehicles can be cost effective compared to diesel vehicles, the comparison is very sensitive to factors such as future energy costs and government support [59].

A crossover between light goods vehicles and bicycles is electric cargo bicycles, which combine the flexibility of bicycles with a slight increase in cargo capacity (and decrease in driver effort) due to small electric motors [53, 54].

1.1.2.4 Increase Capacity

Research has shown that one of the best methods to reduce emissions from the road freight sector is to use higher capacity vehicles [28, 60–62]. In general, the payload mass as a percentage of gross vehicle mass increases as the gross vehicle mass increases [28]. For example, for a 3.5 t van, the payload percentage by mass is typically less than 30% (approximately 1 t). For a large rigid (26 t gross vehicle mass) the percentage is often 60%, and for a long combination vehicle can be as high as 70%. Although any given larger vehicle

consumes more fuel than an equivalent smaller vehicle, the number of vehicles required to move a given pool of freight is less, thus the fleet fuel economy is better.

There are barriers to higher capacity vehicles, particularly in urban environments. These are discussed in more detail in Section 1.1.3.3. The biggest barriers to higher capacity vehicles on the highways are manoeuvrability, braking performance, and legislative barriers (for example ensuring that the vehicle can still pass the standard UK roundabout test [63]).

1.1.3 Overview of the Urban Freight Sector

1.1.3.1 Global Urbanisation

The proportion of the world's population living in urban areas is increasing rapidly. The exact figure depends on the definition of an urban area, which varies significantly between countries, and thus is very difficult to produce. For example by Swedish census methodology, 200 people is considered an urban settlement, whereas in Mali, the minimum is 40,000 [64]. It is widely accepted that more than half of the global population is living in towns or cities, up from 30% in the 1950s [65]. That percentage is expected to rise to 85% by 2050 [66]. In total this corresponds to 3.9 billion people living in urban areas worldwide today, up from just 746 million in 1950. By 2050, an additional 2.5 billion people are expected to be living in towns and cities. This figure is made up of a combination of both population growth and rural to urban migration.

The gap between the developing and developed countries must also be considered. In the UK, the urban proportion of the population (which had been steadily just under 80% since the 1950s) is now at 82% and expected to reach nearly 90% by 2050, a pattern which is repeated across other developed countries [65, 67]. However, despite the lower proportions of urban residents in developing countries, the absolute numbers are higher. Asia alone contributes more than 50% of the world's urban population, whereas Europe contributes just 14%. In terms of growth, the urbanisation process is happening fastest in Africa and Asia (these two continents are expected to generate more than 90% of the increase). India, China and Nigeria alone are predicted to account for 37% of urban population growth by 2050 [65].

An additional distinction is the size of the cities. Of the world's population, only one eighth live in so-called 'mega-cities', with more than 10 million inhabitants [65] (of which there are 28 worldwide). By contrast, more than half live in towns or cities with a population of less than 500,000. Whereas in 1950 the majority of the world's largest cities were found in developed countries, most mega-cities now are found in developing countries. The fastest-growing type of city is mid-sized cities in Africa and Asia, with between 500,000 and 1 million inhabitants [65].

1.1.3.2 Impacts of Urban Freight

High population density creates a number of challenges for providers of goods and services to those populations, which will only increase as the world's population becomes increasingly urban [68]. Transporting goods into and waste out of city centres must be done by road in almost every case, which generates a high volume of vehicles on the roads, both personal and commercial. This usually contributes significantly to congestion, and causes additional problems such as high noise levels, risks for vulnerable road users and greenhouse and noxious gas emissions [68].

Managing urban freight activities can be a complex task, as there are many competing goals to be balanced [69, 70]. These include national authorities seeking to limit Greenhouse Gas emissions; local authorities looking to manage congestion, noise and air quality emissions; operators attempting to minimise costs; residents avoiding noise (particularly outside of working hours), and all parties wishing to improve safety.

McKinnon et al. refer to the concept of negative externalities associated with road freight [38]. These can be considered the 'non-financial costs' of moving freight on the roads. For example the effect on public health of reduced air quality due to freight vehicles in urban areas is a negative externality. (In this case, there is a financial cost, but it is borne by the health service, rather than the freight industry.)

The externalities of road freight in urban centres are different to those on long-haul routes. First, noise pollution becomes a much more significant factor when there are people around to hear it [71]. Secondly, while greenhouse emissions are a negative externality for all freight vehicles, noxious emissions are only really a problem in densely populated areas [72]. Thirdly, congestion is a serious negative impact of increased freight vehicle traffic on urban routes [28]. Finally, there is the risk of damage to infrastructure, or collisions with vulnerable road users [73, 74].

One additional difference between long-haul and urban driving is that drive-cycles in city centres are much lower average speeds, and include a lot more starting and stopping [75, 28]. This makes them ideal candidates for electrification, but in the short term means that the fuel economy and therefore emissions statistics are poorer for urban vehicles than long-haul vehicles.

A simple approach to reducing the negative externalities associated with urban road use is to reduce the number of vehicles on the roads. As well as reducing emissions and noise and improving safety, this would also reduce congestion, which has a further effect on emissions, since vehicles spend less time stationary [28]. Treiber et al. [76] showed that reducing congestion can inherently reduce vehicle emissions by up to 80% in extreme cases, simply by reducing the length of time vehicles spend on the road idling.

1.1.3.3 Barriers to Higher Capacity Urban Vehicles

There are a number of pressures or perceived pressures limiting the size of current urban vehicles.

Negative public perception Negative public perception of heavy goods vehicles has led to strict legislative controls, and reluctance of operators to switch towards larger vehicles. Larger vehicles are generally seen as being more polluting, and more likely to cause damage to structures or to cause accidents involving vulnerable road users [77]. In fact, research into Long Combination Vehicles by Woodroffe showed that larger vehicles are often safer, due to the fact that fewer of them are required, and that operators tend to use their best drivers for their biggest vehicles [78].

Woodroffe's study showed that the crash rate of Long Combination Vehicles operating under a special permit in Alberta was five times less than standard tractor semi-trailers on the same roads [78]. This was partly attributed to the special permit required to operate the vehicles. A report for the Department of Transport in the UK evaluating the trial of longer semi-trailers showed a 70% drop in accidents on a per-km basis for longer semi-trailers compared to standard semi-trailers [79]. Similar results have been observed in the RTMS programme in South Africa [80], and for higher capacity vehicles in Australia [81].

Increasing capacity of freight vehicles will lead to some decrease in traffic congestion [82]. This can be attributed to the reduced number of vehicles required for a given freight task, despite a marginal increase in length per vehicle.

Legislative limits An important barrier to higher capacity vehicles for urban delivery applications is the UK definition of a Light Goods Vehicle (LGV), which must have a Gross Vehicle Weight (GVW) of less than 3.5 t. Consequently vehicles weighing less than 3.5 t do not require drivers to hold an HGV license, or follow HGV driver shift length rules, or the vehicle to be fitted with a tachograph [83]. These would increase operating costs significantly, making it uneconomical to use a vehicle larger than 3.5 t unless a significantly larger vehicle was feasible.

As a response to recent consultation with operator associations, the Department for Transport has relaxed this limit for 'alternatively-fuelled' vehicles to 4.25 t [84]. This is intended to mitigate the payload penalty caused by the increased weight of alternative power-trains, such as battery weight.

For larger vehicles such as tractor semi-trailers, the maximum dimensions are set by the standard roundabout test [63]. To pass, the vehicle must be able to turn through 360° without exceeding an outer radius of 12.5 m, or an inner radius of 5.3 m.

Manoeuvrability If larger vehicles are required to access the same roads as smaller vehicles, then any given vehicle is more likely to cause damage to infrastructure or accident involving other road users, due to the manoeuvrability penalty of being larger [5]. Vehicles with a larger wheelbase have a wider turning circle and so require more space to turn. Vehicles with a longer overall length and therefore longer overhangs from the front and rear wheels have larger ‘frontswing’ and ‘tailswing’, thus can collide with obstacles. These effects will be described in more detail in the following chapters.

Vehicle fill and driver workload Since using a single, larger vehicle instead of a single, smaller one for a given route causes higher fuel consumption, it is clear that unless the larger vehicle can be filled, the smaller vehicle is the more suitable. In other words, if a larger vehicle is not carrying more freight than a smaller vehicle, then the smaller vehicle should be used instead. For some logistics operations a fleet of larger vehicles is less efficient.

Similarly, for operations where increasing capacity means increasing the number of vehicle stops (such as home delivery) rather than the size of each drop, the length of time required to make all the deliveries from a larger vehicle could exceed a sensible driver shift length. This would then incur additional costs of returning to base to swap drivers (in which case the vehicle could be reloaded anyway) or arranging for drivers to meet out on the route. Therefore it is necessary to match the size of vehicles to the number of deliveries that can be completed in a single shift.

1.1.4 Project Motivation

The literature reviewed in the Section 1.1.2.4 sets out supporting evidence for improving the efficiency of road vehicles by increasing their capacity. However, for any specific application, there are practical considerations to be addressed before this strategy can be applied successfully. Possible reasons why this might not be the case fit into two categories: ‘cargo constraints’, and ‘route constraints’, a set of which are presented in Table 1.1. This list is not exhaustive.

Cargo constraints are concerned with ensuring that the cargo is appropriate for the vehicle. The vehicle must have sufficient mass and volume capacity to transport the required freight, and must be able to provide refrigeration for fresh produce, and sufficient suspension cushioning for delicate produce. Additionally, the load space must be of a shape to accommodate the freight—for example a short vehicle cannot carry long, thin goods. A less-considered constraint is inefficiency due to under-utilisation of the vehicle—using a vehicle which is too large for the quantity of freight to be transported generates more emissions than a smaller vehicle. There are many applications where the freight operator does not have enough freight

Table 1.1 Constraints on choice of vehicle for freight task

Cargo Constraints	Route Constraints
Mass Limit	Vehicle Range
Volume Limit	Delivery Windows
Under-utilization	Manoeuvrability
Cargo Cushioning	Driver Shift Length
Cargo Refrigeration	Perishable Produce
Cargo Shape	Safety of Vulnerable Road Users

making a particular journey at a particular time to fill a bigger vehicle, or where the most efficient fleet is made up of smaller vehicles rather than larger vehicles running partially full.

Route constraints refer to selection of a vehicle which is able to complete the required route. The simplest of these is the manoeuvrability constraint, which requires the vehicle to be able to physically fit through narrow gaps or round tight corners. Other considerations include the vehicle's range (which is particularly important for electric vehicles), whether the vehicle can complete a route timed to achieve all required delivery windows, and whether the vehicle's route can be completed within the length of a standard driver shift.

Many of the constraints from Table 1.1 are highly interconnected and require an understanding of the full logistics system to analyse. For example, increasing the length of delivery windows could cause higher utilisation factors for vehicles, since routes will be more efficient and thus more deliveries can be completed without exceeding the vehicle's maximum range. Modelling of the full logistics system was beyond the scope of this work. Two constraints which could be modelled in isolation were the limit on manoeuvrability, and the limit on driver shift length. A need was identified for a method for analysing both of these constraints.

Both of these analyses will be applied to each of the three case studies described in Section 1.2. The first, analysis of driver shift length constraints, will be the focus of Chapter 3. The second, analysis of manoeuvrability constraints, will be the focus of Chapters 4 to 6.

This work is intended to develop enabling methods and technologies to improve the viability of higher capacity vehicles in urban environments, covering the topics of safety, driver workload, and manoeuvrability.

1.2 Case studies

In order to evaluate the methods described in Chapters 3 to 7, three urban freight case studies were selected. These case studies were home delivery of groceries, domestic refuse collection,

and urban store delivery vehicles. This section describes the motivation for selection of these case studies, and an overview of the currently used systems. There were a number of other plausible case studies, including parcel delivery, construction freight, other municipal vehicles such as ambulances and fire engines, and buses. The following sections provide evidence that the greatest benefits to urban emissions can be found from the grocery delivery and refuse collection sectors. The third case study, urban store delivery, is provided as a less specific application, intended to demonstrate the wider applicability of the methods described.

1.2.1 Case Study A: Home Delivery of Groceries

1.2.1.1 Motivation

It is difficult to quantify the contribution of grocery shopping to carbon emissions for several reasons. First, the majority of grocery shopping is done in personal vehicles, for which no loading records are kept, thus making it difficult to track metrics such as tonne-kilometres for the freight being carried. Secondly, much grocery shopping is done as part of journeys which would have occurred anyway, for example on the way home from work. This is known as ‘Journey Chaining’. Thirdly, ‘shopping’ is generally considered both by researchers and consumers to cover both groceries and all other goods, and specific figures for grocery shopping are rarely kept separately. In addition, the effect of grocery shopping on traffic congestion can be significant, thus inflating the emissions of each vehicle. Peak hours at grocery stores typically match morning and evening rush hours on the roads. However, there are some approaches to estimating the effects of grocery shopping on carbon emissions.

Of all the freight being moved in the UK, the most prevalent is food products, comprising 22% of all goods moved by UK-registered HGVs, totalling 30.3 billion tonne-km [85]. This was shown by a survey by the UK Department for Transport (DfT), which considered goods movement by HGVs, although the survey was not limited to cities.

An alternative approach is to consider goods movement from the point of view of households. This takes into account the last mile emissions by car, which are ignored in most freight statistics. Movement of goods by car is rarely measured in tonne-kms, making it difficult to definitively estimate emissions. However, a good approximation can be found by analysing the components of household spending. The Office for National Statistics (ONS) reported that 11% of household spending was on food and non-alcoholic drinks – the fourth largest category behind transport, housing and recreation [86]. When other goods which might be bought on a grocery shopping trip (such as toiletries and alcohol) are included, the percentage of spending rises to 17%.

It has been shown that emissions generated by the last mile are significant compared to the rest of the distribution chain. Browne et al. considered the movement of jeans, finding that a short shopping trip by car could generate as much CO₂ as the rest of the transportation chain [87]. These findings were replicated by Browne et al. for the case of the supply chain of fruit and vegetables [88], by Jespersen for rye bread [89] and by Weber et al. for USB flash drives [90]. This supports the case for investigating the consumer end of the supply chain for impacting carbon emissions of the freight system.

A study by Edwards, McKinnon and Cullinane compared 'last mile' carbon emissions between passenger cars and small delivery vans [91]. The focus of the study was small, non-food items. It found that a 'home delivery operation is likely to generate less CO₂ than the typical shopping trip'.

None of the approaches described above shows conclusively that grocery items are the single largest contributor to urban emissions. However, the literature does provide a compelling argument for focussing on them in order to make a significant impact on urban emissions. Siikavirta et al. estimate that the potential reduction in emissions associated with grocery shopping could be as high as 87% compared to consumers going to the store themselves [92]. Using higher capacity delivery vehicles could reduce the emissions further by requiring fewer vehicles.

1.2.1.2 Current Systems

Although there are subtle differences between the methods used by different retailers for home delivery of groceries, informal interviews with management and staff at three different supermarkets revealed that the underlying methods are similar. Retailers use large outlets, often on the edges of town, as distribution centres for their home delivery operations. Staff pick products from the shelves, according to computer controlled order lists (the approach to assigning products to staff is one of the variations between supermarkets) into small crates known as 'totes'. The totes are labelled with barcodes, so that the computer retains a record of the contents and therefore weight of each tote.

The totes are stacked into 3.5 t home delivery vans by the driver. The supermarkets have different internal vehicle layouts. For example, some vans are accessed by a side panel, whereas other vehicles are accessed through the rear (Figures 1.3a and 1.3b). Most supermarkets use racks to slide the totes to the back, but some have no racking and use stackable totes in piles of four or five. Once the vehicle is loaded with the deliveries scheduled for that shift by the central computer, the computer reports the total weight of the vehicle, alerting the driver to any overloading.



(a) Side-accessed vehicle



(b) Rear-accessed vehicle

Fig. 1.3 Interior layout of home delivery vehicles from two supermarkets (Photo Credit: Alamy)

All retailers interviewed for this work offer one-hour delivery slots. Usually the route planning software allows sufficient time to reach the correct destination. There are however a number of sources of delay such as congestion, or a particularly slow delivery, which could lead to deliveries arriving outside the target window. Drivers sometimes arrive ahead of schedule, requiring them to sit and wait, sometimes for up to an hour. In some cases drivers are permitted to phone ahead to ask for permission to deliver early, but some retailers do not allow this, and sometimes the customer is not available anyway.

Delivery methods are very similar between retailers. The driver unpacks the totes from the van, onto a sack-barrow if there are more than two totes, and takes them to the door. Most supermarkets offer the option for customers to ask drivers to enter the house to unload the totes in the kitchen, but some customers prefer to unload the totes in the doorway. The driver then repacks the empty totes and sack-barrow in the vehicle.

All the supermarkets surveyed require the driver to do some form of paperwork at each delivery. Most require the driver to scan the barcodes on every tote offloaded from the vehicle, as a check against delivery errors. Additionally, most require the drivers to 'sign off' on the delivery using some form of hand-held device.

1.2.2 Case Study B: Refuse Collection

1.2.2.1 Motivation

Waste generation has risen steadily for the last three decades, both as a consequence of increasing populations, and a rising waste rate per capita [93]. In the UK, the total Municipal Solid Waste (MSW) generated is approximately 32 million tonnes per year [94], growing at a rate of up to 7% per year [95]. The majority of this waste is collected by diesel Refuse Collection Vehicles, with an average fuel economy of less than 3 miles per gallon [93]. In



Fig. 1.4 Example Refuse Collection Vehicle (Photo Credit: Veolia)

a case study in Malmo, Sweden, Refuse Collection Vehicles were estimated to account for 10-15% of total freight transportation by volume in the city (but with a higher than average impact on congestion, noise, and noxious emissions due to the stop-start nature of operations) [96].

Research into refuse collection tends to focus on one of two things: the choice of power source for the vehicles, or planning of the most efficient routes. The former has generated several studies comparing the day-to-day and lifetime emissions of existing diesel vehicles to alternatively fuelled vehicles, including Compressed Natural Gas [97], hybrid hydraulic [98], and electric vehicles [99]. Studies on the latter include Bodner [100], Bhat [101], Baptista et al. [102], and Tung and Pinnoi [103] amongst many others. Most of these investigate a specific city as a case study.

There is a gap in the literature covering analysis of the optimum size of refuse collection vehicles.

1.2.2.2 Current Systems

Refuse Collection Vehicles, such as the one shown in Figure 1.4, present an interesting challenge for vehicle design due to the mass and size of the systems required to lift and compact the collected waste. Current vehicles in the UK mount this equipment on the back of the vehicle, behind the rear axle. This leads to high rear axle loads, and also to large tailswing, which is a risk for other road users and infrastructure (tailswing is defined in more detail in Chapters 4 to 6).

The Refuse Collection drive cycle varies according to the specific application. For example trade waste collection requires fewer stops than domestic waste, but a greater mass of waste at each collection. The general cycle involves driving from the refuse collection depot to the urban area, then a large number of accelerations and decelerations, as the vehicle moves between collections. Finally the vehicle returns to the depot. Some duty cycles involve more than one such trip.

1.2.3 Case Study C: Convenience Store Restocking

1.2.3.1 Motivation

Section 1.1.3.2 describes the negative impacts of Heavy Goods Vehicles in an urban environment. However, HGVs are a necessity in city centres to distribute goods to city centre stores. The type and dimensions of HGVs used vary between operators. Holguin-Veras et al. commented on the lack of consideration in the literature of the social impacts of different HGV sizes [62], and no research was found relating to methods for choosing the optimum vehicle for a given task.

1.2.3.2 Current Systems

Whereas edge-of-town supermarkets generally have lots of available space for large vehicles arriving from the trunk network to be unloaded, convenience stores and other stores in city centres have limited space for vehicle parking, and the roads leading to them are often narrow and congested. A description of stock management for convenience stores was presented by Smaros [104]. There are two approaches to restocking convenience stores. One option is to restock the store from an out-of-town distribution centre managed by the same retailer. This allows the retailer to retain control over the supply chain, and group deliveries in the most efficient way. The other approach is for suppliers to deliver to the convenience store directly. This can reduce vehicle kilometres travelled, since one supplier can deliver to several retailers, but it limits the retailer's control over timing of deliveries. Most retailers use a combination of the two approaches, depending on the products.

The second constraint for city centre deliveries is the stock space available at the store. This means that stock cannot be stored off the shelves, necessitating regular, small deliveries, timed to arrive when the shelves are empty. For fresh produce this can require several deliveries per day [104].

Retailers who elect to supply city centre stores directly from distribution centres are likely to find little benefit from increasing the size of vehicles, since the vehicles used can be expected to be sized appropriately to the stock requirements of the store. However, operators



(a) 7.5 t truck



(b) Urban semi-trailer

Fig. 1.5 Two vehicles commonly used for delivery to city centre stores (Photo Credit: Workhorse)

who supply a number of convenience stores could find fuel and emissions reductions by using larger vehicles to deliver to an increased number of stores before having to return to their distribution centre.

A wide range of vehicle configurations are used by different operators for delivery to city centres, ranging from 7.5 t trucks (Figure 1.5a) to urban semi-trailer units (Figure 1.5b), or occasionally full semi-trailers.

1.3 Thesis Outline

One of the largest obstacles to widespread use of larger, heavier vehicles is the public perception of increased safety risks associated with them. Chapter 2 describes technology intended to reduce the risk of incidents involving vulnerable road users, thus lowering the barriers to adoption caused by public perception. It presents a camera configuration and associated algorithm designed to detect and predict the motion of cyclist relative to the side of heavy goods vehicles. This technology is relevant to vehicles currently in common use, as well as higher capacity vehicles.

Chapter 3 investigates the number of deliveries performed during an 8 hour shift of 3.5 t home delivery vans run by two supermarkets. It determines the operational changes needed for drivers to be able to empty 4.25 t vans in the same time.

Chapters 4 to 6 approach finding the the upper bound on vehicle size from the point of view of manoeuvrability, since the vehicles will still be required to access the same delivery locations as the smaller vehicles they replace. The industry approach of specifying the steady-state turning circle radius was considered insufficient. A method is presented for

assessing potential capacity improvements without reducing access. Chapter 7 presents a comparison between this method and the Performance-Based Standards method proposed by Isted et al. which is based on a number of standardised manoeuvres [5]. The impact of rear axle steering as an intervention to improve manoeuvrability is also assessed across these four chapters.

A set of conclusions and some recommendations for further work are presented in Chapter 8.

1.4 Summary

Higher Capacity Vehicles have been demonstrated to provide reductions in emissions and fuel consumption. This is because fewer vehicles are required to move a given pool of freight, although each individual vehicle may generate slightly higher emissions. However, this assumes that the vehicles can be completely filled, which is not necessarily the case. This thesis will investigate methods to enable use of higher capacity vehicles in urban environments, for the purposes of improving fuel efficiency, thereby reducing emissions from the road freight transport sector and mitigating climate change. This will be approached from three perspectives: the safety of vulnerable road users, operational limits due to driver workload, and physical limits due to vehicle manoeuvrability.

Chapter 2

Cyclist Detection

A preliminary version of the work in this chapter was submitted as a thesis towards the degree of Master of Engineering at the University of Cambridge in 2015 [105], and published as a journal article in 2019 [106].

2.1 Introduction and Literature Review

2.1.1 Motivation

In Britain in 2013 there were more than 19,000 road accidents involving cyclists, including more than 100 fatalities [107]. This represents 11% of all road casualties, despite cyclists only accounting for 1% of total traffic. Heavy Goods Vehicles (HGVs) accounted for 23% of cyclist deaths, despite representing only 5% of total road traffic. There is a clear need to address safety issues of cyclist-HGV interactions on UK roads. Figure 2.1 shows a breakdown of cyclist-HGV accidents by configuration during 2006-2008. 43% of accidents occurred when the HGV turned left across the path of the cyclist. This can be attributed to two primary causes: the large blind-spot in this area next to the HGV, and the cut-in behaviour exhibited by HGVs by virtue of their long wheelbase.

The relevance of this particular scenario is further supported by a detailed analysis of 19 fatal cycling accidents involving left-turning HGVs in the UK by Jia [108]. Two of the accidents occurred at roundabouts and 17 at road junctions, mostly with traffic lights. In 15 of the 19 accidents the cyclist's intention was to travel straight ahead, while the vehicle turned left. Only four of the cyclists intended to turn (left) at the roundabout/junction. All of these accidents occurred at speeds of less than 15 km/h. Further, 15 of the HGVs were rigid vehicles (not articulated), and most of these were construction vehicles.

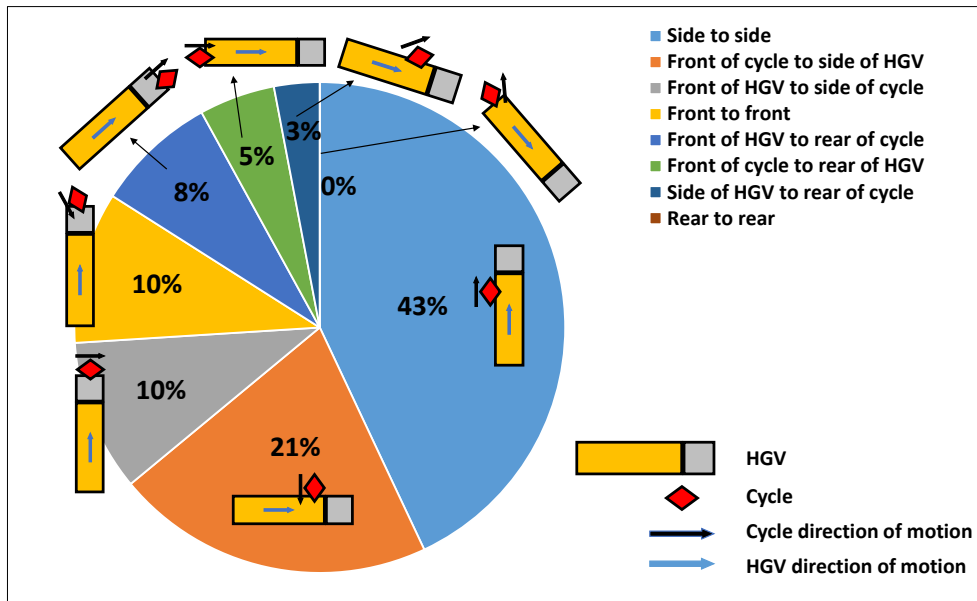


Fig. 2.1 Breakdown of cyclist-HGV collisions by configuration. Data from Robinson and Chislett [3], graphic adapted from Jia [4]

The objective of this work is to develop a system that can detect and accurately locate a cyclist in the left-side blind-spot of an HGV. The system should run in real-time, have a field-of-view which covers the entire length of the vehicle, and be suitably accurate to perform relative motion predictions. The focus is on HGVs in low-speed manoeuvres.

2.1.2 Overview of Existing Cyclist Detection Systems

A number of commercial systems exist to detect and warn drivers of potential low-speed collisions with vulnerable road users. These range from non-discriminating range sensors to high-end combinations of radar and cameras. Simple ultrasonic proximity systems are low cost, but do not discriminate between cyclists or pedestrians and inanimate objects such as roadside furniture. This can cause false alarms giving rise to a risk that drivers may become desensitized to alerts.

‘Cycle Safety Shield’, developed by Safety Shield Systems and Mobileye [109], is a camera-based system which warns the driver of the presence of cyclists. Different versions cover different fields-of-view around the vehicle, however only moving objects trigger an alert.

Cycle Eye[®] is a high-end system that uses a combination of image processing and radar to detect and locate cyclists [110]. The use of radar improves the accuracy in poor light

conditions but adds cost. The manufacturer claims a 98.5% success rate in detecting cyclists over three days' testing in London, including during rush hour.

A system based entirely on an array of ultrasonic sensors was developed by Jia and Cebon in the Cambridge Vehicle Dynamics Consortium (CVDC) [111]. The system is intended to predict future cyclist motion and actuate the vehicle brakes to execute an emergency stop in the event of a predicted collision. This strategy was shown to be effective at preventing reconstructed accidents in simulation and was successfully proven in low-speed field trials on a prototype system [111]. A deficiency of this system is its inability to distinguish between multiple cyclists, items of road furniture, and parked cars.

2.1.3 Vision Technologies for Vehicle and Cyclist Detection

The use of wheel detection techniques has been popular in vehicle and cyclist detection applications, owing to the ubiquity and consistency of the features. Ardeshiri et al. [112] investigated the use of ellipse-fitting methods to detect bicycle wheels, using reflective wheel-rims and dark backgrounds to limit the number of pixels to process. The system used the Hough transform [113, 114] to detect ellipses (and hence wheels), though it was noted that this approach is very computationally expensive unless steps are taken to limit the number of input pixels processed. Variations on the Hough transform, such as the Randomized Hough Transform [115, 116], or the approach described by Xie and Ji [117], can reduce computation time, but are error-prone in noisy or partially occluded conditions.

The Hough transform was also used by Lai and Tsai [118] to detect the wheels of passing cars, using the orientation and centre of the wheel to calculate relative heading and position of the two vehicles.

More general feature descriptors include Haar Features [119]. These are commonly used for face detection, using Adaboost to train classifiers [120, 121] and a cascade architecture. The cascade allows background regions to be quickly ignored by the simplest classifiers, so that more computation time can be spent by the higher-level classifiers on promising 'object-like' regions of the image. An implementation of the Haar Cascade classifier is available as part of the OpenCV computer vision library [122].

This approach was used effectively by Chavez-Aragon et al. [123] to detect parts of nearby vehicles. Real-time processing was achieved by using geometric arguments to limit the region of image searched to a 'Feasible Search Zone', drastically reducing computation time.

More complex methods for image feature detection and classification exist, such as part-based models [124], often used for pedestrian detection. Although part-based models can be very accurate, they are generally computationally demanding.



Fig. 2.2 Camera and ultrasonic setup

In vehicle-based pedestrian detection work by Bertozzi et al. [125], an innovative camera calibration method was devised, in order to create an efficient mapping of the ground plane from image to world coordinates. The method avoided the need for full camera calibration and image distortion correction. Initial images of a calibration grid on the ground captured by the system allowed the generation of a direct pixel-to-ground coordinate mapping. This enabled efficient real-time processing.

2.2 System Outline

The aim of this work was to investigate whether a vision-based system could be used to measure cyclists' motion relative to an HGV with one or two cameras instead of the 10 or 12 ultrasonic sensors needed by the CVDC ultrasonic system. The primary advantages of a vision-based system compared to an ultrasonic system are discrimination between different types of objects, and identification of multiple cyclists. This could reduce false alarms due to detection of street furniture or walls. Although complex vision-based systems for object detection exist, it was proposed that simple shape-based detection might be sufficiently accurate.

The effectiveness of the proposed vision system is dependent on the type of imaging system used (for example the choice of lens) and the configuration in which it is installed on the vehicle (location, orientation and number of cameras). In establishing a suitable combination of these factors, the following criteria were considered:

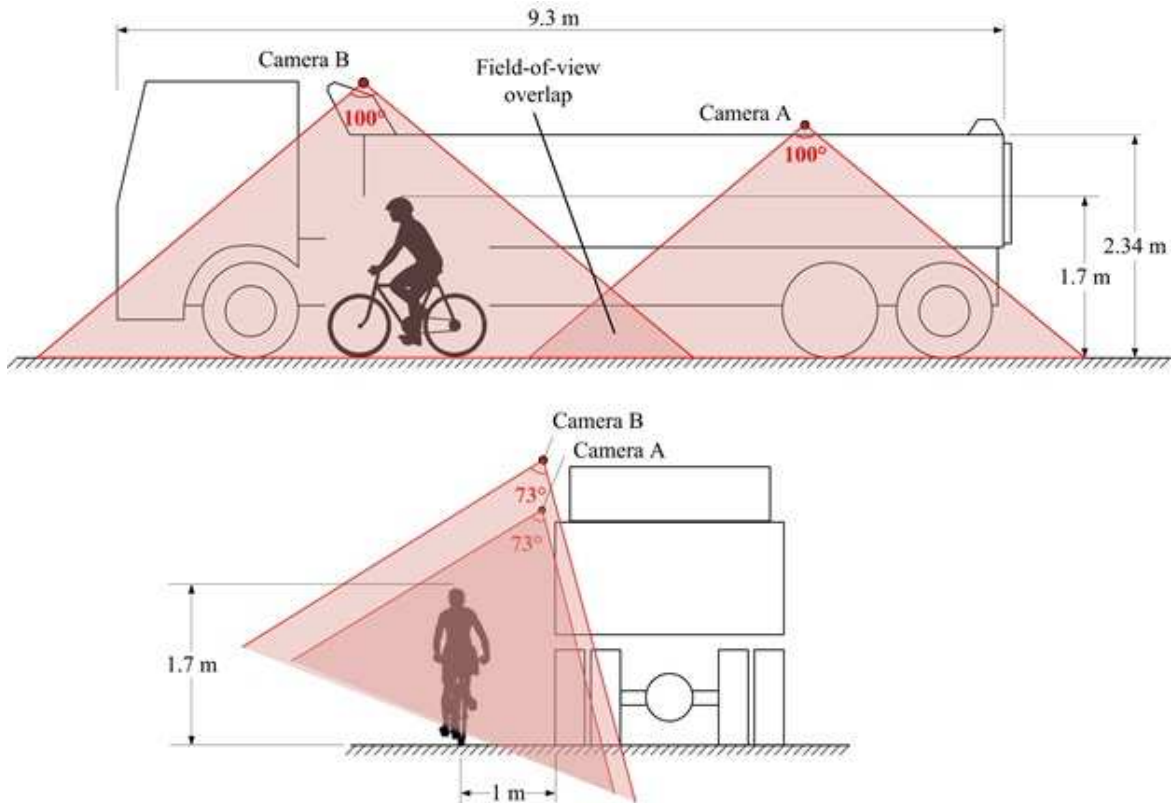


Fig. 2.3 Camera configuration and field-of-view, shown approximately to scale with a cyclist at 1 m from the HGV

- (i) The ground area covering the full length of the HGV should be visible, using the minimum number of cameras possible.
- (ii) The field-of-view should cover the region of interest but should minimise the inclusion of background scenery and other moving objects.
- (iii) Potential classification features such as wheels should be visible.
- (iv) Occlusion problems should be minimised in instances where more than one cyclist is present.

The system was mounted on the same rigid construction vehicle used in tests by Jia [111] (see Figure 2.2). Sample images were obtained from various points on a vehicle to determine the best location for the camera. The chosen configuration is illustrated in Figure 2.3. The vehicle is shown to scale and a representative silhouette of a cyclist is included for reference.

The high mounting point of the cameras was a key decision in the design of the system. An important benefit of the top-down view is that lateral position errors arising from image

processing are minimised, because a single pixel uncertainty in the measurement in image coordinates corresponds to a much smaller lateral distance if the cameras are looking almost straight down compared to if the cameras are mounted at wheel height and looking ‘across’ the ground plane. This vantage point also addresses the fourth criterion above, by minimising potential occlusion. The visibility of potential classification features (as in the third criterion) may be slightly reduced, compared to lower mounting points, but this was shown not to be prohibitive.

To address the first and second criteria, two ultra-compact Point Grey Flea3[®]. USB 3.0 cameras fitted with Fujinon 2.8 to 8 mm wide-angle lenses with a maximum field-of-view of 100° were selected [126, 127]. The cameras were located high on the side of the vehicle and spaced longitudinally so as to achieve maximum coverage along the full length of the vehicle. There was a region of overlap between the two views which was important for the transition of tracking information between the two cameras. The front camera (camera “B”) was mounted slightly higher than the rear camera (camera “A”) due to the available height at that point on the tipper bucket. A small outwards tilt to the cameras extended the lateral viewing distance.

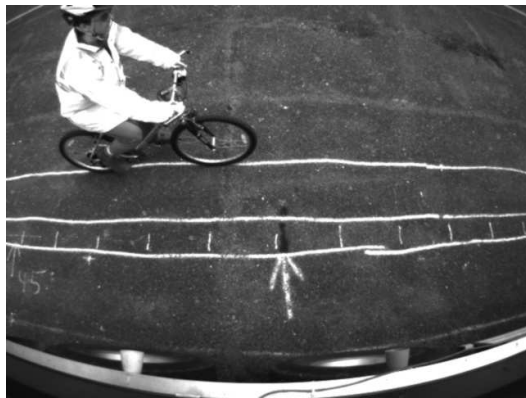
2.3 Test Program

Tests were carried out on an open area of tarmac at Bourn Airfield, near Cambridge, UK. Parallel passing manoeuvres between the test vehicle and a cyclist were carried out at various passing distances.

A straight line was marked on the road as a guide for the driver to follow, such that the line roughly approximated the left side of the HGV. Parallel to this, lines were marked at distances of 0.75 m, 1 m and 1.5 m as guidelines for the cyclist. Transverse tick marks at 0.5 m spacing were included in order to estimate cyclist and vehicle speed during post-processing. The lines are visible in Figure 2.4.

Three runs of each test were conducted to allow for variations. A total of 18 sets of data were recorded, six each at 0.75 m, 1 m and 1.5 m spacing (consisting of three repetitions at HGV speeds of 5 km/h and 8 km/h).

A schematic of the instrumentation layout is shown in Figure 2.5. The cameras were connected via USB 3.0 to a dedicated computer located inside the driver’s cab. Synchronous greyscale images were captured from both cameras at 20 frames per second (fps) with a resolution of 640×480. A slave computer running MATLAB[®]’s xPC Target toolbox was used for data-logging, and a laptop computer was used as the primary user interface. CANbus was used for communication between the camera computer and xPC slave unit.



(a) Camera A, cyclist at 1.5 m



(b) Camera B, cyclist at 1 m



(c) Camera A, cyclist at 0.75 m



(d) Camera A, cyclist at 1.5 m, sunny

Fig. 2.4 Sample images at various lateral separations and lighting intensities

2.4 Image Processing

2.4.1 Strategy

The idea behind the image processing system is to locate the points of contact between bicycle wheels and the ground, and to calibrate the ground plane so that the contact points can be converted into the (x, y) coordinates of the wheel relative to the HGV.

Although the selected camera system and its particular configuration has a number of benefits, it also presents some challenges. Firstly, the elevated camera positioning results in the cyclist's shape varying with lateral distance. For example, circular wheels are viewed as thin ellipses from above at close range, and the proportion of head and torso in the cyclist's silhouette grows with proximity to the vehicle. Similarly, the cyclist's shape is variable from the left to the right of the camera field-of-view, due to camera position and lens distortion. These effects are highlighted in Figure 2.4a to 2.4c.

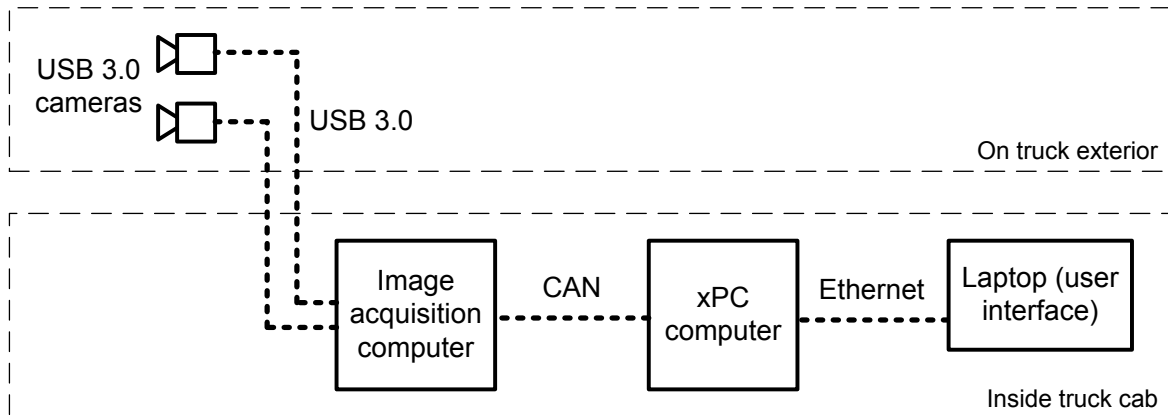


Fig. 2.5 Instrumentation schematic for image acquisition

Secondly, as with any vision-based system, variations in lighting can be problematic. Figure 2.4d shows the effects of strong light conditions on an image. The shadow covering the rear wheel makes it more difficult to distinguish from the background.

The overall image processing strategy of the system can be summarised into five parts:

- (i) Calibration: generate coordinate map.
- (ii) Wheel detection: identify the presence of a cyclist in the image.
- (iii) Contact point location: locate the positions of the contact points between wheels and road.
- (iv) Coordinate conversion: map image coordinates to world coordinates.
- (v) Cyclist tracking: mitigate spurious or occluded detections and predict trajectories using a bicycle model and Kalman Filter.

The first stage, calibration, is performed only once, on installation of the cameras. The final four stages are carried out for every image frame. The five stages are discussed separately in the following sections.

2.4.2 Calibration

A method was required for converting the detected cyclist's position into a world coordinate system. One approach to this would be to rectify the distorted images, and then use known camera parameters to perform a full 3D calibration. However, this would add a computationally expensive processing stage. Ground mapping was proposed as a simpler alternative, which does not require an undistorted image.

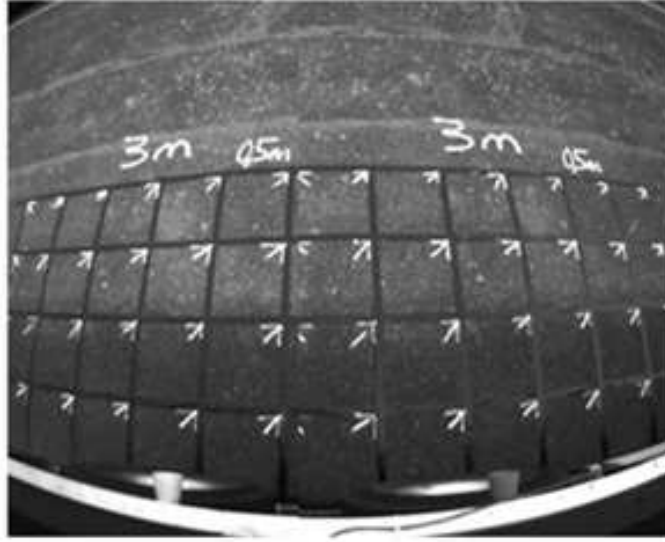


Fig. 2.6 Calibration grid processed to cover the entire image

The aim of the ground mapping process was to convert the coordinates of the points of contact between the bicycle wheels and the ground from the image coordinate system to a global coordinate system (relative to the HGV). The point on the ground directly below the front left corner of the vehicle was chosen for the origin of the HGV coordinate system. Defining bicycles in the ground plane by their contact points simplified the calibration of the camera to a planar mapping.

The cameras were calibrated by positioning the vehicle next to a calibration grid (Figure 2.6).

The image coordinates (u, v) of the grid intersection points were extracted manually; the world coordinates of each grid intersection point (x, y) were already known. The camera lenses introduced barrel distortion which is approximately quadratic [128]. Therefore, a quadratic shape-function was used to approximate the transformed shape of the grid in both dimensions. Shape-function-based interpolation was used to generate a map from image to world coordinates, as described by Silva et al. [129]. The mapping is described as follows:

$$u(x, y) = c_1 + c_2x + c_3y + c_4x^2 + c_5xy \dots \\ + c_6y^2 + c_7x^2y + c_8xy^2 \quad (2.1)$$

$$v(x, y) = d_1 + d_2x + d_3y + d_4x^2 + d_5xy \dots \\ + d_6y^2 + d_7x^2y + d_8xy^2 \quad (2.2)$$

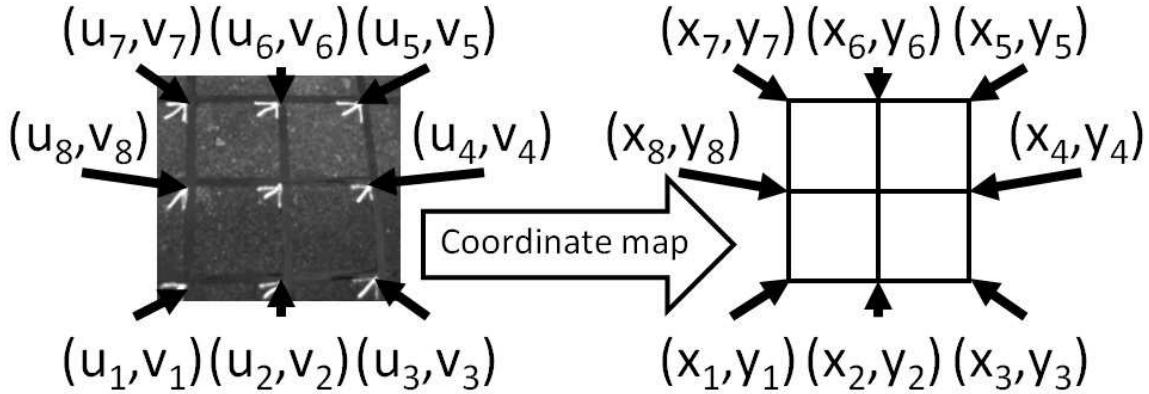


Fig. 2.7 General illustration of coordinate mapping

where c_i and d_i are constant coefficients. For an example intersection point (x_1, y_1) the mapping to (u_1, v_1) would be as follows:

$$u_1(x_1, y_1) = c_1 + c_2x_1 + c_3y_1 + c_4x_1^2 \dots \quad (2.3)$$

$$+ c_5x_1y_1 + c_6y_1^2 + c_7x_1^2y_1 + c_8x_1y_1^2$$

$$v_1(x_1, y_1) = d_1 + d_2x_1 + d_3y_1 + d_4x_1^2 \dots \quad (2.4)$$

$$+ d_5x_1y_1 + d_6y_1^2 + d_7x_1^2y_1 + d_8x_1y_1^2$$

A one-meter square as shown in Figure 2.7 has intersection coordinates (x_1, y_1) to (x_8, y_8) , where $(x_1, y_1) = (0, 0)$, $(x_2, y_2) = (0.5, 0)$, $(x_3, y_3) = (1, 0)$, $(x_4, y_4) = (1, 0.5)$, $(x_5, y_5) = (1, 1)$, $(x_6, y_6) = (0.5, 1)$, $(x_7, y_7) = (0, 1)$ and $(x_8, y_8) = (0, 0.5)$. These values of (x_i, y_i) can be substituted into Equations 2.1 and 2.2 to yield values of u_i and v_i for $i = 1$ to 8. For example:

$$u_2(0.5, 0) = c_1 + 0.5c_2 + 0.25c_4 \quad (2.5)$$

$$v_2(0.5, 0) = d_1 + 0.5d_2 + 0.25d_4 \quad (2.6)$$

These expressions for all eight intersection points can be written in matrix form:

$$\mathbf{u} = \mathbf{A}\mathbf{c} \quad (2.7)$$

where

$$\mathbf{u} = [u_1 \ u_2 \ u_3 \ u_4 \ u_5 \ u_6 \ u_7 \ u_8]^T \quad (2.8)$$

$$A = \begin{bmatrix} 1 & 0 & 0 & 0 & 0 & 0 & 0 & 0 \\ 1 & 0.5 & 0 & 0.25 & 0 & 0 & 0 & 0 \\ 1 & 1 & 0 & 1 & 0 & 0 & 0 & 0 \\ 1 & 1 & 0.5 & 1 & 0.5 & 0.25 & 0.5 & 0.25 \\ 1 & 1 & 1 & 1 & 1 & 1 & 1 & 1 \\ 1 & 0.5 & 1 & 0.5 & 0.5 & 1 & 0.25 & 0.5 \\ 1 & 0 & 1 & 0 & 0 & 1 & 0 & 0 \\ 1 & 0 & 0.5 & 0 & 0 & 0.25 & 0 & 0 \end{bmatrix} \quad (2.9)$$

$$\mathbf{c} = [c_1 \ c_2 \ c_3 \ c_4 \ c_5 \ c_6 \ c_7 \ c_8]^T \quad (2.10)$$

Similarly

$$\mathbf{v} = A\mathbf{d} \quad (2.11)$$

Given a set of known image coordinates (\mathbf{u}, \mathbf{v}) , \mathbf{c} can be found by

$$\mathbf{c} = A^{-1}\mathbf{u} \quad (2.12)$$

$$\mathbf{d} = A^{-1}\mathbf{v} \quad (2.13)$$

This process of finding \mathbf{c} and \mathbf{d} from images of the ground grid constitutes the only calibration needed for the cameras. Given a world coordinate point (x, y) , the coordinates of the transformed point in the image (u, v) can be found by substituting $x = x_1, y = y_1, c_1$ to $c_8 = \mathbf{c}$ and d_1 to $d_8 = \mathbf{d}$ into Equations 2.3 and 2.4.

However, given image coordinates (u, v) , the corresponding point (x, y) is not directly obtainable. To calculate (x, y) an initial guess of the world coordinates is made and mapped to image coordinates. This is compared to the target point and the guess adjusted according to the error. This process is repeated until the transformed coordinates converge to the target point. A separate ground plane calibration map was required for each camera in this case, owing to their different heights and small variations in pitch and internal parameters.

To speed up the real-time element of the program the conversion was calculated in advance for every pixel, and stored in a lookup table. The calibration process should only be required once per vehicle unless the cameras are moved.

From the 40 grid intersection points shown in Figure 2.6, only eight are required for each 2D quadratic approximation. To maximise the accuracy, the calibration image was split into ten patches, in two rows of five, with overlap between the two rows to ensure continuity in the more critical lateral direction. Each patch was treated separately. This introduced small discontinuities between the patches which could be reduced by using a finer calibration

grid, but this was not considered necessary. All measurements of position and velocity were transformed into *relative* measurements between cyclist and vehicle.

The resolution of the images limited the precision of the manual extraction of grid coordinates to approximately ± 3 pixels which can be shown to correspond to an error in world coordinates of up to 4 cm. This calibration assumes the HGV was perfectly aligned with the grid while the calibration images were taken, which was not necessarily the case. This could introduce an additional offset to the final position outputs. In total, errors due to the coordinate conversion of up to 7 cm are likely, although the uncertainty will vary across the field-of-view with higher uncertainty corresponding to regions of highest distortion on the images.

2.4.3 Wheel Detection

Wheel detection was used to detect the presence of a cyclist in the images. Both ellipse-based and classifier-based methods for wheel detection were explored. Wheels were chosen as recognisable features since they are common to all bicycles with only minor variations. Ellipse-fitting methods considered included Edge Following [130, 131], Genetic Algorithm-based approaches [132], and the Hough transform [117]. The approach to the Hough Transform described by Xie and Ji [117] was implemented in Python. The calculations required for each frame took almost 0.1 s, so a maximum frame rate of 10 fps was achieved. However, the algorithm is not robust to occlusion of one side of the wheel, which was a common occurrence.

The classifier-based method of Viola and Jones [119] was implemented in Python, using the OpenCV computer vision library [122]. The output of the classifier is a bounding box surrounding the detected wheel feature. This method was found to be most suitable, and yielded an acceptable frame rate of more than 20 fps.

Training data for detection and classification work is available for cyclists, including the SUN [133] and KITTI [134] databases. However, the cyclist images in these datasets are largely from a ground level reference and are not suitable for the highly oblique view which results from our raised camera setup. As a consequence, the data from two of the three runs of each test were used as training data for the third run. This is of course not suitable for a generalised system which should be robust to varied cyclists and backgrounds. However, it was deemed suitable at this proof-of-concept stage. More generalised training data will be obtained and used to retrain the classifiers in future work.

Due to the relatively small number of training images available (approximately 900 images per camera for each test run), separate classifiers were trained for each lateral distance

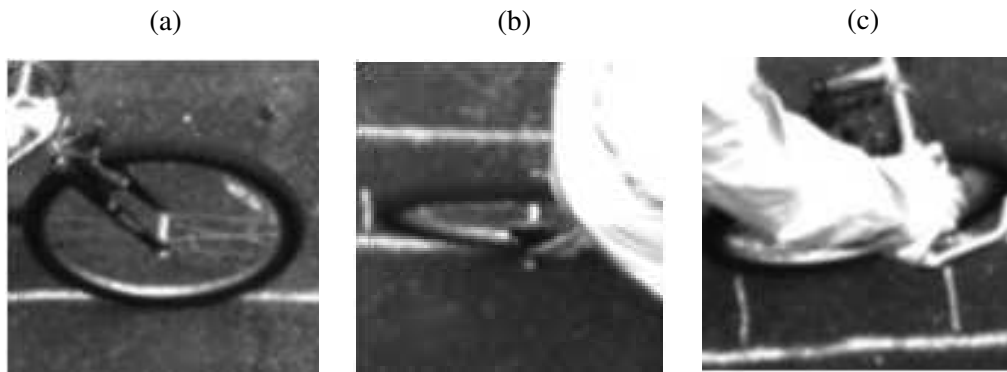


Fig. 2.8 Examples of positive training images

from the HGV. Positive image regions were marked manually and images without wheels visible were used as negative training data.

Figure 2.8 shows examples of positive training images. Between 150 and 300 positive images were used to train each classifier, depending on how many frames the wheels were visible for. The positive samples were scaled to 24×24 pixels. Only 75 negative images were used due to lack of variation between the images.

This method was fast enough for real-time implementation. However, the location accuracy was not sufficiently precise since the detection bounding box could move relative to the feature it enclosed. Due to the relatively small amount of training data available, the classifiers were not very robust. In order to guarantee detection of the wheels, the detection threshold was kept low, which led to a high rate of false positive detections. Figure 2.9 shows example outputs of the detection step.

It should be noted that this combination of testing and training images is insufficient for robust implementation. First, the number of negative training images should be significantly larger than the number of positive training samples, and secondly, both testing and training were carried out on the same style of bicycle. This is due to the lack of availability of training data for the oblique camera angles used in this work. Some ad-hoc testing has been carried out on classifiers trained with multiple different cyclists and bicycles and found to work well [135].

The current work is intended as a proof-of-concept of the detection-location-tracking-prediction system as a whole, thus it was considered that a partially-trained classifier would give sufficiently accurate results. Future work should include training the classifier on a much larger database of images collected from the elevated camera angle.

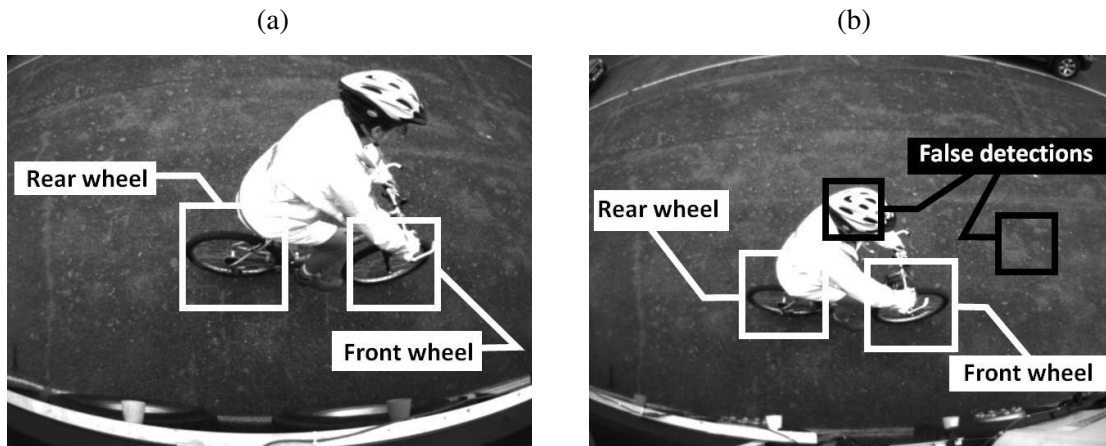


Fig. 2.9 Examples of (a) correctly and (b) wrongly detected features

2.4.4 Contact Point Location

Once wheels have been detected, the contact point with the road must be determined. Several methods were considered for finding the ground-wheel contact point within the detected bounding boxes. The methods considered and their performance are summarised as follows.

- (i) The Hough transform [117] was used to fit ellipses inside the feature bounding box.
- (ii) Fitzgibbon's algorithm [136] was used to fit ellipses, combined with RANSAC [137] to remove outliers.
- (iii) A simplified version of the Starburst algorithm [138] was used to limit the number of pixels in the box.
- (iv) The ground point was assumed to be a fixed distance down the centreline of the bounding box, where the distance varied according to the passing distance between HGV and cyclist in order to prevent loss of accuracy at close range.
- (v) The ground contact point was taken as the lowest point on an edge in the cropped image (Figure 2.10a). A grey-scale threshold of 50 was first applied to remove bright patches, such as road markings (Figure 2.10b), then the images were normalised to maximise the contrast between the tyres and the road (Figure 2.10c), and finally Canny edge detected [139] with a high threshold to ensure that noise from the road surface was removed (Figure 2.10d). The cropped image was then searched in columns to find the lowest edge pixel (Figure 2.10e). The threshold and normalisation steps largely remove susceptibility to lighting conditions, though more work is needed to ensure complete robustness.

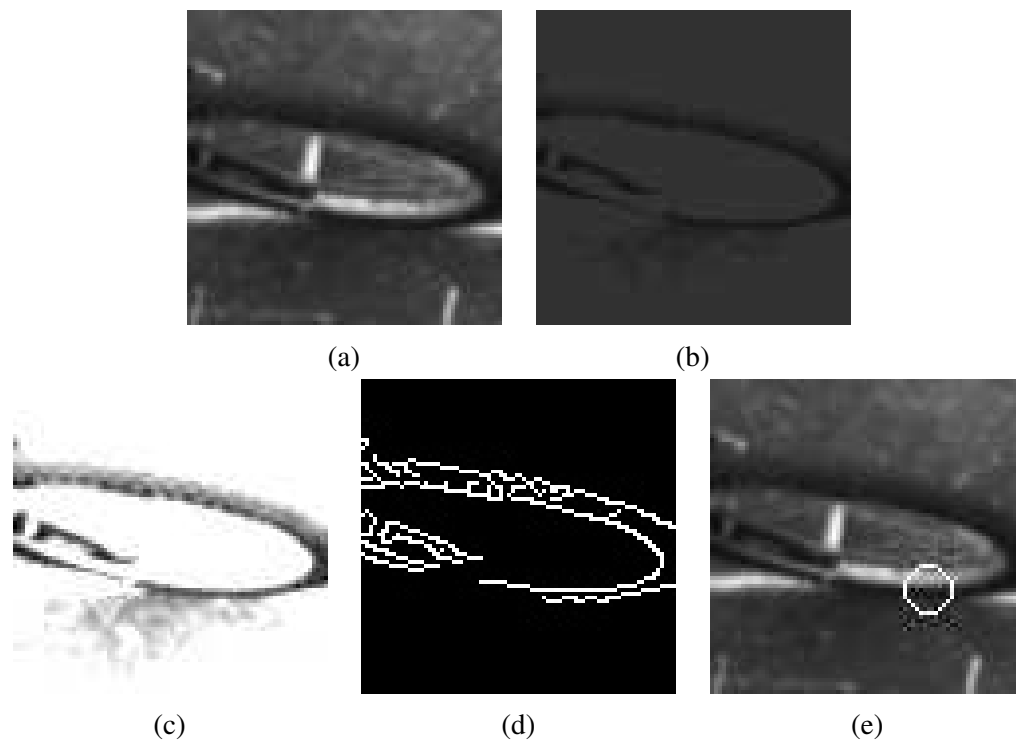


Fig. 2.10 Stages in the extraction of the ground contact point. (a) Cropping (b) Thresholding (c) Normalisation (d) Edge Detection (e) Selection of the lowest pixel

For methods (i) to (iii), the cropped images were first pre-processed with a Gaussian blur and Canny edge detection [139]. The Hough transform (i) was computationally expensive and unreliable due to noise and occlusion in the images. Combining Fitzgibbon's algorithm with RANSAC (ii) was a more reliable method of ellipse fitting, but still took too long to run. The simplified Starburst algorithm (iii) was inaccurate due to the noise and occlusion in the images. Using the full Starburst algorithm might be more accurate, but would again be computationally expensive. Assuming a fixed position within the bounding box (iv) was accurate when the wheel was near to the centre of the field-of-view but introduced errors of up to 3 cm at the edges of the image due to the camera distortion. This approach has the benefit that the contact point can be estimated even when it is occluded by the cyclist. Edge detection and minimum point selection (v) was fast and accurate but was less accurate if the contact point was occluded. Therefore this was the method chosen except for close range tests where the fixed location method was used instead. It is possible for the contact point to be occluded in the tests at longer range. However method (v) simply returns the location of the edge point which is closest to the truck, which is likely to be whatever is obscuring the wheel. This method is therefore still fairly accurate, and so can be used, especially at longer test distances where accuracy is less critical because the cyclist is further from danger.

2.4.5 Coordinate Conversion

Once the image coordinates of the wheel-ground contact points were extracted from the images, they were passed through the coordinate map, and then translated so as to be relative to the origin under the front left corner of the HGV.

2.4.6 Cyclist Tracking

In order to track the cyclist's motion using a Kalman Filter, the cyclist was modelled by converting the coordinates of the contact points of the front and rear wheels to a yaw angle, wheelbase and position of the centre-of-mass of the cyclist. Due to the relatively high rate of false positive detections of the wheels, the positions of the front and rear wheels were used to validate each other: a bicycle detection would not be confirmed unless both wheels were detected in the correct relative positions. This check was performed in world coordinates and so the acceptable relative position was governed by an approximate bicycle wheelbase of 1.2 m, and a maximum expected yaw angle of $\pm 5^\circ$ relative to the x -axis.

Any detection with a plausible wheelbase was compared to detections from the previous frame, and a maximum velocity limit of 25 cm per frame in the direction of travel and 8 cm per frame laterally was imposed at 20 fps. These values were determined from an assessment of feasible cyclist motions. The bicycle was then tracked and its future position predicted, so that in future frames only one wheel needed to be detected, and checked against the expected position.

A simple Kalman Filter [140] was added to reduce measurement noise. Constant accelerations both parallel and perpendicular to the direction of motion were assumed. This also had the effect of providing motion estimates even in ranges where detections were missed. The positions of the front and rear wheels were averaged to output a list of positions of the approximate centre of the cyclist (mid-wheelbase) in each frame.

The prediction equations of the Kalman Filter were:

$$\hat{\mathbf{X}} = \mathbf{X}_{k-1} + \dot{\mathbf{X}}_{k-1}\Delta t \quad (2.14)$$

$$\mathbf{p} = \mathbf{P} + \mathbf{Q} \quad (2.15)$$

where \mathbf{X} is the state vector (lateral and longitudinal displacement and velocity of the center of the cyclist's wheelbase), $\hat{\mathbf{X}}$ is the prior estimate of the state vector, \mathbf{P} is the error in the estimate, \mathbf{p} the prior estimate of the error, and \mathbf{Q} is the process covariance.

The update equations were:

$$\mathbf{K} = \mathbf{p}(\mathbf{p} + \mathbf{R})^{-1} \quad (2.16)$$

$$\mathbf{X}_k = \hat{\mathbf{X}} + \mathbf{K}(\mathbf{z} - \hat{\mathbf{X}}) \quad (2.17)$$

$$\mathbf{P} = (1 - \mathbf{K})\mathbf{p} \quad (2.18)$$

where \mathbf{z} is the observed states, \mathbf{R} is the model covariance, and \mathbf{K} is the Kalman gain.

The prediction equations produce estimates of the system states and their uncertainties. The update equations take these estimates and the observations from the image processing and calculate a weighted sum, giving a higher weighting to the more certain predictions. The model covariance was set to 1 for all states, and the process covariance set to 1.2 for the position states and 2 for the velocity states. These values were approximated from inspection of the covariance of the unfiltered states and then adjusted to give suitable results.

A Python implementation of the whole algorithm ran at an average of 7.7 fps on a 3.6 GHz laptop. Analysis by Jia [111] showed that for effective intervention in the HGV motion, the system should predict 1.5 seconds ahead. At typical closing speeds, this requires a minimum of 7.5 fps. The algorithm frame rate was therefore deemed suitable.

2.4.7 Error Analysis

As no ‘ground truth’ position of the cyclist was available, the position of the ground contact point was manually extracted from each of the images in order to remove the effect of imperfect following of the nominal position lines by both cyclist and HGV. However, there are errors associated with this process, both in the mapping itself and due to imperfect alignment between the vehicle and the calibration grid during the capture of calibration images.

This manual measurement was designated M , the camera system’s measurement C and the ‘true’ position of the cyclist T . The maximum uncertainty between the manual measurement and the true position, $\varepsilon_{MT,max}$ was approximated as the sum of two components—a 3 cm uncertainty in the drawing of the calibration grid, and a three pixel uncertainty in the accuracy of manually selecting points from images. This three pixel uncertainty was converted to world coordinates at different lateral distances from the vehicle, representing increasing distances at higher separation as anticipated from the angle of the cameras, equalling 2 cm at 0.75 m, 3 cm at 1 m and 4 cm at 1.5 m. Combined with the 3 cm uncertainty from drawing the grid, this gave $\varepsilon_{MT,max} = 5$ cm, 6 cm and 7 cm at 0.75 m, 1 m and 1.5 m respectively.

The standard deviation of the uncertainty, σ_{MT} was estimated from the maximum error between the manually-extracted position and true position. Assuming the errors followed a Gaussian distribution, 99% of the data lie within three standard deviations of the mean, leading to $\sigma_{MT} \approx \varepsilon_{MT,max}/3$ giving $\sigma_{MT} = 1.67$ cm at 0.75 m, 2.00 cm at 1 m, and 2.33 cm at 1.5 m. The mean uncertainty was assumed to be zero. Although a slight bias possibly occurred

due to the nature of the data extraction task, this was likely to be small and impossible to quantify.

The error between the camera measurement and the manual measurement (ϵ_{CM}) had a different mean and standard deviation for each test run. The total error between the camera measurement and true position ϵ_{CT} was calculated as the sum of ϵ_{CM} and ϵ_{MT} . The mean (μ) and standard deviation (σ) were found by assuming that the errors ϵ_{CM} and ϵ_{MT} were uncorrelated, according to:

$$\epsilon_{CT} = \epsilon_{CM} + \epsilon_{MT} \quad (2.19)$$

$$\mu_{CT} = \mu_{CM} + \mu_{MT} \quad (2.20)$$

$$\sigma_{CT}^2 = \sigma_{CM}^2 + \sigma_{MT}^2 \quad (2.21)$$

The standard deviations were also normalised as a percentage of the nominal passing distance.

The camera system can continue to make estimates of the cyclist's position using the Kalman Filter if a previously-detected wheel becomes occluded, so there is no loss of data at the edges of the fields-of-view of the cameras. This contrasts with the manually-extracted position data points, which cannot be extrapolated in the case of an occluded cyclist and therefore do not cover the same longitudinal range as the camera-measured position. There are data points missing in the region around $X = 5$ m and at the highest and lowest values of X . This corresponds to points close to the edge of either camera's field-of-view, where one wheel is occluded, so manual position extraction is impossible. The camera system can detect a wheel even if the contact point is fully occluded, if the view of the cyclist is sufficiently similar to training images. Additionally, the camera system can predict from previous positions, or from detection of a single wheel. This loss of data points is more significant at $d = 0.75$ m where the wheels are occluded further from the edges of the camera field-of-view.

As an initial validation of the wheel detection algorithm, the relative longitudinal velocity between cyclist and HGV was compared with manual measurements taken from the lateral tick marks on the ground. The manual extraction was approximate due to discretisation errors: there may not be an image at the exact moment a wheel passes a tick mark. The manual speed measurement was smoothed by taking a moving average.

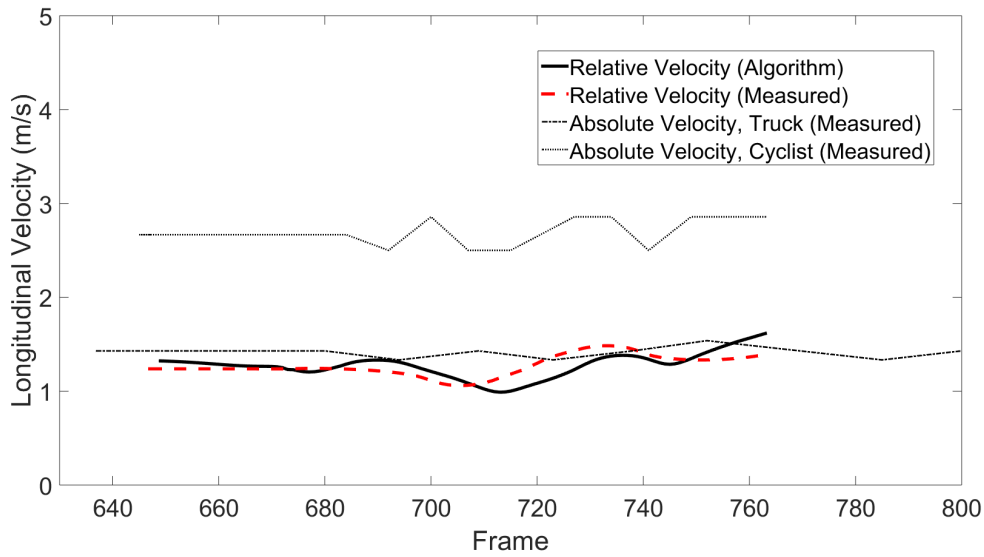


Fig. 2.11 Comparison of calculated and measured longitudinal velocities

2.5 Results

Figure 2.11 shows the relative and absolute longitudinal velocities of the HGV and cyclist, for the cyclist nominally at a lateral distance of 1 m from the side of the HGV ($d = 1$ m). The results indicate reasonable agreement between the algorithm and the measured speeds.

Figure 2.12 shows the trace of the camera-estimated position for three of the test runs at different lateral distances. The nominal position is the location of the marked lines on the road at $d = 0.75$ m, 1 m and 1.5 m from the HGV, shown in dashed lines on the figure. These results show reasonable performance in the estimation of the cyclist's position relative to the nominal position, although comparison to the nominal position is of limited value as the cyclist and the HGV may not have followed their respective lines precisely. However, the estimated position is within a 10 cm window of the nominal line in most cases. Errors are higher at smaller values of d because the wheels were more often occluded by the cyclist's body. This reduced the number of observations, thus reducing the robustness of the Kalman Filter. The occlusion of the wheels at the edges of the fields-of-view of the separate cameras also contributed to the large discontinuity in position at the join between the left and right cameras at $X \approx -4.5$ m for $d = 0.75$ m, as the position estimate there was based on prediction rather than observations.

In total, 18 sets of testing images were recorded—six each at 0.75 m, 1 m and 1.5 m. These included a range of passing speeds between the HGV and the cyclist, and a range of lighting conditions, from overcast to bright sunlight, with combinations of HGV and cyclist

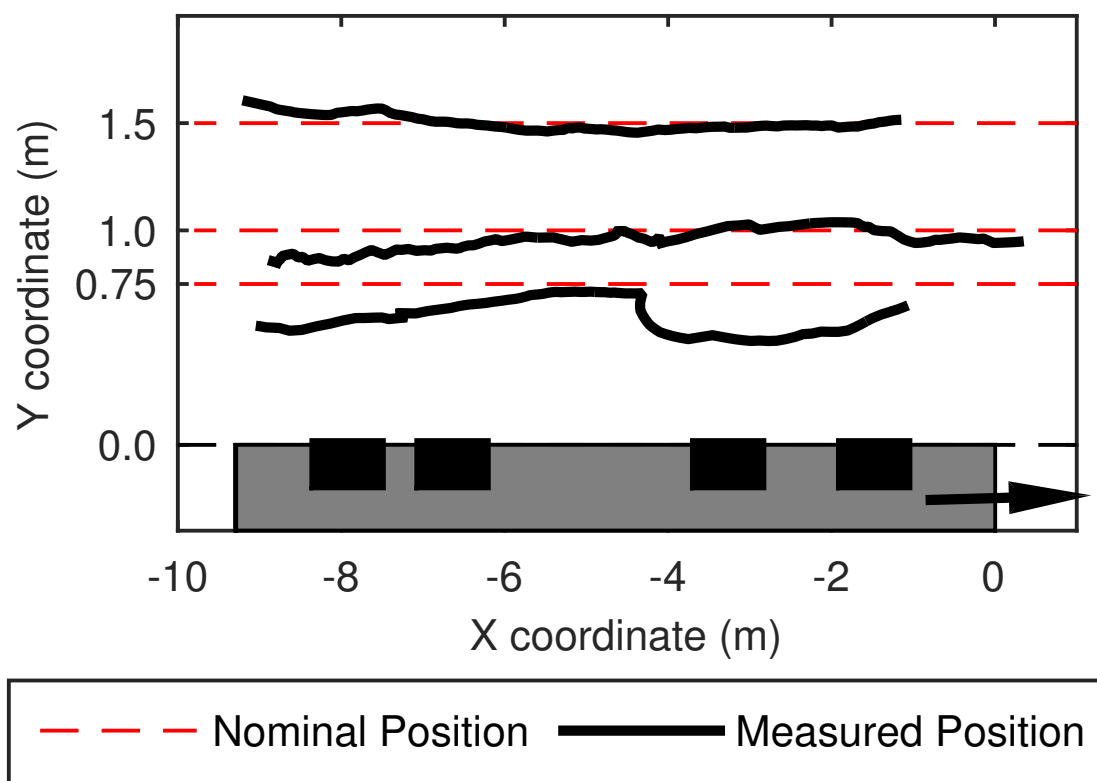


Fig. 2.12 Output of camera-based detection system over three different lateral distances from the side of the HGV

shadows in different orientations. The lighting conditions had no noticeable effect on the accuracy of the detection. Table 2.1 summarises the average results for each of the three test distances.

Figure 2.13 shows a comparison of the camera-measured position and the manually-extracted position for one test run at each of the test distances.

At 1.5 m distance (Figure 2.13a), the camera detection matches closely the manually extracted positions, with a maximum error of 4.1 cm at $X = -9.1$ m. This is close to the width of the bicycle tyre and also to the uncertainty introduced by the calibration system at that distance which had a standard deviation of ± 1.67 cm.

Across all six test runs at a nominal spacing of 1.5 m, the camera system performed very well. The errors between the camera system and the manually extracted coordinates were very small, with a standard deviation across all six runs of only 3.27 cm—only slightly greater than the tyre width. The error between the camera measurements and manual measurements

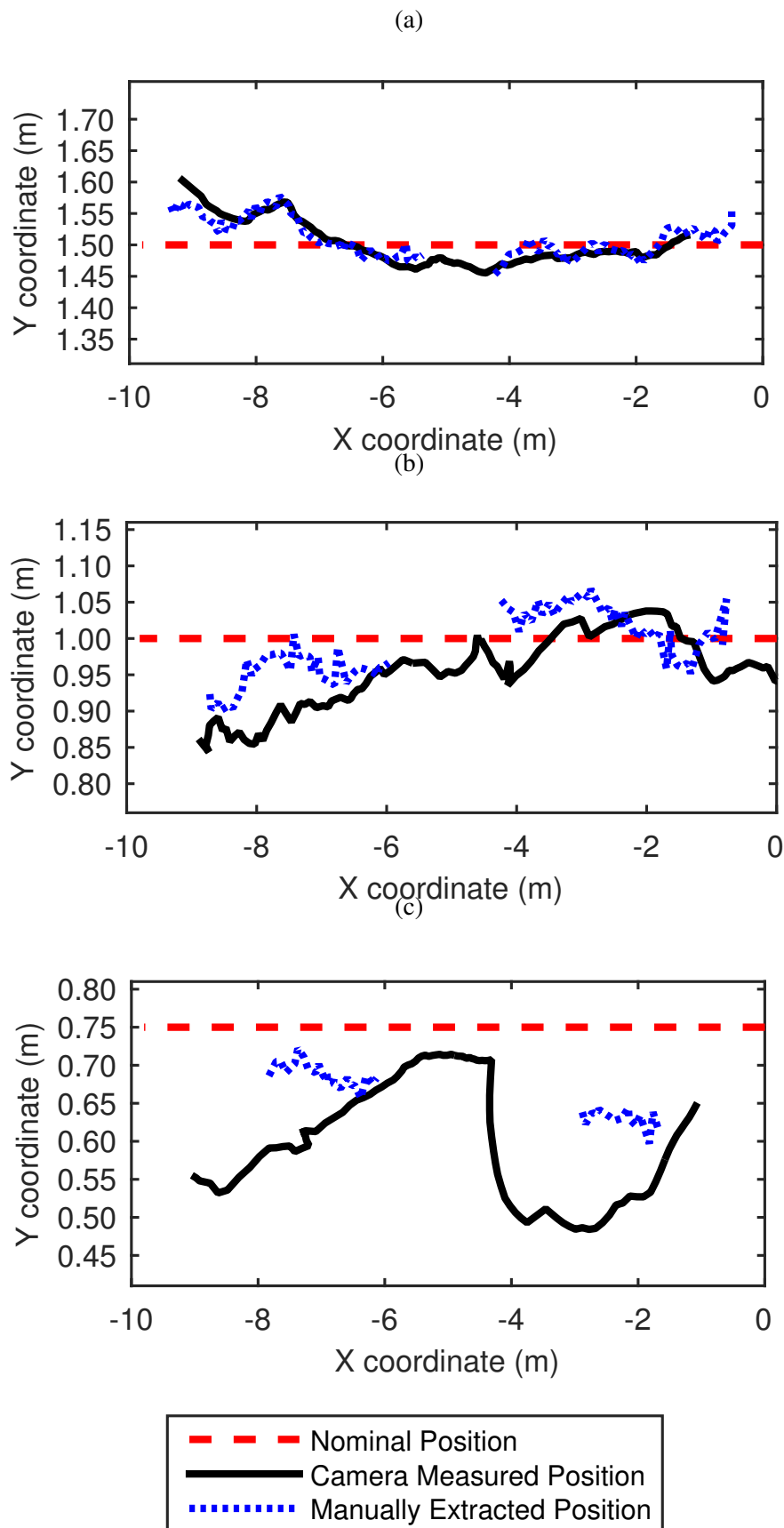


Fig. 2.13 Comparison between camera measurements and manually-extracted data points for a single run at (a) 1.5 m separation (b) 1 m separation (c) 0.75 m separation

Table 2.1 Average detection errors across all tests.

Nominal distance (m)	1.5	1.0	0.75
σ_{CM} (cm) (measured)	3.27	3.66	4.72
σ_{MT} (cm) (estimated)	1.67	2.00	2.33
σ_{CT} (cm) (calculated)	3.67	4.17	5.26
Normalised σ_{CT}	2.4%	4.2%	7.0%

dominates the error between the manual measurements and true value. This implies that the calibration process is very accurate and reliable, even at $d = 1.5$ m.

At 1 m distance (Figure 2.13b), occlusion prevents manual measurements between the two cameras ($X = -6$ m to -3 m). The errors relative to the manually extracted position are slightly larger, but still close to the 3 pixel uncertainty window (corresponding to 3 cm at $d = 1$ m), again implying that the image processing system can find the ground contact point at least as accurately as a human. The maximum error for the displayed test run was 10.9 cm at $X = -7.4$ m, but the standard deviation across all tests was 3.66 cm. The higher maximum error suggests that the camera system is slightly less robust at closer range, as the wheels become more liable to occlusion, but the overall accuracy is similar. As predicted, at closer range, the uncertainty in the calibration process drops, as the camera ‘looks down’ on the closer points instead of ‘across’ them, allowing the ground point to be more accurately defined. This causes the errors due to the detection stage to become even more dominant as the range reduces.

At 0.75 m distance (Figure 2.13c), the camera system is much less reliable. Occlusion strongly limits the areas where manual extraction can be performed. The maximum errors are much larger (15.2 cm at -2.7 m), although the standard deviation is still under 8 cm across all the test runs. The calibration process is more accurate at the closer distance, so the errors in the detection stage dominate, leading to a standard deviation in the error between the camera measurement and the true position of up to 5 cm. This is largely due to significant occlusion of the wheels at close range by the cyclists body. Since the classifier training dataset included images of partially occluded wheels the system can still estimate the position of the wheel, but accuracy is reduced compared to the fully visible case.

The errors at the closest nominal distance were noticeably larger than at further distances. Inspection of the output of the detection stage for these runs shows significant loss of accuracy at the gap between the images taken by the two cameras. This often caused the Kalman Filter to fail for all or part of the test, without enough observations to inform the model. This loss of detections was most significant at the closest distance because the wheels are more

easily occluded when the cyclist is close to the camera, leaving only two small patches, one in the centre of each camera's field-of-view where the detection system was working well. This pattern was consistent across all the runs at 0.75 m. Reducing the separation between the cameras, or increasing the number of cameras would eliminate this blind-spot in the field-of-view, and improve the accuracy significantly.

2.6 Discussion

Jia [111] quoted the accuracy of the ultrasonic measurement system as a standard deviation of 3.4 cm at a nominal passing distance of 1 m. This is very similar to 3.92 cm for the camera system in a similar test. However it should be remembered that a component of this value is an uncertainty in the manually extracted position (as the true position was unknown, unlike the ultrasonic tests) and the standard deviation of the camera detection alone was 3.66 cm. The output of the camera system is the world coordinates of the point midway between the ground contact points of the bicycle's wheels, whereas the output of the ultrasonic system was the distance of the cyclist's shoulder from the side of the HGV. The translation from the ground point to the shoulder would introduce discrepancies between the camera and ultrasonic systems due to roll motion of the cyclist, and the position and angle of the cyclist's torso relative to the bicycle. However, for the purposes of predicting trajectories rather than merely detecting proximity, the point in the ground plane is the more reliable predictor of future motion, which is a benefit of the camera system.

A significant disadvantage of the camera system compared to the ultrasonic system is the loss of accuracy at close range. However, this could be mitigated by smaller separation between the cameras (possibly increasing the number of cameras required) and also by lowering the camera, to reduce the angle between the camera and the ground plane, thus reducing occlusion of the wheels by the cyclist's torso.

The camera system addresses many of the limitations of the ultrasonic system, including complexity and cost of installation and the ability to differentiate between multiple cyclists. A hybrid system using cameras to identify cyclists and a few ultrasonic sensors to accurately locate them would be a possible enhancement.

2.7 Conclusions

- (i) A camera system was developed to measure the motion of cyclists on the nearside of Heavy Goods Vehicles. The system consisted of two downward-facing cameras mounted high on the side of the vehicle. A calibration grid marked on the ground

was used for locating contact points. Cyclist wheels were detected using boosted classifiers and geometrical arguments. The point of contact between the wheel and the ground was extracted and converted into world coordinates using a coordinate mapping generated from the calibration grid.

- (ii) The system was evaluated using test data from a number of parallel passing manoeuvres between a cyclist and HGV. The system was generally able to track the position of the cyclist to within 10 cm at distances of 1 m or greater from the HGV. The detection step was accurate to ± 4 cm (standard deviation) at most points. The remainder of the error was introduced by the mapping to world coordinates. At lateral distances of less than 1 m the system was found to be significantly less accurate due to occlusion and distortion of the image features. Quantification of the error was hampered by the lack of a 'ground truth' to compare to.
- (iii) The system was slightly less accurate than Jia's ultrasonic system, most significantly when the cyclist was close to the HGV. The camera-based approach also suffers in poor lighting or weather conditions, meaning a solely camera-based approach is likely to be unrealistic.

The primary conclusion from this work was that the system described in this chapter is promising but not sufficient to provide a robust detection system for all conditions, due to the loss of accuracy at close range, and the impracticality in low-light conditions. It is likely that the most suitable solution would be a hybrid system fusing image and ultrasonic data. This would combine the accuracy and robustness of the ultrasonic system with the ability of image processing to discern a single cyclist from the background or from a group of cyclists. It was decided to leave this separate major project to be completed by another researcher in order to focus on vehicle capacity and manoeuvrability issues.

Chapter 3

Analysis of Urban Delivery Systems

3.1 Introduction

This Chapter presents an analysis of some logistical aspects of urban delivery systems, in the context of the three case studies described in Chapter 1. First, in-service data from two grocery delivery providers were presented, allowing a comparison to be made between the two providers. These data were used to assess a statistical model of shift lengths in multi-delivery operations, with the intention of ensuring that drivers are not required to work excessively long shifts due to the use of higher capacity vehicles, which can complete more deliveries in one shift. Secondly, in-service data from four refuse collection vehicles were used to analyse shift lengths for domestic waste collection operations, in order to predict the impact of higher capacity vehicles. Finally the impact of higher capacity vehicles on urban store restocking was discussed. Analysis of this case study required modelling of an entire logistics system, and a wide-ranging data collection project to inform the model, which was considered beyond the scope of this project.

3.2 Case Study A: Grocery Delivery Vehicle

In order to assess the possible effects of using higher capacity vehicles on the home delivery system, data were collected from grocery delivery vehicles for two supermarkets in Cambridge. These data were used in two ways. First, qualitative and quantitative comparisons were made between the delivery operations for these two supermarkets. The aim was to identify target areas where each supermarket could work towards a 'best practice' standard. Secondly, a statistical analysis evaluated the potential impact of increasing size of the delivery vehicles on the system as a whole. In this application, a key constraint is the length of time

taken to complete the delivery route, which must not exceed the driver's 8 hour working day. Possible methods for reducing delivery times were also considered.

3.2.1 Data Collection Methods

Data were collected by three different methods. First, a qualitative assessment of each of the supermarkets was performed through informal interviews with consumers. Secondly, one vehicle from each of the supermarkets was fitted with a logging device, and vehicle data was collected for four days of typical in-service use. Finally, an observer spent two days with a driver from each supermarket taking qualitative observations, and completing a simple study of time taken to complete aspects of the delivery task.

Two supermarket chains were considered for this analysis, designated Supermarket A and Supermarket B. Both are in the top eight UK supermarkets in terms of market share.

3.2.1.1 Qualitative Analysis

Both supermarkets considered in this analysis were researched, in order to understand the qualitative differences between them. Informal interviews were conducted with a small number of consumers, questioning their impressions of the two supermarkets, both in general and in some specific areas, including value for money, typical customer profile, and quality of customer service. Although the sample size was small, results were very consistent, and can be matched to patterns in the quantitative data.

3.2.1.2 Vehicle Data

Data from the vehicles were captured using a bespoke android application. This application, known as the 'SRF logger', captured several data channels, and transmitted the data to a Cambridge University server. The data channels were captured from three sources: the android device's GPS module, the android device's internal accelerometers and gyroscopes, and the On-Board Diagnostics (OBD) port of the vehicle (through a bluetooth module). The data channels recorded are listed in Table 3.1.

Of the parameters listed in Table 3.1, only the GPS-based position and OBD-port vehicle speed were used in this analysis. Potential uses for the other data channels will be presented in the final chapter of this thesis. Chowdhury et al. showed that GPS-based speed measurement can be more accurate than that reported by the OBD port [141]. However, due to the design of the SRF logger, GPS data were sometimes not available at the start of a journey, and so the OBD port measurement was used, as it was more reliable. Similarly, the mass air flow measurement was known to be an unreliable measure of fuel consumption for diesel vehicles,

Table 3.1 Data channels captured by the SRF logger

GPS	On-Board Sensors	OBD Port
Position (-)	X,Y,Z acceleration (m s^{-2})	Engine speed (rpm)
Speed (m s^{-1})	Yaw, Pitch, Roll rates (rad s^{-1})	Vehicle speed (m s^{-1})
		Mass Air Flow (kg)
		Throttle position (%)

hence fuel consumption and emissions were instead calculated using a numerical model described below.

The data collected by the logging device were separated by ‘key-off’ events (i.e. when the vehicle was switched off). This allowed consideration of the data as a series of ‘legs’. Each leg was taken to be the journey from one delivery to the next; each day of driving was made up of a number of legs. This assumption allowed statistics for each leg to be considered, but there were a few errors.

First, some legs did not start and end at a delivery location. From the information gathered (as described in section 3.2.1.3), it is believed that some of the legs showed driving from a delivery to a location where the driver took a break, or from the break location to the next delivery. These events were omitted from the analysis.

Secondly, it appears that the engine was not always switched off at delivery locations. Some legs show a long stationary period before continuing to move, indicating that the period between two key-off events covers two deliveries instead of one. These legs were also removed from the analysis. Although consideration of these events would be interesting from the point of view of reducing engine idling time, they would introduce errors into the driving distance per delivery investigated here.

3.2.1.3 Driver Observations

Researchers were able to spend two days at each supermarket shadowing a driver during delivery shifts. These were not the same days for which the logging device was fitted to the vehicle. On these days, the researchers were able to take observations, with the intention of identifying areas in which to improve the efficiency of the process. Additionally, the researchers completed a simple study of the time spent completing various tasks during each delivery. The tasks were divided into:

- (i) Completing paperwork.
- (ii) Unloading the delivery from the van (usually onto a trolley).

- (iii) Delivery to the customer (including time spent walking between the vehicle and the customer's door).
- (iv) Repacking the trolley and empty totes into the van.

As well as observations of the drivers, researchers observed the 'warehouse' side of the operation, from product picking to vehicle loading.

3.2.1.4 Fuel consumption modelling

Due to the unreliability of the fuel consumption measurement reported by the vehicle OBD-port, a numerical model was developed using the Advanced Vehicle Simulator (ADVISOR) [142]. ADVISOR models have been validated against other simulations, showing total simulated fuel use and emissions within 5% of measured values [143]. Comparison to test data for a Hybrid Electric Vehicle showed errors in energy consumption of less than 1% [144]. This simulation used the speed measured from the OBD-port as an input drive cycle, and a model of a light delivery vehicle, with an engine appropriately sized to be able to complete the drive cycle. The mass was kept constant as if the vehicle was fully loaded. Although in practice the mass of the vehicle decreased throughout the shift as deliveries were made, the effect was assumed to be small compared to the mass of the vehicle (a single delivery comprises approximately 1.4% of the mass of the full vehicle), and expected to be consistent across both supermarkets.

3.2.2 Comparison between Supermarkets

3.2.2.1 Qualitative Analysis

There is a significant perceived difference between the socio-economic profiles of the two supermarkets. Supermarket A is considered to offer better value for money than Supermarket B. Products tend to be towards the less expensive end of the spectrum, and in general the typical customer falls into a lower income bracket compared to Supermarket B. This tends to be reflected in analysis of customer addresses. The tendency is for Supermarket A customers to live around the outskirts of Cambridge, whereas Supermarket B customers often live in the small villages in the surrounding countryside.

These perceptions of the two supermarkets are subjective, and somewhat generalised, but are supported by multiple informal interviews with consumers, as well as price comparison reports.

3.2.2.2 Vehicle Data

The following paragraphs analyse the data collected using the in-service logging application.

GPS-based position Figure 3.1 shows GPS traces captured by the logging device across both supermarkets for each of the four days of data collected. Data for both supermarkets are displayed on the same scale. The figure gives a strong impression of the difference between the areas covered by each vehicle during a typical shift, which are larger for Supermarket B than for Supermarket A. This supports the statement that customers of Supermarket A tend to live close to the city, either in the centre or on the outskirts, whereas customers of Supermarket B often live in the surrounding villages.

The GPS data displays some features of interest. In a number of places, the vehicle appears to have travelled out and back along the same road, without a delivery marked at the point when it turned round. In some cases this is due to temporary failure of the logging device, and in other trips it appears the driver used the closest opportunity to turn round. However, in some cases no obvious reason was identified. It is believed that these events occur when the driver is ahead of schedule and needs to find a place to wait until the next delivery can be made. This hypothesis is supported by observations of the driver, described in Section 3.2.1.3.

Distance travelled The vehicle position can also be summed to give the total distance travelled. Figure 3.2a shows a box and whisker plot of the distance travelled for each leg by each supermarket. The edges of the box show the 25th and 75th percentile, the lines across the necks indicate the mean value, and the tips of the whiskers represent the extreme values. Supermarket B clearly has to travel on average further between each delivery than Supermarket A, evidenced by greater mean, quartile and maximum values. These data are also expressed as a probability density function in Figure 3.2b. Figures 3.3a and 3.3b present the histograms of the driving distance data along with the fitted probability distribution. A Gamma function was chosen to best represent the data, initially by assumption, but which was then shown to represent the data well [145]. From this point, all the data will be shown in the form of the fitted distribution rather than the underlying histogram, to enable easier visualisation of the comparisons.

As Figure 3.2b shows, the mode distance per delivery (the peak of the probability density function) is similar for both supermarkets: 0.9 km for Supermarket A and 1.0 km for Supermarket B. However, the tail of the probability density function for Supermarket B is much longer than the tail for Supermarket A. This supports the findings from the previous section, suggesting that Supermarket B delivers to customers in the surrounding villages, as

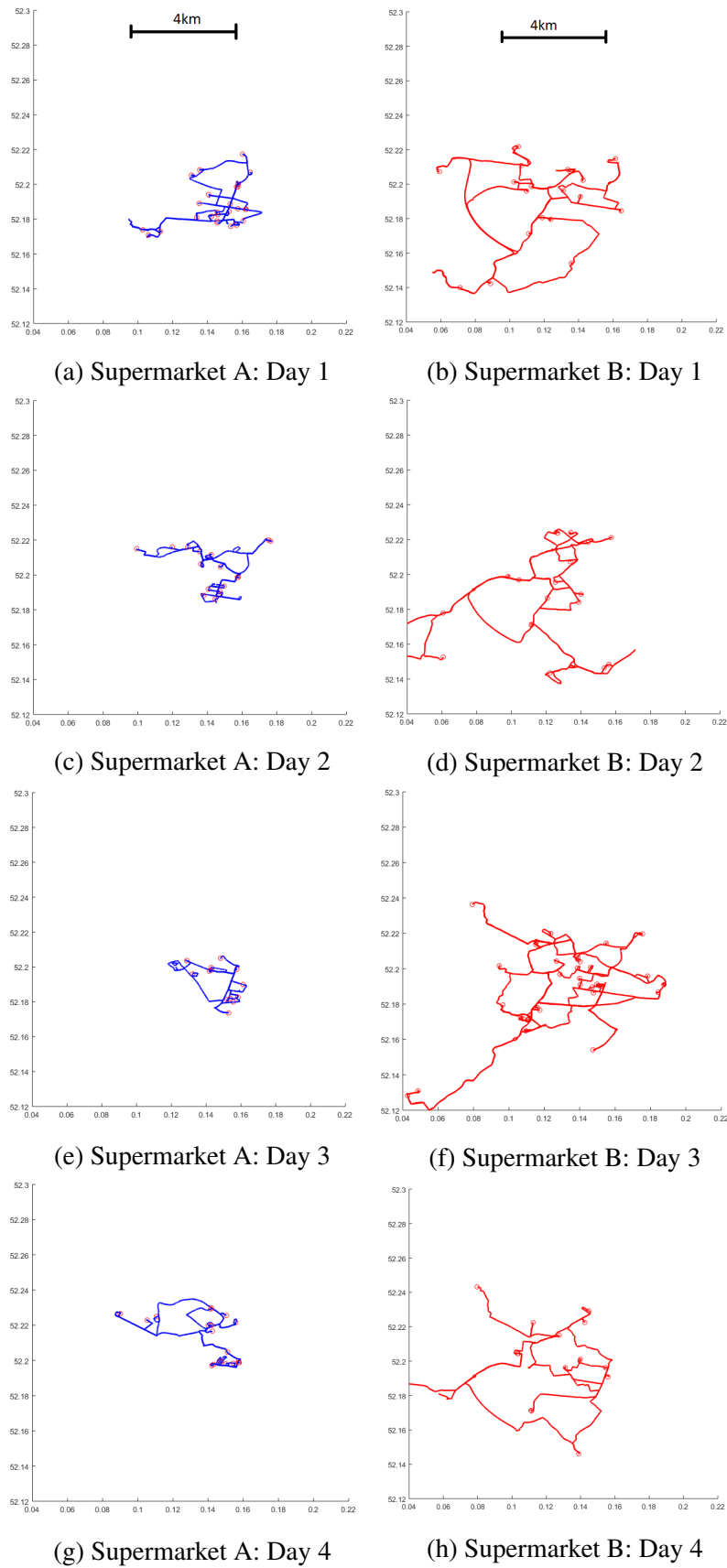


Fig. 3.1 GPS traces of supermarket vehicles

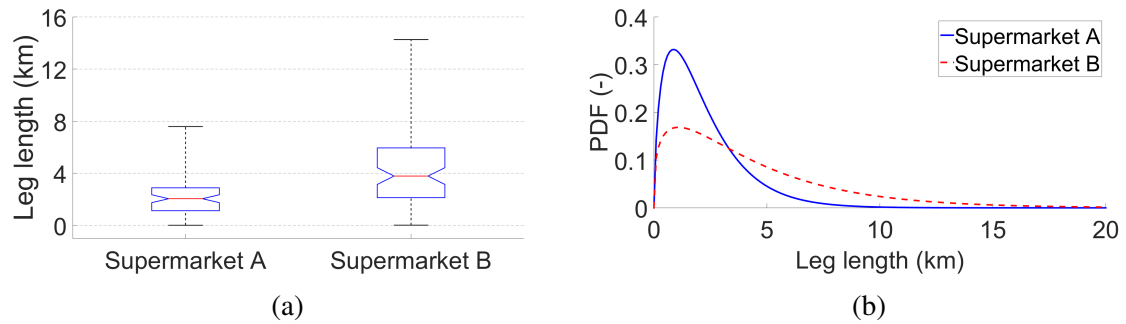


Fig. 3.2 Box and whisker plot and probability density function for distances travelled between deliveries by each supermarket

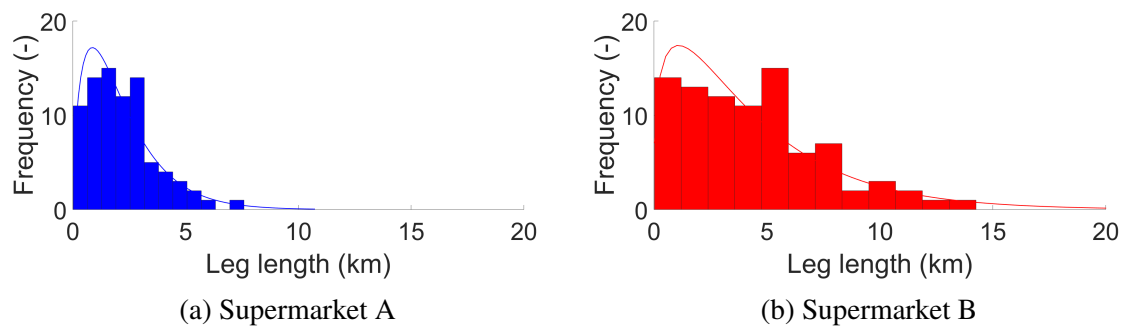


Fig. 3.3 Histograms of distance travelled between deliveries for each supermarket, showing fitted Gamma probability distributions

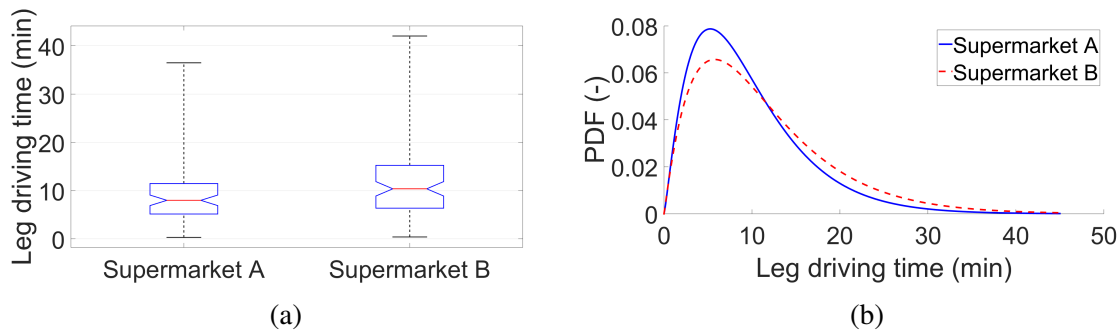


Fig. 3.4 Box and whisker plots and probability density functions of time spent travelling per leg for each supermarket

well as to customers in the centre of town, as made by Supermarket A. The mean distance travelled per leg was 2.2 km for Supermarket A, and 4.4 km for Supermarket B.

The total distance travelled by the vehicle on each of the four recorded days was also calculated. Supermarket A's vehicle averaged 44.7 km/day, whereas Supermarket B's vehicle travelled on average 95.8 km/day, both within an 8 hour shift.

Driving time The time spent driving for each leg was also computed. The box and whisker plot and probability density function of the times spent driving for each leg by each supermarket are presented in Figure 3.4.

Although Figure 3.2b shows that the vehicles of Supermarket B drove further between deliveries on average than those of Supermarket A, Figure 3.4b shows that the time taken to complete those journeys was fairly similar, implying that the average speed of vehicles from Supermarket B was significantly higher. This links to the analysis of locations of Supermarket B customers. Although customers in the villages surrounding Cambridge are further away, the speed limits on the roads are higher, and the likelihood of significant traffic congestion is lower on these routes.

The median driving time was 8.0 minutes for Supermarket A, and 10.4 minutes for Supermarket B.

OBD-port vehicle speed To verify the conclusions of the previous paragraphs, the average speeds of the vehicles from the two supermarkets were compared. Figures 3.5a and 3.5b show the box and whisker plots and probability density functions respectively of the average speed for each leg (leg length divided by leg driving time) by each supermarket.

The average leg speed for Supermarket A rarely exceeds 30 km h^{-1} , and the mode average speed is 11 km h^{-1} . In contrast, the mode average speed for Supermarket B is 17 km h^{-1} , and the tail of the probability density function has average speeds exceeding 30 km h^{-1} in

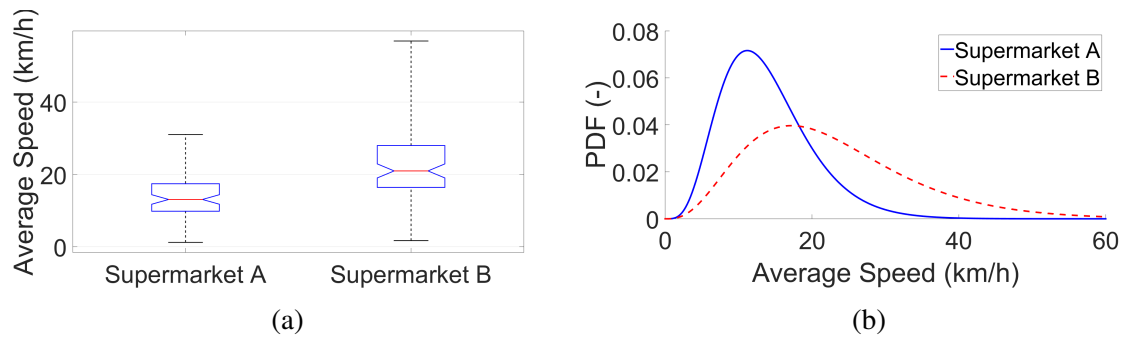


Fig. 3.5 Box and whisker plot and probability distribution function for average speed of travel between deliveries by each supermarket

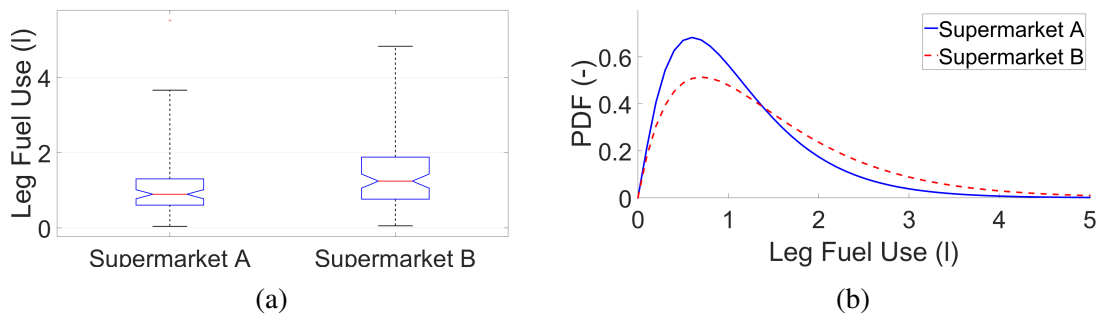


Fig. 3.6 Box and whisker plot and probability distribution function for total fuel consumption per delivery by each supermarket

some cases, supporting the conclusion that vehicles from Supermarket B generally travel at higher speeds than vehicles from Supermarket A.

Fuel consumption The average fuel consumption per leg and average fuel consumption per 100 km of each vehicle were compared in simulation using ADVISOR, taking the collected OBD-port vehicle speed as an input drive cycle. Figure 3.6 shows the distribution of fuel consumption across all the legs for each supermarket. These figures indicate that the total fuel consumption per leg was very similar for both supermarkets on average.

However, to account for the increased driving distance of Supermarket B, Figure 3.7 gives the comparisons for fuel consumption per 100 km. Four anomalously high data points (legs with a fuel consumption of more than 200 l/100km) were attributed to legs with long idling times, and were removed from the figures.

The cost of the increased distances travelled by Supermarket B is offset by the higher travel speeds and lower congestion compared to the short, urban routes travelled by Supermarket A. An example drive cycle for each supermarket is presented in Figure 3.8, demonstrating the higher travel speeds and reduced starting and stopping for Supermarket B.

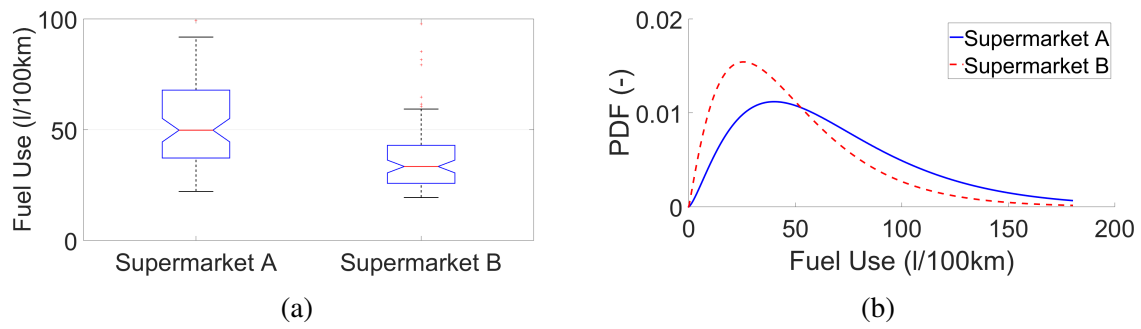


Fig. 3.7 Box and whisker plot and probability distribution function for average fuel consumption per 100 km by each supermarket

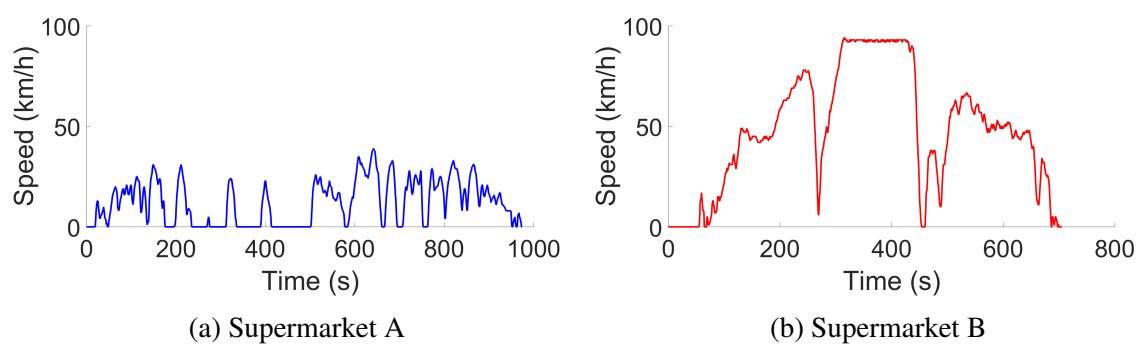


Fig. 3.8 Example drive cycles for Supermarkets A and B

3.2.2.3 Driver Observation Data

The following paragraphs present conclusions drawn from observations of the drivers and the ‘picking’ and ‘loading’ operations.

Stock picking and vehicle loading Both supermarkets had a similar approach to stock picking. Goods were picked by employees (not the vehicle drivers) from the supermarket shelves, and packed into totes which were stacked in a holding area for the drivers to load into the vehicles. There were subtle differences between the computer systems controlling how tasks were allocated to pickers, partly necessitated by the different layouts of the two stores. These differences are beyond the scope of this work and not investigated further.

Both vehicles were loaded by their drivers, in reverse order, i.e. the first delivery was closest to the rear doors. The two vehicles had significantly different racking strategies. The strategy of Supermarket A required the driver to climb into the back of the van, whereas the totes from Supermarket B could be loaded from outside the vehicle (with the aid of a hooked pole for some of the later deliveries). The loading of both vehicles was observed to take a comparable length of time, although this was not recorded.

Informal conversations with the drivers revealed some systematic problems with the loading. First, loading dock space was limited at Supermarket A, meaning that sometimes drivers had to load from the ground instead of from a dock at the height of the vehicle floor. This delayed the journey. Secondly, the computer system could not predict overweight vehicles until after the loading was complete, occasionally resulting in vehicles being unloaded and deliveries reallocated. Neither of these problems were observed at Supermarket B, where vehicles were always loaded from ground level, and the system allocating deliveries to vehicles could predict overweight vehicles in advance.

In summary, the systems used by both supermarkets were very similar, with only minor differences in the computer systems controlling allocation of pickers, drivers, and vehicles.

Qualitative observations of drivers The driver activities were also similar between supermarkets. There were, however, two primary differences. First, it was more common for the driver from Supermarket B to enter the houses and carry deliveries inside than for the driver from Supermarket A (formally both supermarkets have the same policy of being willing to carry deliveries inside on request). This is likely to be partly due to the demographic of the consumers at each supermarket, and also partly due to the reputation for particularly excellent customer service of Supermarket B. Both of these comments are subjective, but supported by observation and Section 3.2.1.1.

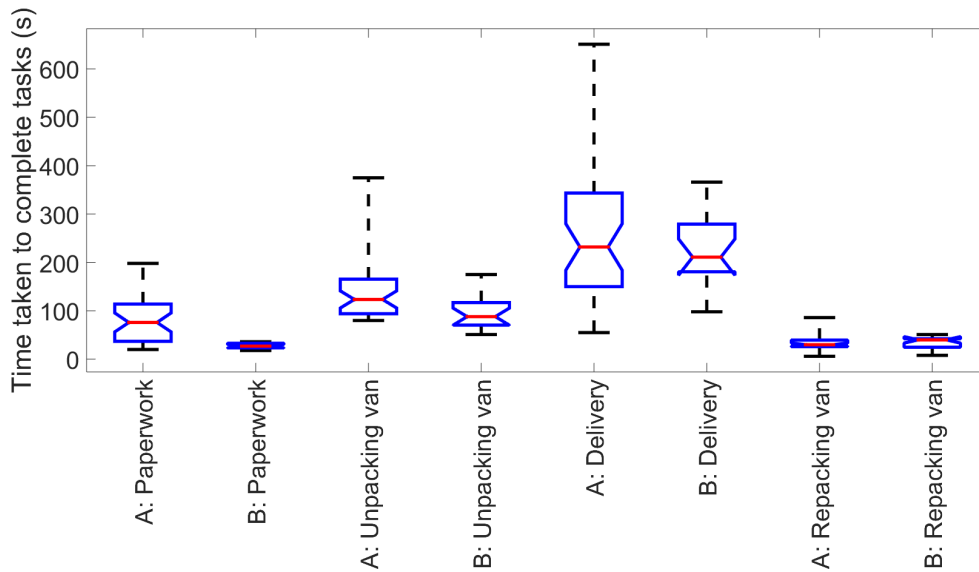


Fig. 3.9 Time taken to complete delivery tasks for each supermarket

Secondly, drivers from Supermarket A often had to walk further than those from Supermarket B to the customer's door. Parking was less readily available in the city centre, hence drivers regularly had to load totes onto a trolley and walk to the address. While common with both supermarkets, it was seen more often for Supermarket A.

As with the picking and loading operations, differences between the drivers of the two supermarkets were minimal, and irregular, such that they are difficult to define, except by statistical analysis of their impact on the time taken to complete certain tasks.

Task completion-time analysis While observing the drivers, measurements were taken of the time taken to complete four tasks: (1) completing any required paperwork, (2) unpacking the correct totes from the van, (3) making the delivery, and (4) repacking the van with empty totes. These times were measured by stopwatch and rounded to the nearest second. Potential inaccuracies were introduced into the measurements by the variable nature of the task. For example, at some deliveries the driver would unpack half of the totes and deliver them to the door, where the customer would empty them while the driver unpacked the second half of the totes. In other cases, the driver would unpack all the totes to make the full delivery in one transfer. This made it difficult in some cases to know which task to attribute periods of time to. The results presented below represent a close estimate.

Figure 3.9 shows a comparison between the average time taken to complete the four tasks for each supermarket. Table 3.2 shows the mean times taken to complete each task.

Table 3.2 Mean time taken to complete delivery tasks

	Supermarket A		Supermarket B	
	Time (s)	Percentage of total (%)	Time (s)	Percentage of total (%)
Paperwork	82	16	28	7
Unpacking van	143	28	98	26
Delivery	258	50	221	58
Repacking van	34	6	33	9
Total	517	100	380	100

Several trends are visible in comparison between the supermarkets. First, the spread of times for Supermarket A is much greater than the spread for Supermarket B. There were more data points recorded for Supermarket A (38) than for Supermarket B (17), which could account for some of the difference, but there may be an impact of driver experience, or some aspect of the systems used by Supermarket B (no such difference was observed). Further study is required to understand this difference.

Secondly, the most time consuming aspect of the task is the delivery itself. This is difficult to analyse, as the tasks involved in this varied between deliveries. For example, some customers unpacked in the doorway, while others carried the totes inside their house. Supermarket B spent on average 37 s less on the delivery than Supermarket A. One possible explanation for this is brand loyalty: Supermarket B customers are more likely to be familiar with the delivery system, and have their own systems in place for quick unpacking of the totes. Equally this could be attributed to differences between individual drivers.

Thirdly, Table 3.2 shows that unpacking the van of Supermarket A is considerably slower than for Supermarket B. This may be linked to the loading system, which requires the driver to get into the back of the vehicle, as opposed to being able to retrieve the totes from outside.

Table 3.2 shows that the Supermarket B stops took an average of 137 seconds less than those of Supermarket A. Over the course of 20 deliveries in a typical day, this equates to a time saving of over 45 minutes for Supermarket B. Of this 45 minutes, approximately 15 minutes is accounted for by the unpacking of the van, and a further 12 minutes by the actual delivery. The final 18 minutes is attributed to the time spent completing paperwork.

Impact of bagged deliveries A brief investigation was conducted into the impact of using single-use plastic bags to package deliveries, to assess whether the removal of plastic bags increases the time required to complete the delivery. Since the introduction of a carrier bag charge in the UK aimed at reducing plastic waste, most supermarkets have asked the

Table 3.3 Effect of single-use plastic bags on the mean time to complete delivery

	Supermarket A	Supermarket B
With bags (s)	165	179
Without bags (s)	263	150
Impact of bags (s)	-98	+29

customer to ‘opt-in’ to use of plastic bags, for an additional small fee. If plastic bags are not used, each tote has to be unpacked item-by-item to complete the delivery.

Table 3.3 shows the effect of the use of bags on the mean delivery time (not including the other three tasks). The results are inconclusive, showing a significant speed increase for Supermarket A, and a small decrease in speed for Supermarket B. This discrepancy is likely due to the small sample size.

It is believed that Supermarket A customers usually unpack in the doorway, carrying products from the doorway to the kitchen individually. The use of plastic bags has a significant positive effect on the speed in this case. Contrastingly, Supermarket B customers tend to ask the drivers to carry totes through to the kitchen, reducing the effect on the total delivery time.

3.2.3 Analysis of Shift Length

Due to the small sample size of the collected data, it was difficult to draw any significant conclusions on the effect of increasing the number of deliveries on the drivers’ shift length. It was decided instead to use the collected data to inform a model of the driver’s shift, and perform a Monte Carlo simulation to calculate the statistical likelihood of the shift length exceeding eight hours.

3.2.3.1 Method

The method was developed as follows:

- (i) Generate a ‘target’ probability distribution of driving distance per stop for each supermarket from the measured data, and sample this distribution N times, in order to create a randomised delivery shift of N deliveries with the target statistics.
- (ii) Convert each driving distance into a driving time (see method below).
- (iii) Generate a probability distribution of kerb time per stop for each supermarket from the measured data, and sample this distribution N times.

Table 3.4 Model parameters for statistical model of driver activities

	Supermarket A	Supermarket B
Driving distance		
k	1.66	1.33
θ	1.31	3.32
Driving time		
E	300	307
F	0.85	0.59
Kerb time		
k	7.81	14.1
θ	68.4	30.4

- (iv) Assess an approximate length of break time taken by the driver.
- (v) Sum all the times above to give the total length of shift for this sample day.
- (vi) Repeat steps (i) to (v) M times to give a distribution of the probable length of shift for N deliveries.
- (vii) Adjust N , the scale of the probability distribution of driving distances, and the scale of the probability distribution of kerb times and repeat steps (i) to (vi) to assess the impact of these parameters on shift length.

3.2.3.2 Driving distance probability distribution

For each of the two supermarkets, the driving distance from every leg collected was plotted, and a Gamma distribution fitted to the data points (shown in Figure 3.3). A Gamma distribution was found to fit the measured data well. A Gamma distribution is parameterised by a shape parameter, k , and a scale parameter, θ , with a probability density function given by:

$$\frac{1}{\Gamma(k)\theta^k} x^{k-1} e^{-\frac{x}{\theta}} \quad (3.1)$$

where Γ is the Gamma function [145]. Values for the shape and scale parameters for each supermarket are given in Table 3.4. These parameters were selected using a built-in distribution-fitting Matlab function.

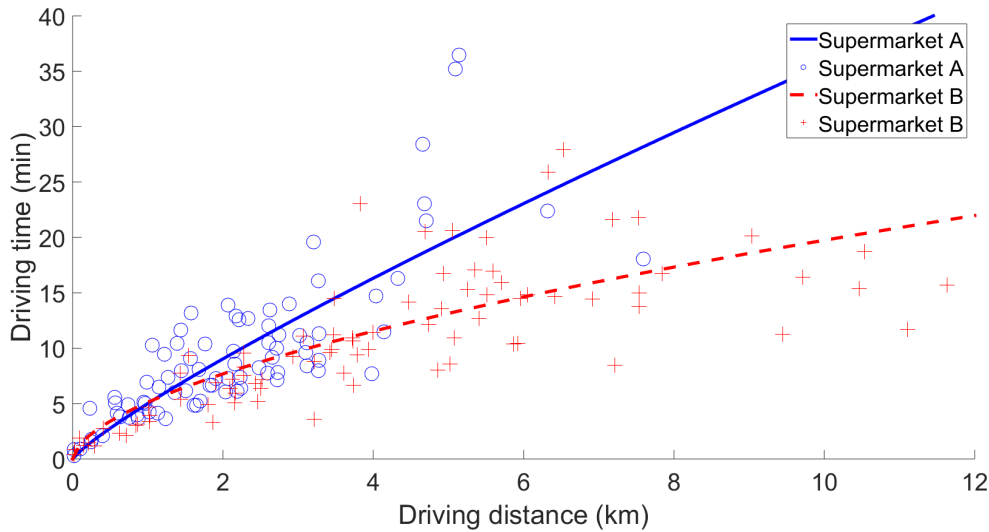


Fig. 3.10 Function to convert from driving distance to driving time

3.2.3.3 Conversion from distance to time

There were some legs from the collected data that contained artefacts that needed to be removed. For example, long stationary periods with the engine switched on while not at a delivery point were interesting from a qualitative point of view, but skew the driving time data unrealistically. Therefore, the drive cycle data was clipped to remove any stationary time of more than five minutes.

Figure 3.10 displays a scatter graph of driving distance, d_D , against driving time, t_D , along with a power series model fitted to the data for each supermarket. This allowed quick conversion from driving distance to driving time. The fitted curve was given by:

$$t_D = E (s_D)^F \quad (3.2)$$

where the parameters E and F are given in Table 3.4 for each supermarket.

The data display a large variance, in some cases up to 45%. However, in the region of the figure where most deliveries are (less than 5 km) the errors are typically less than 2 minutes, which was considered acceptable. The fit was not valid for distances greater than 12 km due to lack of data.

The two curves have a similar gradient for distances less than approximately 2 km, and then diverge. This seems to reflect the typical driving requirements of the two supermarkets. Below 2 km, both vehicles are driving in the city centre. Above 2 km, most journeys for Supermarket B are out of the city on roads with greater average speed. In contrast, almost all driving for Supermarket A is in the city centre, where congestion reduces the

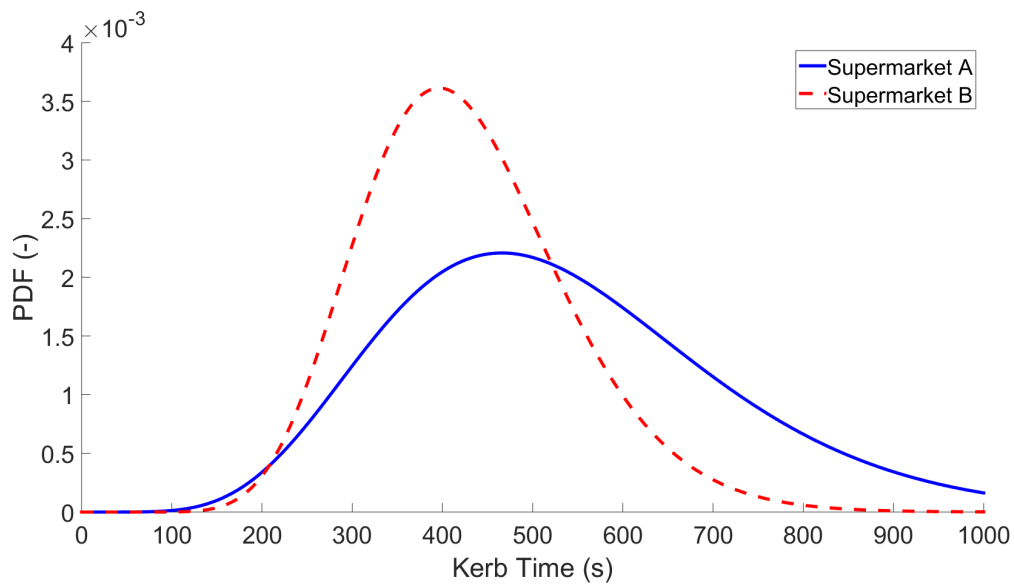


Fig. 3.11 Probability density function showing time spent on each delivery for each supermarket

average speed. Therefore, the corresponding time taken to complete legs is greater for longer distances than for Supermarket B. This trend was not expected to continue to higher distances, therefore the investigation was limited to 12 km. It could be argued that both supermarkets should be assessed using the same curve (perhaps a curve fitted to combined leg data from both supermarkets), to minimise the effect of customer demographic. However, since the demographic and location of the customers is inherently tied to the brand identity, and therefore outside the scope of this project, it was decided to keep separate curves for each supermarket.

3.2.3.4 Create kerb time probability distribution

Figure 3.11 shows the distribution of the total time spent on each delivery for each supermarket. This was calculated by summing the times for each individual task from Table 3.2. A Gamma probability density function was again used, where the parameters k and θ for each supermarket are given in Table 3.4. A Gamma distribution was preferred to a Normal distribution because all values were positive.

As with the driving time, it was decided to use each supermarket's curve for further calculations, despite the fact that Supermarket B appears to outperform Supermarket A, rather than taking an 'optimum' kerb time distribution and using it for both supermarkets.

3.2.3.5 Typical day generation

Each sampled day was composed of three parts: (1) driving between deliveries, (2) time spent at each delivery, and (3) a rest period for the driver. The rest period was fixed to 90 min per day, which approximately corresponded to driver observations (there is no legislatively fixed required break for drivers of light goods vehicles). The other two periods were calculated by sampling the driving distance and then the kerb time probability density functions N times, converting the distances to times as described above, and then summing all the times. The sum of the three periods gave a total time for the shift.

It was assumed that the first and last deliveries of the day were close enough to the vehicle's base that the 'end effects' at the start and end of the day could be neglected.

Inspection of the preliminary results revealed that a work shift of 8 hours with typical driving distances allowed for approximately 20 deliveries. This corresponded to observations of and discussions with drivers about real world activities, and hence was taken as the baseline value for N . In the simulation N was varied between 10 and 40.

3.2.3.6 Repeat simulation

Due to the statistical nature of the analysis, each sample day was simulated $M = 100$ times, yielding a distribution of shift lengths for a given set of parameters for the input distributions. The output variable extracted from this analysis was the likelihood of any given delivery shift exceeding eight hours. This allowed more realistic reasoning than simply extracting the mean shift length, enabling the system to retain a certain percentage (for example 75%) of shifts below eight hours. 75% was chosen as the percentage which most closely matched the current operation, found both from qualitative observations, and by analysis of the results described below.

This analysis did not take into account the degree by which a shift overran. Therefore solutions where a high percentage of shifts overran by a small amount were less highly rated than solutions where most shifts were under eight hours, but a small number of shifts exceeded eight hours by a large margin.

3.2.3.7 Varying the probability distributions

The goal of this work was to assess methods for increasing the number of deliveries, while keeping the length of the delivery shift below eight hours. The two options considered were reducing the driving distance between deliveries and reducing the kerb time. In practice, these options could be achieved in a number of different ways.

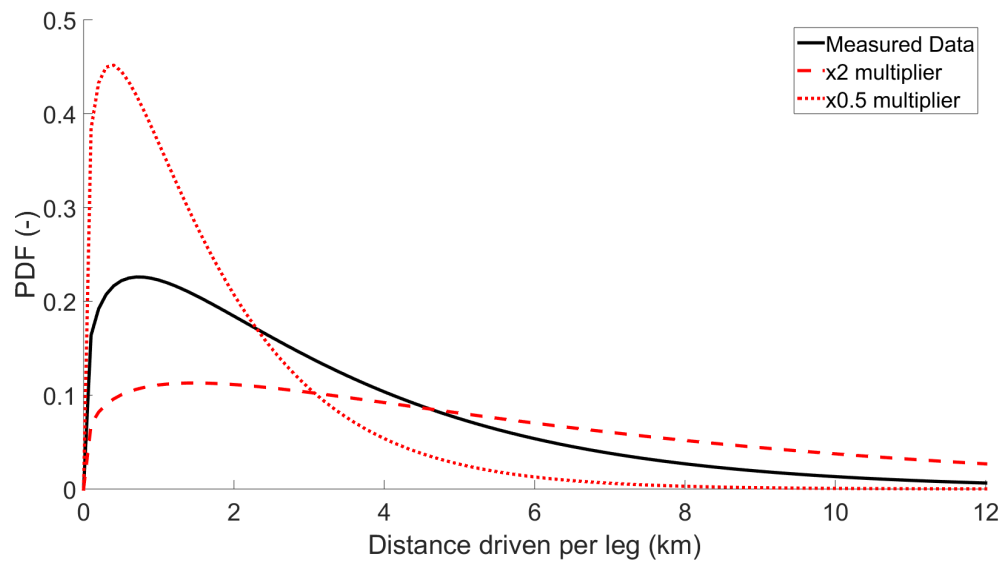


Fig. 3.12 Effect of multiplying the measured data by a factor of 2 or 0.5 before fitting Probability Density Function

The driving distance for any one vehicle could be reduced by increasing the number of deliveries in a given area known as the drop density. Methods for achieving this are discussed in Section 3.2.4.2.

Direct manipulation of the probability density functions by changing the parameters was considered unhelpful due to the lack of physical interpretation of the shape and scale parameters of the Gamma distribution. Instead, the probability distribution functions were found by multiplying the measured data by a scale factor, then fitting a new distribution to the scaled data (see Figure 3.12).

It was also recognised that the most useful variation might be truncation of any distance above a set threshold. This would represent having a separate vehicle to do the long distance drops, leaving the vehicle considered in this work to do only the short stops. Setting excessive values to the threshold would result in a spike at the threshold, hence for this approach values above the threshold were removed before fitting the probability distribution. Figure 3.13 shows the effect on the probability density function of removing the high value data.

To reduce the kerb times, three scenarios were considered.

- (i) The paperwork component of the delivery task was removed. In practice this involved subtracting the mean paperwork time, 66 s, from all data.
- (ii) A scenario was considered where the unpacking and repacking of the van was automated, and took no time, thus subtracting 150 s.

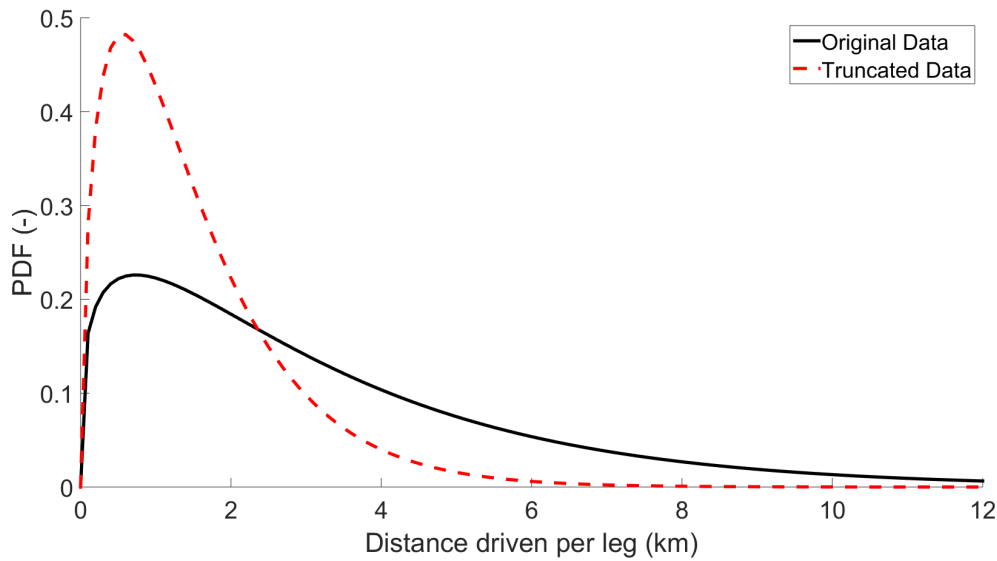


Fig. 3.13 Effect of truncating the measured data above a threshold of 3 km before fitting Probability Density Function

(iii) Both of these variations were applied together.

For each scenario, the probability distribution was calculated by modifying the input data and then refitting the distribution to the modified data. The effect of these reductions on the kerb time probability density function are shown in Figure 3.14.

3.2.4 Results and analysis

3.2.4.1 Effect of number of deliveries

Figure 3.15 shows the effect of changing the number of deliveries, while keeping the drop density constant. The figure shows that increasing the number of deliveries per day beyond 20 dramatically increased the likelihood of the shift exceeding 8 hours. Shifts with 25 or more deliveries were almost guaranteed to take longer than 8 hours. These results were similar across both supermarkets, and it has been shown in previous sections that the driving time between deliveries is similar for both supermarkets.

3.2.4.2 Effect of driving distance

Figures 3.16 and 3.17 show how the likelihood of a shift exceeding 8 hours varies with both the number of stops, N , and the mean distance between stops. The results for both supermarkets were fairly similar. The baseline case was taken to be at $N = 20$, and at a

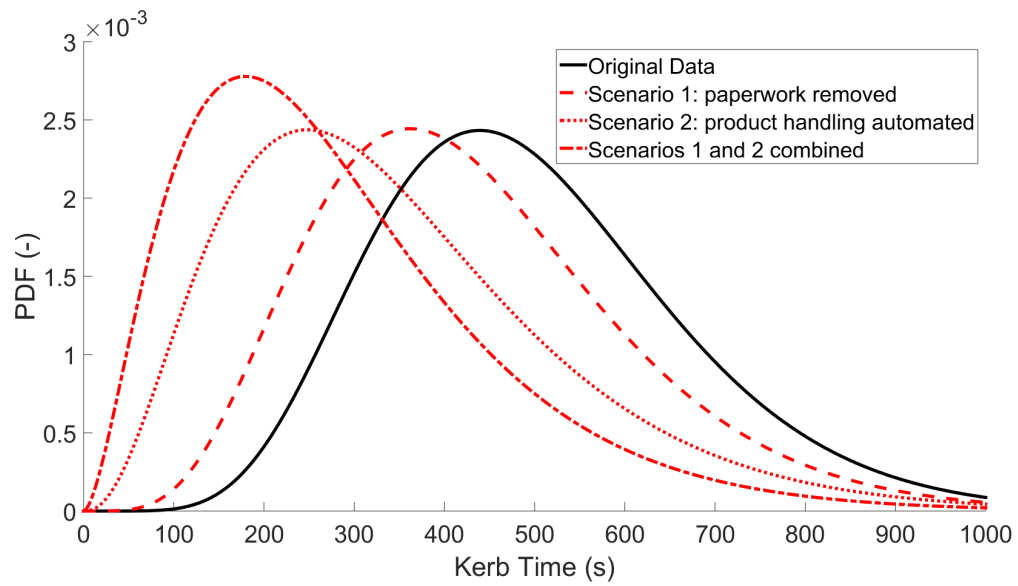


Fig. 3.14 Effect on probability density function of different kerb time reduction scenarios compared to the measured data

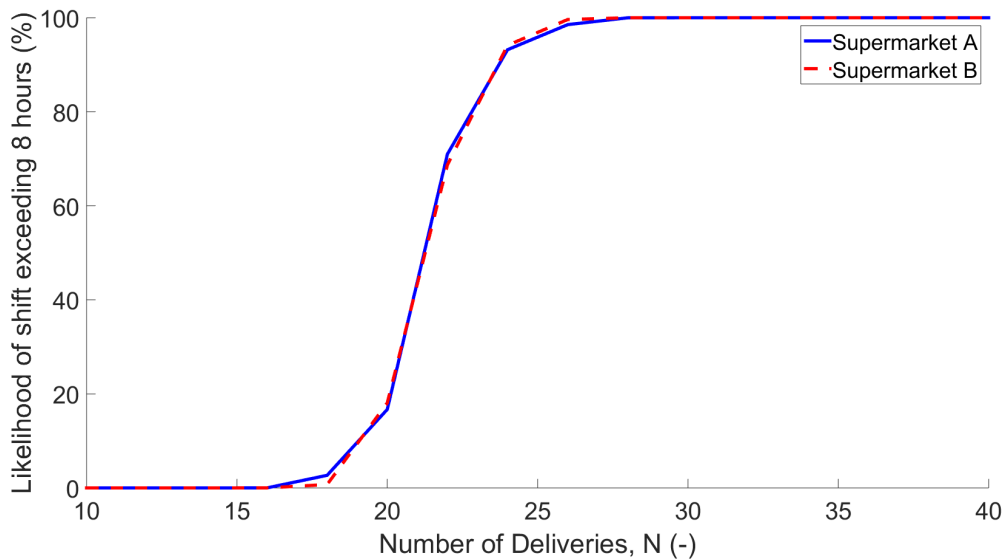


Fig. 3.15 Likelihood of shift length exceeding eight hours for varying number of deliveries, assuming no change to drop density

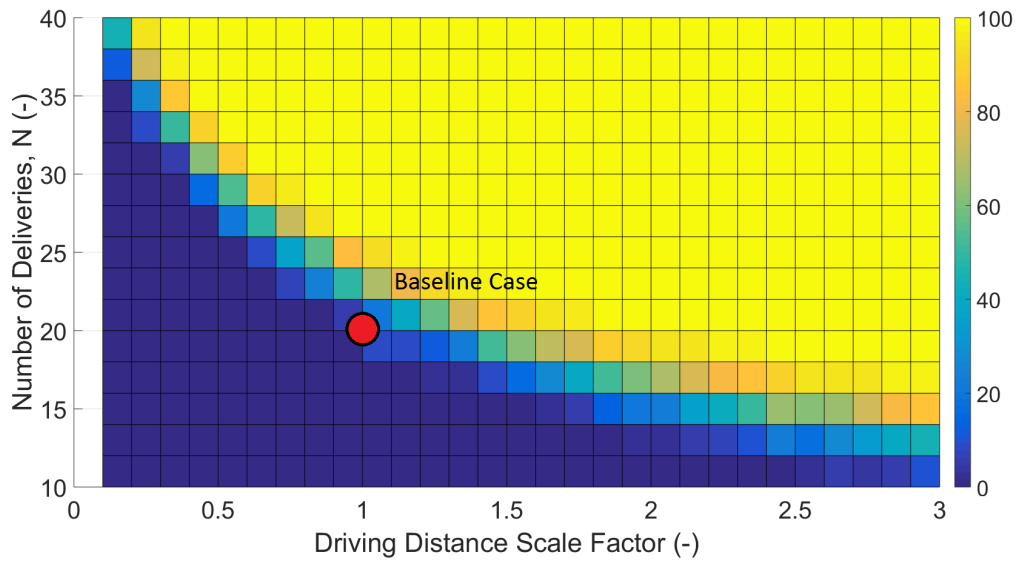


Fig. 3.16 Likelihood of shift length exceeding eight hours with varying number of stops and distance between stops for Supermarket A

Driving Distance Scale Factor of 1, marked on the figures, for which both supermarkets showed a likelihood of the shift length exceeding 8 hours of approximately 25%, which agrees with observations. This value of 25% for the baseline system was considered the limiting case, not to be exceeded. For both supermarkets, increasing the number of deliveries by 50% would require reducing the driving distance by 70% compared to the baseline system, in order to not increase the likelihood of the shift exceeding 8 hours. This would reduce the mean driving distance from 2.2 km to 0.7 km for Supermarket A, and 4.4 km to 1.3 km for Supermarket B.

The approach of multiplying the distances travelled by a scale factor in order to simulate travelling less distance may not be the most realistic representation of a real world method. Figures 3.18 and 3.19 show the output of the same method as Figures 3.16 and 3.17, except that the driving distances were modified by removing all distances above a certain threshold from the input data.

These results showed more divergence between Supermarket A and Supermarket B, as predicted, since legs for Supermarket A rarely exceeded 5 km, and thus the impact on the shift length was very minimal until the threshold was very small. On the other hand, the longer legs from Supermarket B were affected even with a large threshold. Using this measure, limiting the maximum leg distance travelled by Supermarket A vehicles to approximately 1.5 km could increase the capacity of the vehicles by 50% without increasing the shift

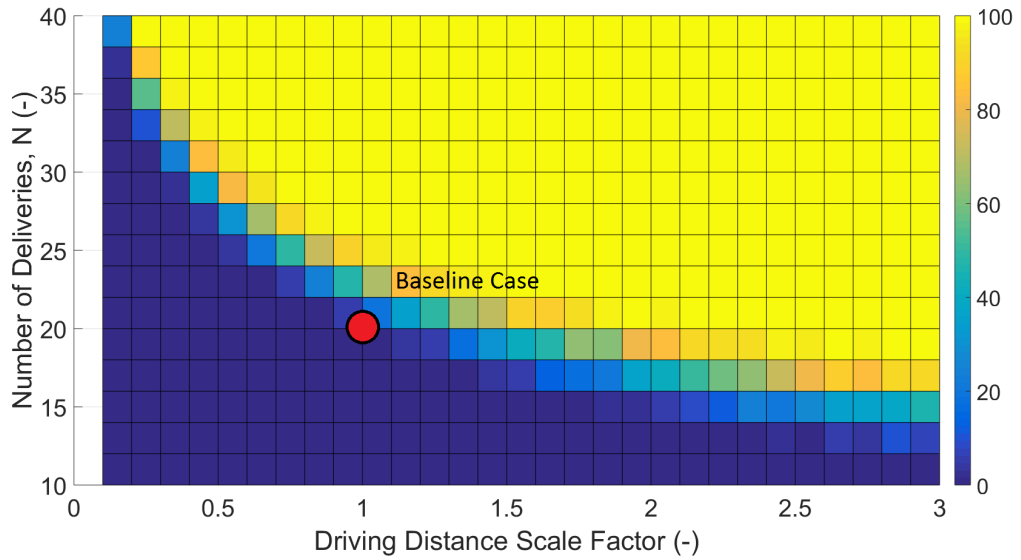


Fig. 3.17 Likelihood of shift length exceeding eight hours with varying number of stops and distance between stops for Supermarket B

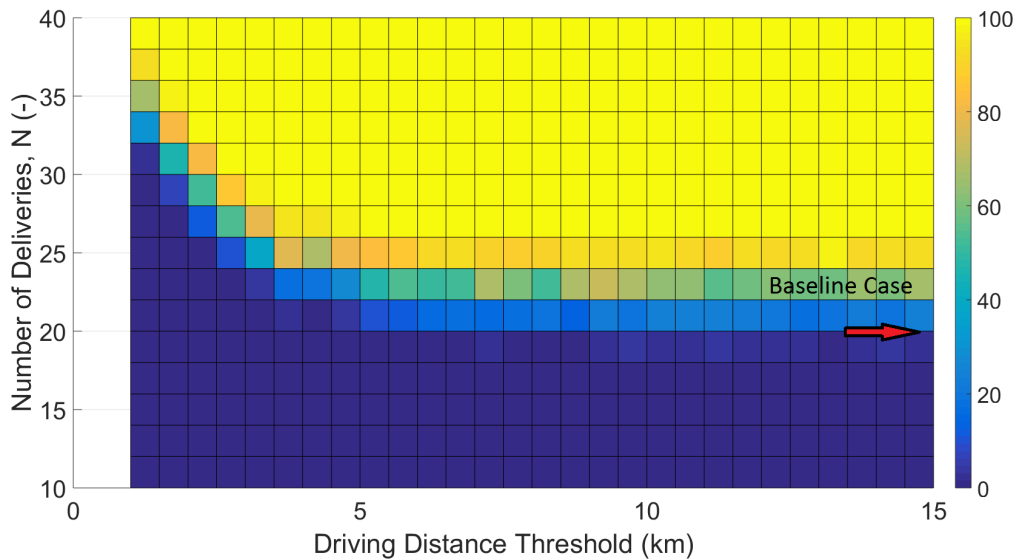


Fig. 3.18 Likelihood of shift length exceeding eight hours with varying number of stops and maximum distance between stops for Supermarket A

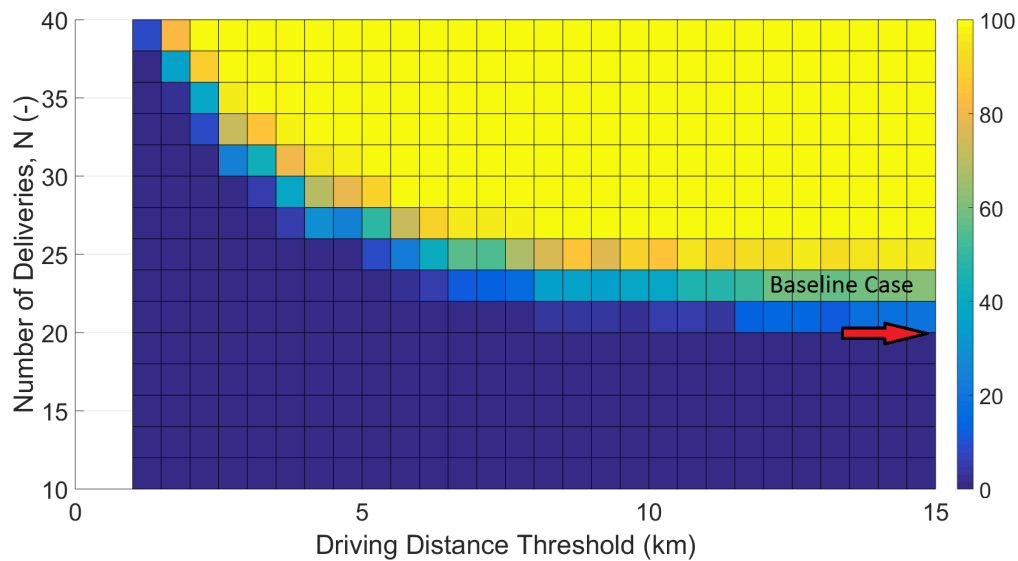


Fig. 3.19 Likelihood of shift length exceeding eight hours with varying number of stops and maximum distance between stops for Supermarket B

length. Similarly, limiting the distance to 2.5 km for Supermarket B could give the same 50% increase in capacity, and limiting the distance to 1.5 km could double the vehicle's capacity.

There are several methods by which this reduction in driving distance could be achieved. First, increasing the uptake of home delivery services would lead to more customers per supermarket in any given area. Therefore, the distance between deliveries would decrease. The number of vehicles required to service all the deliveries might well increase, but the vehicle efficiency would improve. The assumption that this is a 'better' solution than the current system relies on the assumption that customers not using home delivery services are currently shopping for groceries in personal vehicles, thus efficiency would be improved by increasing uptake of home delivery services. Secondly, there is scope for collaboration between supermarkets. If the areas covered by Supermarkets A and B combined could be split in half geographically rather than by customer choice of supermarket, the drop density in each geographical area would increase and the driving distance travelled by all vehicles from both supermarkets would decrease. However, this would require a level of cooperation between supermarkets not seen in the current system.

3.2.4.3 Effect of kerb time reduction scenarios

In order to compare the different scenarios for reducing kerb time, a single contour was extracted from each of the surface plots shown in the previous section. Since the baseline case corresponds approximately to a 25% chance of the shift taking longer than 8 hours,

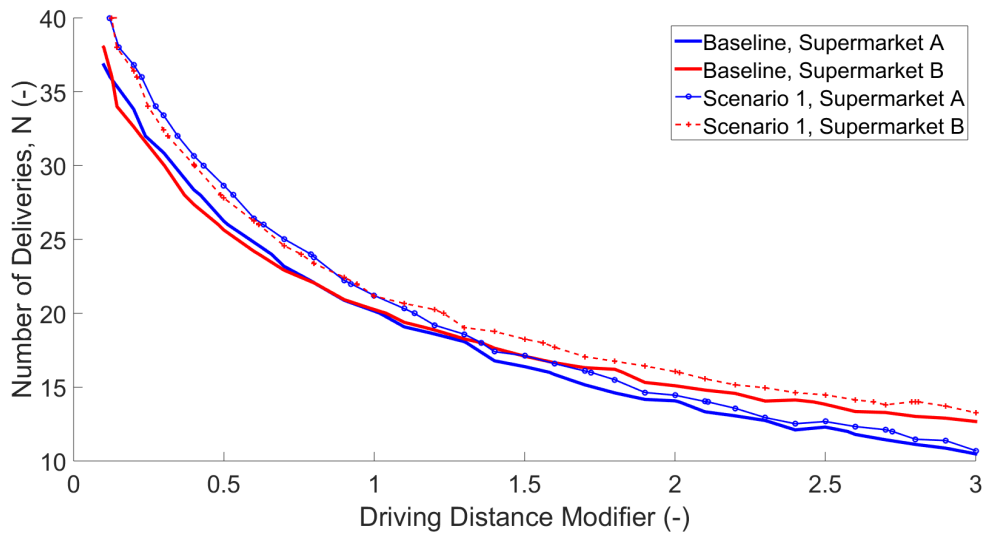


Fig. 3.20 Effect of kerb time reduction scenario 1 (removing paperwork) on the 25% chance contour of the shift length exceeding 8 hours

the 25% contour was used for comparison. Figures 3.20 to 3.22 show the 25% likelihood contour for the baseline case and the three kerb time reduction scenarios for each of the two supermarkets. These scenarios were removing paperwork, automating product handling, and a combination of the two. These required reducing the kerb times by 66 s, 150 s, and 216 s respectively as described in Section 3.2.3.7.

Measurements taken from these figures are summarised in Table 3.5. Each Supermarket was assessed on the percentage increase in the number of deliveries which which could be completed in under 8 hours (with 25% confidence as described above) under each kerb time reduction scenario. This percentage was calculated assuming first no change in the driving distance, and then a 50% reduction in the driving distance. This would involve reducing the mean driving distance from 2.2 km to 1.1 km for Supermarket A, and from 4.4 km to 2.2 km for Supermarket B.

Both Supermarkets can achieve 20 deliveries (with 25% success rate) under the current kerb time assumptions. Removing time spent doing paperwork from the driver workload permits a 5% increase for both supermarkets (a single additional delivery). Automating the product handling allows a 15% increase for both supermarkets, and combining the two scenarios to reduce the kerb time further increases the allowed number of deliveries for both supermarkets by 25% (5 additional deliveries).

However, greater increases in the number of deliveries can be achieved by simultaneously reducing the driving distance while reducing the kerb time. For scenario 3, removing paperwork and automating product handling, if the driving distance could be reduced by

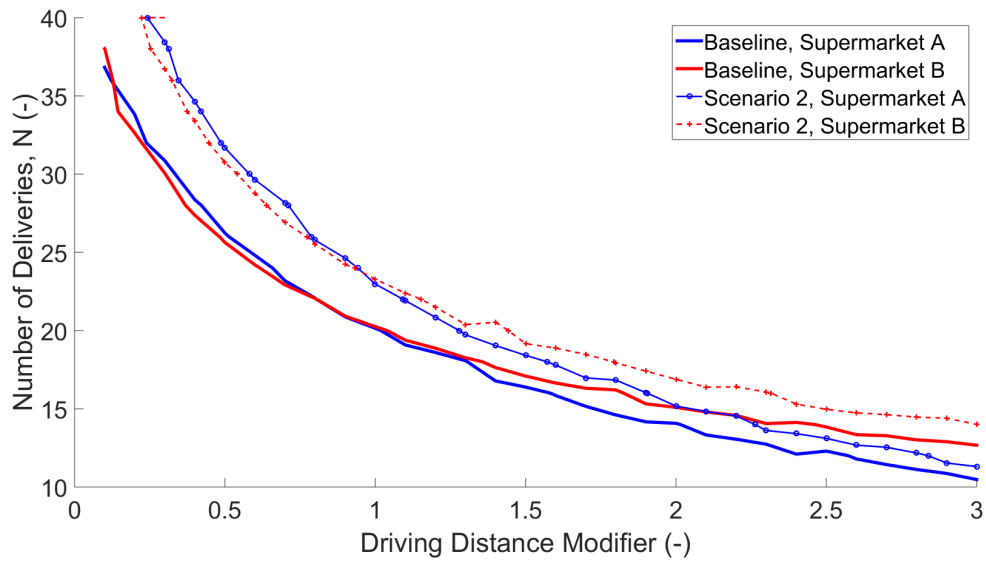


Fig. 3.21 Effect of kerb time reduction scenario 2 (automating material handling) on the 25% chance contour of the shift length exceeding 8 hours

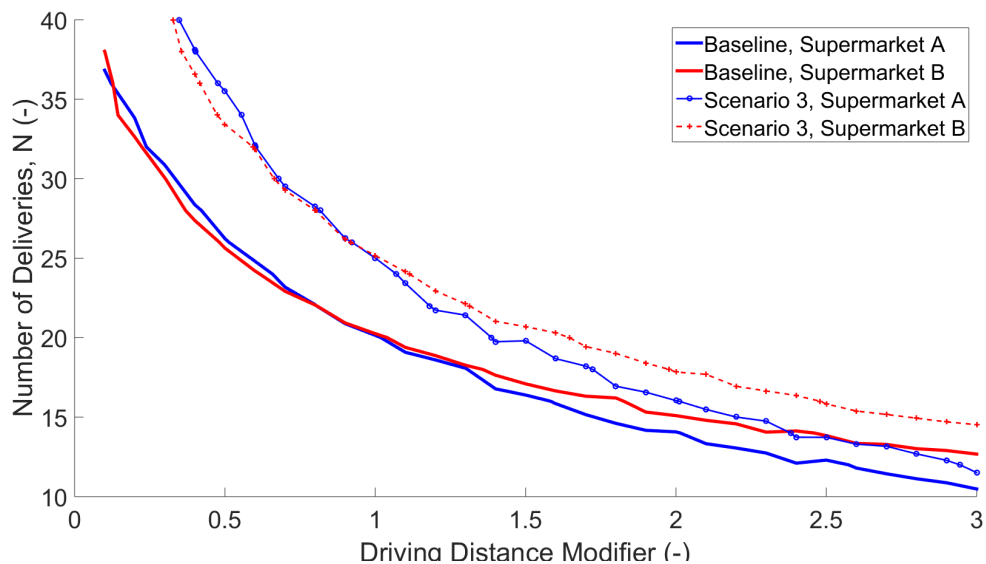


Fig. 3.22 Effect of kerb time reduction scenario 3 (removing paperwork and automating material handling) on the 25% chance contour of the shift length exceeding 8 hours

Table 3.5 Increase in number of deliveries which can be completed in 8 hours for different kerb time reduction scenarios, using the baseline driving distance and a reduced driving distance (50% reduction from the baseline)

	Supermarket A		Supermarket B	
	Baseline driving distance (%)	Reduced driving distance (%)	Baseline driving distance (%)	Reduced driving distance (%)
Baseline	0	30	0	30
Paperwork removed	5	45	5	40
Product handling automated	15	60	15	55
Combined	25	80	25	65

50% (reducing the mean driving distance by 1.1 km for Supermarket A, and 2.2 km for Supermarket B) the number of deliveries completed in an 8 hour shift could increase by 80% for Supermarket A (from 20 to 36 deliveries) and by 65% for Supermarket B (from 20 to 33 deliveries).

In general, reducing the kerb time by any of the three scenarios presented has a greater impact proportionally on Supermarket A, compared to Supermarket B. This matches expectations since, as presented earlier, the shift length for Supermarket B is dominated by driving time over kerb time, as compared to Supermarket A.

3.2.5 Summary

Analysis of the home delivery system used by two supermarkets revealed the potential for increasing the capacity of the vehicles under certain conditions. The analysis showed that increasing the number of deliveries would lead to a high likelihood that the time taken to complete the delivery shift would exceed 8 hours. It was shown that by reducing the distance between deliveries by 50%, the number of deliveries which could be completed in under eight hours could be increased by 30% for both supermarkets. It was also shown that if the kerb time could be reduced by eliminating paperwork and automating the product handling so as to reduce the time spent packing and unpacking the van, this increase in capacity could be as much as 80% for Supermarket A, and 65% for Supermarket B, for the same reduction in driving distance.

Methods of achieving these reductions in driving distance were described. These were increasing the attractiveness of home delivery systems to consumers, such that the drop den-

sity increases as more houses in a given area require deliveries, and encouraging cooperation between supermarkets, such that each supermarket's vehicles cover a smaller area.

Additionally, comparisons were made between the two supermarkets for which data were collected. It was shown that the driving distances travelled by each supermarket were significantly different, and hypothesised that it could be due to the socio-economic profile of the customers at each supermarket. However, it was also shown that there was a difference between the length of time spent by each supermarket on certain components of the delivery task. It was suggested that Supermarket A could reduce the length of time spent at each delivery by adopting a more streamlined approach to unpacking goods from the back of the vehicle, and also by reducing the amount of time spent completing paperwork, to bring Supermarket A's kerb times into line with Supermarket B.

3.3 Case Study B: Refuse Collection Vehicle

The typical daily cycle of a refuse collection vehicle, as shown by Nicolaidis, contains periods of refuse collection, and periods of more sustained motion as the vehicle travels to the depot (either a landfill site or recycling centre) to be emptied once full [16]. The impact on this analysis is that there is only significant advantage in increasing the capacity of the vehicle if one or more trips to the depot can be eliminated.

Analysis of data collected by Nicolaidis in Cambridge showed that collection vehicles for domestic waste operate on a two-week cycle. Two distinct collection patterns were identified in the data:

- (i) **Single Trip:** The vehicle completed a single round trip taking on average 5.5 hours, leaving from and returning to the collection point.
- (ii) **Two Trips:** The vehicle completed two round trips, the first typically taking on average 4.3 hours, and the second taking on average 1.7 hours.

It is believed that the first of these patterns corresponds to a collection route where collections are widely spaced, and thus it takes longer to fill the vehicle. The second pattern corresponds to closely-spaced collections where the vehicle is quickly filled and must be emptied to continue collection. Four refuse collection vehicles were analysed across a single two week cycle. There were 41 days of data (Monday to Friday for two weeks for each of four vehicles, and one Saturday for a single vehicle), and a total of 70 trips. 17% of days were completed in a single trip, while the other 83% required a double trip. A second collection trip increases costs substantially for two reasons. First, there is a fuel cost (and

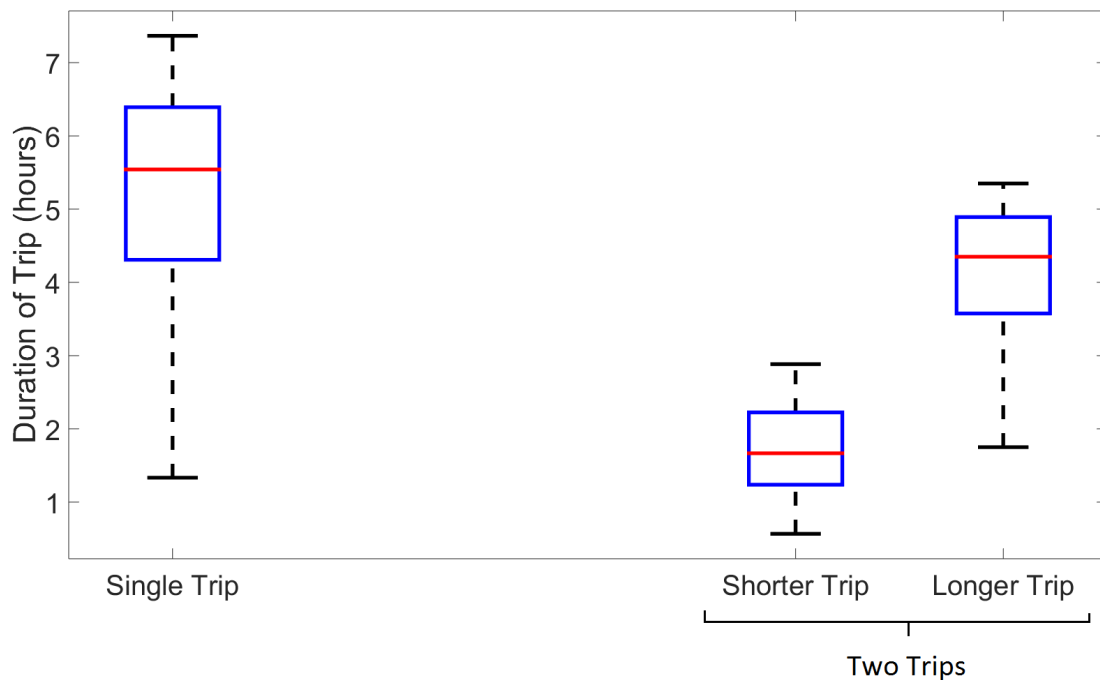


Fig. 3.23 Box and whisker plots showing the duration of refuse collection trip for different collection patterns

associated emissions) required by driving back to the depot to empty the vehicle between trips. Secondly, that journey (including the time taken to empty the vehicle) typically takes 60-90 minutes, which represents lost productivity.

Figure 3.23 shows box and whisker plots for the duration of collection trips. On days where the vehicle completed two trips, separate box plots are plotted for the shorter trip and the longer trip. There was no pattern to which of these trips was the first.

Without intervention to reduce the time taken for each collection or the time spent driving to and from the collection point, there is no benefit to increasing the size of vehicle on around 17% of collection routes (Pattern 1). However, for the 83% of days when the vehicle is following Pattern 2, fuel consumption and emissions could be reduced by completing both sets of collections in one trip, thus eliminating the cost of returning to the depot between trips. To increase collections from just the longer of the two trips (on average 4.3 hours) to both the longer and shorter trips combined (on average 6 hours) requires an increase in collection duration of 40%. If it is assumed that the vehicle fills at an approximately constant rate on these days, the percentage increase in required capacity to eliminate the second trip is the same as the required increase in the time the vehicle can collect for.

Therefore an increase in capacity of 40% would remove the requirement for the vehicle to return to the collection point during a shift, which is currently required on 83% of shifts. There is therefore a case for increasing capacity of Refuse Collection Vehicles in order to reduce emissions, provided the increase in capacity is at least 40%. The following chapters will assess whether an increase of vehicle capacity of this magnitude is feasible from the perspective of vehicle manoeuvrability.

3.4 Case Study C: Urban Store Vehicle

The vehicles used to restock city centre stores typically travel relatively large distances on the highway network to transport products from a regional or national distribution centre to the store in question. This means that to deliver to an additional store in the same city represents only a small proportional increase in driving distance and time, and so it can be assumed that driver shift length is not a limiting factor in assessing the suitability of higher capacity vehicles.

The key factor in this case is the relationship between the capacity of the vehicle, and the required capacity to service a given store. Urban stores tend not to have significant spare space for stock, thus stock is usually provided on a just-in-time basis. This means that the stock requirements for the store are effectively set by consumers, beyond the scope of this project. In practice this means that the vehicle must service a discrete number of stores, each of which will require a significant proportion of the vehicle's capacity (as opposed to home delivery vehicles, where adding an additional delivery requires only a small increase in capacity).

Analysis of this relationship would require modelling of an entire logistics system, which was considered beyond the scope of this project.

Chapter 4

Manoeuvrability Modelling: Methodology

4.1 Introduction

4.1.1 Overview

As argued in Chapter 1, one of the most effective ways to increase the efficiency of HGVs is to increase the capacity of vehicles. This reduces the number of vehicles on the roads, thus reducing congestion, noise, and both greenhouse and noxious emissions. The most significant impediment to increasing the capacity of HGVs is the penalty to manoeuvrability, and therefore the places that the vehicle can access.

Careful consideration is needed in the design of HGVs to ensure that they can complete the necessary manoeuvres required to reach their destinations, without damaging infrastructure, road furniture, or endangering other road users. The conventional approach to HGV design focuses on ‘steady-state’ manoeuvres, with little consideration for how vehicles manoeuvre in the real world. An example of this is the Performance-Based Standards approach (described in Chapter 7), which uses standardised simple manoeuvres to assess vehicles. A method is presented here to apply real-world context to the design of HGVs. The method can be generalised to be used for any set of design parameters, for example overall length, wheelbase, steering lock angle, width or height, but this work will focus on optimising vehicles for overall length and wheelbase only. All other parameters will be set by making practical assumptions, as described in this chapter. Throughout this thesis, ‘t’ or ‘tonnes’ will be used as a unit of mass, despite not being an SI unit, in line with industry standards.

This Chapter presents a method for design of HGVs. The kinematic and mass distribution models described in the following sections are used as standard in the industry: the most

significant novel contribution of this work is the graphical visualisation demonstrated in Section 4.6, which allows direct comparison between different vehicle configurations.

4.1.2 Conventional Approach

4.1.2.1 Rigid Vehicles

The most common approach to designing a two-axle, rigid HGV with unsteered rear axle, is to consider the steady-state turning circle. A maximum radius of turn can be defined, within which a vehicle must be able to pass. Figure 4.1 shows the geometry of a rigid vehicle in a constant radius turn. Given a fixed steering lock angle, δ_f , the outer turn radius, ρ_o , is governed only by the wheelbase, $(a + b)$, and the front overhang, d . Therefore the allowable outer turn radius puts an upper limit on the allowable wheelbase. The inside turn radius, ρ_i , is governed by the wheelbase, thus minimising the wheelbase is desirable also to minimise cut-in. Although both ρ_i and ρ_o are dictated by the wheelbase, the relationship between their acceptable values determines which controls the performance.

The remaining parameter, L , can then be set by considering the allowable axle loads. For a given wheelbase, the greater the value of L , the greater the total mass of the vehicle, and the greater the proportion of the load carried on the rear axle. Increasing the proportion of the vehicle mass carried by the rear axle increases the likelihood that the rear axle load limit is exceeded before the vehicles maximum volumetric capacity is filled, as the vehicle is loaded.

A common addition to this approach is to consider the transient phase of typical manoeuvres, for example a 90° turn. This is governed by the front and rear overhangs. The front overhang is considered fixed in this work, but the rear overhang, c , is dictated by the wheelbase and the total length according to

$$c = L - (a + b) - d \quad (4.1)$$

Provided $c < \frac{L}{2}$, in the steady state, the outer turn radius will always be governed by the front outside corner (Figure 4.1). However, in the transient part of the manoeuvre, the rear of the vehicle can swing out (known as tailswing), thus L must be chosen to give a value of c which limits tailswing to an acceptable value (the Road Vehicles (Construction and Use) Regulations, 1986 specifies this maximum value as 0.8 m for rigid vehicles [63]).

There is no UK legislation governing the choice of ρ_i and ρ_o for rigid vehicles specifically (although those used for articulated vehicles as described below provide lower and upper bounds respectively, since rigid vehicles must also conform to these). Suitable values must be estimated from road geometry.

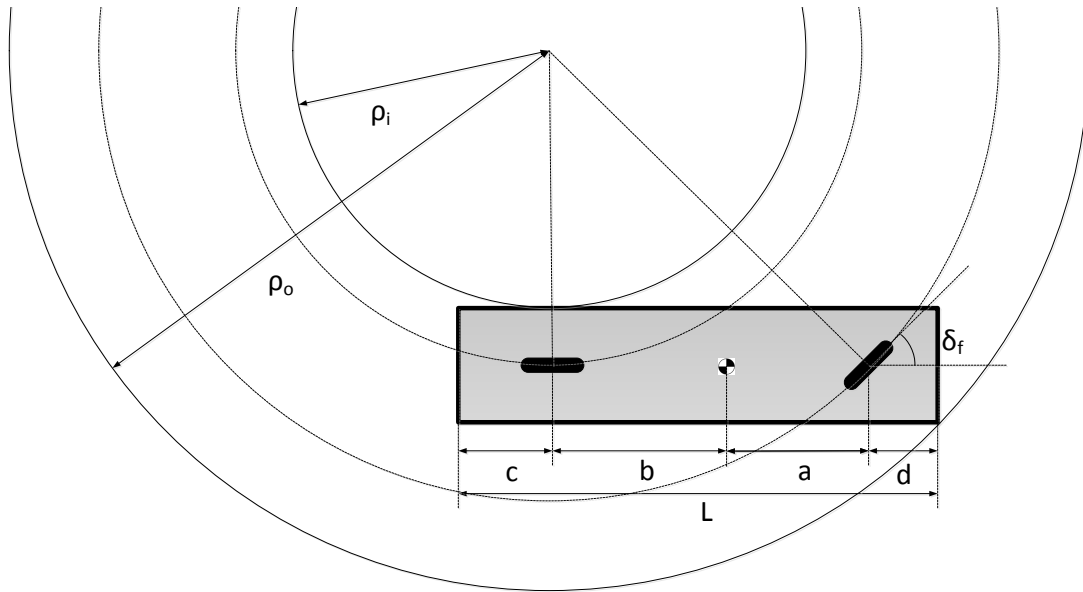


Fig. 4.1 Standard turning circle analysis of manoeuvrability for a rigid vehicle

There are no formal limits on the rear axle load for rigid vehicles, as the axle loads are not expected to exceed those generated by articulated vehicles, which are generally larger.

4.1.2.2 Articulated Vehicles

Figure 4.2 shows the equivalent construction for an articulated vehicle. In this case, ρ_o is still governed by the outside front corner, and thus is dictated by the wheelbase of the tractor unit, $(a_1 + b_1)$ (assuming d_1 and the front steering lock angle are fixed as above). This also has the effect of defining the path of the fifth wheel (assuming e_1 is fixed). With the path of the fifth wheel defined, the inner turn radius ρ_i is determined by the effective wheelbase of the trailer unit, $(a_2 + b_2)$. As for the rigid vehicle, the relationship between the allowable values of ρ_o and ρ_i determines which controls the performance.

As for the rigid vehicle, the second design parameter, L_2 is set by consideration of rear axle loads, under the caveat that the tailswing must again be limited to an acceptable value.

For articulated vehicles, European Council directive 97/27/EC governs the permitted values of ρ_o and ρ_i [146]. The standard roundabout test requires the vehicle to pass between an outer radius of 12.5 m and an inner radius of 5.3 m, with a tailswing on entry of less than 0.8 m.

The load limits on axles depend on the configuration of axles used. However, an upper bound on the design of articulated vehicles is a limit of 24 t across all three axles of a tri-axle

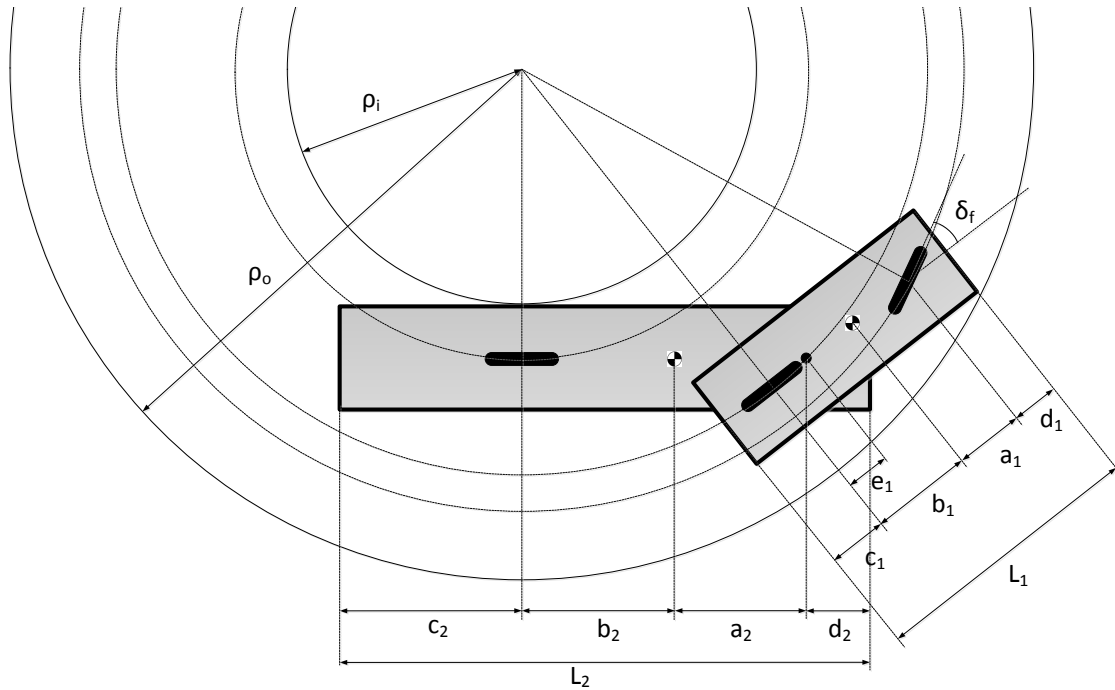


Fig. 4.2 Standard turning circle analysis of manoeuvrability for an articulated vehicle

group. Additionally, there is a limit of 11.5 t on the drive axle of a tractor unit, provided it has ‘road-friendly’ (air) suspension.

4.1.3 Alternative Approach

The above method does not take into account the complexity of real-world manoeuvres. An alternative approach is proposed for designing vehicles with maximised capacity, whereby vehicles are simulated attempting real-world manoeuvres, and scored according to their success. The stages of the method are as follows:

- (i) Collect route information (e.g. from in-service GPS data) from the class of vehicle to be considered (such as home delivery vehicles).
- (ii) Identify from the route information a library of the most difficult manoeuvres.
- (iii) Use satellite images to convert each manoeuvre into a set of constraints on the vehicle motion. The pavement kerbs should be identified, as well as limits such as lampposts or street furniture.
- (iv) Simulate a vehicle attempting each manoeuvre.

- (v) Vary the two design parameters L and $(a + b)$, select rigid or articulated vehicle and a rear axle steering strategy, and generate a chart that shows the percentage of manoeuvres that can be completed by a vehicle of given dimensions in a single pass (i.e. without reversing in mid-manoeuvre).
- (vi) Plot additional constraints on the chart such as axle load limits and infeasible vehicle configurations.
- (vii) Select the vehicle concept as the set of dimensions which maximises capacity without violating any constraints, and can complete at least the same percentage of manoeuvres as the existing vehicle.

4.1.3.1 Model Requirements

In order to implement this method, several simulation models are required. The design space for a freight vehicle is very large, with a wide range of different vehicle configurations to select from, each with a range of parameters to be optimised. For the scope of this investigation, several commonly used vehicle configurations were selected to be investigated, and the parameters to be set were chosen to match existing vehicles as closely as possible. A fleet operator or vehicle builder using this approach with a more specific end-goal in mind could use different vehicle configurations and optimisation parameters.






The configurations considered for each of the Case Studies from the previous chapters are listed in Table 4.1, and described in more detail in the following sections. For each configuration, a manoeuvrability model, and a mass distribution model are required.

Only rigid vehicles were considered for Case Study A, as the relatively small size of vehicles for this application made articulated vehicles unnecessary. Both Case Study B and Case Study C considered both rigid and articulated vehicles—the difference between the vehicles for the two case studies being the bin lifting and compacting equipment required at the rear of the vehicle for Case Study B. Different freight densities were used for all three case studies, as described in Section 4.5.

Existing vehicles matching the larger of these configurations would typically have 2 or more rear axles (on any of a rigid vehicle, a tractor unit or a trailer unit), but have been modelled with the rear axles combined into one equivalent axle, which is acceptable for manoeuvrability calculations.

The parameters to be optimised for the articulated vehicle (length and wheelbase) refer to the trailer.

Table 4.1 Vehicle configurations to be considered

(1)	Case Study A	Rigid	
(2)	Case Study B	Rigid	
(3)	Case Study B	Articulated	
(4)	Case Study C	Rigid	
(5)	Case Study C	Articulated	

4.2 Literature Review

This project will require simulations of vehicles attempting to complete manoeuvres. A brief review of different approaches to vehicle motion modelling was carried out, followed by an investigation into different approaches to improving manoeuvrability: rear-axle steering, torque vectoring, and torque-actuated axle steering.

4.2.1 Vehicle Models

4.2.1.1 Dynamic Modelling

Dynamic vehicle modelling is concerned with the equilibrium of forces acting on a vehicle. The main forces to consider are the weight, inertial forces, forces generated by the tyres, and any external forces such as aerodynamic forces [147]. The simplest approach to modelling yaw-plane motion of vehicles is the single-track or ‘bicycle’ model, by which all wheels on any one axle are considered as one equivalent wheel located on the centreline of the vehicle [148–152]. This approximation is particularly effective at low speeds, where roll characteristics are not important, but can be applicable at higher speeds if roll motion is expected to be small. Using a bicycle model removes the complexity of modelling steering linkages and considering Ackerman steering geometry [153], as well as the effects of roll-motion on high-speed dynamics.

4.2.1.2 Tyre Modelling

A dynamic vehicle model requires a method for modelling tyre forces. A number of different approaches are commonly used for modelling tyre characteristics for truck tyres. Two of the more detailed models are the Fancher model [154] which is based on a brush model with parameters based on physical properties, and the ‘Magic Formula’ [155] which is entirely empirical. The different models were compared by Eichberger and Schittenhelm [156]. Preliminary work with dynamic models for this project used the Fancher model to allow validation against work by Morrison [157].

4.2.1.3 Multi-body Modelling

An alternative method is to use a specialist multi-body simulation software package as described by Cheng [158] and in more detail by Blundell and Harty [159], which considers the motion of vehicle components such as wheels and chassis separately. This approach allows precise simulation, since all aspects of the vehicle motion are taken into account, with

very few simplifying assumptions. However, for low-speed applications where roll motion and lateral accelerations are small, sufficiently accurate simulations can be achieved with less complexity.

4.2.1.4 Kinematic Modelling

For low-speed applications, a kinematic vehicle model is often more simple than a dynamic model. These assume no slip between the wheels and the road, and use simple geometric arguments, derived in Section 4.3 to calculate the position of the vehicle for each time-step. A comparison between kinematic and dynamic simulation is provided by Rimmer [160]. Because the simulations in this project were at low speed, it was decided that a kinematic model would provide sufficient accuracy for very low computational cost.

4.2.2 Manoeuvrability Interventions

The following sections review the literature on possible methods for improving the manoeuvrability of vehicles.

4.2.2.1 Rear-axle steering

Steering the rear axle or axles of a vehicle can improve the vehicle's manoeuvrability, by shortening the effective wheelbase and therefore moving the turn centre closer to the side of the vehicle. It can also reduce tyre wear, by eliminating scrubbing from multi-axle groups. A comprehensive overview of the literature on trailer steering systems is presented by Jujnovich [161]. His work focussed on articulated vehicles but many of the principles described are relevant to both rigid and articulated vehicles. Jujnovich divided steering systems into two groups: passive systems and active systems. This work will focus on one particular strategy from each group: Command-Steer (for passive systems) and Path-Following steering (from active systems).

The disadvantage of rear axle steering is the increased cost of the steered rear axle, and the weight penalty due to the actuation hardware required (either mechanical linkages or hydraulic pumps, actuators, and accumulators).

4.2.2.2 Command-Steer

The Command-Steer strategy requires steering one or more of the rear vehicle axles in proportion to some reference angle. For articulated vehicles this is usually the articulation

angle (using the tractor steering angle was shown to be less effective by Lukowski and Fiedler [162]). For rigid vehicles the front steering angle is used.

This strategy is designed to minimise Swept Path Width in low-speed steady state cornering, but exhibits poor transient behaviour [163, 161]. In particular, because the front of the vehicle enters turns before the rear, the rear steering angle is applied before the rear of the vehicle reaches the turn. This leads to a phenomenon known as ‘tailswing’. Significant tailswing can lead to collisions with other road users or infrastructure. The main benefit of this strategy is that Command-Steer can be achieved with a mechanical linkage between the front and rear of the vehicle. This minimises cost and complexity [164].

The most common implementation of Command-Steer for rigid vehicles involves steering only the rear-most axles in a multi-axle group. This causes the effective rear axle position to move from the centre of the group to level with the front axle of the group. Therefore the vehicle behaves at low speed like a fixed rear axle vehicle with a shorter wheelbase. This does not cause such excessive tailswing as the full Command-Steer method, but also does not reduce the cut-in by as much. This strategy in this work will be known as Partial Command-Steer.

4.2.2.3 Path-Following Steering

To mitigate the problems with Command-Steer, Jujnovich proposed a Path-Following controller, in which a ‘follow point’ at the rear of the vehicle follows the path of a ‘lead point’ at the front of the vehicle for all manoeuvres and speeds. The control algorithm was based on matching the heading angle of the follow point to the heading angle of the lead point at the same distance down the path [165]. The controller was based on a simpler controller designed by Hata et al. [166]. Hata’s work focussed on rigid vehicles and was extended to articulated vehicles by Jujnovich. An alternative approach was developed by Cheng [158] who used a PID controller to guide the rear of the vehicle along the path of the front of the vehicle.

Some rear-axle steering algorithms can lead to instability at high speed [167]. However, it is possible to lock axles above a given speed threshold in order to eliminate this problem. Alternatively, the approaches adopted by Jujnovich and Cheng eliminate this problem by ensuring accurate path tracking and stability for all speeds.

4.2.2.4 Skid Steering

Skid steering refers to supplying more torque to the drive axles on one side of a vehicle than the other, thus generating a yaw moment [168]. The most common example is tracked

vehicles such as tanks. Kinematic models for skid-steered, wheeled robots are presented by Yi et al. [169], Zhang et al. [170], and Mandow et al. [171]. A similar model for tracked vehicles is described by Yi et al. [172].

A comparison between skid-steer and conventional Ackerman steering for heavy trucks by Maclaurin [173] showed that Ackerman-steered vehicles are usually understeered, whereas skid-steered vehicles are usually neutral or oversteered, and involve high power consumption. Work by Morales et al. investigates the modelling of frictional losses at low speeds for skid-steered, wheeled robots [174, 175].

Another consideration is tyre wear. Skid-steer causes the tyres to slip relative to the road, which causes wear, as well as increasing power consumption. Basic tyre wear characteristics are described by Grosch and Schallamach [176], and Schallamach and Turner [177].

The differential torque is usually applied by the drive systems, but can also be generated by braking. Boada et al. proposed a controller for distributing brake forces between the front wheels [178]. This improved the vehicle handling, although conventional steering was still required. Pusca et al. proposed the use of four electric motors to control all four wheels independently [179]. This method offered excellent manoeuvrability at the expense of power consumption.

Although it was initially proposed that application of skid steering could improve the manoeuvrability of heavy goods vehicles, review of the literature, and preliminary modelling work showed that this approach could generate only minor improvements to low-speed manoeuvrability, and came at the cost of increased tyre wear and energy consumption [180]. This approach was therefore discontinued in favour of rear axle steering.

4.2.2.5 Torque-Actuated Axle Steering

A less common approach to using differential torque to improve manoeuvrability is to fit a steering axle at the rear of the vehicle without actuation (either mechanical or computer-controlled hydraulics). The axle is locked at high speeds, but at low speeds the steering angle is controlled by applying differential torques to the wheels on opposite sides. This generates a steering moment. This strategy has been used to assist front axle steering in passenger cars, [181, 182], but control of the rear steering angle was not covered in the literature. In trailers this could be achieved by applying the brakes more on one side (although this would require a fast acting and highly controllable brake valve). With new developments in electric drive vehicles, this could also be achieved by using hub motors and directly controlling drive torques to the rear wheels.

This strategy has the benefits associated with actuated rear axle steering—improved manoeuvrability and reduced tyre wear—since the control strategy can be designed to match

any rear axle control strategy (for example Path-Following), without the weight penalty of requiring heavy hydraulic actuators to control the steering angle, instead using components already on the vehicle (hub motors or brake valves).

For the remainder of this thesis, it will be assumed that vehicles described as having steered rear axles can achieve the required steering angles using low-cost, low-weight methods such as torque-actuated axle steering, without directly considering the details of implementation.

4.3 Manoeuvrability Models

In order to simulate the vehicle attempting the library of manoeuvres, vehicle models were developed for both rigid and articulated vehicles. The rigid vehicle model was used to simulate vehicles (1), (2) and (4) from Table 4.1, and the articulated vehicle model was used for vehicles (3) and (5) from Table 4.1. The vehicle speed, U , was assumed to be low throughout this section of work, and the slip angles of the wheels assumed to be zero, thus a kinematic vehicle model could be used. The vehicle was treated as a single-track model, with the wheels located at the centre of their axles.

4.3.1 Rigid Vehicle

4.3.1.1 Model Assumptions

There are many parameters to be considered in the design of an HGV. In order to focus on the most significant results, the approach was simplified by fixing the values of a number of parameters and making certain design decisions. The rear axles were assumed to be capable of steering for the purposes of modelling the vehicles. The steering control strategies are defined in Section 4.4. The geometry of the rigid vehicle is shown in Figure 4.3, and the following assumptions were made:

- (i) The front overhang, d , was fixed at 1 m.
- (ii) The half-width of the vehicle, w , was fixed at 1 m.
- (iii) The front steering lock angle, $\delta_{f,max}$, was fixed at 40° .
- (iv) The rear steering lock angle for vehicles with rear steering, $\delta_{r,max}$, was fixed at 25° .

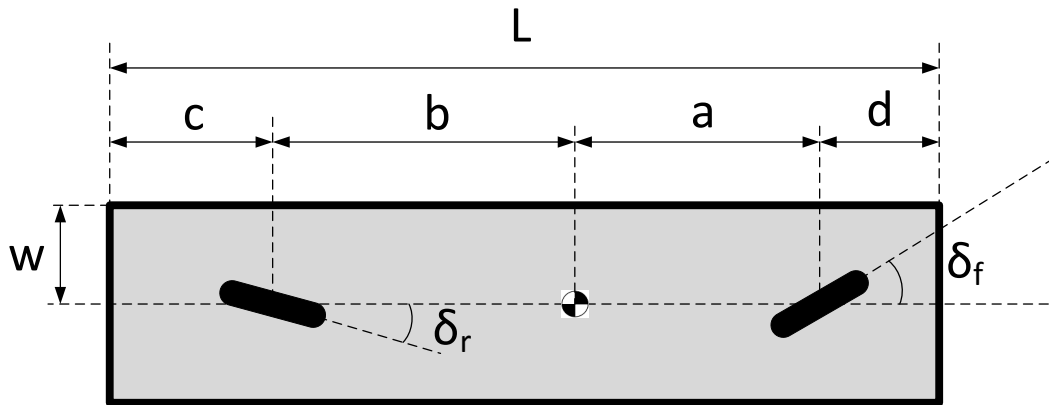


Fig. 4.3 Configuration of a rigid vehicle under certain design assumptions

These assumptions were based on the design of an existing Mercedes Sprinter 3.5 t home delivery vehicle. The vehicle was always treated as having a single rear axle. Although multi-axle groups are not uncommon on large, rigid HGVs, it was assumed that any multi-axle group could be considered as a single equivalent axle, with a load rating equal to the total load rating of the multi-axle group, and at a wheelbase equal to the effective wheelbase of the multi-axle group.

The parameters available to vary were:

1. The wheelbase, $(a + b)$.
2. The overall length of the vehicle, L .
3. The steering strategy of the rear axle (including 'unsteered').

4.3.1.2 Vehicle Model

At each time step, n , the heading angle, γ , of the lead point (the centre of the front axle) was determined from the vehicle yaw angle, ψ , and the front steering angle, δ_f , according to

$$\gamma = \psi + \delta_f \quad (4.2)$$

as shown in Figure 4.4, and the position of the lead point, (x_n, y_n) , was updated by moving a distance Δs in the direction γ , as shown in Figure 4.5.

$$x_n = x_{n-1} + \Delta s \cos \gamma_{n-1} \quad (4.3)$$

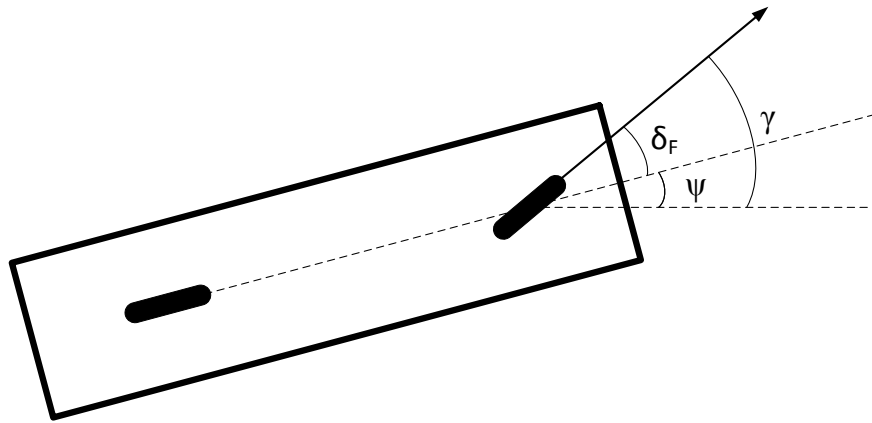


Fig. 4.4 Calculation of Heading Angle for a Rigid Vehicle

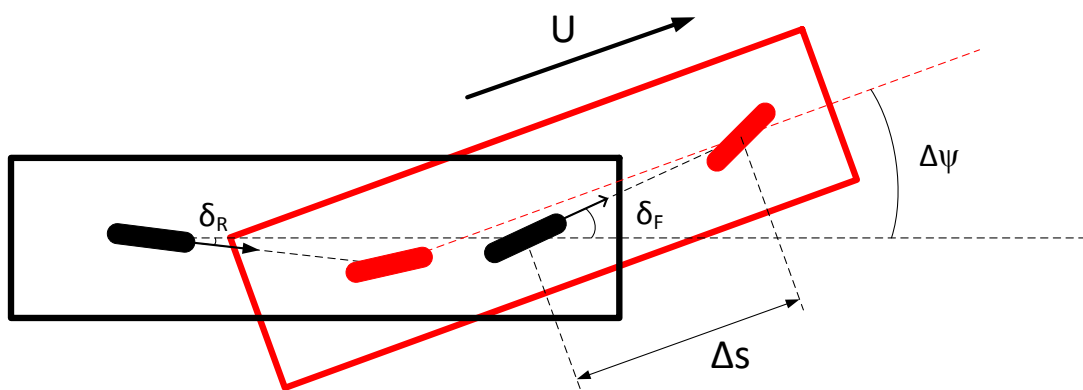


Fig. 4.5 Kinematic model of a rigid vehicle

$$y_n = y_{n-1} + \Delta s \sin \gamma_{n-1} \quad (4.4)$$

where Δs was calculated from the speed of the vehicle U and the time step Δt as

$$\Delta s = U \Delta t. \quad (4.5)$$

The change in yaw angle of the vehicle, $\Delta \psi$ was then calculated as a function of the front and rear steering angles and the wheelbase, according to

$$\Delta \psi = \Delta s \frac{\sin(\delta_f - \delta_r)}{(a + b) \cos \delta_r}. \quad (4.6)$$

δ_r was set to zero for the conventional vehicle without rear steering. The yaw angle was calculated by

$$\psi_n = \psi_{n-1} + \Delta \psi. \quad (4.7)$$

The state of the vehicle was fully defined by the position of the lead point and the yaw angle. The positions of the four corners of the vehicle were then calculated using the dimensions of the vehicle.

4.3.2 Articulated Vehicle

4.3.2.1 Model Assumptions

The assumptions made in the design of the articulated vehicle were similar to those for the rigid vehicle, as shown in Figure 4.6. The parameters of the tractor unit were set, and the corresponding parameters to the rigid vehicle design variables were the overall length and wheelbase of the trailer unit (taken as the distance between the rear axle and the fifth wheel).

1. The front overhang of both tractor and trailer units, d_1 and d_2 , were fixed at 1.5 m.
2. The half-width of both vehicle units, w , was fixed at 1 m.
3. The front steering lock angle, $\delta_{f,max}$, was fixed at 40° .
4. The steering lock angle on the trailer axle for vehicles with rear steering, $\delta_{r,max}$, was fixed at 25° .
5. The offset between the fifth wheel and the rear axle, e_1 , was fixed at 0 m.
6. The tractor wheelbase, $(a_1 + b_1)$, was fixed at 2.65 m.

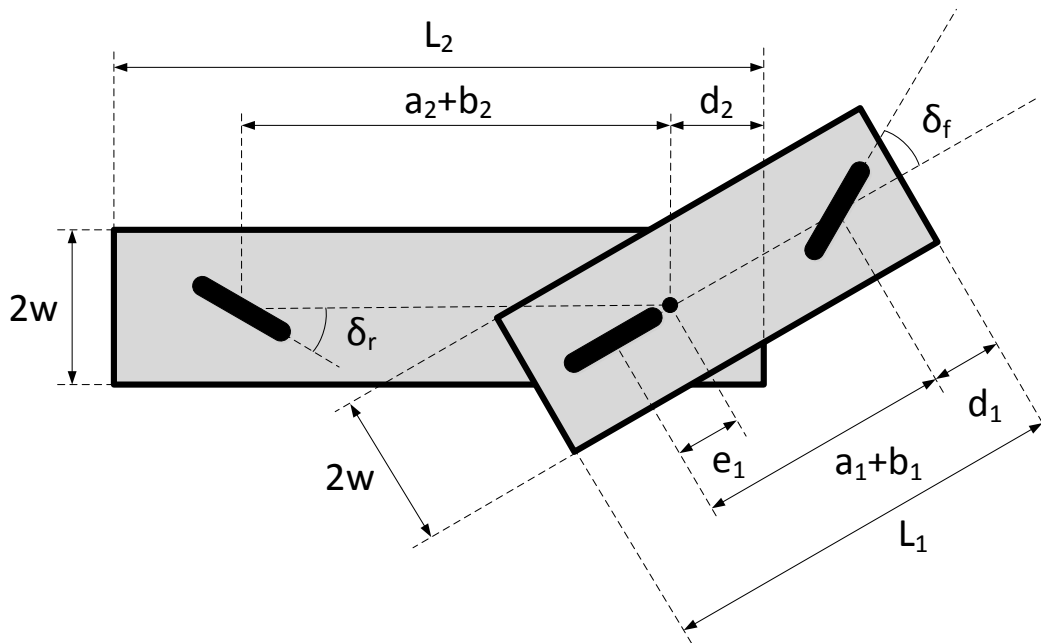


Fig. 4.6 Configuration of an articulated vehicle under certain design assumptions

7. The tractor length, L_1 , was fixed at 4.70 m.

These tractor parameters represent a Mercedes Antos urban tractor unit. As with the rigid vehicle, multi-axle groups on the trailer were always considered as a single equivalent axle. The half-width of the existing Mercedes vehicle is greater than 1 m. However, in order to allow direct comparison with the rigid vehicles, the same half-width was used.

The parameters available to vary were:

1. The trailer wheelbase, $(a_2 + b_2)$.
2. The overall length of the trailer, L_2 .
3. The steering strategy of the trailer axle (including 'unsteered').

4.3.2.2 Vehicle Model

The articulated vehicle was simulated by treating the tractor unit as a rigid vehicle and simulating it as described in Section 4.3.1, using the notation shown in Figure 4.6. The position of the fifth wheel was calculated from the states of the tractor unit and the geometry as

$$x_{FW} = x_{LP} - (a_1 + b_1 - e_1) \cos \psi_1 \quad (4.8)$$

$$y_{FW} = y_{LP} - (a_1 + b_1 - e_1) \sin \psi_1. \quad (4.9)$$

The heading angle of the fifth wheel to reach this new position, and the distance travelled were given by

$$\gamma_{FW,n} = \tan^{-1} \left[\frac{y_{FW,n} - y_{FW,n-1}}{x_{FW,n} - x_{FW,n-1}} \right] \quad (4.10)$$

$$\Delta s_{FW,n} = \sqrt{(x_{FW,n} - x_{FW,n-1})^2 + (y_{FW,n} - y_{FW,n-1})^2}. \quad (4.11)$$

The trailer unit was then treated as a second rigid vehicle, by taking the fifth wheel as the lead point, and using Equations 4.6 and 4.7 to update the trailer yaw angle, ψ_2 . The distance travelled by the lead point was $\Delta s_{FW,n}$, the wheelbase was the distance between the fifth wheel and the rear trailer axle, $(a_2 + b_2)$, and the front steering angle was given by

$$\delta_{f,2} = \gamma_{FW,n} - \psi_2. \quad (4.12)$$

4.4 Rear-axle Steering Systems

The simplest way to reduce the turning circle of a vehicle is to reduce its wheelbase, e.g. by moving the rear axle forward. This moves the centre of rotation forwards and closer to the side of the vehicle, reducing the radius of turn. However, moving the rear axle forward increases the proportion of the mass of the vehicle which is carried by the rear axles relative to the front axle, which reduces the load that can be carried without exceeding axle load limits, and reduces the normal loads on the front tyres, reducing their ability to provide lateral steering forces. Higher capacity axles are more expensive, and increasing the proportion of the total load carried by the rear axles increases the likelihood that the rear axle load limit will be exceeded before the vehicle is full. For these reasons, it is preferable to minimise increases in rear axle load.

An alternative method to improve manoeuvrability of a vehicle is to steer the rear axles as well as the front. This moves the effective wheelbase forwards along the vehicle without moving the real wheelbase. Therefore the load balance between front and rear axles is unchanged, but the vehicle benefits from the increased manoeuvrability of the shorter effective wheelbase.

The kinematic model described in the previous section takes a rear steering angle as one of its inputs. There are a number of different algorithms which could be used to select the rear steering angle.

4.4.1 Rear Unsteered

The rear steering angle could be set to zero at all times. This is the case for almost all existing small rigid commercial vehicles. This steering type will be referred to as ‘Rear Unsteered’ for this work.

4.4.2 Command-Steer

The rear steering angle can be made proportional to the front steering angle for a rigid vehicle, or to the articulation angle for an articulated vehicle. This approach is commonly used for large commercial vehicles with rear axle steering. The method is very simple to implement in articulated vehicles: the rear steering angle can be generated through a mechanical linkage or electro-hydraulic system, and the cut-in of the vehicle is reduced during steady-state manoeuvring, as intended. However, because the front of the vehicle turns in before the rear of the trailer has reached the turn, the rear steering angle is applied too early, causing increased tailswing. Importantly, the rear of the vehicle swings out into parts of the road that the front of the vehicle did not pass through that are in the driver’s blind spot, making manoeuvring through narrow obstacles difficult for drivers.

The Command-Steer gain can be set such that during the steady state, the ‘follow point’ (the centre of the rear bumper) follows the path of the lead point (centre of the front axle). For the rigid vehicle, this can be achieved by implementing the following:

$$\delta_r^{CS} = \tan^{-1} \frac{\left(\frac{a+b-c}{2}\right) \sin \delta_f}{\left(\frac{a+b+c}{2}\right) \cos \delta_f}. \quad (4.13)$$

This equations is commonly linearised to the form

$$\delta_r^{CS} = K^{CS} \delta_f \quad (4.14)$$

by assuming small angles, but this work allows for large steering angles, thus Equation 4.13 was used.

For the articulated vehicle, the corresponding equation is

$$\delta_r^{CS} = \tan^{-1} \frac{\left(\frac{a_2+b_2-c_2}{2}\right) \sin \Gamma}{\left(\frac{a_2+b_2+c_2}{2}\right) \cos \Gamma - a}. \quad (4.15)$$

It should be noted that the rear steering gain for articulated vehicles is calculated using the fifth wheel as the lead point. If the rear axle of the tractor unit is unsteered, the lead point will cut-in from the front axles of the tractor unit, but if the wheelbase of the tractor unit is short, this effect is small [164].

As described above, this steering strategy generates tailswing in the transient part of the manoeuvre. This can be significant, and is dependent on the position of the rear axle. The limit in the EU on tailswing is 0.8 m [146]. Therefore the Command-Steer gain for this work is limited to either the gain that would generate a tailswing at that limit, or the gain given in Equations 4.13 and 4.15, whichever is the least.

4.4.3 Partial Command-Steer

A variation on the Command-Steer method is commonly seen on large vehicles with a twin-axle group at the rear. Full Command-Steer as described above is rarely used on rigid vehicles due to the excessive tailswing it generates. Instead, the rear-most axle in the rear axle group is steered (in proportion to the front steering angle) while the other axle is left unsteered. This has the effect of moving the instantaneous centre of the turn forwards, until it is level with the unsteered axle. (For vehicles with no rear axle steering it is level with the middle of the axle group). This does not reduce the turning radius as much as the full Command-Steer method, but is still an improvement from the rear unsteered case, and does not have such a large effect on the tailswing.

The greatest impact of this method is not on the manoeuvrability of the vehicle, but on reducing tyre wear, which is high on vehicles with unsteered multi-axle groups as at least some of the axles in the group experience high slip.

The implementation of this algorithm is very simple, as the vehicle behaves exactly as a rigid vehicle with a single rear axle at the position of the front-most axle in the axle group of the original vehicle. Therefore the simulation model is the same as for the unsteered case, but with the wheelbase shortened.

4.4.4 Path-Following Steering

An alternative to Command-Steer is to steer the rear of the vehicle such that a 'follow point' at the rear of the vehicle follows the path of the 'lead point' (either the centre of the front

axle, or the fifth wheel) at all times. This is known as Path-Following steering. In practical systems this is done by using a vehicle model to calculate the heading of the lead point at all times, from the vehicle's speed and steering angle [165]. This is then stored in a buffer which is used as a lookup table to calculate the required heading angle of the follow point. The rear axle is steered to achieve this heading angle according to a geometric relationship between the rear overhang and the current yaw angle of the vehicle.

In the context of this work, the effect of Path-Following steering can be achieved more simply, by placing the rear of the vehicle on the intersection between the path of the lead point and an arc centred on the lead point, with length equal to the wheelbase, $(a + b)$. In some cases achieving this position of the follow point relative to the previous position of the follow point would imply saturation of the rear steering angle. In these cases, the new yaw angle of the vehicle is calculated by using the standard vehicle model, with full lock on the rear steering angle.

4.5 Mass Distribution Models

There is a compromise in the position of the rear axle, between optimising manoeuvrability and equalising the load distribution between the front and rear axles. Reducing the wheelbase improves manoeuvrability, as a vehicle with a short wheelbase will exhibit less cut-in. However, a simple force balance shows that placing the rear axle too far forward, towards the centre of the vehicle increases its axle load, as opposed to placing the rear axle further back, where the load is shared more equally. Increasing the rear axle load decreases payload capacity (because the vehicle is more likely to exceed the rear axle load limit before being full) and increases the cost of the required axle, hence the compromise.

In order to assess this compromise, simple mass distribution models of the vehicles were created, and calibrated using the plated axle weights of existing vehicles. This was then extended to calculate the axle weights for different vehicle dimensions, enabling contours of constant rear axle load to be plotted, to act as either a constraint or a guideline in the vehicle design.

Separate model parameters were required for all the vehicle configurations given in Table 4.1, because rigid and articulated vehicles required different models, and a different payload density was assumed for each case study. The models were calibrated using three existing vehicles: the Mercedes Sprinter van used for home delivery; a Refuse Collection Vehicle consisting of a Mercedes Eonic chassis, fitted with a Dennis Eagle Olympus body; and the Mercedes Antos Urban Tractor unit with a DSV curtain trailer (forming a standard 44 t articulated vehicle).

4.5.1 Rigid Vehicle

4.5.1.1 Standard Vehicle

The mass distribution model comprised 5 elements—two axles, the chassis, the engine and gearbox, and the payload. Each element was described by its mass and the position of its centre of mass, as shown in Figure 4.7. The vehicle mass was assumed to be evenly distributed through its width, i.e. only the longitudinal direction was considered. The masses of the 5 elements were denoted as follows: both axles were treated as having the same mass, $m_{a,1} = m_{a,2} = m_a$, the mass of the engine and gearbox was given by m_e , the mass of the chassis, m_c , was calculated from a fixed mass per unit length, q_c , multiplied by the length of the vehicle, L , and the mass of the payload, m_p , was calculated from the payload density, ρ_p , multiplied by the payload volume.

The other parameters were the position of the centre of mass of the engine and gearbox element relative to the front bumper, p_e , and the length of the cab, L_{cab} , from which the length of the payload section, $L_p = L - L_{cab}$, was derived. The payload volume was calculated as $2whL_p$, where w was the half-width of the vehicle, and h was an estimated height of the payload. It was assumed that the payload was evenly distributed such that the centre of mass of the payload was at its geometric centre, and the centre of mass of the chassis was at the centre of the vehicle. The distance of the front axle from the front bumper, d , was fixed at 1 m as described in the previous section. This combination of fixed parameters and assumptions allowed the vehicle to be completely defined by only its wheelbase and overall length.

The total mass of the vehicle was then given by

$$M = 2m_a + m_c + m_e + m_p \quad (4.16)$$

where $m_c = q_c L$, and $m_p = \rho_p 2whL_p$.

The front axle load was found by taking moments about the rear axle, and the rear axle load found from the difference between the vehicle weight and the front axle load. Both axle loads were then divided by the acceleration due to gravity to give the value in kilograms rather than Newtons.

$$R_f = \frac{\left[m_a (a + b) + m_e (a + b + d - p_e) + m_c \left(a + b + d - \frac{L}{2} \right) + m_p \left(a + b + d - L_{cab} - \frac{L_p}{2} \right) \right] g}{a + b} \quad (4.17)$$

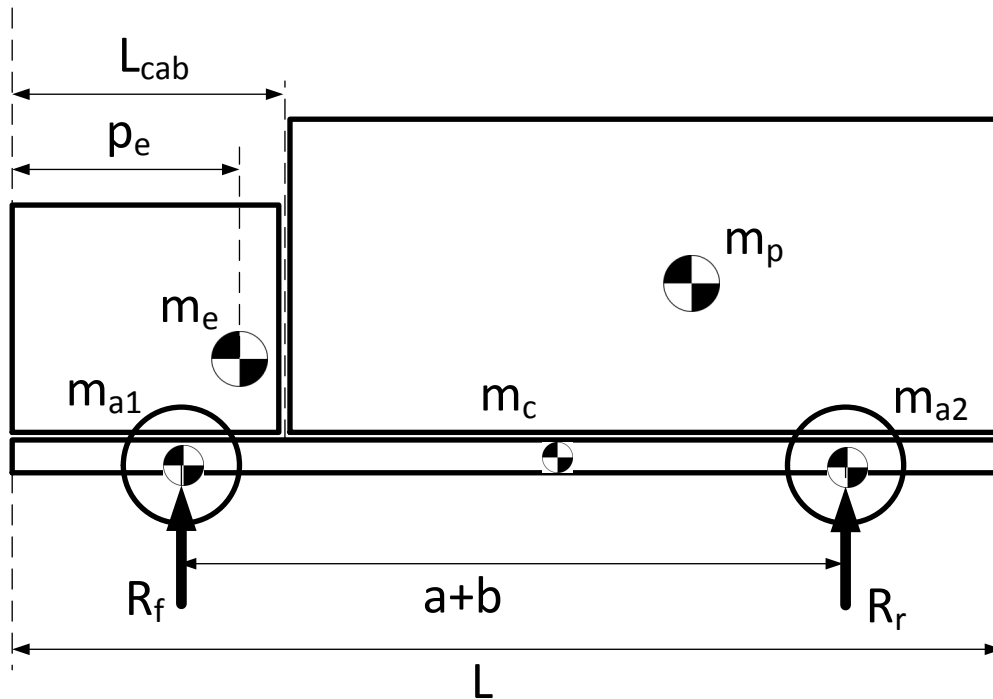


Fig. 4.7 Mass distribution model of a rigid vehicle

$$R_r = Mg - R_f \quad (4.18)$$

4.5.1.2 Refuse Vehicle

The Refuse Collection Vehicle is configured slightly differently to the standard home delivery vehicle in that it carries a significant amount of bin-lifting and rubbish-compacting equipment on the back. A separate load model was defined for this case, presented in Figure 4.8.

The additional parameters considered were the mass and length of the extra equipment, m_{equip} and L_{equip} . The length of the payload section in this case was given by $L_p = L - L_{cab} - L_{equip}$, and the equations for M and R_f included additional terms.

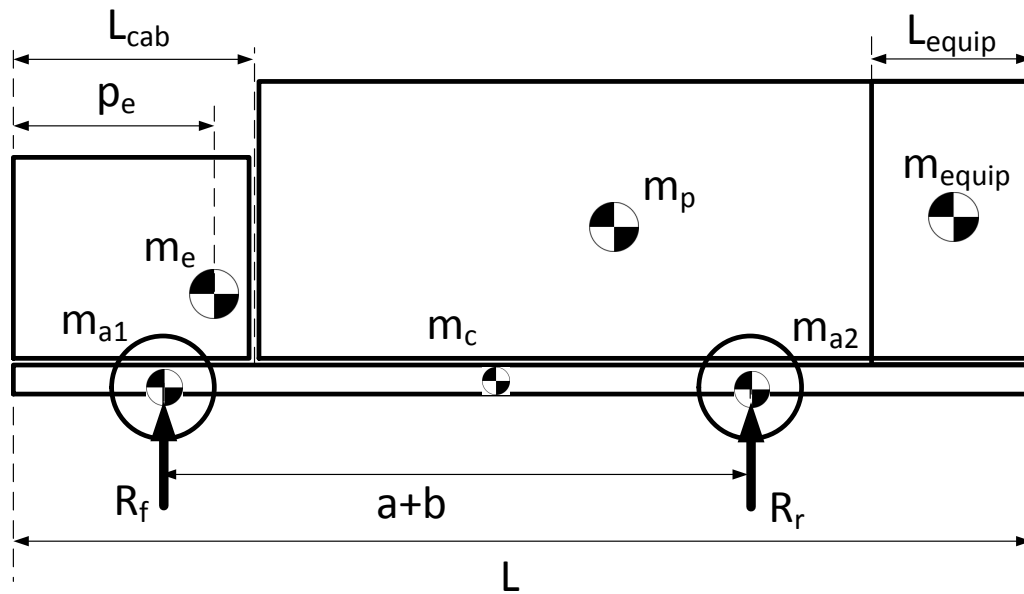


Fig. 4.8 Mass distribution model of a rigid refuse collection vehicle

4.5.2 Articulated Vehicle

4.5.2.1 Standard vehicle

The elements used for the corresponding model of an articulated vehicle are shown in Figure 4.9. The tractor unit was modelled as a 10 t rigid vehicle for the purposes of calculating the Gross Vehicle Weight. The loads on the tractor axles were not modelled, as the load on the trailer axle was assumed to be critical. The trailer was assumed to have a single axle. For a multi-axle group, both the mass of the axle units and the load carried by them were summed to be equivalent to a single axle unit positioned at the centre of the group.

Dimensions not shown on Figure 4.9 are as shown in Figure 4.6.

The trailer payload was given by $m_p = \rho_p 2whL_2$, and the masses of the chassis and axle are as defined in the same way as for the rigid vehicle, although different values were used, which will be set in Section 4.5.3. The load on the trailer axles, R_2 , was calculated by taking moments about the fifth wheel, given by the following equation:

$$R_2 = \frac{\left[m_c \left(\frac{L_2}{2} - d \right) + m_p \left(\frac{L_2}{2} - d \right) + m_a l_2 \right] g}{l_2}. \quad (4.19)$$

The Gross Vehicle Weight, M , was calculated according to

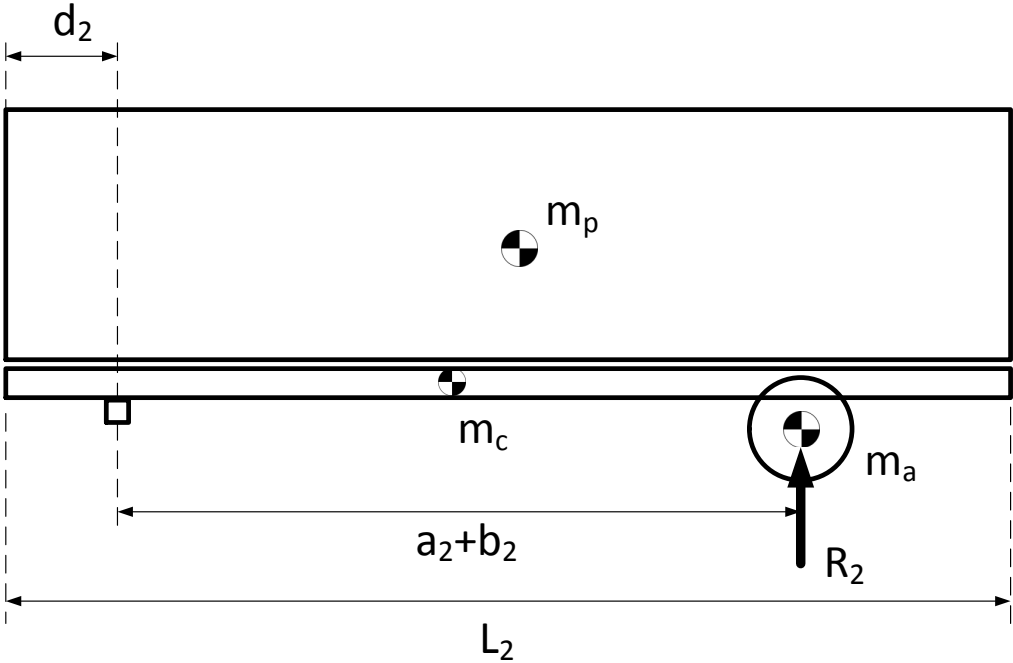


Fig. 4.9 Multi-body model of an articulated vehicle

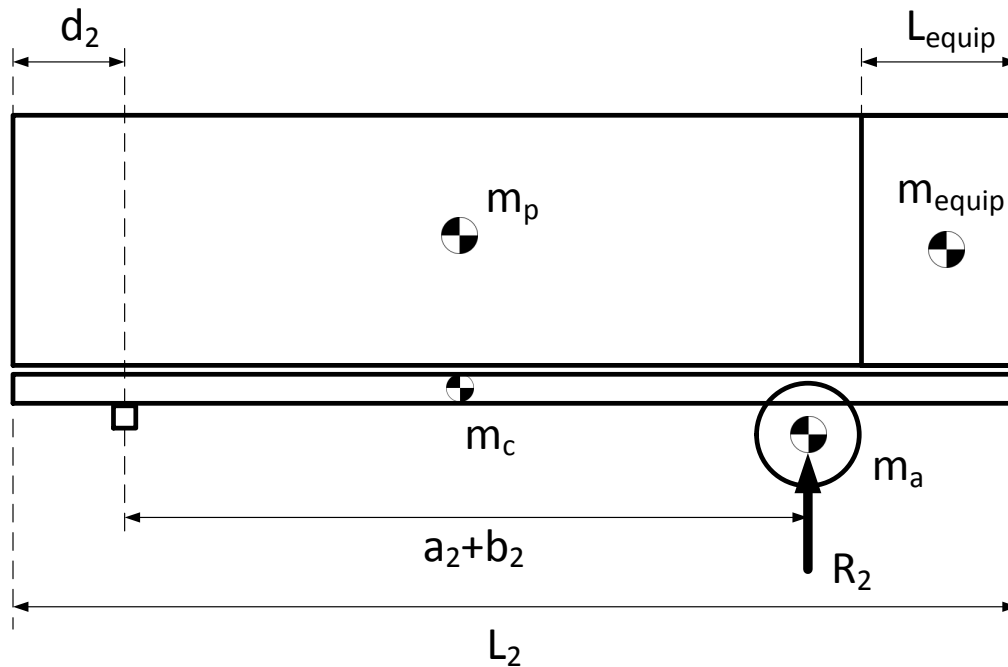


Fig. 4.10 Multi-body model of an articulated refuse vehicle

$$M = m_c + m_p + m_a + M_T \quad (4.20)$$

where M_T is the mass of the tractor unit.

4.5.2.2 Refuse Vehicle

As for the rigid vehicle, an articulated refuse truck model was developed, with the additional mass of the lifting and compacting equipment taken into account. This vehicle is shown in Figure 4.10.

4.5.3 Mass Distribution Model Calibration

The models described above were calibrated against three existing vehicles, to overcome the difficulty of estimating some parameters such as the average density of the chassis. Due to the simplicity of the models, some parameters do not precisely represent physical values, but were adjusted to ensure the best fit to known data. In particular the height, h , was used to represent the effective payload height, rather than the height of the cargo space of the vehicle.

4.5.3.1 Home Delivery Vehicle

A 3.5 t Mercedes Benz Sprinter van with a wheelbase, $(a + b)$, of 3.66 m, used by several home delivery operations, was used to validate the model. The following parameters were estimated:

$$p_e = 1.8 \text{ m}$$

$$L_{cab} = 2.5 \text{ m}$$

$$m_a = 300 \text{ kg}$$

$$m_e = 600 \text{ kg}$$

$$q_c = 206 \text{ kg m}^{-1}$$

$$h = 1.5 \text{ m}$$

$$\rho_p = 90 \text{ kg m}^{-3}$$

Additionally, the known wheelbase $(a + b) = 3.66 \text{ m}$, and vehicle length $L = 6.23 \text{ m}$ were used. The payload density of $\rho_p = 90 \text{ kg m}^{-3}$ was estimated to equate to the known maximum load capacity of 1000 kg.

Equations 4.16, 4.18, and 4.17 then yielded the following values:

$$M = 3.49 \text{ t}$$

$$R_r = 2.10 \text{ t}$$

These were required to match the fully loaded GVW of 3.5 t and the rated rear axle load for the calibration vehicle of 2.25 t. Both values were within 10% thus the model was considered sufficiently accurate. Differences between the plated values and the modelled values arise from the simplicity of the model. Using more model elements would increase accuracy but this was considered unnecessary for this application.

4.5.3.2 Refuse Vehicle

The refuse collection vehicle model was calibrated using a Mercedes Econic chassis, fitted with a Dennis Eagle Olympus body, with a total gross vehicle weight of 26 t. The following parameters were used:

$$p_e = 1.8 \text{ m}$$

$$L_{cab} = 2.5 \text{ m}$$

$$m_a = 300 \text{ kg}$$

$$m_e = 7000 \text{ kg}$$

$$q_c = 600 \text{ kg m}^{-1}$$

$$h = 1.5 \text{ m}$$

$$L_{equip} = 1.15 \text{ m}$$

$$m_{equip} = 200 \text{ kg}$$

$$\rho_p = 540 \text{ kg m}^{-3}$$

The effective wheelbase of the vehicle was $(a + b) = 4.72 \text{ m}$ and the total length was $L = 10.42 \text{ m}$. A payload density of 540 kg m^{-3} was used, as defined by Dennis Eagle. This model yielded a volumetric capacity of 20.3 m^3 , and a maximum payload of 11.0 t , compared to the manufacturers values of 21.4 m^3 and 11.6 t . The GVW and rear axle loads when fully loaded were 25.0 t and 18.8 t respectively, compared to the targets of 26 t and 19 t . All of these metrics were within 6% of the targets, therefore the model was considered to be sufficiently accurate without requiring more elements.

4.5.3.3 Standard Semi-Trailer

The third vehicle used for calibration was a fully loaded standard UK semi-trailer (a DSV curtain trailer) pulled by a Mercedes Antos urban tractor unit weighing 10 t . The following parameters were used:

$$m_a = 300 \text{ kg}$$

$$q_c = 220 \text{ kg m}^{-1}$$

$$h = 1.5 \text{ m}$$

$$\rho_p = 450 \text{ kg m}^{-3}$$

$$M_T = 10 \text{ t}$$

Additionally, the trailer wheelbase for the calibration vehicle was $(a_2 + b_2) = 7.60$ m and the total length was $L_2 = 13.6$ m. A payload density of 450 kg m^{-3} was used. This model yielded a maximum payload of 30.6 t, compared to the manufacturers values of 32.8 t. The GVW and trailer axle loads when fully loaded were 43.9 t and 23.7 t respectively, compared to the expected GVW of 44 t and the UK limit for load on a tri-axle group for a full loaded semi-trailer of 24 t.

4.6 Example Plot Construction

In order to validate the approach, a preliminary case was considered, using simple geometric arguments to assess the success or failure of the vehicle, instead of simulating an entire library of manoeuvres. The vehicles were assumed to have unsteered rear axles.

The parameter space to be searched was defined for rigid vehicles as wheelbases between 2 m and 14 m, and overall lengths between 3.5 m and 15 m. The legal limit on length for a rigid vehicle in the UK is 12 m but longer vehicles were considered in case of any future changes in legislation. Articulated vehicles were considered with trailer effective wheelbases from 2 m to 14 m, and trailer lengths between 6 m and 16 m. The limit in the UK on tractor and trailer combined is 16.5 m, which under the design assumptions about tractor size above corresponds to a limit on trailer length of 13.9 m, but again longer trailers were considered.

Four constraints were applied to the parameter space: a constraint on vehicle ‘feasibility’, a constraint on manoeuvrability, a constraint on axle loads, and a constraint on the Gross Vehicle Weight. The optimum design was then the selection of parameters which yields the highest capacity without violating any of the constraints.

4.6.1 Vehicle Feasibility Constraint

The parameter space was first restricted by discounting any vehicles for which the rear axle was at a position further aft than the length of the vehicle, as well as any vehicles where the rear axle was more than half the vehicle length away from the rear. These regions are shown in red in Figure 4.11.

4.6.2 Manoeuvrability Constraint

The second constraint on the parameter space is related to manoeuvrability. As described above, for validation of the method, the manoeuvrability constraint was determined by simple geometric arguments rather than the full simulation approach.

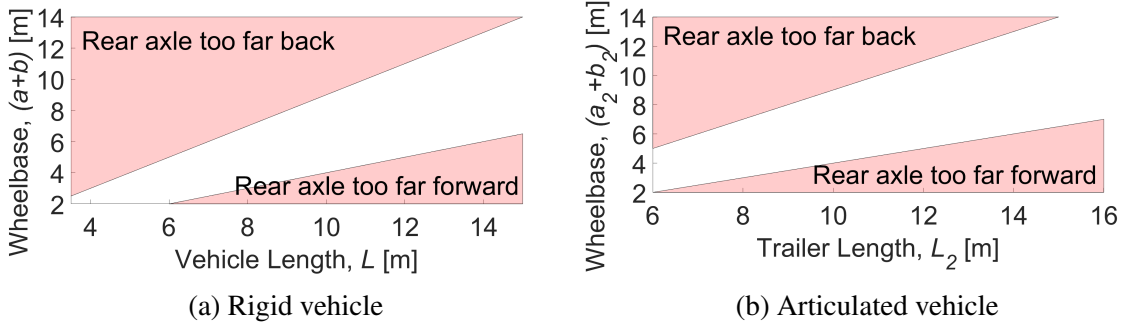


Fig. 4.11 Feasibility constraints

4.6.2.1 Rigid Vehicle

A single critical manoeuvre was determined for rigid vehicles by discussion with operators of home delivery vehicles for groceries, and the approximate dimensions extracted. The manoeuvre was a 90° turn, with an outer radius of 8.75 m, and an inner radius of 3 m. To be considered successful, the vehicle must be able to stay between these two radii in steady state cornering.

The steady state turn radius of the outside front corner for a rigid vehicle can be calculated by geometric arguments to be

$$\rho_{o,f} = \sqrt{(a+b+d)^2 + \left(\frac{(a+b)}{\tan \delta_f} + w \right)^2} \quad (4.21)$$

and similarly, the steady state turn radius of the outside rear corner is given by

$$\rho_{o,r} = \sqrt{c^2 + \left(\frac{(a+b)}{\tan \delta_f} + w \right)^2}. \quad (4.22)$$

The second of these equations will not be significant, because the critical point will always be the front corner in steady state, provided $c < \frac{L}{2}$, which is guaranteed according to section 4.6.1. Equation 4.21 can be rearranged to solve for the value of δ_f required to yield the maximum outer turning radius of 8.75 m. Any vehicle which required a steering angle greater than $\delta_{f,lock}$ was considered to have failed.

The inner turn radius, ρ_i , was then calculated for that wheelbase and steering angle, according to

$$\rho_i = \frac{(a+b)}{\tan \delta_f} - w \quad (4.23)$$

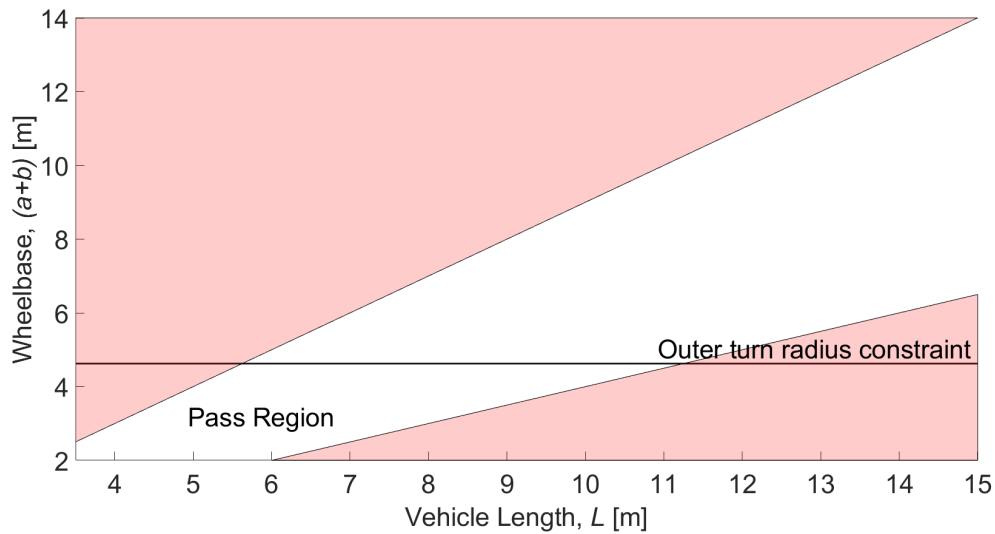


Fig. 4.12 Manoeuvrability constraint by geometric arguments for a rigid vehicle

and vehicles where ρ_i was less than the minimum value of 3 m were considered to have failed. All other vehicles, which could therefore achieve the required outer and inner radii without exceeding the steering lock angle were considered to have passed. Figure 4.12 shows the outer turn radius constraint separating successful vehicles from unsuccessful ones. The contour was horizontal, confirming that the vehicles success at the steady-state roundabout manoeuvre was determined by the wheelbase, and governed by the path of the outside corners.

For vehicles with a very large total length but a short wheelbase, the rear outside corner of the vehicle governed, rather than the front, so the overall length (or more specifically the length of the rear overhang) became important. However, in this region, the rear axle was forward of halfway along the vehicle, so this region was discounted as described in section 4.6.1.

4.6.2.2 Articulated Vehicle

For the articulated vehicle, the standard UK roundabout test [63] was used for defining the limiting radii, instead of the 8.75 m radius turn used for the rigid vehicles. To be considered successful the vehicle must be able to turn through 360° without exceeding an outer radius of 12.5 m, or an inner radius of 5.3 m.

The steady state turn radius of the outside front corner can be calculated as if the tractor unit were a rigid vehicle, thus equation 4.21 can be used, substituting rigid vehicle parameters for tractor parameters as follows:

$$\rho_{o,f} = \sqrt{(a_1 + b_1 + d_1)^2 + \left(\frac{(a_1 + b_1)}{\tan \delta_f} + w \right)^2}. \quad (4.24)$$

The dimensions of the tractor unit were kept constant for this analysis, therefore the steering angle required to achieve an outside turn radius of 12.5 m will be constant. Equation 4.24 yields $\delta_f = 16.2^\circ$ when rearranged. The outside rear corner of the tractor unit will not exceed the turning radius of the front for the reasons described above for rigid vehicles. The outside corners of the trailer can also be assumed not to exceed the turning radius of the front of the tractor because the trailer will cut in unless the rear overhang c_2 is unacceptably large.

For $\delta_f = 16.2^\circ$, the radius of curvature of the path of the fifth wheel is fully defined as

$$\rho_{FW} = \sqrt{e_1^2 + \left(\frac{(a_1 + b_1)}{\tan \delta_f} \right)^2} \quad (4.25)$$

which for the tractor unit used for this analysis yields $\rho_{FW} = 9.9$ m. As expected, for the articulated vehicle, the cut in of the tractor unit is small. The smallest radius of turn, ρ_i , is traced by the point level with the trailer axle on the inside of the vehicle, and can be calculated according to

$$\rho_i = \sqrt{\rho_{FW}^2 - (a_2 + b_2)^2} - w. \quad (4.26)$$

Any vehicles where ρ_i was less than 5.3 m was considered to have failed. Figure 4.13 shows the manoeuvrability constraints for the articulated vehicle. As expected the trailer wheelbase is the dominant factor, this time due to the cut in of the trailer axle.

The lower part of the constraint is caused by the tailswing of the vehicle causing the rear of the trailer to exceed the outer turning radius of the front corner of the tractor. As expected, this only happens when the rear axle of the trailer is forwards of the centre of the trailer, thus is already discounted.

4.6.3 Axle Load Constraint

4.6.3.1 Rigid Vehicle

The load distribution model described in Section 4.5 was used to calculate the rear axle loads at each point in the parameter space, assuming a constant load density equivalent to that typically carried by the home delivery vehicle. Instead of a fixed constraint, indicating an upper bound on the allowable rear axle load, contours of constant rear axle load were plotted, and the results shown in Figure 4.14. Contours of 2 t, 3 t, 4 t and 5 t were plotted, as well

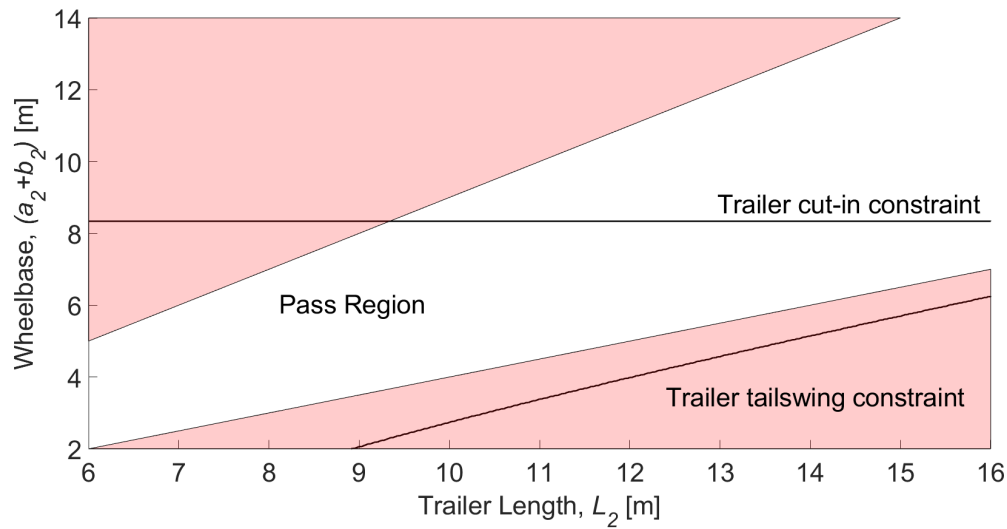


Fig. 4.13 Manoeuvrability constraint by geometric arguments for an articulated vehicle

as 2.25 t, which corresponds to the axle load rating of the baseline home delivery vehicle. Although the vehicle can be designed for any rear axle load, a higher load rating corresponds to a higher cost of the axle, and a reduced capacity.

4.6.3.2 Articulated Vehicle

Figure 4.15 shows the output from the load distribution model of the articulated vehicle. In the UK, the limit on axle load for a triaxle group is 24 t shared equally between the three axles. Therefore the 24 t contour forms a hard constraint. For smaller vehicles, the axle load contours are not hard constraints, but a higher axle load relates to higher likelihood of exceeding rear axle load limits without filling the vehicle, resulting in reduced payload capacity.

4.6.4 Gross Vehicle Weight Constraint

A final consideration was the Gross Vehicle Weight (GVW) of the vehicle. This was also calculated from the load distribution model, by summing the masses of all the components of the mass distribution model.

4.6.4.1 Rigid Vehicle

Contours of constant GVW were plotted, corresponding to common vehicle weights, specifically the standard 3.5 t home delivery van, the 4.25 t home delivery van, and a larger 7.5 t

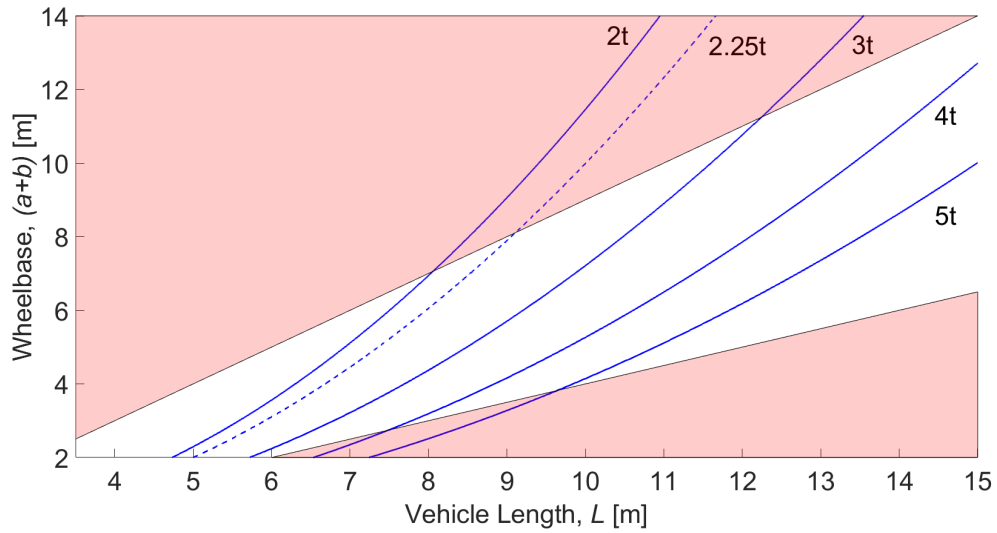


Fig. 4.14 Contours of constant rear axle load for a rigid vehicle with known payload density

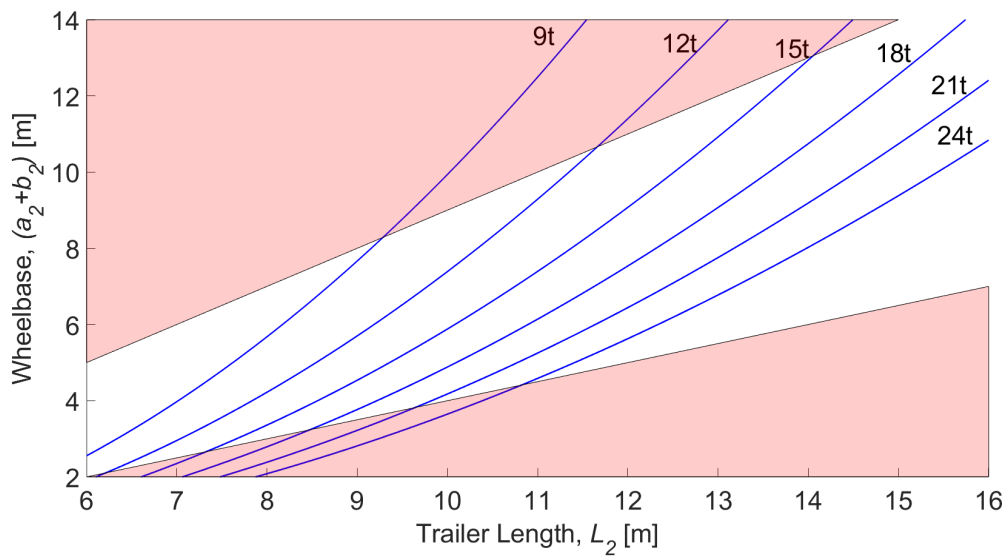


Fig. 4.15 Contours of constant trailer axle load for an articulated vehicle with known payload density

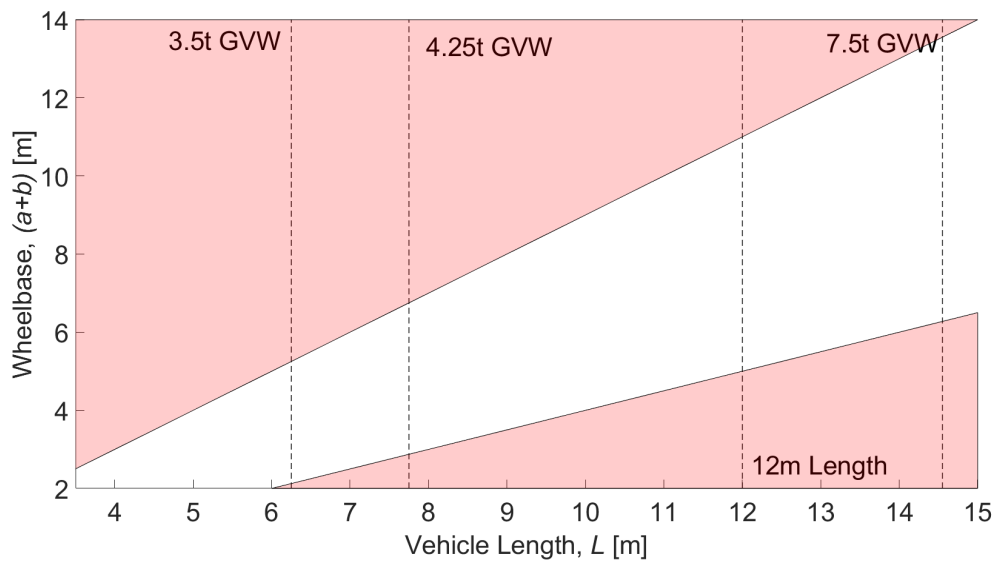


Fig. 4.16 Contours of constant Gross Vehicle Weight for a rigid vehicle

truck. These contours are shown in Figure 4.16. The UK limit on overall rigid vehicle length, 12 m is also shown.

A theoretical 7.5 t grocery delivery vehicle is also marked on the figure, at 14.6 m vehicle length. This is significantly longer than a conventional 7.5 t vehicle (which are typically less than 9 m long). This is because the density of groceries in the form carried by home delivery vehicles is low in comparison to the roll cages carried in larger vehicles. This demonstrates one of the difficulties involved in trying to use a significantly larger vehicle (such as a 7.5 t) for grocery delivery: a larger vehicle will exceed capacity limits well before exceeding load limits.

4.6.4.2 Articulated Vehicle

For the articulated vehicle, the GVW is less relevant, as the example HGV carrying groceries will almost always be volume-limited rather than weight-limited. For higher density freight, the 44 t limit would become relevant, as shown in the case studies considered in Chapter 6. A related constraint is the overall length of the vehicle, which varies only with L_2 under this model, as does GVW. Figure 4.17 shows constraints corresponding to a total vehicle length of 15.5 m and 16.5 m. The former can be broken if the vehicle is capable of completing the standard roundabout test as described above.

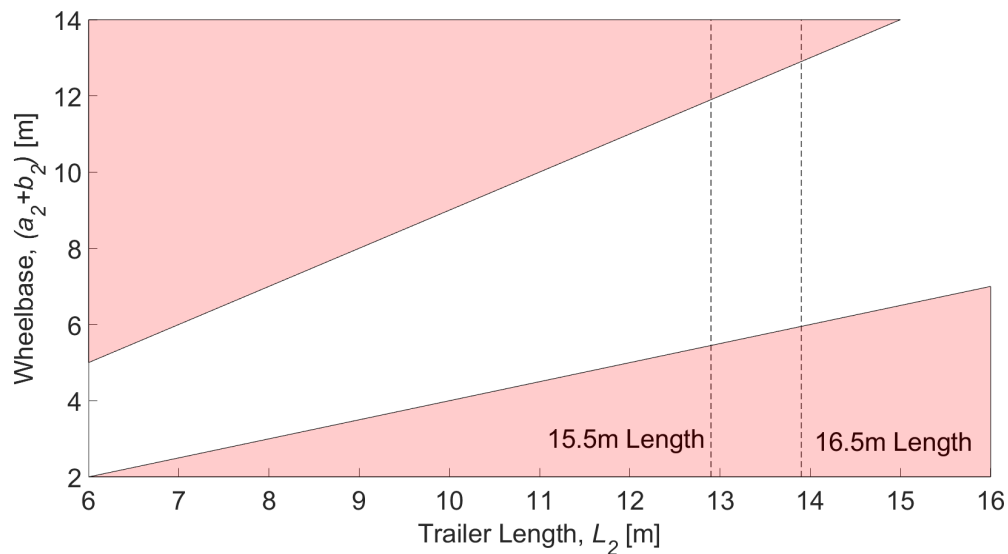


Fig. 4.17 Contours of constant total combination length for an articulated vehicle

4.6.5 Discussion

4.6.5.1 Rigid Vehicle

The set of constraints on the dimensions of the vehicle are shown all together in Figure 4.18. The dimensions of the existing home delivery vehicle are shown as a red circle at $L = 6.23$ m, $(a + b) = 3.67$ m. The design aim is to maximise the load capacity of the vehicle. For the model described in Section 4.5, this is achieved by maximising the length, L , regardless of the wheelbase. In other words, the operating point should be as far to the right of Figure 4.18 as possible without violating any constraints.

The figure shows that the current design of the vehicle appears to be a good compromise. The 3.5 t limit on the vehicle weight prevents larger vehicles from being used. This corresponds with anecdotal observations from drivers, who note that the vehicles are almost always weight-limited, rather than volume-limited.

One potential method for improvement is to raise the GVW. This would ordinarily cause the vehicle to fall into the category of HGV, requiring stricter and more expensive driver training and licensing, and tachograph equipment. However, new legislation aims to increase the definition of HGV from 3.5 t to 4.25 t [183], thus the vehicle length could be increased up to 7.75 m without requiring the costly switch to HGV licensing.

However, as Figure 4.18 shows, increasing L without changing the wheelbase $(a + b)$ causes the rear axle load to increase. In other words, as the rear axle moves forward on the vehicle, the proportion of the total load it carries compared to the front axle is increased.

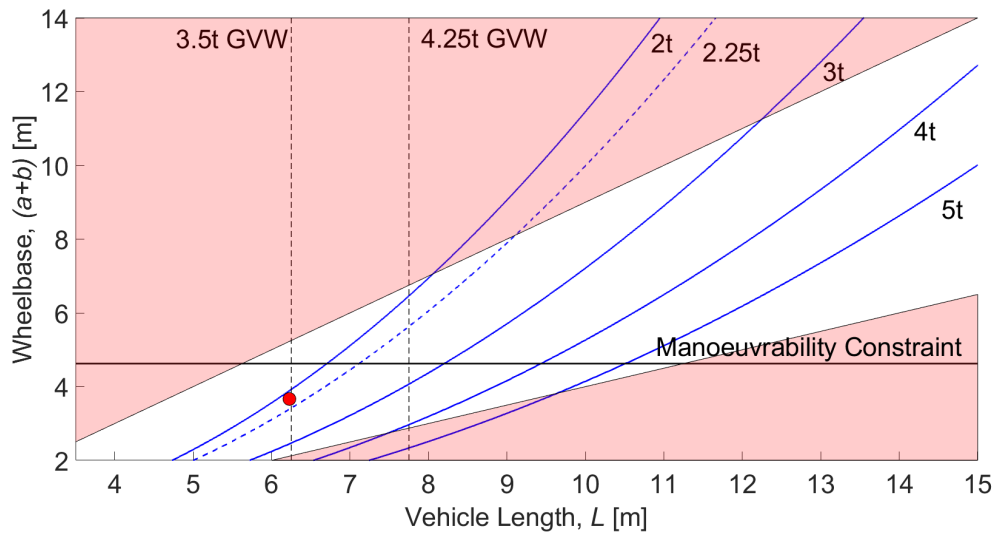


Fig. 4.18 Response of a rigid, unsteered vehicle to a steady-state roundabout manoeuvre, including load limits

Increasing L to 7.75 m would raise the rear axle load to approximately 3 t, exceeding the 2.25 t rating of the current axle. Heavier axles are more expensive, thus the movement up the contours of constant axle load is undesirable.

The alternative is to increase the wheelbase as the total length is increased, i.e. following the 2.25 t contour upwards. This avoids violating any of the load constraints, but would exceed the limit on manoeuvrability. This highlights the need for interventions to improve the manoeuvrability of large vehicles, such as rear axle steering, thus changing the shape of the manoeuvrability constraint. This is considered further in Chapter 6.

4.6.5.2 Articulated Vehicle

Similarly, the full set of constraints for the articulated vehicle are shown in Figure 4.19.

The figure shows that conventional articulated vehicles are close to the optimum dimensions for manoeuvrability, and for limiting trailer axle loads to 24 t. Increasing the capacity of conventional semi-trailers would require both relaxation of the 16.5 m maximum combination length, and either some intervention to decrease the rear axle loads (or increase the legal rear axle load limits), or to improve the manoeuvrability of the vehicle, such as trailer axle steering.

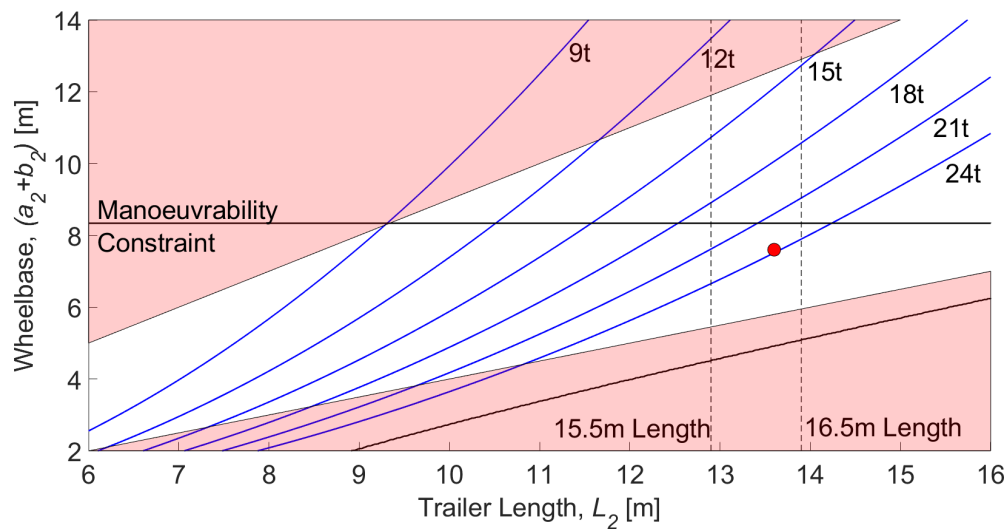


Fig. 4.19 Response of an articulated, unsteered vehicle to a steady-state roundabout manoeuvre, including load limits

4.6.5.3 Applicability of Results

The position of the manoeuvrability constraint in this example is determined by simple geometric analysis (based on a steady-state turning circle) so as to provide a suitable demonstration of the method. The purpose of the following chapter is to determine the position of the manoeuvrability constraint in a more realistic manner. This will affect the conclusions. In particular, as well as relating the parameters of the vehicle to the dimensions of its turning circle, the full approach to assessing manoeuvrability will need to take into account the transient part of the manoeuvre. In particular, tailswing in the entry to corners is likely to penalise vehicles with long rear overhang, i.e. those with high L and low $(a + b)$. This is expected to provide insight into the question of whether a full analysis of ‘real-world’ manoeuvrability is required, or whether the steady-state analysis is sufficient.

4.7 Conclusions

- (i) Kinematic models were developed for a rigid vehicle, allowing the movement of the vehicle to be simulated under the effect of a steering angle input. Models were developed for both rigid and articulated vehicles, and for several rear axle steering strategies, namely unsteered, Partial Command-Steered, Command-Steered, and Path-Following.

- (ii) Simple mass distribution models of both rigid and an articulated vehicles were developed, allowing estimation of the Gross Vehicle Weight, and rear axle loads, given an assumption about its payload density, and the vehicle dimensions. These models were calibrated against three existing vehicles, corresponding to the three case studies described in previous chapters.
- (iii) A parameter space was defined, where the vehicle overall length and vehicle wheelbase varied. The models described above were used to constrain the space, by limiting the Gross Vehicle Weight (or overall vehicle length in the case of the articulated vehicle), the rear axle load limit, and the steady-state turning ability of the vehicle by simple geometric arguments.
- (iv) Under this particular set of constraints, the capacity of an existing home delivery vehicle was found to be approximately optimised, although applying rear-axle steering to change the position of the manoeuvrability constraint would allow an increase in length and therefore capacity.
- (v) Increasing the GVW from 3.5 t to 4.25 t is essential for any increase in the capacity, as confirmed by fleet operators for home delivery of groceries. Increasing the axle load limits would allow greater capacity, but would require a more expensive axle for the same level of manoeuvrability.
- (vi) The capacity of the standard articulated vehicle cannot be increased without intervention to remove at least two of the constraints. As for the rigid vehicle, applying trailer steering would change the position of the manoeuvrability constraint, allowing greater volumetric capacity without increasing the load on the trailer axles.
- (vii) A more detailed investigation of the effect of the manoeuvrability constraint is required, to be pursued in the following chapter.

Chapter 5

Manoeuvrability Modelling: Algorithm Selection

5.1 Method and Limitations

The approach to designing HGVs described in the previous chapter requires a method for simulating the HGV attempting a series of manoeuvres. The simulation models are described in the previous chapter, but all require a method of route planning to dictate the path of the lead point. There are many route-planning methods described in the literature. However, most are intended for open scenarios, where many solutions exist and the search is for the most suitable. The problem described here is to investigate a very tightly constrained manoeuvre, and to identify whether or not a solution exists. The four algorithms investigated were: Rapidly-exploring Random Trees (RRT), Model Predictive Control (MPC), Single- and Multi-segment splines (SMS), and N Control Point splines (NCPS).

5.1.1 Method Overview

The aim of this Chapter was to locate a performance envelope in $(L, a + b)$ space separating vehicles which can, and vehicles which cannot complete a specific manoeuvre. Examples of this envelope are shown in Figure 5.1: the black region marks vehicles which were unsuccessful at the manoeuvre, while the white regions show vehicles which were successful. Discovery of the location of this envelope required simulating all vehicles in the parameter space attempting the manoeuvre using the vehicle models described in the previous chapter, assigning each a pass or fail result, and drawing an envelope around the successful vehicles. In order to speed up the search for the performance envelope, the values of L and $(a + b)$ for each simulation were selected by following particular rules, rather than searching all possible

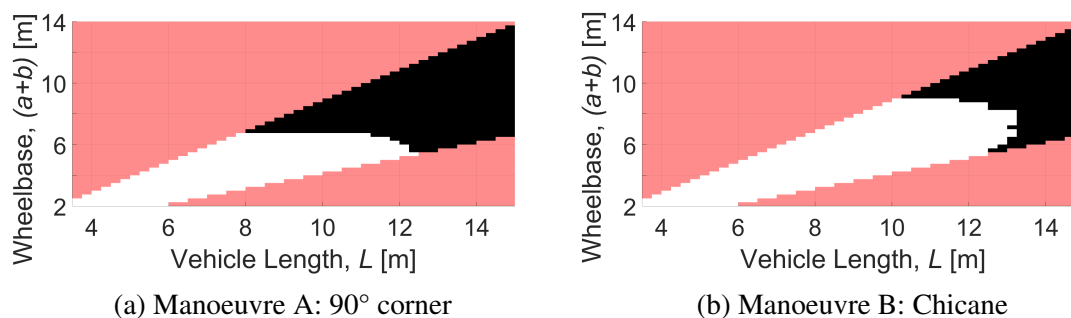


Fig. 5.1 Performance envelopes for the representative manoeuvres

values. It is clear that if a manoeuvre can be completed by a vehicle with a given wheelbase and length, any vehicle with the same wheelbase, but shorter overall length can complete the same manoeuvre. This means that for any vehicle which passes, all vehicles with the same $(a + b)$ but smaller L can also be judged to have passed. For every row of the plot (i.e. every value of $(a + b)$) the value of L was increased until the vehicle failed the manoeuvre. If the vehicle initially failed, the value of L was decreased until it passed. In this manner, the edge of the performance envelope at that value of $(a + b)$ was located. The edge of the performance envelope for the next value of $(a + b)$ was assumed to be at a similar value of L thus this was used as the starting point. Typically this reduced the number of vehicles to be simulated from several thousand to approximately one hundred (the exact number depended on the shape of the envelope).

The constraints on vehicle path for each manoeuvre were defined as described in the previous chapter, by manually drawing boundaries on satellite images. Equations for converting image coordinates to world coordinates are given in Section 5.3. Additionally, an example path was defined through each manoeuvre, by manually marking points on the manoeuvre, and joining them with splines. This was required for several of the simulation methods described below, but did not represent the optimal path through the manoeuvre, and it was not guaranteed that any vehicle would be able to follow the path without collisions with the boundaries.

The vehicles were then simulated attempting the manoeuvre. The path of the lead point was determined by one of the methods described below, and the path of the follow point was determined by the vehicle model (and rear steering controller), described in the previous chapter.

5.1.2 Limitations

In contrast to the way drivers would approach difficult manoeuvres in the real world, it was decided to remove the option of reversing—in other words the vehicle was only considered successful if it could complete the manoeuvre in one continuous forward motion. In the real world, drivers presented with an impossible manoeuvre would reverse to draw a cusp. However, had reversing been permitted, an upper limit on the number of reversing manoeuvres which were allowed would have been required to prevent vehicles passing by using a very large number of very small cusps (an option which a driver would not have the patience to do in the real world). Since this limit would have been arbitrarily decided, it was decided to set that limit to zero for the sake of limiting the complexity of the simulation.

It should also be noted that the definition of the manoeuvre constraints introduced errors. First the extraction of the constraints from the satellite images had a finite precision (approximated to be ± 3 pixels, corresponding to approximately 0.16 m). Second, the constraints made no distinction between ‘hard’ and ‘soft’ boundaries. An example of a ‘hard’ boundary would be a wall, which no part of the vehicle could cross. A ‘soft’ boundary would be a kerb, which the wheels could not cross, but the front and rear overhangs could. In this work, all constraints were considered ‘hard’. The lack of distinction in the definition of the constraints is not a significant issue, since the intended use for the method is to compare vehicles. Provided both vehicles to be compared are to be judged by the same criteria, the difference between the two types of constraint is not important.

5.1.3 Algorithm Assessment Criteria

In order to assess the success of the algorithms described below, with the aim of selecting the most suitable, two representative manoeuvres (A and B) were identified. These were a 90° corner, and a chicane. These manoeuvres were selected by inspection of a set of manoeuvres identified as difficult by local drivers. Measurements were taken of road widths and offsets to match the representative manoeuvres to typical real manoeuvres. However, the representative manoeuvres were constructed manually from straight lines rather than using real world manoeuvres, so as to minimise noise in the results and make them more predictable. The representative manoeuvres are shown in Figure 5.2, including potential points of collision with the constraints.

The ‘ground truth’ for the performance envelope was not known. Therefore, an approximation was found by manually driving simulated vehicles of different sizes around the manoeuvres, by directly controlling the steering angle. Although this did not give provably the exact location of the complete performance envelope, enough attempts were made to

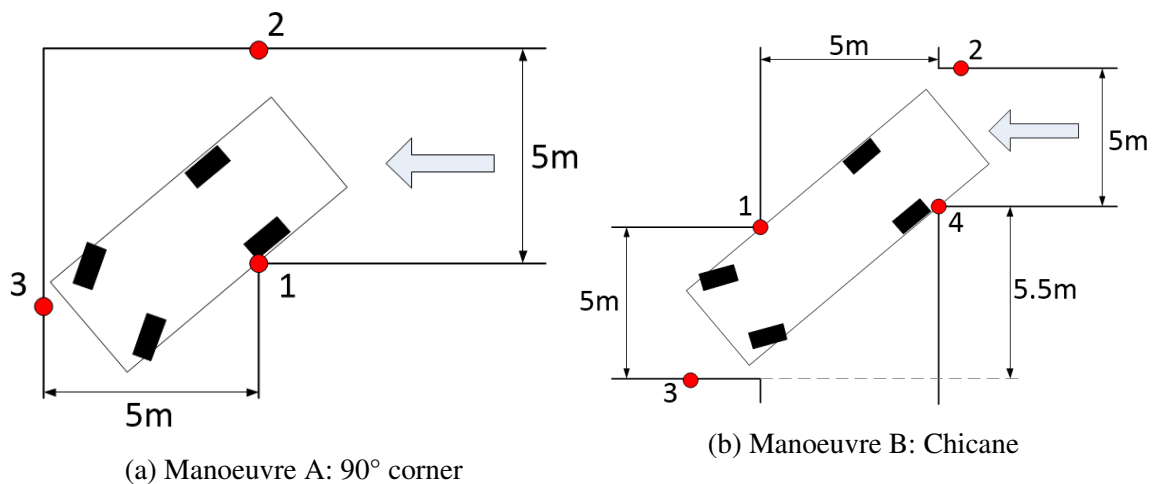


Fig. 5.2 Representative manoeuvres used for assessing path-planning algorithms

allow conviction that the envelope was sufficiently accurate. The score for each simulation algorithm was then given as the difference in area between the performance envelope output by the algorithm and the manually approximated performance envelope. The completed envelopes for the two representative manoeuvres are shown in Figure 5.1. The white region shows successful vehicles, while the black shows failed vehicles. The red regions represent infeasible vehicles, as described in Section 4.6.1.

Both plots show a clear maximum wheelbase, across a range of vehicle lengths. This suggests that for both manoeuvres, the critical performance condition is the cut-in (collision at point 1 from Figure 5.2), rather than the tailswing (collision at point 2 for manoeuvre A, or point 2 or 4 for manoeuvre B). This may be a result of the choice of manoeuvres, both of which consist of sharp corners, with few obstructions on the outside of the turn to penalise tailswing. For manoeuvre A, for example, an obstruction such as a parked car at point 2 would shift the required balance back towards minimising tailswing.

However, manoeuvre B also shows a clear maximum length, for a range of wheelbases. The implication is that manoeuvre B also penalises tailswing, although to a lesser extent than cut-in. This is supported by inspection of Figure 5.2b for which the second part of the manoeuvre (the left-hand steering after crossing the centre) is obstructed by a second potential collision at point 4.

This analysis supports the argument for the necessity of this work. Although conclusions can be drawn from the representative manoeuvres about the feasible dimensions for vehicles required to complete them, those conclusions can be quickly invalidated by relatively small changes in the shape of the manoeuvre, for instance the additional obstacle of a parked car, or street furniture such as bollards.

The calculations were timed, to ensure that they could generate a full set of results across all vehicles and all manoeuvres in a reasonable amount of time. In practice, all of the algorithms could generate a full map of all manoeuvres for a single vehicle type on a standard desktop computer¹ in under 12 hours of elapsed time, and so were considered acceptable.

5.2 Literature Review

It would be impractical to manually define the optimum path through every manoeuvre for every vehicle, thus a path-planning strategy is required. An alternative approach would be to treat route planning as a control problem, and try to optimise the vehicle's direction at every step, thus a review of both approaches is presented here.

The problem of finding a path through an environment from a start to a goal configuration is well researched for a number of applications. Vehicle path planning methods are important in the field of driverless cars [184], and driver assistance systems such as automatic parking [185]. Path planning is important for mobile robots, such as factory pickers [186], and also for applications such as manipulator arms, which are required to move to a goal configuration efficiently and without collisions [187]. An overview of path-planning concepts is presented by Rimmer [160].

For this work, it was assumed that the motion planning algorithm had perfect information about the constraints on the manoeuvre being attempted. This removed the need for any kind of sensor simulation to imitate detecting the environment. Additionally, there was no requirement for the vehicle to take the most efficient path through the manoeuvre, so algorithms which dedicate computation resources to finding the optimum path were not considered.

The idea of proving the existence of a feasible path is more difficult than finding the optimum path if one exists. Most path planning algorithms explore the search space but cannot be proved to have evaluated every possibility. There is little in the literature to document approaches to proving the existence of a feasible path. Several promising approaches are listed below, with a brief overview of the relevant literature.

5.2.1 Rapidly-exploring Random Trees

The 'Rapidly Exploring Random Trees' approach was presented by LaValle [188]. Points are randomly sampled from the search space, and added to the tree if a feasible path can be found from the randomly sampled point to the nearest node of the tree. Once the tree includes

¹Windows 8 64-bit, Intel i7-4790 3.6GHz processor, with 8GB of RAM

the goal configuration, a path is traced along branches of the tree (using an optimisation algorithm if required). This method can be very fast, but random, so there is no guarantee of an optimal path without using a second, optimisation stage [160]. Methods for biasing the random selection of points are described by Urmson et al. [189].

Use of the RRT algorithm for vehicle path planning is widespread, but requires constraints on the branches of the tree due to the non-holonomic vehicle property [190]. Kuwata et al. described the alterations to the RRT algorithm required to make it applicable to non-holonomic wheeled vehicles [191]. A dynamic path planner was presented by Pepy et al. [192].

5.2.2 Model Predictive Control

Model Predictive Control (MPC) is a control scheme intended to “optimize, over the manipulable inputs, forecasts of process behavior”, according to a tutorial overview provided by Rawlings [193]. Reviews of MPC technology appear regularly, such as [194, 195]. Model Predictive Control has been used on vehicles for several applications including stability control [196], energy management strategies [197], and obstacle avoidance for autonomous vehicles [198]. The latter paper presents a local path planner for obstacle avoidance.

5.2.3 Spline-Based Methods

Dubins demonstrated the use of straight lines and arcs to make up longer paths [199]. Although Dubins’ work was later extended, the discontinuities in gradient between segments are a common feature in the output of global path planning algorithms [200]. These discontinuities increase the travel time, because the vehicle has to stop and turn. Lau et al. proposed a controller designed to minimise the time taken to traverse a route, by generating smooth spline segments [200]. A similar approach was used by Shiller et al. [201]. Likhachev and Ferguson used the idea of a motion primitive—a short segment of path which could be simply defined, such as a straight line, or an arc—to generate longer routes made up of sets of motion primitives [202]. Lecture notes by Cipolla give an overview of working with splines [203]. Rimmer combined motion primitives to develop paths for reversing of long combination vehicles [160].

5.2.4 Geometric Proofs

The ‘Piano Mover’s’ problem is to find a path for a polygon (in two dimensions) from a starting configuration to a goal configuration [204]. This problem is constrained by the

presence of obstacles between start and goal configurations, and in the case of a road vehicle, by the non-holonomic property. An attempt at a general solution was presented by Canny using Voronoi diagrams [205].

Basch et al. attempted to disprove the existence of a feasible path [206]. The method was to look for simple proofs of when the motion planning problem is ‘clearly impossible’. However, this effectively generates a lower bound on impossible solutions, rather than the truly critical case. The authors state that the method is unsuitable for borderline cases.

Vasseur et al. used a set of connected, convex polygons to attempt to prove the existence of a path [207]. At the entry position to each polygon, motion primitives were defined to show the possible configurations at exit of that polygon, and continuity enforced across polygons. This was shown to be successful in relatively unconstrained environments, but was less successful in more complex environments where the number of polygons required for all polygons to be convex was high, and therefore the size of polygons was low.

No comprehensive proof of the non-existence of a path between two configurations for a car-like vehicle was found in the literature.

5.3 Coordinate Conversion

The set of constraints extracted from the satellite image were initially in an image-based coordinate system, (u, v) . The scale factor of the image λ , from pixels to meters was extracted from the image using a scale bar visible in the image and used with the height of the image in pixels, H , to convert the constraint data into a world-based coordinate system, (x, y) , according to

$$x = u\lambda \quad (5.1)$$

$$y = (h - v)\lambda \quad (5.2)$$

in which all calculations were performed.

5.4 Rapidly-exploring Random Trees (RRT)

The Rapidly-exploring Random Trees (RRT) algorithm is a method for quickly finding a path from a start to a goal configuration [188]. A ‘tree’ is grown from the start configuration, expanding into unexplored space until it reaches the goal. Branches of the tree represent possible motion of the vehicle (Figure 5.3). The algorithm has two significant features. First, the tree expands preferentially into the largest unexplored regions of space, thus assisting

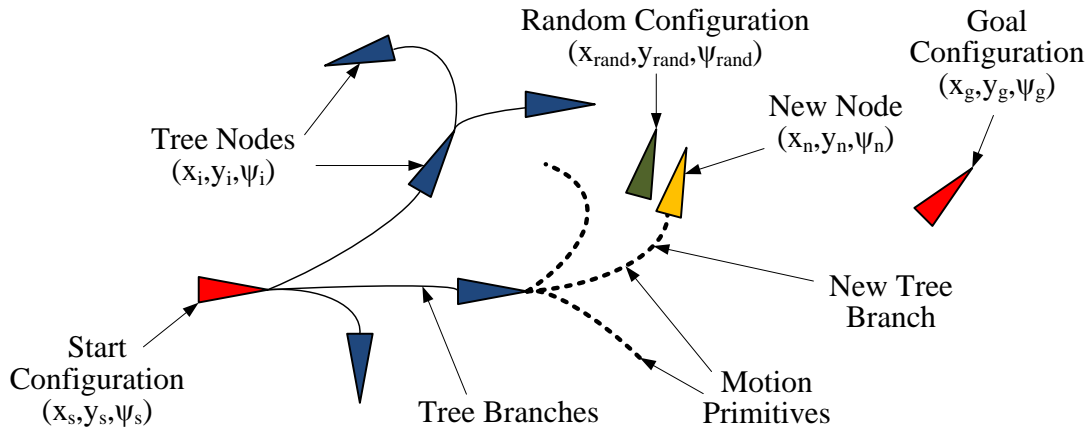


Fig. 5.3 Illustration of the RRT algorithm

faster convergence. Second, although the algorithm cannot provide proof that a solution does not exist, if run for a sufficiently long time, the tree will tend towards covering the entire search space, thus ensuring that a solution will be found, if one exists.

5.4.1 Method

The aim of the standard RRT algorithm is to construct a tree from a start configuration, (x_s, y_s, ψ_s) , to a goal configuration, (x_g, y_g, ψ_g) , via node configurations, connected by branches. The algorithm consists of four steps, which are discussed in the following sections, and illustrated in Figure 5.3:

Select a random configuration, $(x_{rand}, y_{rand}, \psi_{rand})$, from the search space. The standard RRT algorithm selects a random value for all three states of the vehicle: the position, (x, y) , of the lead point and the yaw angle, ψ , of the vehicle, $(x_{rand}, y_{rand}, \psi_{rand})$.

The tree was biased to grow towards the goal configuration, to improve the convergence time, by applying a 10% probability that the randomly selected configuration would be the goal configuration.

Find the closest node of the tree, (x_i, y_i, ψ_i) , to the random configuration. All nodes, (x_i, y_i, ψ_i) , in the current tree were awarded a score, H_i , based on their proximity to the randomly selected node, according to

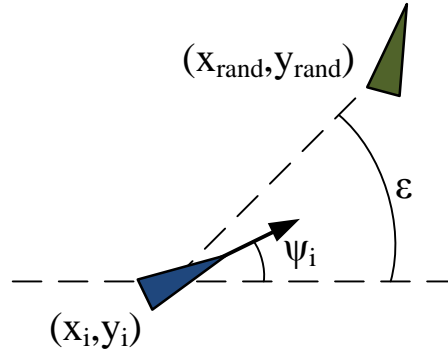


Fig. 5.4 Illustration of parameters required to calculate H_i

$$H_i = (x_i - x_{rand})^2 + (y_i - y_{rand})^2 + K_\psi |\psi_i - \varepsilon_i| \quad (5.3)$$

where K_ψ was a gain set empirically to 2, and ε_i was given by

$$\varepsilon_i = \arctan\left(\frac{y_i - y_{rand}}{x_i - x_{rand}}\right) \quad (5.4)$$

as shown in Figure 5.4. The purpose of this term was to favour nodes where the vehicle is oriented towards the random node, over nodes which might be closer in (x, y) but where the vehicle is pointing away from the random node.

The node in the tree with the lowest value of H_i was the seed point for the new branch to grow from.

Extend motion primitives from the closest node towards the random configuration, and place a new node, (x_n, y_n, ψ_n) , at the end of the motion primitive which ends closest to the random node. Growth of the tree branch consisted of generating a set of motion primitives by sweeping the range of possible steering angles and steering rates, and using Equations 4.2 to 4.12 to calculate the resulting states of the vehicle. The update equations forming the vehicle model are given in Chapter 4. Each motion primitive was scored according to the Euclidean distance from the end of the path to the random node that the tree was growing towards. The highest scoring motion primitive became the new branch of the tree, with its endpoint stored as a new node.

At every step along the branch, the position of the vehicle was checked for collisions with the manoeuvre constraints. If a collision was detected, the branch was terminated at the previous step.

Repeat these stages until a node falls sufficiently close to the goal configuration. The Euclidean distance between any new node and the goal position was calculated, and the tree growth process was terminated if that distance was below a given threshold of 2 m. The orientation of the vehicle in the goal configuration was not considered.

Once the tree growth process was terminated, the indices of linked nodes were traced back from the final node to the start configuration to output the final path.

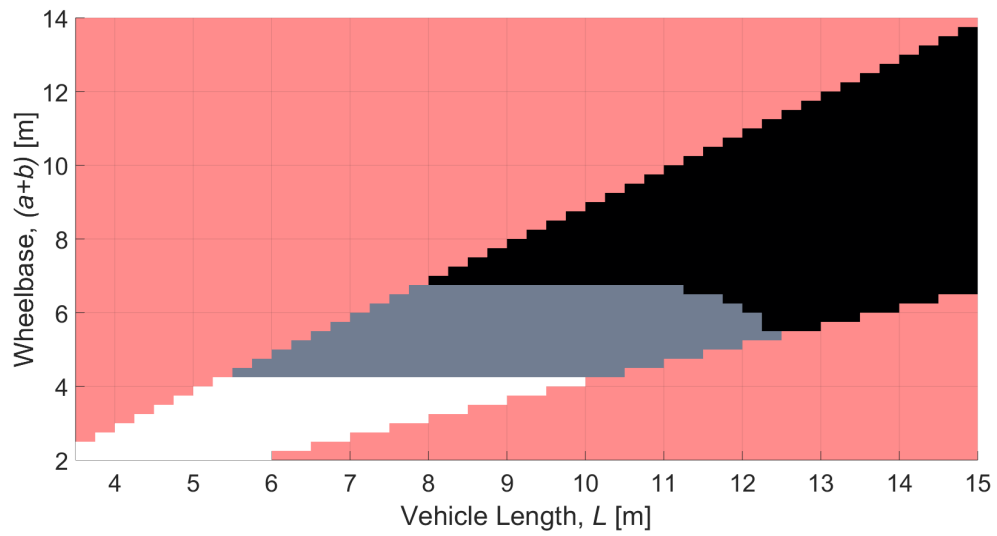
5.4.2 Results

The comparison between the performance envelope generated by the RRT algorithm (in white) and the true performance envelope (in grey) is shown in Figure 5.5. The results clearly show that the RRT algorithm was ineffective at locating successful paths through the manoeuvres for larger vehicles. The RRT algorithm discovered only 40% of the vehicles which were shown to be viable by the true performance envelope for representative manoeuvre A, and 33% of vehicles for representative manoeuvre B, based on the areas of the performance envelopes in Figure 5.5.

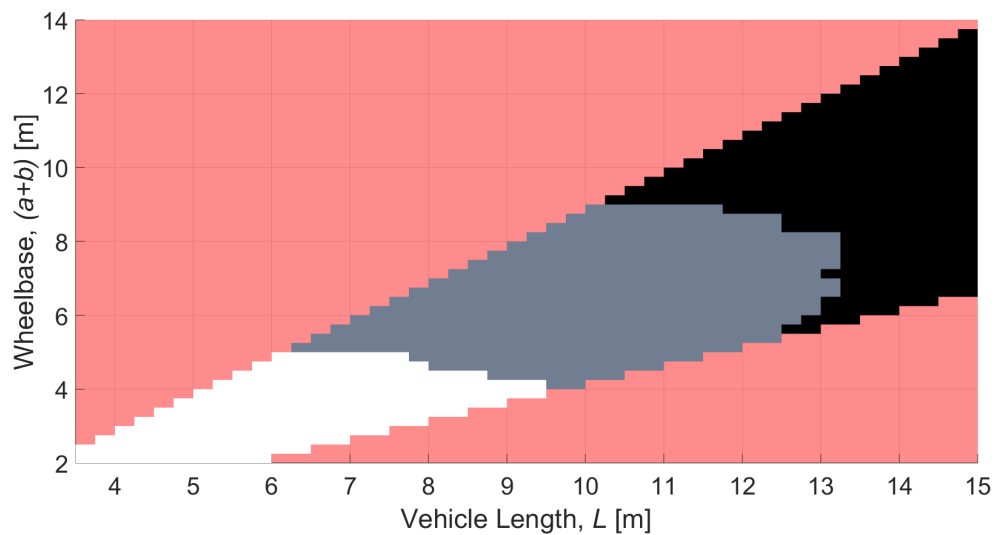
Although the algorithm has been shown in general to be a viable method for path planning in open environments, in the case of the tightly constrained manoeuvres considered here, which require location of a single viable path with high precision, RRT was unsuitable.

The reason for this is illustrated in Figure 5.6. The first few iterations of the tree growing process in this example generated nodes 1 and 2 (which are considered close together) from the start node 0. The next point in the tree which is required for a successful path is in the vicinity of configuration 3. When a point close to configuration 3 is randomly selected, the algorithm must select one of the existing nodes to expand the tree from. If nodes 1 and 2 are close together, then any point sufficiently close to configuration 3 to form a successful path will always make the same selection, no matter what method is used (in this example closest Euclidean distance will always select node 2, but a different method might always select node 1). However, the route 0–1–3 yields a successful path whereas the route 0–2–3 intersects with a boundary, therefore it is required that some points close to configuration 3 select node 2 to grow from, while others select node 1.

In open environments this effect is not seen because if nodes 1 and 2 are close enough together to create the problem then either node generates a successful path. This allows the algorithm to be successful at finding paths for relatively small vehicles. This problem can be



(a) 90° corner



(b) Chicane

Fig. 5.5 Success boundaries as found by RRT algorithm

- Unrealistic Vehicles
- True Performance Envelope
- RRT Performance Envelope
- Unsuccessful Vehicles

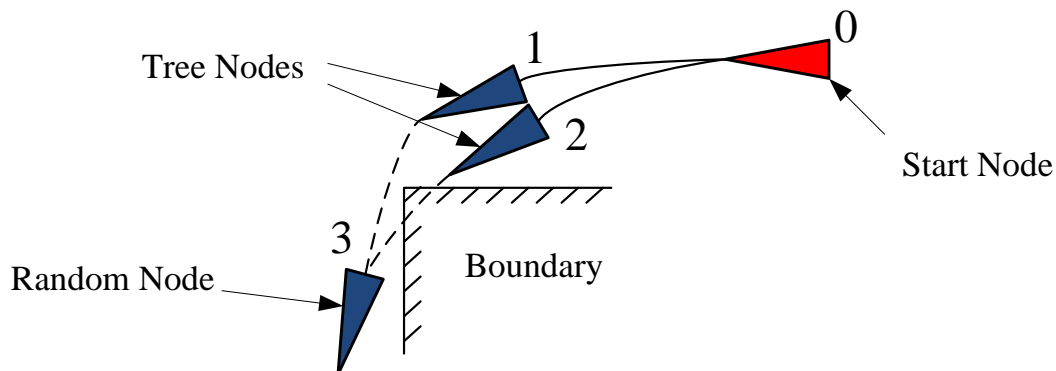


Fig. 5.6 Illustration of the challenges associated with the RRT algorithm

removed by increasing the resolution of the entire tree growing process, such that the effective distance between nodes 1 and 2 grows, however the calculations become prohibitively expensive. An adaptation to the RRT algorithm used nearest neighbour searching to identify a set of nodes within a threshold distance to the random configuration, and selected one node randomly from this sample. However this caused tree growth towards the goal to become very slow, as the random selection was not biased towards reaching the goal.

The results from the RRT algorithm show several positive features. First, the performance envelopes for both manoeuvres exhibit the same general shape as the true boundaries, despite being smaller. This suggests that the algorithm was generating sensible paths, but was not precise enough to find the exact required path. Secondly, the performance envelopes are very smooth, compared to the inconsistency generated by some of the other methods. This implies that the method is reliable and repeatable.

5.5 Model Predictive Control (MPC)

5.5.1 Method

Model Predictive Control (MPC) is a control strategy designed to identify the set of inputs to a system which generate the most suitable outputs, according to some cost function [193]. The main steps of a standard MPC algorithm are as follows:

- (i) Measure the current states of the system.
- (ii) Generate a set of input trajectories.

- (iii) Pass each trajectory through a system model, and evaluate a cost function for each.
- (iv) Select the trajectory that gives the lowest cost, and take the first step along this trajectory.
- (v) Repeat these steps.

In the case of the vehicle system, the states were the (x, y) position of the lead point of the vehicle, and the yaw angle, ψ . In the case of an articulated vehicle, the articulation angle formed a fourth state. Initially, the only input to the system was the front steering angle δ_f . The input trajectories were chosen as constant steer angles, thus each input trajectory formed a ‘motion primitive’. However, it was found that these motion primitives offered no incentive for the vehicle to ‘counter-steer’ before turning—this is an approach commonly seen in real-world driving of large vehicles, where the driver steers the lead point in the ‘wrong’ direction first to reduce the effective cut-in later in the manoeuvre. This caused the vehicle to fail by cutting in, when it still had space on the outside to use. An alternative set of motion primitives was defined, using the initial steering angle and steering rate as two inputs. These allowed the vehicle to steer outwards first, without being penalised for the effect of the ‘tail’ of the motion primitive.

For each combination of initial steering angle and steering rate, the vehicle model described in the previous chapter was used to advance the lead point by one step in the direction prescribed by the steering angle, and to calculate the new yaw angle of the vehicle. At each time step, the cost function increment, ΔJ , was calculated and added to the total cost for that steering angle and steering rate, J .

It should be noted that in the case of vehicles with rear axle steering, the system was still treated as having a single input. The rear steering angle, δ_r , was considered to be dependent on the front steering angle, either directly proportionally (through Command-Steer), or indirectly (through Path-Following steering).

The most significant component in the measure of each motion primitive was the distance travelled by the vehicle before colliding with a boundary. The greater this distance, the better. Because the vehicle travelled in discrete steps, using this parameter alone generated a highly non-linear, ‘stepped’ cost function, without a clearly defined trough. Additional parameters were therefore used, with a lower weighting, specifically the perpendicular distances from the front corners to the closest boundaries and the perpendicular distance from the front of the vehicle to the nearest boundary. Finally, in order to prevent the vehicle finding local minima, and to ensure it took the right ‘general route’ through the manoeuvre (for example turning right instead of left at a junction) a target path was defined, and the perpendicular distance from the lead point to the target path was used as an additional factor in the cost function. These parameters are illustrated in Figure 5.7.

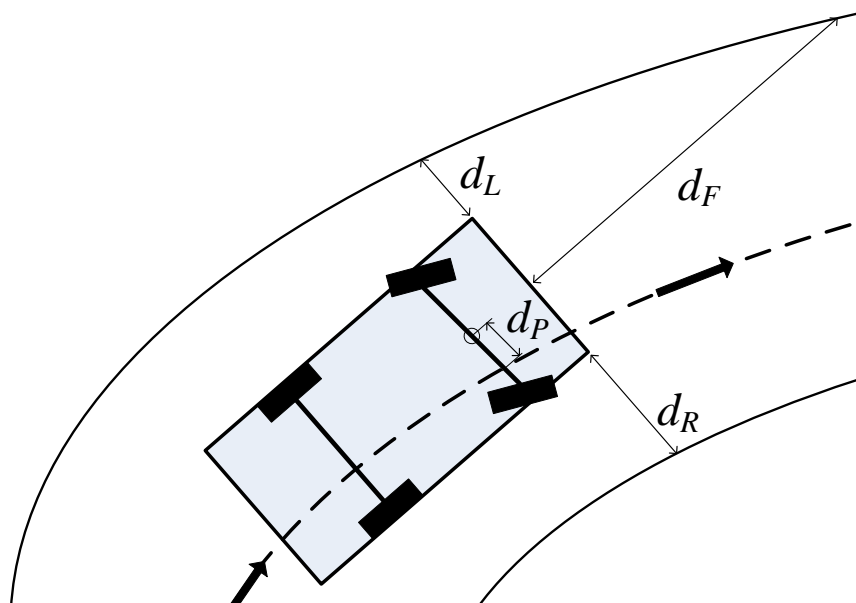


Fig. 5.7 Illustration of parameters used to evaluate the MPC cost function

The cost function was given by the following equation:

$$\Delta J = e^{-K_e k} (K_L d_L + K_R d_R + K_F d_F + K_P d_P) \quad (5.5)$$

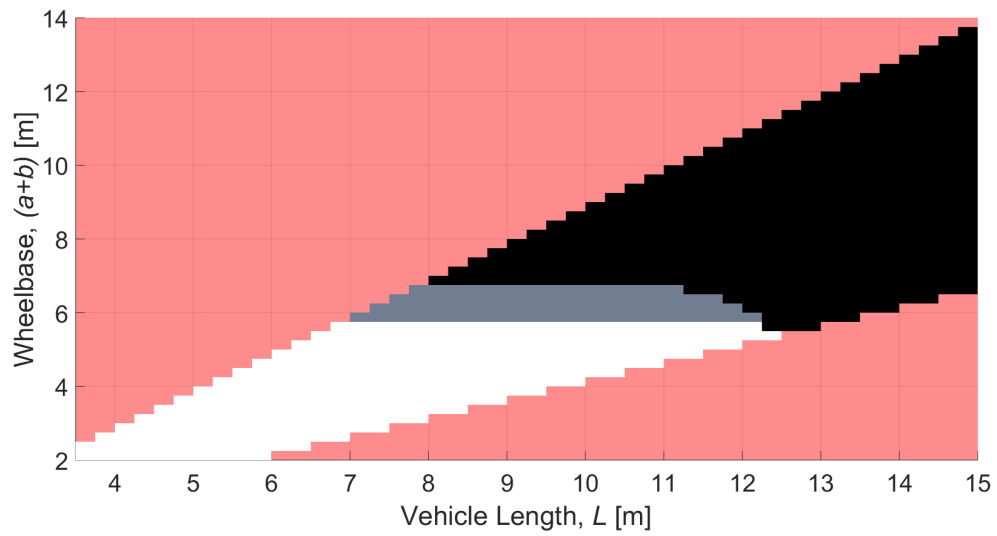
where K_L , K_R , K_F , and K_P are weights on the parameters shown in Figure 5.7, and K_e is an exponential gain intended to prioritise the part of the path closest to the current position.

The cost, J , for each motion primitive was a function of two variables: initial steering angle, $\delta_{f,i}$, and steering rate, $\dot{\delta}_f$. To optimise this, a Genetic Algorithm was used. A Genetic Algorithm generates a set of starting parameter values, and evaluates the cost function for these parameters. Sets of parameter values which score highly are passed down with some mutations and random inclusions to the next ‘generation’ to be evaluated.

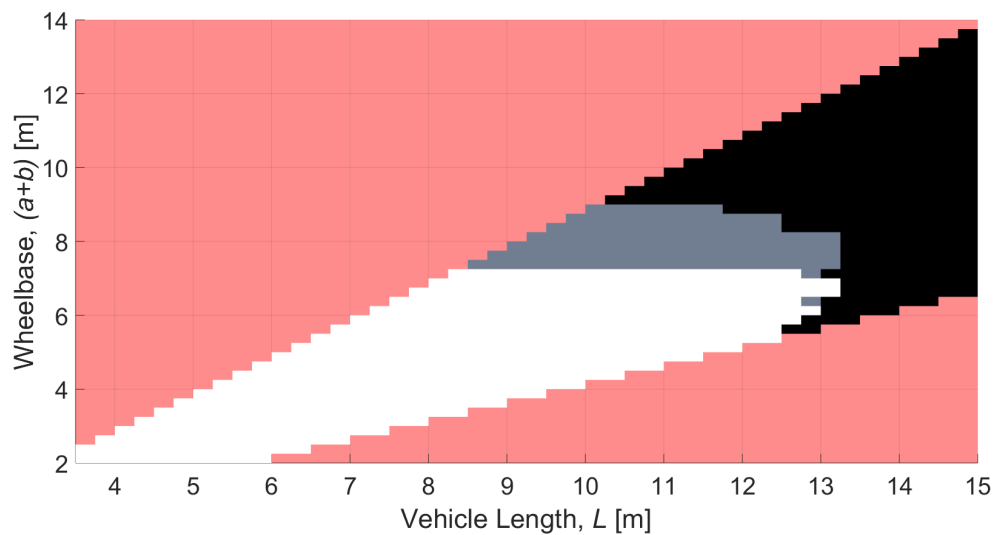
5.5.2 Results

The MPC algorithm performed reasonably well, scoring 79% for both of the representative manoeuvres. Figure 5.8 shows the performance envelopes as found by the MPC algorithm compared to the true envelopes.

These figures show a clear pattern, specifically that the MPC algorithm is unsuccessful at locating the viable path through a manoeuvre once the vehicles wheelbase reaches a certain value relative to the dimensions of the manoeuvre. The algorithm performs well, locating the



(a) 90° corner



(b) Chicane

Fig. 5.8 Success boundaries as found by MPC algorithm

- Unrealistic Vehicles
- True Performance Envelope
- MPC Performance Envelope
- Unsuccessful Vehicles

true performance envelope accurately, when the vehicle is at its maximum successful length for that manoeuvre. This also corresponds to the region of the envelope plot where the rear overhang of the vehicle is greatest.

This pattern matches expectations of the algorithm. If the rear axle of a vehicle moves forwards on the vehicle, from the rear bumper towards the centre of the vehicle, the effect on the swept path of the vehicle is to shift the swept area towards the outside of the corner, as cut-in reduces and tailswing increases. The algorithm was known to be poor at managing cut-in, as shown by the initial design of ‘constant steer angle’ motion primitives, which failed because they could not avoid cutting in. This problem was reduced by the new, more complex motion primitives, but not completely overcome. At long wheelbases, the wheels are close to the rear of the vehicle, hence the cut-in is large compared to the size of the vehicle, and the MPC algorithm fails because it cannot find suitable motion primitives to cause it to counter-steer prior to the corner. The algorithm could be improved by using a library of more complex motion primitives, but this would increase the computation time. It was preferable to restructure the algorithm using the control point-based approach described below.

This implementation of MPC used a short control horizon and a long preview horizon. An alternative implementation would be to use a longer control horizon, such that the algorithm optimises the control inputs at all points along the path, rather than just the first time step. It was believed that this approach would require the same compromise between resolution and computation time as the RRT method, and so would not offer an advantage. However, this was not tested, as other methods were found to be sufficiently accurate.

5.6 Single- and Multi-segment Splines (SMSS)

An alternative to the MPC approach was to use cubic splines to define a path through the manoeuvre, using a similar cost function to the MPC approach to evaluate the success of the path. Several different methods for defining the splines were investigated, as described below. An optimisation method was used to find the combination of parameters which defined the highest-scoring spline, and the vehicle was considered to have passed if it could reach the end of that spline without colliding with the manoeuvre constraints. This was performed using the Matlab Global Optimisation Toolbox. A Genetic Algorithm was chosen as the optimisation algorithm, because the objective function was expected to be highly non-linear, and the shape of the function was very unpredictable. It was found that very few ‘generations’ were required to give reasonable results, so the algorithm was run with a limit of ten generations, and was modified to exit early if the vehicle could reach the end of a tested spline.

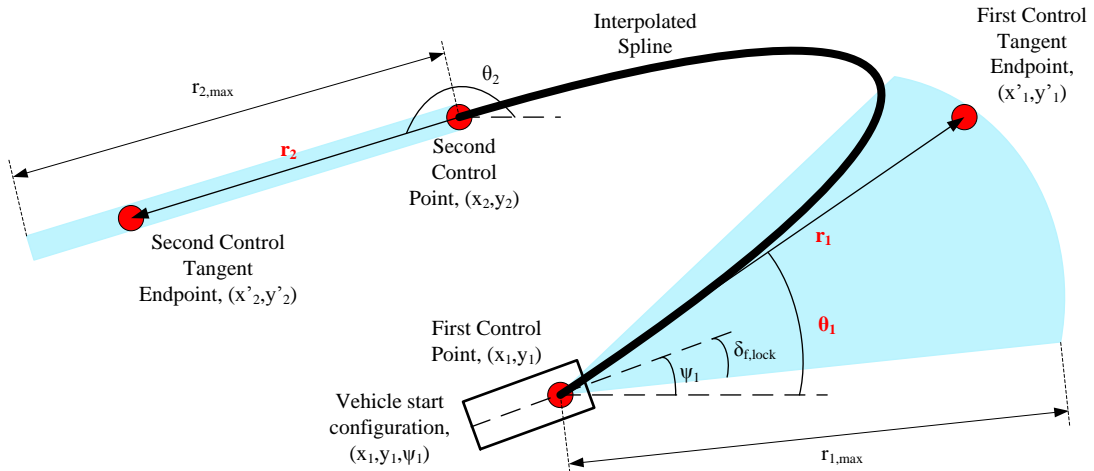


Fig. 5.9 Parameters required to define a single-segment spline

5.6.1 Single-segment Splines

5.6.1.1 Method

A single Hermite spline segment is described by the positions of two control points, (x_1, y_1) and (x_2, y_2) , and the endpoints of tangents to the ends of the path, (x'_1, y'_1) and (x'_2, y'_2) at the control points, as shown in Figure 5.9. In this work, the control points (the start and end points of the manoeuvre) were the start and end points of the example path through each manoeuvre, created when the manoeuvre was defined (as explained in Section 5.1.1), thus of the eight parameters required to define the spline, four, (x_1, y_1, x_2, y_2) , were fixed by the definition of the manoeuvre. In order to provide limits on the upper and lower bounds of the other four parameters, (x'_1, y'_1, x'_2, y'_2) , these parameters were redefined as $(r_1, \theta_1, r_2, \theta_2)$ where

$$x'_1 = r_1 \cos \theta_1 \quad (5.6)$$

$$y'_1 = r_1 \sin \theta_1 \quad (5.7)$$

$$x'_2 = r_2 \cos \theta_2 \quad (5.8)$$

$$y'_2 = r_2 \sin \theta_2 \quad (5.9)$$

To reduce the number of parameters required, the angle at which the spline arrives at the goal position, θ_2 , was fixed manually when the manoeuvre was defined. Therefore, three parameters were required to fully define the spline, (r_1, θ_1, r_2) , shown in Figure 5.9.

The maximum and minimum values of θ_1 were taken as $\psi_1 - \delta_{f,lock} < \theta_1 < \psi_1 + \delta_{f,lock}$, where ψ_1 was the yaw angle of the vehicle in the start configuration, so that the vehicle could not exceed its steering lock angle in the first time step. The radii, r_1 and r_2 , were limited to a maximum value of 100 m. This value was determined by inspection of plausible splines.

These limits generate a sector of plausible locations for the endpoint of the first control tangent, and a line of plausible locations for the endpoint of the second. Both areas are shaded in Figure 5.9.

Any parametric cubic curve can be defined as

$$x(t) = a_x t^3 + b_x t^2 + c_x t + d_x \quad (5.10)$$

$$y(t) = a_y t^3 + b_y t^2 + c_y t + d_y \quad (5.11)$$

for $0 \leq t \leq 1$. In matrix form this is written as

$$\mathbf{Q}(t) = \mathbf{T}\mathbf{C} \quad (5.12)$$

where $\mathbf{Q}(t)$ is the coordinates of the curve, $[x(t), y(t)]$, \mathbf{T} is the parameter matrix $\begin{bmatrix} t^3 & t^2 & t & 1 \end{bmatrix}$ and \mathbf{C} is known as the coefficient matrix, given by

$$\mathbf{C} = \begin{bmatrix} a_x & a_y \\ b_x & b_y \\ c_x & c_y \\ d_x & d_y \end{bmatrix} \quad (5.13)$$

Differentiating yields

$$\mathbf{Q}'(t) = \begin{bmatrix} 3t^2 & 2t & 1 & 0 \end{bmatrix} \mathbf{C} \quad (5.14)$$

where $\mathbf{Q}'(t) = \begin{bmatrix} x'(t) & y'(t) \end{bmatrix}$.

The four control points described above then provide four boundary equations which can be written as

$$\begin{bmatrix} x_1 & y_1 \\ x_2 & y_2 \\ x'_1 & y'_1 \\ x'_2 & y'_2 \end{bmatrix} = \begin{bmatrix} T_1^3 & T_1^2 & T_1 & 1 \\ T_2^3 & T_2^2 & T_2 & 1 \\ 3T_1^2 & 2T_1 & 1 & 0 \\ 3T_2^2 & 2T_2 & 1 & 0 \end{bmatrix} \mathbf{C} \quad (5.15)$$

where $T_1 = 0$ and $T_2 = 1$. From this, \mathbf{C} can be found by

$$\mathbf{C} = \begin{bmatrix} T_1^3 & T_1^2 & T_1 & 1 \\ T_2^3 & T_2^2 & T_2 & 1 \\ 3T_1^2 & 2T_1 & 1 & 0 \\ 3T_2^2 & 2T_2 & 1 & 0 \end{bmatrix}^{-1} \begin{bmatrix} x_1 & y_1 \\ x_2 & y_2 \\ x'_1 & y'_1 \\ x'_2 & y'_2 \end{bmatrix} \quad (5.16)$$

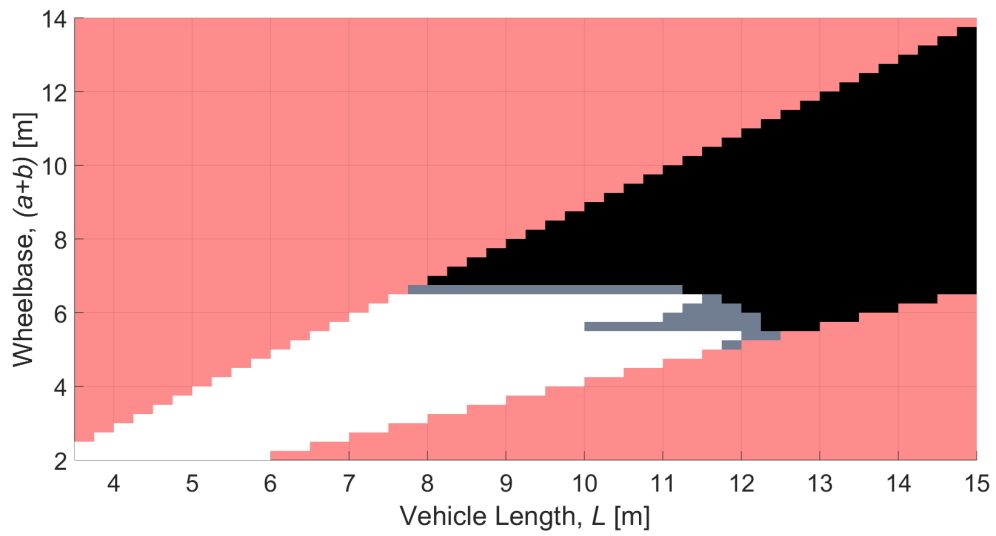
With the coefficients of the matrix \mathbf{C} known, the full set of coordinates for the path can be defined by solving Equation 5.12 for a finely spaced set of values of t between 0 and 1.

5.6.1.2 Results

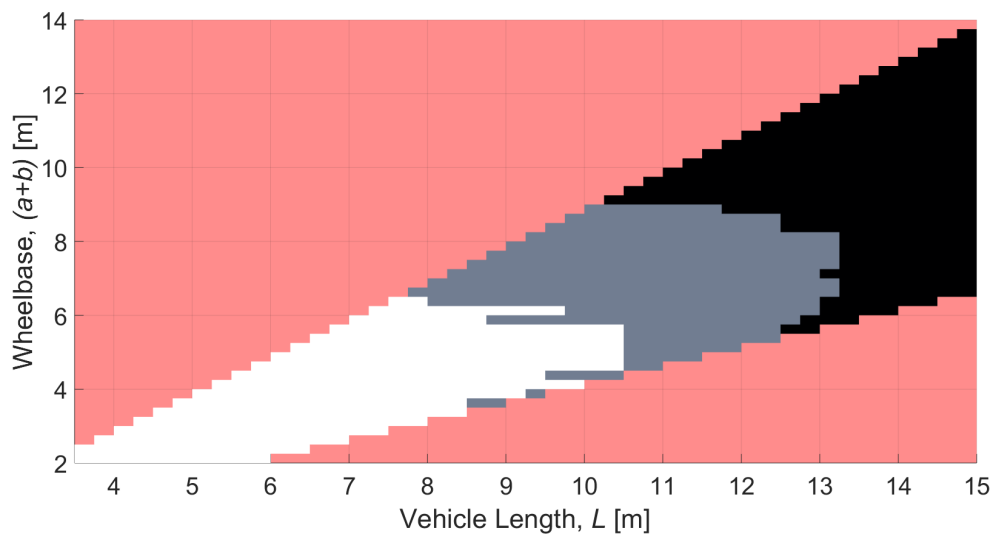
Figure 5.10 shows the success boundaries generated by the Single-segment Spline algorithm. The algorithm performed well on the first manoeuvre, scoring 89%, but badly on the second, scoring 51%.

Inspection of the two manoeuvres shows the cause of the poor performance on the second manoeuvre. The 90° corner seen in the first manoeuvre requires only one change of direction, and can be easily defined by a cubic function with four control points. Varying the control points slightly will yield a range of slightly different splines which can be evaluated. By contrast, the second manoeuvre requires two changes of direction. Although this can in theory be represented by a spline defined by four control points, in practice the spline becomes very sensitive to the position of the control points. This makes it difficult to achieve the fine control over the spline required to generate a set of similar splines to evaluate. This is a significant disadvantage to this method, assuming that not all manoeuvres can be completed with a single change of direction. The following section, on Multi-segment Splines, attempted to address this problem by providing an intermediate control point, thus reducing the sensitivity of the spline to the positions of its control points.

Another feature of interest in the figures are the ‘missing rows’ visible at 5.5 m wheelbase for the first manoeuvre, and 5.75 m for the second. The test programs were repeated, and the position of these artefacts was not consistent. Their presence suggests that the algorithm is prone to falling into local minima, rather than finding the global optimum. This is unexpected, since the spline was optimised using the Genetic Algorithm, which should be able to robustly find the global minimum for a simple system. As explained above, defining the relatively complex spline with only four control points causes high sensitivity to the position of those inputs. It is thought that the global optimiser was not able, or not given sufficient time to locate the position in the parameter space of the correct solution to a sufficient degree of precision. Initial tests, allowing more generations of the Genetic Algorithm appeared to confirm this, however the calculation ran slowly. Consequently reducing the sensitivity to the control points by adding more spline segments was preferred as a solution.



(a) 90° corner



(b) Chicane

Fig. 5.10 Success boundaries as found by Single-segment Spline algorithm

- Unrealistic Vehicles
- True Performance Envelope
- SMSS Performance Envelope
- Unsuccessful Vehicles

5.6.2 Multi-segment Splines

5.6.2.1 Method

Any single spline can be split into multiple segments. Each additional segment requires one additional control point, (x_i, y_i) , and the endpoint of the tangent to the curve at that point, (x'_i, y'_i) , converted to (r_i, θ_i) as described above, leading to four additional parameters, x_i, y_i, r_i and θ_i . An initial estimate of the position of the additional control point was taken as the midpoint of the example path (described in Section 5.1.1), and the algorithm was permitted to search around this starting point as described below.

Figure 5.11 shows a spline composed of two segments, with three control points, and three control tangent endpoints, requiring 12 parameters to define. Of those 12 parameters, the same five were considered fixed for a given manoeuvre, x_1, y_1, x_3, y_3 and θ_3 , leaving seven parameters to optimise over. The computational complexity could have been reduced by fixing (x_2, y_2) at the same time as the start and goal configurations were defined, but this would have increased the likelihood of missing a valid solution. Instead, the coordinates (x_2, y_2) were allowed to vary by a radius of up to 4 m from their initial position (as set at the definition of the manoeuvre). This maximum radius was defined by inspection of maximum road widths for the manoeuvres.

The search spaces for the parameters governing the start and goal tangent endpoints were the same as for the single segment, but for the middle control point, r_2 was limited to 25 m by inspection, and θ_2 was allowed to vary between $\psi_2 - \pi$ and $\psi_2 + \pi$. ψ_2 was fixed by the manoeuvre definition. This could not be limited further by the steering lock angle as for θ_1 because it was not known in advance at what angle the vehicle would approach the control point at.

The coordinates of the different spline segments were calculated separately according to the method described for the single spline segment. Continuity between the spline segments in position and gradient was ensured by using the same control point and control tangent endpoint, for the end of the first segment and the start of the second. There is an argument to suggest that enforcing continuity between spline segments is not true to the real world behaviour of a driver attempting a tight manoeuvre. Enforcing continuity in gradient corresponds to requiring no instantaneous change in the steering angle, which will not necessarily be the case if the driver finds he cannot complete the manoeuvre without changing the steering angle while stationary. However, it was decided to limit the search to manoeuvres which could be completed by a single spline with gradient continuity enforced.

The same analysis gives 11 parameters to optimise over for a three segment spline. Additional spline segments increases the dimension of the search space significantly, and

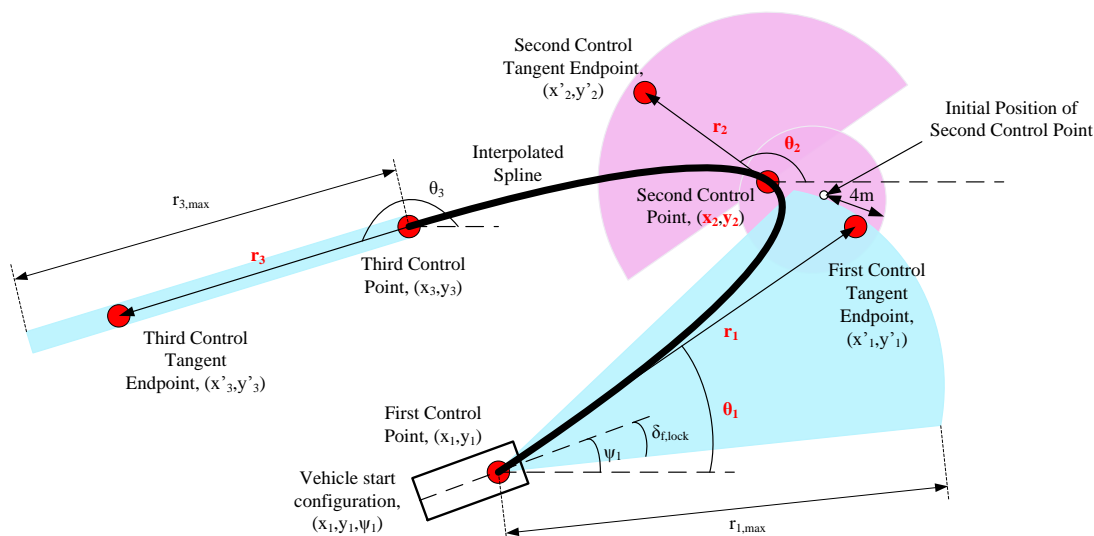


Fig. 5.11 Parameters required to define a spline composed of two segments

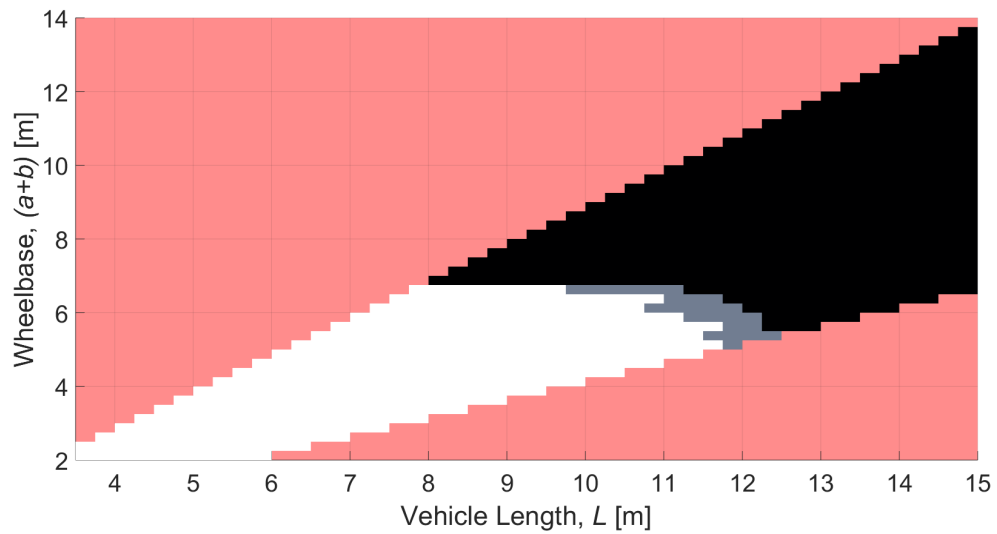
risks over-defining the manoeuvres, which were all simple enough to be defined by 4 control points (3 spline segments), so splines with more than 3 segments were not considered.

5.6.2.2 Results

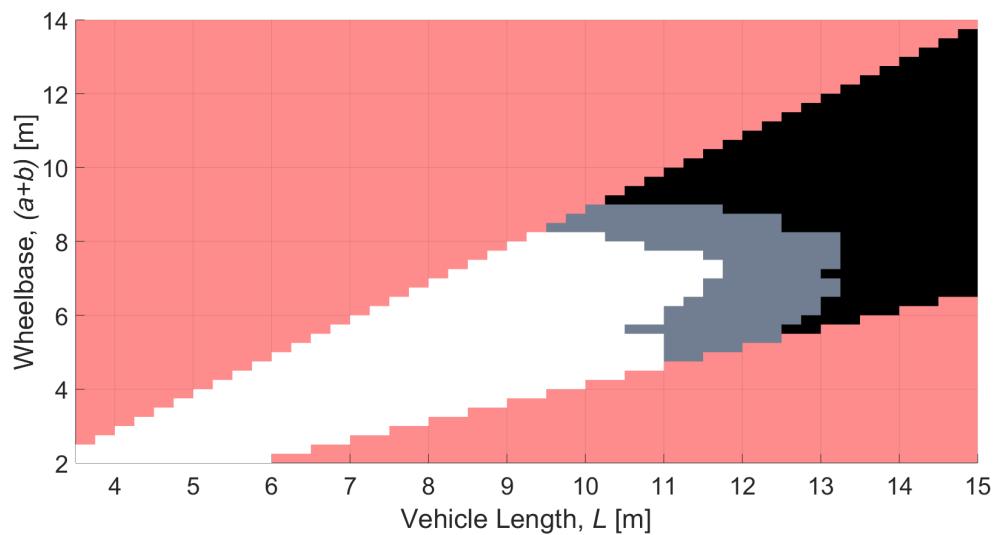
The results for two-segment and three-segment splines are shown in Figure 5.12 and Figure 5.13 respectively. Both algorithms show good results for the first manoeuvre, scoring 90% and 94%, and slightly worse performance on the second manoeuvre, scoring 75% and 76%.

As predicted, the subdivision of the spline into multiple segments reduced the sensitivity to the location of the control points, reducing artefacts such as the local minima problems present in the results from the Single-segment Spline method. This also reduced some of the performance deficit for the chicane manoeuvre, although the results are still worse than for the corner manoeuvre.

These results suggest that the performance of the algorithm can be improved by increasing the number of control points used to define the splines. However, in the Multi-segment Spline implementation, every additional control point requires 4 additional parameters to be optimised, which slows the algorithm. An alternative structure was proposed, in order to allow investigation of larger numbers of control points.



(a) 90° corner



(b) Chicane

Fig. 5.12 Success boundaries as found by Two-segment Spline algorithm

- Unrealistic Vehicles
- True Performance Envelope
- SMSS Performance Envelope
- Unsuccessful Vehicles

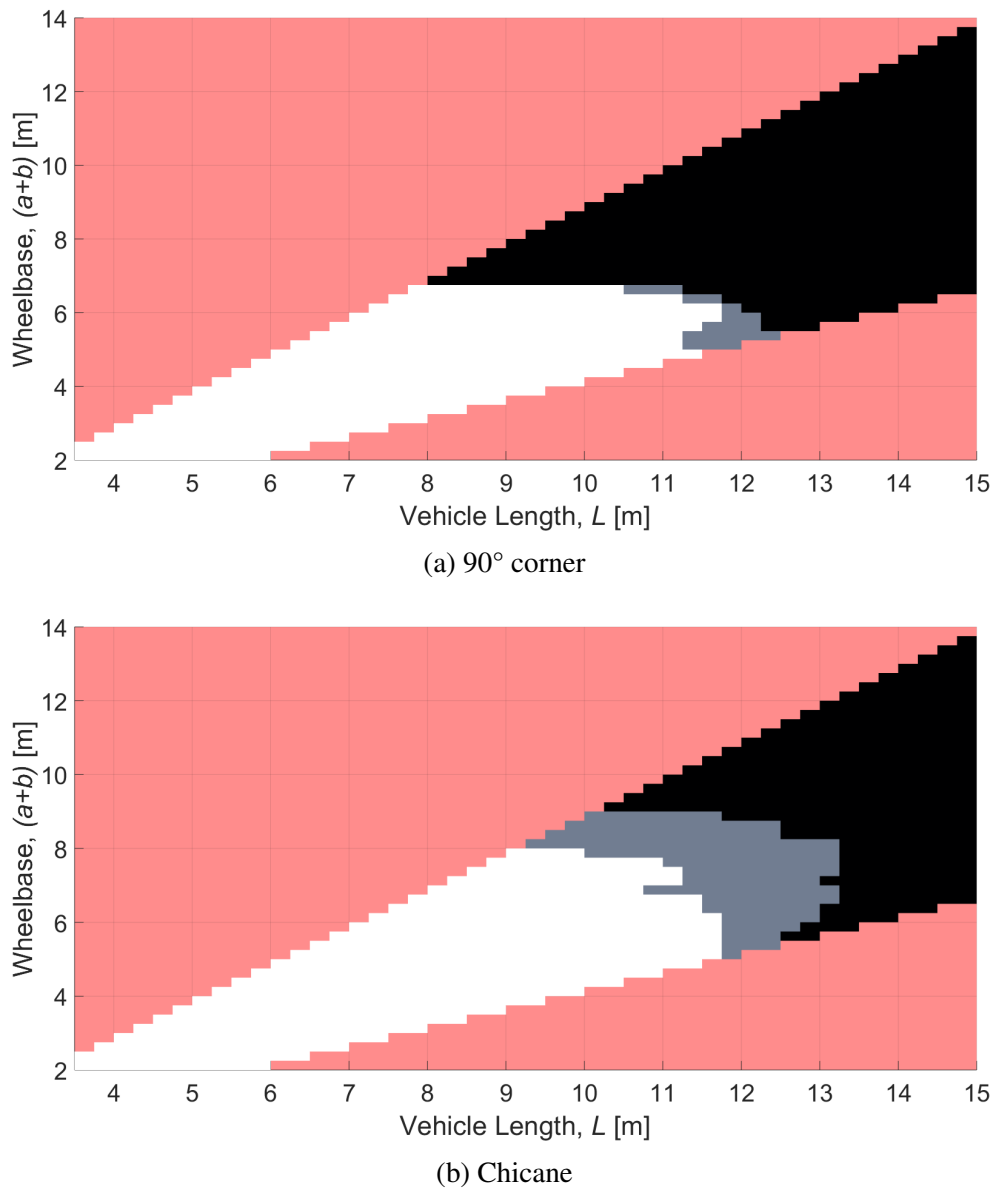


Fig. 5.13 Success boundaries as found by Three-segment Spline algorithm

- Unrealistic Vehicles
- True Performance Envelope
- SMSS Performance Envelope
- Unsuccessful Vehicles

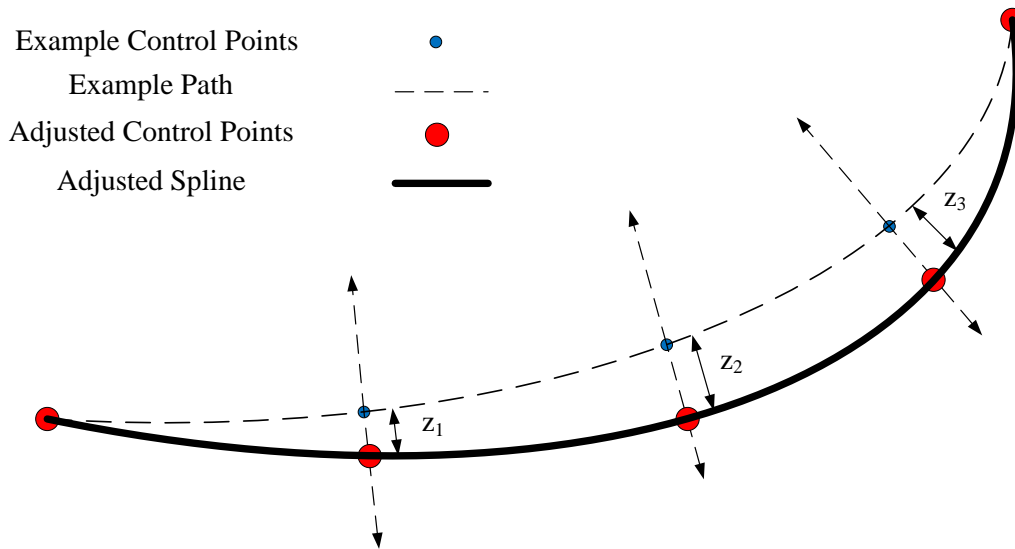


Fig. 5.14 Definition of a spline with many segments using few parameters

5.7 N Control Point Splines (NCPS)

5.7.1 Method

In order to give a higher degree of control over the spline, without requiring an excessive number of parameters to optimise over, a further method was investigated. An example path was generated manually and subdivided into n spline segments, requiring $n + 1$ control points to define it. The control points were equally spaced along the example path. Perpendicular lines to the example path were defined at each of the control points, and the optimisation variable for each control point was the distance along these perpendiculars to the example spline away from the initial position, z_i , ranging from -3 m to 3 m. The spline was required to pass through all the control points as shown in Figure 5.14. The method to enforce this is described below. In this way, only one optimisation parameter was required to define the position of each control point, and none were needed for the start and end point, so a spline with n segments was defined by $n - 1$ parameters. This compares very favourably to the method used in section 5.6.2 which required $4(n - 1) + 3$ parameters. For a ten segment spline, this corresponds to nine parameters instead of 39. Using as many as ten spline segments is likely to cause over-fitting, or oscillations in the spline. However, it allows increased flexibility for the critical, tightly-constrained vehicles.

This type of spline is known as a Catmull-Rom spline [203]. A single spline segment passing through four control points, $C_1 - C_4$, can be defined by

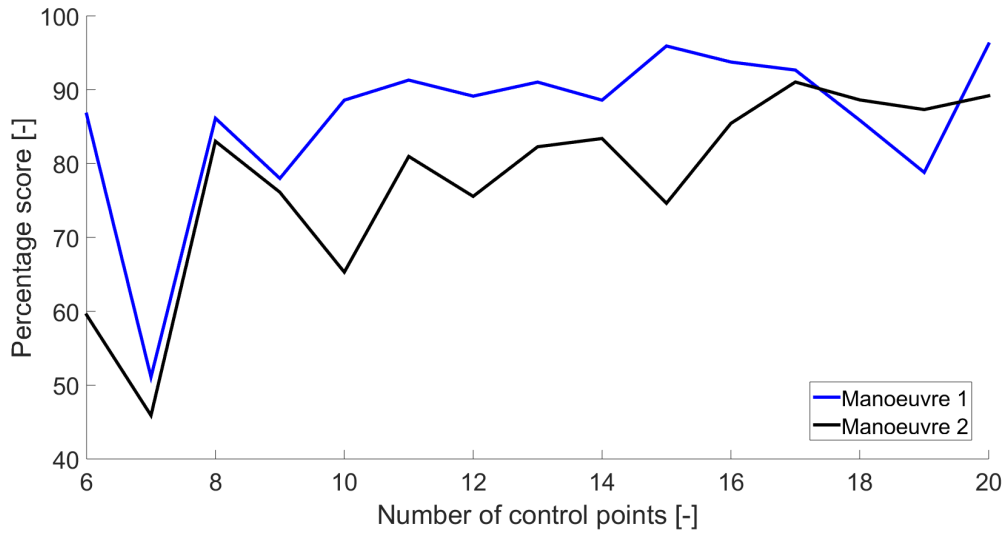


Fig. 5.15 Variation of the algorithm score for each manoeuvre with the number of control points used to define the spline

$$\mathbf{Q}(t) = \mathbf{TC} \quad (5.17)$$

where \mathbf{Q} is the coordinate for that particular spline segment, \mathbf{T} is defined as above, and \mathbf{C} is the coefficients matrix that encodes the control points. Following the method used above to find \mathbf{C} from the boundary conditions yields

$$\mathbf{C} = \frac{1}{2} \begin{bmatrix} -1 & 3 & -3 & 1 \\ 2 & -5 & 4 & -1 \\ -1 & 0 & 1 & 0 \\ 0 & 2 & 0 & 0 \end{bmatrix} \begin{bmatrix} x_1 & y_1 \\ x_2 & y_2 \\ x_3 & y_3 \\ x_4 & y_4 \end{bmatrix} \quad (5.18)$$

The outer two control points, C_1 and C_4 , are used to define the gradients at points C_2 and C_3 , thus the interpolation is only valid between C_2 and C_3 . In other words, at C_2 , $t = 0$ and at C_3 , $t = 1$. Continuity between the segments can be ensured by sharing control points.

5.7.2 Results

5.7.2.1 Investigation of the effect of number of control points

In order to assess the effect of the number of control points on the algorithm, success boundaries were plotted for a range of values of n . Figure 5.15 shows the effect of the number of control points on the score for the manoeuvre.

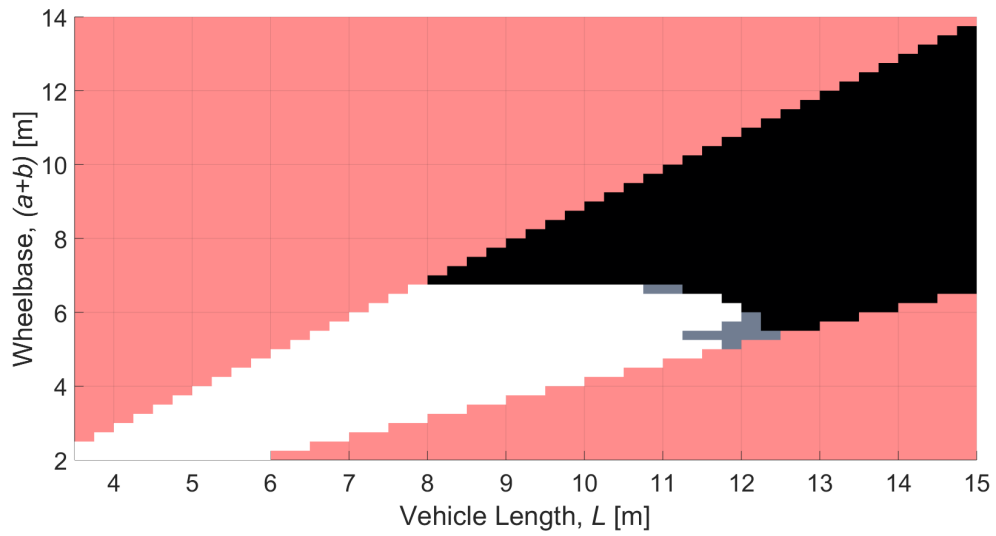
The plots for both manoeuvres show a significant drop in performance at seven control points, compared to six or eight. Analysis of the example manoeuvres shows that, for these particular manoeuvres, an odd number of control points leads to one of the control points being directly in the centre of the manoeuvre, at the critical point. When the number of control points is even, the critical centre of the manoeuvre is not explicitly defined by a control point, but instead by the spline joining the control points on either side, which allows greater freedom. At higher numbers of control points, this effect is less pronounced, since the distances between the control points are lower, and therefore the positioning of the control points along the spline is less crucial.

Figure 5.15 suggests that more control points gives better performance, with peaks at 20 control points for the first manoeuvre and 17 control points for the second. Tests with more than 20 control points were slow to solve because of the increased number of optimisation variables. In addition, a spline with more than 20 control points can exhibit significant oscillation. This firstly increases the solution time, and secondly may yield a very unrealistic path. For this reason, it was decided to generate the results using 20 control points.

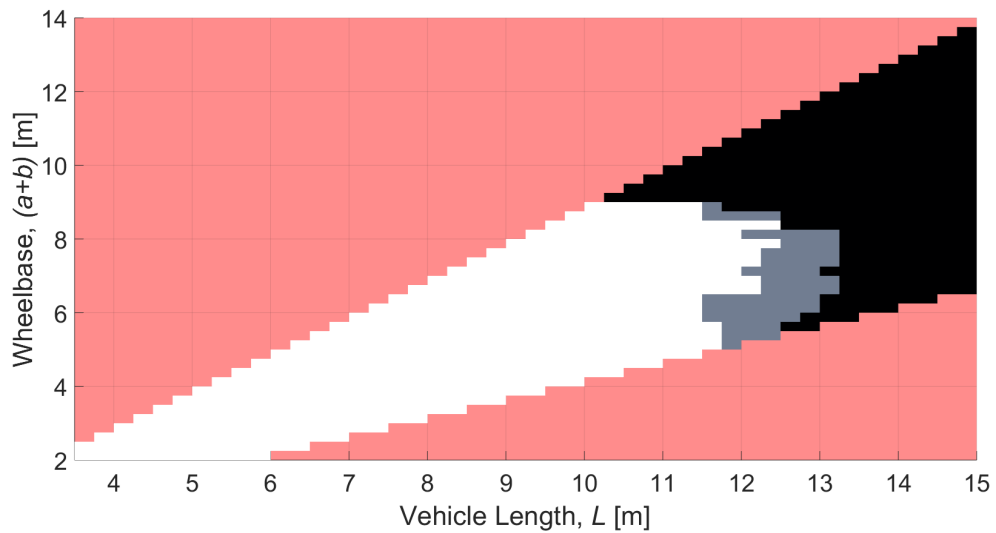
5.7.2.2 Results for 20 control points

Figure 5.16 shows the success boundaries for the two representative manoeuvres. The percentage of successful vehicles discovered was 96% for the first manoeuvre and 89% for the second manoeuvre. The algorithm was successful at locating the maximum wheelbase for both manoeuvres. This suggests that the algorithm is capable of planning paths which either counter-steer or overshoot the corner, unlike some of the other algorithms. The algorithm performs relatively poorly as the rear overhang increases. This is likely to be an effect of the oscillations previously described, as vehicles with very long rear overhangs will exhibit significant tailswing in the transient region of manoeuvres, which for a path with oscillations is a significant proportion of the path.

One adaptation of the algorithm was considered, where the freedom of movement of each control point varied. For example control points near the start and end of the manoeuvre were allowed only a small amount of movement, while control points near the centre could move much further from their starting position. However it was decided that this restricted the algorithm on manoeuvres where the most crucial part was not at the centre.



(a) 90° corner



(b) Chicane

Fig. 5.16 Success boundaries as found by Multiple Control Point Spline algorithm with 20 control points

- Unrealistic Vehicles
- True Performance Envelope
- NCPS Performance Envelope
- Unsuccessful Vehicles

Table 5.1 Evaluation of path-planning algorithms

Algorithm	Variant	Accuracy 1 (%)	Accuracy 2 (%)	Time(s)
RRT		40	33	13.8
MPC		79	79	46.9
SMSS	Single-segment	89	51	4.8
	Two-segment	92	75	46.9
	Three-segment	94	76	67.4
NCPS	6 Control Points	87	60	15.4
	7 Control Points	51	46	15.5
	8 Control Points	86	83	19.0
	9 Control Points	78	76	20.4
	10 Control Points	89	65	22.1
	12 Control Points	89	76	26.9
	15 Control Points	96	75	29.5
	20 Control Points	96	89	35.8
MPC + NCPS(20)		99	96	82.7

5.8 Algorithm Selection

5.8.1 Quantitative Evaluation

Table 5.1 shows the percentage of successful vehicles discovered by each algorithm for both manoeuvres. The table also shows the average time taken to simulate each vehicle across both manoeuvres. All of these times corresponded to a time of less than 90 minutes to generate the full performance envelope. The time taken to generate the full performance envelope depends on the number of vehicles which must be simulated, thus varies with the size and shape of the envelope. It was approximated that a computation time per simulation of less than 90 s would correspond to a time to generate the full envelope of less than 90 minutes, which was considered acceptable. The speed of most of the algorithms can be improved, but at the cost of performance. For example, limiting the number of Genetic Algorithm generations will reduce the time taken, but could lead to viable paths being missed.

5.8.2 Qualitative Evaluation

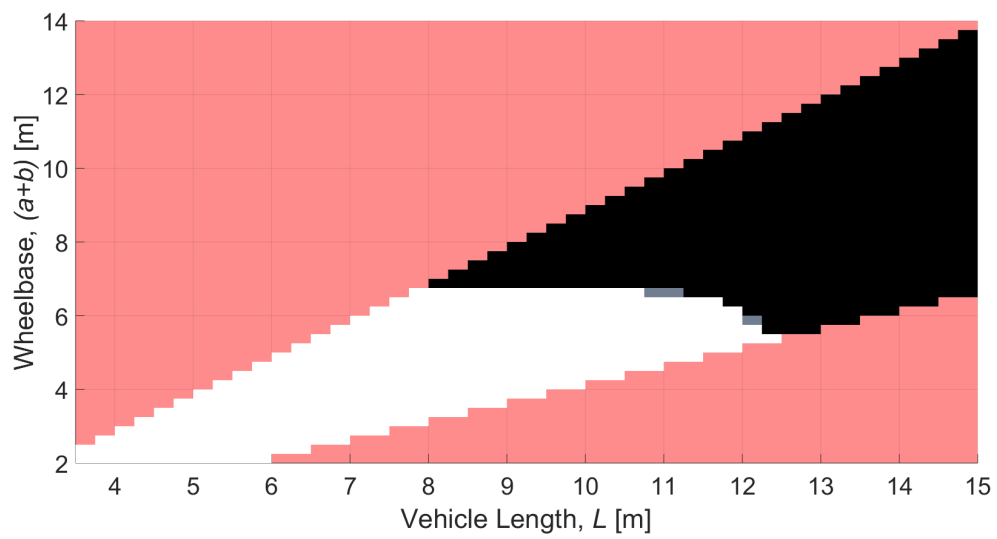
None of the algorithms successfully revealed the true performance envelope accurately. Of the four possibilities, the RRT algorithm can be discounted, for its poor performance at the critical points of the map, where the vehicle is large and tightly constrained. Similarly, the Single-segment Spline method can be discounted, due to its inefficacy on manoeuvres with more than one change of direction. The Multi-segment Spline approaches were reasonably accurate but ran slowly relative to their performance.

Analysis of individual tests showed certain characteristics of each algorithm which penalised different forms of vehicle. The most pronounced of these were the MPC algorithm, which penalised vehicles with a long wheelbase, and the NCPS algorithm, which penalised vehicles with a long rear overhang. These two methods complement each other, such that the sum of the two maps located 99% of the performance envelope for the 90° corner and 96% of the boundary for the chicane. These envelopes are compared with the true performance envelope in Figure 5.17.

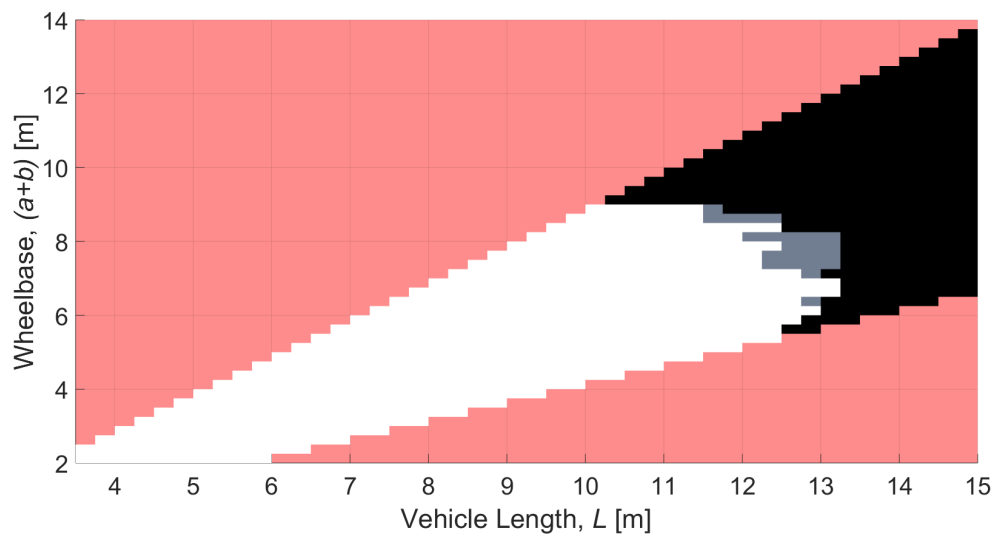
The combined time for these two algorithms was 82.7 s per simulation, which corresponds to approximately 72 minutes per full map. Although more than any individual algorithm, this was considered acceptable. It would also be possible to increase the speed by using the very fast Single-segment Spline method for the smaller vehicles which are more likely to pass, and switch to the other methods close to the boundary.

5.9 Conclusions

- (i) A method was required to locate the boundary in $(L, a + b)$ space separating vehicles which can, and vehicles which cannot complete a specific manoeuvre. This required a path-planning algorithm so that large numbers of vehicles could be simulated attempting many manoeuvres.
- (ii) A number of simplifications and assumptions were required. First, reversing was not considered, and secondly all obstacles were considered ‘hard’ obstructions to any part of the vehicle (whereas in reality, some ‘soft’ obstacles such as kerbs will constrain the wheels but not the front or rear overhangs).
- (iii) Four path-planning algorithms were designed and written. These were Rapidly-exploring Random Trees (RRT), Model Predictive Control (MPC), Single- and Multi-segment Splines (SMS) and N Control Point Splines (NCPS).



(a) 90° corner



(b) Chicane

Fig. 5.17 Success boundaries found by the combination of the MPC and NCPS algorithms

- Unrealistic Vehicles
- True Performance Envelope
- MPC and NCPS Combined Performance Envelope
- Unsuccessful Vehicles

- (iv) None of the methods could successfully locate the boundary perfectly, but a combination of the MPC and NCPS algorithms successfully located 99% and 96% of the viable vehicles for the first and second manoeuvres respectively.

Chapter 6

Manoeuvrability Modelling: Case Studies

6.1 Introduction

Chapter 4 describes a method for assessing the manoeuvrability of Heavy Goods Vehicles. This chapter will apply this method to three case studies: Grocery Delivery Vehicles, Refuse Collection Vehicles, and Urban HGVs such as those used to restock supermarkets and convenience stores. Two libraries of manoeuvres were collated. First, a set of ‘residential’ manoeuvres, applicable to home delivery vehicles and refuse trucks, and secondly, a set of ‘urban’ manoeuvres, expected to be more suitable for larger vehicles such as those used to restock stores in city centres. The method consists of the following steps:

- (i) Identify a library of manoeuvres, suitable for the application the vehicle will be used for. These could be identified from GPS data collected from similar vehicles.
- (ii) Convert each manoeuvre in the library into a set of boundary constraints, by extracting the positions of obstacles such as kerbs, walls, or traffic furniture.
- (iii) Simulate a set of vehicles with different lengths, L , and wheelbases, $(a + b)$, attempting the manoeuvre using the path-planning algorithms described in Chapter 5, and display the results as a set of contours in L and $(a + b)$ space corresponding to the percentage of manoeuvres from the library which a vehicle of those dimensions could complete.
- (iv) Locate an existing vehicle on the plot. The percentage of manoeuvres passed by the existing vehicle will form the minimum target for any new design. Using the existing vehicle instead of an arbitrary baseline calibrates against the effects of inaccuracies and assumptions about the constraints.

- (v) Simulate the same for vehicles utilising interventions to aid manoeuvrability such as rear axle steering or articulation joints, and plot the resulting contours.
- (vi) Apply additional constraints or contours, including:
 - (a) Maximum Gross Vehicle Weight (or contours of constant Gross Vehicle Weight)
 - (b) Maximum axle load (or contours of constant axle load)
 - (c) Remove vehicles where the rear axle is off the back of the vehicle, or in the front half of the vehicle
- (vii) Locate the point on the plot (with or without manoeuvrability interventions such as rear axle steering) which allows the maximum load capacity without violating any of the constraints, and can pass at least the same percentage of manoeuvres as the existing vehicle. For this work, the capacity is a function only of the vehicle length, so the point of optimum design point is the point with the greatest value of L .

It was expected that the addition of rear axle steering to a vehicle would increase the percentage of manoeuvres it could complete. This would mean that a longer vehicle could complete the same percentage of manoeuvres as the unsteered, baseline vehicle. However, initial simulations showed that the addition of rear axle steering in some cases reduced the percentage of manoeuvres the vehicle could complete. In order to confirm the validity of these results, Section 6.2 presents an investigation of the effects on manoeuvrability of different steering strategies.

6.2 Comparison of Steering Strategies

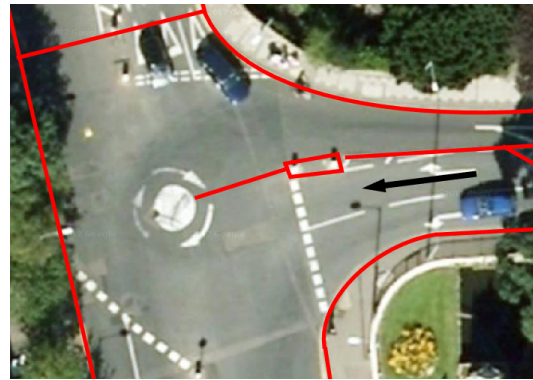
A number of rear axle steering strategies are defined in Chapter 4, and simulation models developed for each of them. The aim of this section is to analyse the effect of different steering strategies for specific manoeuvres. The four strategies used were ‘Rear Unsteered’ (a conventional, fixed rear axle), ‘Command-Steer’, ‘Partial Command-Steer’, and ‘Path-Following’.

Figure 6.1 shows a subset of manoeuvres from the ‘residential’ library. The performance envelopes for these manoeuvres for a rigid vehicle with four different rear axle steering strategies are shown in Figure 6.2.

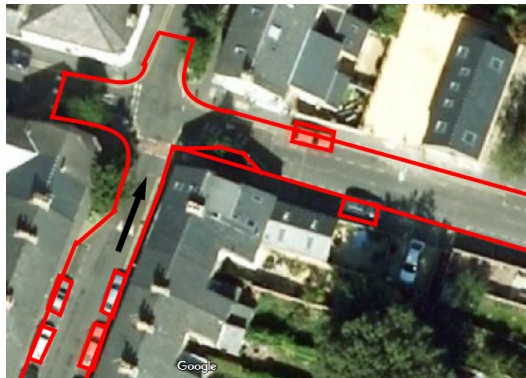
The results across all the manoeuvres show a fairly consistent pattern, with minor differences between manoeuvres. These differences can be attributed to the specifics of the manoeuvre. For example for some of the manoeuvres the entry is narrow compared to the



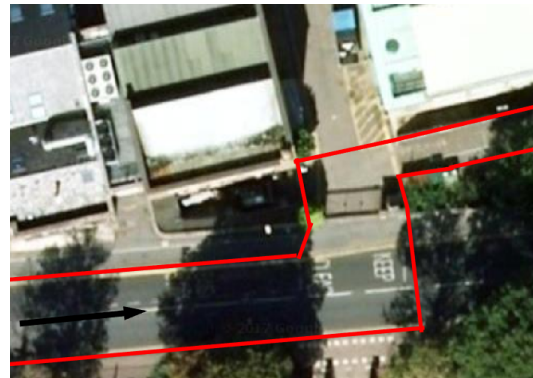
(a) Manoeuvre 1



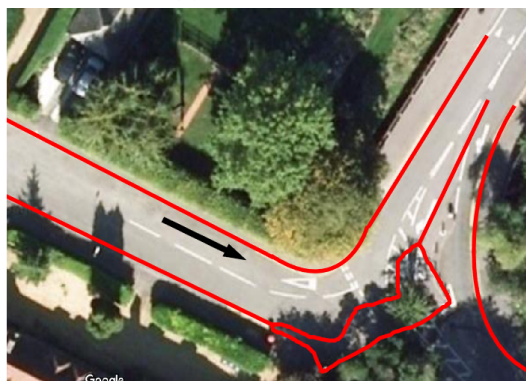
(b) Manoeuvre 2



(c) Manoeuvre 3



(d) Manoeuvre 5



(e) Manoeuvre 10



(f) Manoeuvre 13

Fig. 6.1 Subset of manoeuvres from the 'residential' library

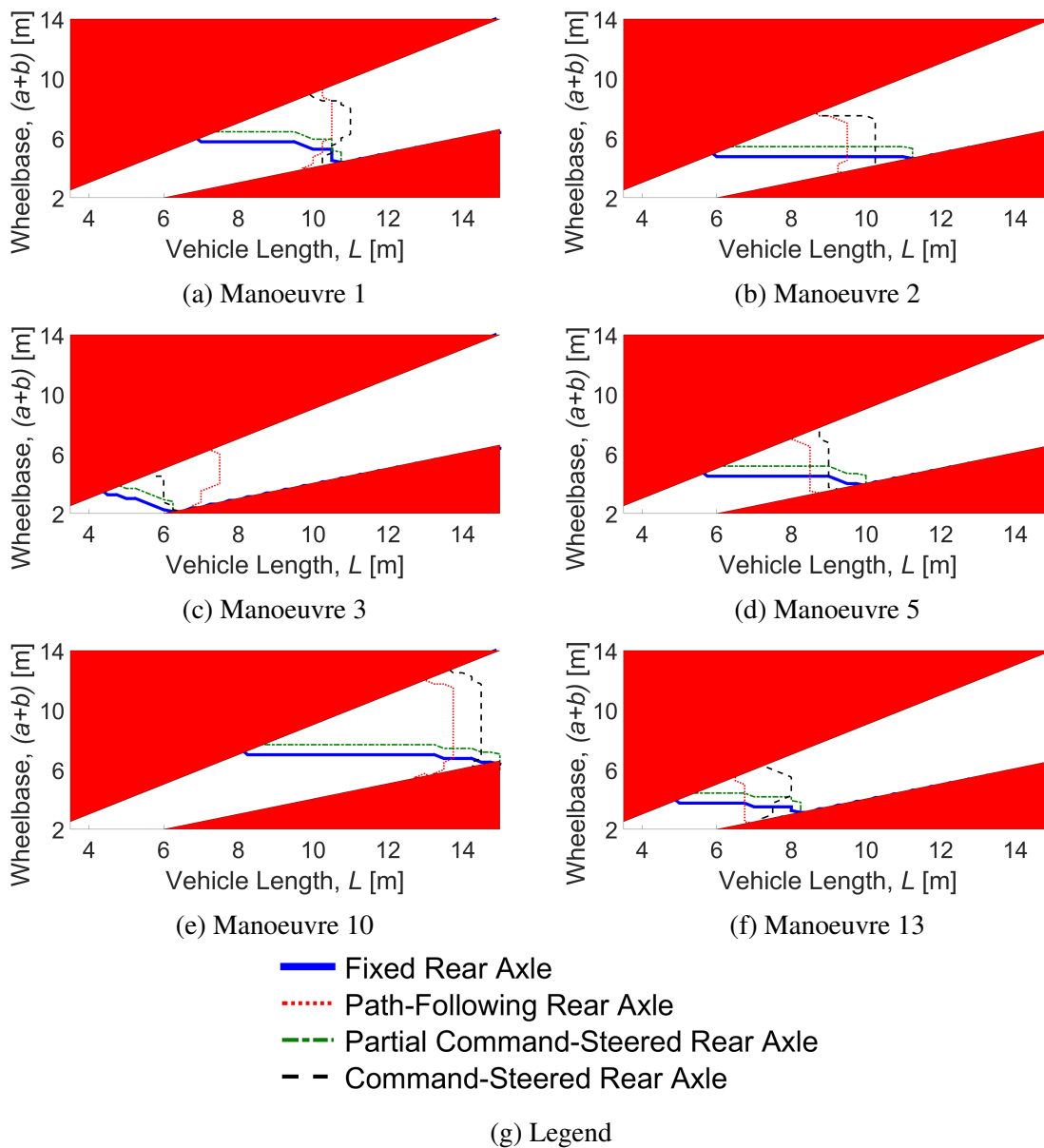


Fig. 6.2 Comparison between success boundaries for vehicles with and without rear axle steering for a selection of manoeuvres

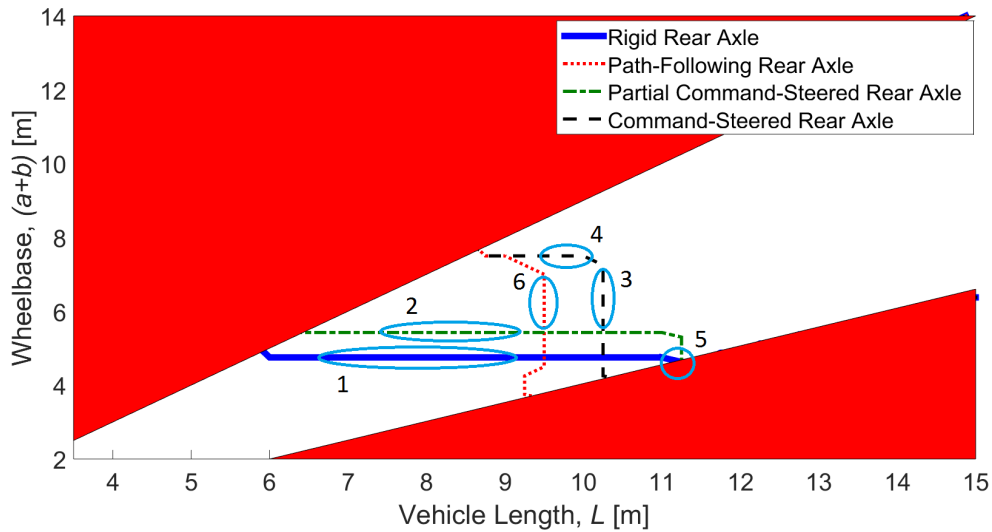


Fig. 6.3 Annotated results for Manoeuvre 2 from the residential library

exit, thus penalising tailswing (the outside rear corner of the vehicle swinging outside the line of the side of the vehicle). Contrastingly, manoeuvres with a wide entry but narrow exit penalise cut-in (the side of the vehicle on the inside of the turn moving in towards the centre of the turn) as the driver cannot ‘overshoot’ the corner. Thus some manoeuvres penalise vehicles with short wheelbases (and therefore long rear overhang and large tailswing) while others penalise long wheelbase vehicles (for increased cut-in).

Most manoeuvres show six consistent trends, the causes of which will be explained in Section 6.2.1. Figure 6.3 highlights key regions of the plot corresponding to these trends for Manoeuvre 2. (Manoeuvre 2 is shown in Figures 6.1b and 6.2b). The trends are as follows:

- (1) There is a limiting wheelbase for the Rear Unsteered vehicle.
- (2) The Partial Command-Steer strategy yields an identical success boundary to the Rear Unsteered case, but at a longer wheelbase.
- (3) With a fully Command-Steered rear axle, there is a maximum vehicle length which can be achieved across most wheelbases.
- (4) With a fully Command-Steered rear axle, there is also a limit on the maximum wheelbase.
- (5) The maximum successful length across all strategies is often found on the plot without rear axle steering, at short wheelbases.

- (6) The use of the Path-Following algorithm, as opposed to the Command-Steer algorithm, to control the rear steering angle generates the same pattern (a maximum achievable length) but the maximum length is reduced.

6.2.1 Expected Results

From the list above, the first two trends can be explained by considering the steady state turning circle of the vehicle. The minimum turning radius for a fixed rear axle vehicle is proportional to the tangent of the front steering lock angle, $\delta_{f,max}$, (which is considered fixed for this work) and the wheelbase, $(a + b)$. It is therefore clear that for a vehicle to achieve a particular turn radius in the steady state there is an upper limit on the wheelbase. The Partial Command-Steer vehicle is equivalent to a Rear Unsteered vehicle with a shorter wheelbase.

Conversely, with full Command-Steer, the effective wheelbase can be moved to any position on the vehicle (subject to the limit on the rear steering lock angle). Chapter 4 describes this process. Since the effective wheelbase can always be as far forward as it needs to be, the real wheelbase has no impact. Therefore with a steered rear axle the limit is instead on vehicle length, which can be achieved at any wheelbase (Trend (iii), Figure 6.3).

Not every effective wheelbase can be achieved for a given real wheelbase, because the rear steering angle is limited by the clearance available outside the frame rails of the vehicle chassis. Based on previous implementations, the maximum rear axle steering angle was set to $\delta_{r,max} = 25^\circ$. This creates a saturation region in the graph (Trend (iv) on Figure 6.3). In this region the effective wheelbase is still forward of the real wheelbase, but cannot reach the centre of the vehicle (where the Command-Steer algorithm aims to place it) because the rear steering angle saturates. Thus in this region the wheelbase is the limiting variable. This hypothesis was confirmed by running the simulation without a limit on the rear steering angle.

The fifth and sixth trends from the previous section are counter-intuitive. Figure 6.3 shows a region where the vehicle with fixed rear axle is successful whereas the addition of rear axle steering causes it to fail. A thorough analysis of this phenomenon was carried out and is described in the following section.

6.2.2 Command Steer: Analysis

The basic operating principle behind the Command-Steer algorithm for a rigid vehicle is that the steering angle of the axle to be steered should be proportional to the front axle steering angle. The choice of gain between the front and rear steering angles controls the effective wheelbase. The best gain for steady-state turning causes a follow point at the rear of the

vehicle to follow the path of a lead point at centre of the front axle during the steady-state region of a manoeuvre. This is equivalent to placing the effective rear axle almost in the middle of the vehicle (halfway between lead and follow points). However, in the transient part of the manoeuvre this causes extreme tailswing, and thus longer effective wheelbases may be more appropriate for real-world applications.

In the region of Figure 6.3 labelled '5', the vehicle represented is long, with a very short wheelbase (like a bus). The bottom of that region (shaded red) marks the boundary where the rear axle of the vehicle is halfway between the front axle at the rear bumper (i.e. at the point the Command-Steer algorithm aims to position the effective rear axle). Two vehicles, both with rear axles in the centre of the vehicle, one Rear Unsteered and the other Command-Steered, might be assumed to be identical if the Command-Steer gain is chosen such that the effective rear axle is also in the centre of the vehicle. However, this is only the case in steady-state turning. The effective axle position of the Command-Steered vehicle moves backwards and forwards along the vehicle as the vehicle moves through the manoeuvre, in proportion to the changing front steering angle. This accounts for the difference between the fixed and steered rear axle vehicles, which might have been assumed to be identical.

6.2.2.1 General Manoeuvre Analysis

This effect was investigated by simulating a long vehicle with a short wheelbase (i.e. a vehicle from the region of Figure 6.3 labelled '5') completing a 90° left turn with a 12.5 m radius. Figures 6.4 and 6.5 show the tailswing and cut-in, and the Swept Path Width respectively, for vehicles with fixed rear axle and Command-Steered rear axle. The tailswing was measured as the perpendicular distance of the outside rear corner of the vehicle from the path of the centre of the front axle. The cut-in was measured as the maximum perpendicular distance of any point on the inside of the vehicle from the path of the lead point. The Swept Path Width was the sum of the absolute values of tailswing and cut-in.

The differences between the two vehicles are small, as expected since in region 5 of Figure 6.3 the rear axle position is close to the Command-Steer target effective axle position (near the centre of the vehicle), thus the Command-Steer angles are small. However, there is a clear increase in tailswing of 0.08 m at step 185, caused by the application of rear axle steering. For the level of precision required by this method, that is enough to cause one vehicle to fail and the other to pass.

The counterpoint to this is that the cut-in at this step is very similar between the two vehicles, giving an increase in Swept Path Width of 0.07 m. Therefore the vehicle is unable to enter the manoeuvre further to the inside of the corner to compensate for the increased tailswing, because this will cause a collision on the inside of the vehicle.

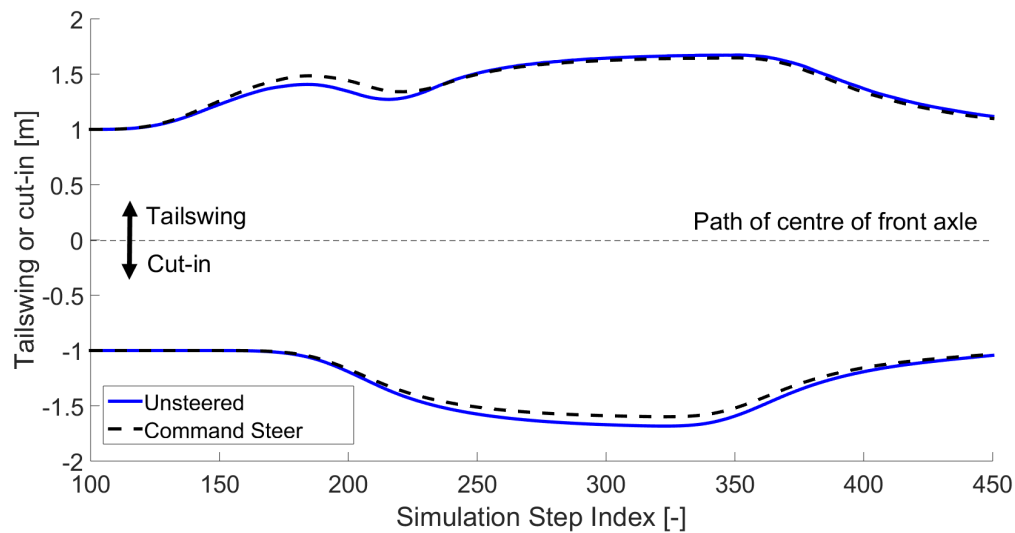


Fig. 6.4 Comparison of tailswing (positive values) and cut-in (negative values) between different steering strategies for an example manoeuvre. The vehicle had $L = 10.40$ m and $(a + b) = 4.72$ m

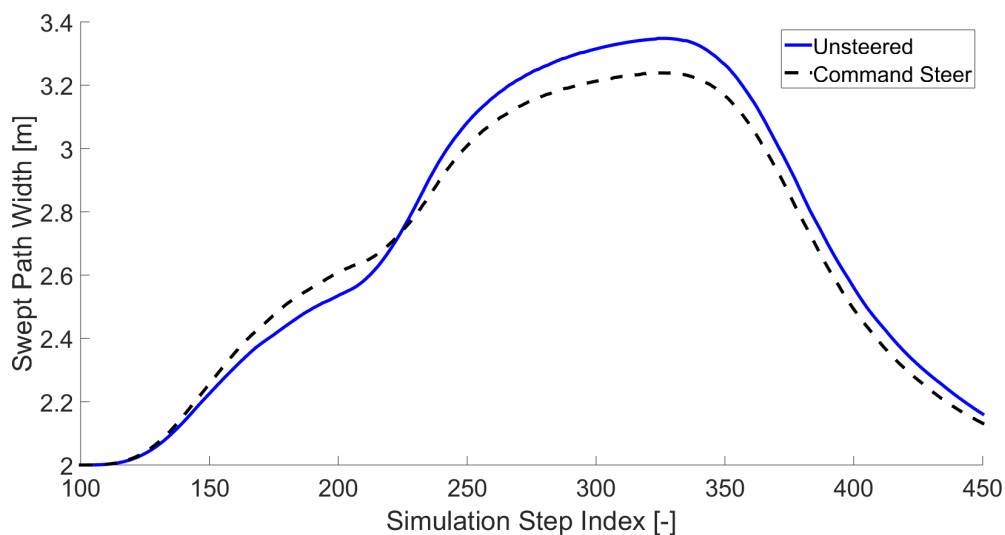


Fig. 6.5 Comparison of Swept Path Width between different steering strategies for an example manoeuvre. The vehicle had $L = 10.40$ m and $(a + b) = 4.72$ m

Through the steady-state region of the manoeuvre, between approximately step 260 and step 340, the cut-in (and therefore Swept Path Width) is reduced by the addition of rear axle steering, although this vehicle only gains a small improvement of 0.09 m, because the rear axle is so far forward. It is therefore shown that although the use of the Command-Steer algorithm reduces Swept Path Width through the apex of the turn (once the vehicle reaches steady-state) it has a negative effect on the Swept Path Width through the transient part of the manoeuvre. Therefore, vehicles are less likely to succeed on manoeuvres with a narrow entry, even if the exit is wide.

This highlights one of the effects that the shape of the manoeuvre has on the ability of vehicles of certain lengths and wheelbases to complete it.

6.2.2.2 Specific Manoeuvre Analysis

The effect of this behaviour on the success envelopes was investigated by simulating Manoeuvre 1 from the library (Figures 6.1a and 6.2a). A vehicle was chosen ($L = 9.75$ m, $(a + b) = 4.70$ m) which was just small enough to pass in both Command-Steer and Rear Unsteered configurations, and the separations to the most relevant obstacles measured at various points through the manoeuvre. Figure 6.6 shows the simulated position for the Command-Steered vehicle, annotated with the minimum clearances for both vehicles at the key points. Since the real rear axle position was close to the target position for the Command-Steer effective axle (halfway between the front axle and the rear bumper), the rear steering angles were small and therefore the paths were similar, but the difference in minimum clearances was significant.

Three areas of potential contact were obvious from the figure. First, a traffic island on the outside of the entry to the corner was a potential point of contact with the tail of the vehicle as it swung out. Secondly, the cut-in around the apex of the corner came very close to the inside pavement. Thirdly, on the exit of the corner, the front outside corner of the vehicle narrowly avoided a parked car.

As the two vehicles (Rear Unsteered and Command-Steered) enter the manoeuvre, they behave very similarly. Since the rear axle is close to the middle of the vehicle, both exhibit some tailswing. Although the Command-Steer angles are small because the rear axle is so far forward, they do cause a difference between the two vehicles, in the form of a slight increase in tailswing for the steered vehicle. This is shown in Figure 6.6 by the clearances in area 1, which are less than half as large for the Command-Steered vehicle. This is despite the fact that the clearances in area 2 are also significantly lower, so the vehicle cannot steer any further left to increase the clearance in area 1. This supports the reasoning that the Swept

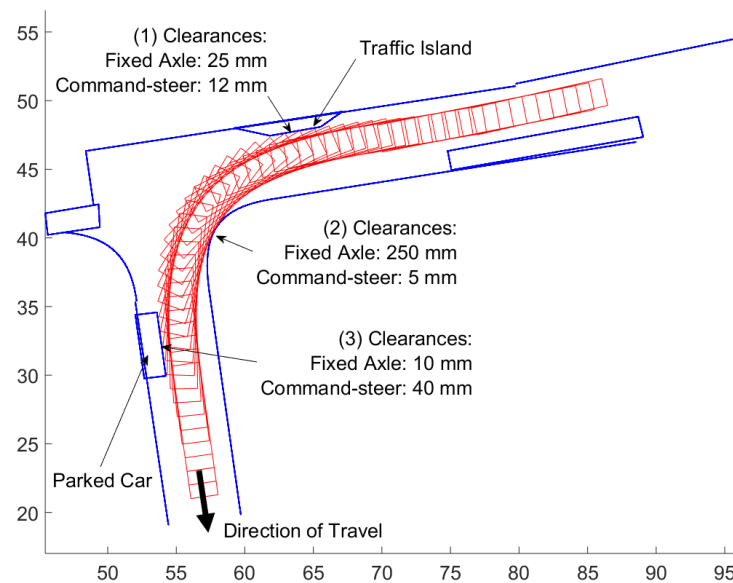


Fig. 6.6 Measurements of clearances around critical obstacles for example manoeuvre. The vehicle had $L = 9.75$ m and $(a + b) = 4.70$ m

Path Width in the early part of the manoeuvre is greater for the steered vehicle. This means that as the vehicle size is increased, the Command-Steered vehicle is the first to fail.

The benefit of the rear-steering algorithm comes in the second part of the manoeuvre, given that the clearance in area 3 is significantly greater for the Command-Steered vehicle. This is because the rear axle steering allows the vehicle to achieve higher yaw rates, so the vehicle is fully rotated by this point, as opposed to still swinging round as it is for the fixed rear axle vehicle. The Swept Path Width through this part of the manoeuvre is decreased by the addition of rear axle steering. It should be noted that there are other benefits of rear axle steering, such as improved load distribution, but this section is only concerned with investigating the apparent reduction in manoeuvrability at very low wheelbases.

This behaviour can be further confirmed by comparison between Manoeuvres 1 and 10 from the library. It can be seen from Figure 6.1a that early tailswing is likely to be penalised in this manoeuvre by the traffic island at the entry. Therefore, reducing the wheelbase (which therefore increases rear overhang and tailswing) will reduce performance (i.e. reduce the maximum length which can pass the manoeuvre). Figure 6.2a confirms that for a Command-Steered vehicle, reducing the wheelbase (e.g. from 7 m to 4 m) reduces the maximum length of vehicle which can complete the manoeuvre.

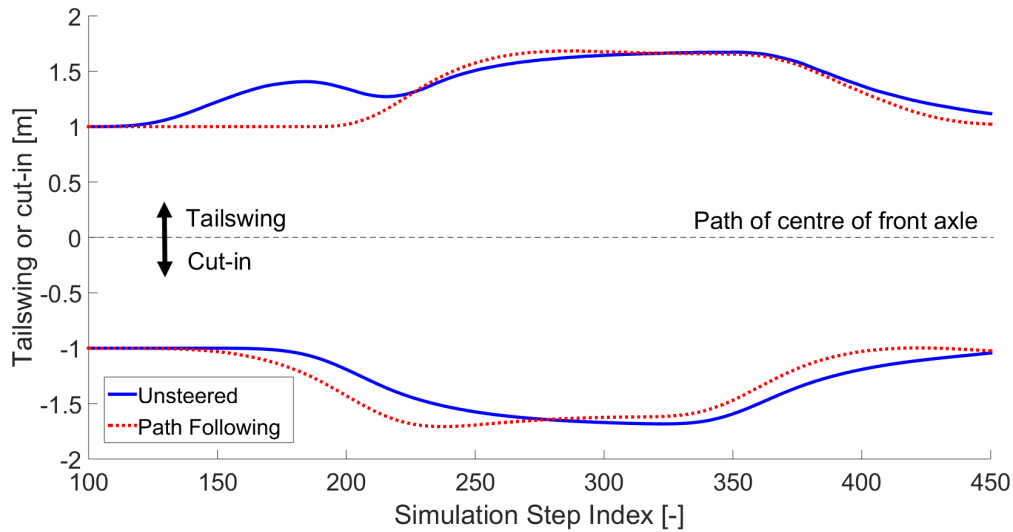


Fig. 6.7 Comparison of tailswing (positive values) and cut-in (negative values) between different steering strategies for an example manoeuvre. The vehicle had $L = 10.40$ m and $(a + b) = 4.72$ m

No such obstruction exists in Figure 6.1e and the road at the entry to the manoeuvre is wide, whereas the apex and exit are narrow, penalising cut-in instead. Therefore vehicles with a short wheelbase (and large tailswing) will not perform poorly. Figure 6.2e indicates that reducing the wheelbase has a much smaller impact on the maximum length which can pass Manoeuvre 10 than it does on Manoeuvre 1. This confirms that a vehicle which is likely to exhibit tailswing is not penalised as heavily on Manoeuvre 10 than on Manoeuvre 1.

Other manoeuvres were shown to exhibit similar behaviour, thus the contours representing the sum of all the manoeuvres also exhibits this behaviour at many points on the graph.

6.2.3 Path Following: Analysis

The Path-Following vehicle was assessed in the same way as the Command-Steered vehicle, in order to understand the reason for the reduction in maximum length compared to the Command-Steered case.

6.2.3.1 General Manoeuvre Analysis

The previous section demonstrated that an increase in the Swept Path Width can lead to a reduction in maximum length of a vehicle that can pass a manoeuvre with a particular characteristic (such as a narrow entry). If many manoeuvres in the library share the same characteristic then this trend will be visible in the sum of all the manoeuvre results.

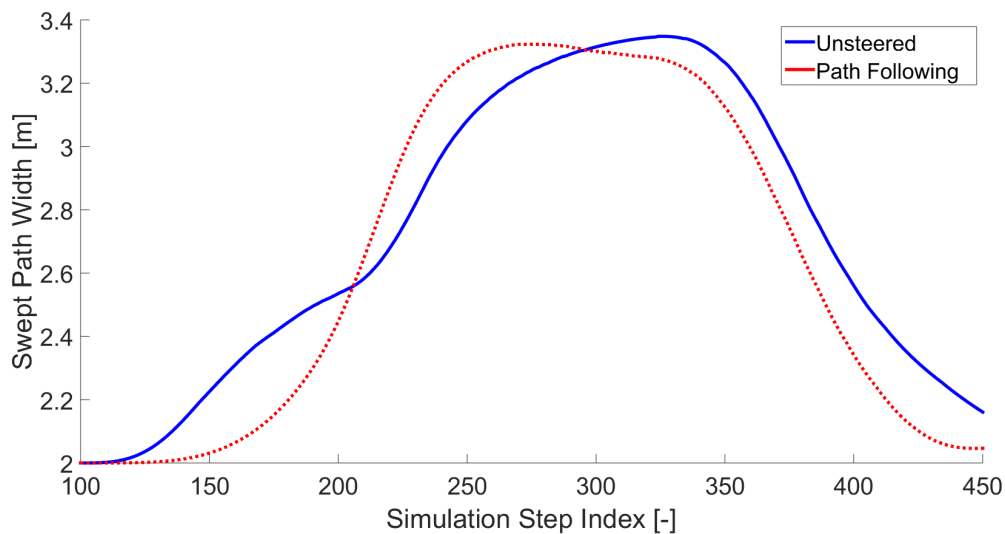


Fig. 6.8 Comparison of Swept Path Width between different steering strategies for an example manoeuvre. The vehicle had $L = 10.40$ m and $(a + b) = 4.72$ m

Figures 6.7 and 6.8 show the tailswing and cut-in, and Swept Path Width respectively for the vehicle with fixed rear axle and one using the Path-Following algorithm attempting the 12.5 m radius, 90° left turn. Figure 6.8 clearly shows a region in which the Swept Path Width is greater for the Path-Following vehicle than the Rear Unsteered vehicle (between step 200 and step 275). The reason for this is obvious from Figure 6.7 which shows that although the tailswing early in the manoeuvre is removed by the Path-Following algorithm, this has the effect of increasing cut-in in the next part of the manoeuvre, approaching the apex. Although on average the Swept Path Width of the Path-Following vehicle is lower across the whole manoeuvre, the presence of the region of higher Swept Path Width may cause failure if the manoeuvre exhibits obstacles at that particular point.

6.2.3.2 Specific Manoeuvre Analysis

Figure 6.9 shows the minimum clearances to the most restrictive constraints for the Path-Following and Rear Unsteered vehicles attempting Manoeuvre 1. A smaller vehicle was used than those from Section 6.2.2 to ensure that the Path-Following vehicle could complete the manoeuvre ($L = 9.50$ m, $(a + b) = 4.70$ m). The reduced clearance around the second potential collision point for the Path-Following vehicle compared to the Rear Unsteered vehicle corresponds to the part of Figure 6.8 where the Swept Path Width is higher for the Path-Following vehicle. The Path-Following vehicle does have room to move further to the right in the entry to the manoeuvre (the first potential collision point) but the vehicle needs

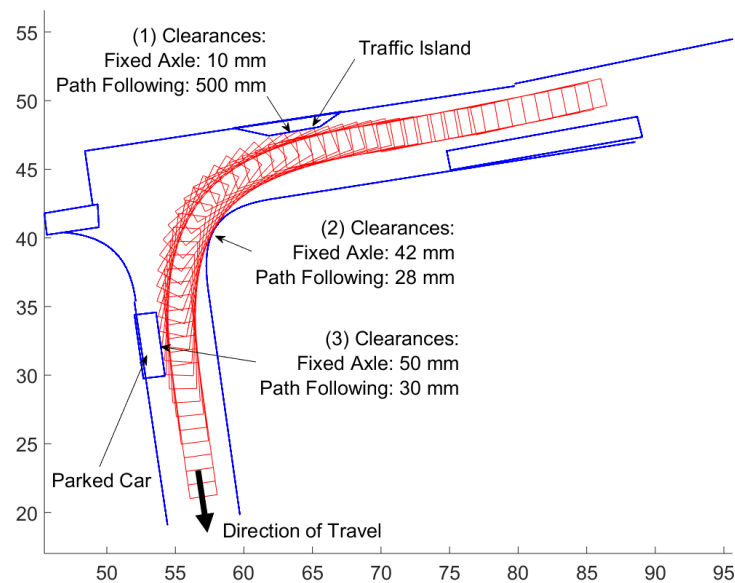


Fig. 6.9 Measurements of clearances around critical obstacles for example manoeuvre. The vehicle had $L = 9.50$ m and $(a + b) = 4.70$ m

to stay left, or it will not be able to achieve a high enough yaw rate to avoid colliding with the third potential collision point, where the clearance is lower than for the fixed rear axle vehicle.

6.2.4 Summary

The use of rear axle steering can, in certain cases, reduce the maximum length of vehicle which can complete a manoeuvre. For the Command-Steer strategy this is because the strategy can cause increased tailswing which can cause a vehicle to fail if the manoeuvre is narrow around the entry. For the Path-Following strategy, the tailswing is reduced to zero, but this is achieved by increasing cut-in later in the manoeuvre, which can cause the vehicle to fail if the manoeuvre is narrow between the entry and apex of the manoeuvre. In the real-world, this behaviour is not noticed because human drivers leave sufficient margin for error that the difference in Swept Path Width between steered and unsteered rear axles at entry and exit does not cause collision. This means that the much larger difference in Swept Path Width between steered and unsteered rear axles in the steady-state part of the manoeuvre is the main differentiator between rear axle steering strategies, thus the steered rear axle apparently performs better.

The intention of this investigation was to confirm that the shape of the results shown in Figure 6.2 is correct. Some aspects of the shape of these graphs were as expected, while others were not. The above investigation confirmed that the aspects of those results which were unexpected were due to true phenomena and not errors in the simulation. It was therefore considered appropriate to use this method to analyse the case studies described below.

6.3 Case Study A: Grocery Delivery Vehicle

The first Case Study to be investigated was home delivery of groceries. Personal vehicles are a highly inefficient method for transporting groceries, because each vehicle only carries deliveries for one household. Existing home delivery systems can fit the deliveries for up to approximately 25 households into a 3.5 t, 6.3 m-long van, which takes up a comparable amount of space on the road to the average (in the UK) 4.8 m-long personal vehicle. This suggests that home delivery of groceries, as opposed to collection in personal vehicles, could save a significant number of vehicle journeys, thus reducing congestion, as well as greenhouse and noxious emissions.

In order to maximise the benefits of using home delivery, one way to improve the efficiency of the system would be to increase the capacity of the vehicles used. If the vehicle can make additional deliveries in a single journey before returning to its collection point, fewer kilometres are spent travelling to and from its 'base'. Additionally, increasing capacity requires fewer vehicles on the roads (assuming demand remains constant), thus further reducing congestion and emissions. The impacts of maximising capacity of freight vehicles are discussed in Chapter 1.

However, the higher capacity vehicle is required to have comparable manoeuvrability to standard personal vehicles, as it must be able to access the same areas. The framework described in the previous section would therefore be applicable, to attempt to quantify the potential for increasing the size of the current vehicles, without limiting their access to the required areas.

6.3.1 Current Vehicle

6.3.1.1 Description

For this case study, the baseline vehicle used is a Mercedes Sprinter van, with a 3.7 m wheelbase and an overall length of 6.3 m. The Gross Vehicle Weight (GVW) is 3.5 t, with a

payload capacity of 1 t. The vehicle has a fixed rear axle. This is representative of the vehicle used by a number of major supermarkets in the UK.

The vehicle payload is carried in plastic trays known as ‘totes’. The layout of the totes in the baseline vehicle is shown, approximately to scale, in Figure 6.10. The totes used by the supermarket operating the baseline vehicle are 0.6 m long, 0.4 m wide, and 0.24 m high, which is comparable to those used by other supermarkets. This has an impact on the minimum sensible increase in dimensions of the vehicle. For this investigation, it was assumed that no change to the size and shape of the totes was possible.

Different operators take different approaches to the layout of the totes in the vehicle, so in order to provide fair comparison the same layout as the baseline vehicle was used. The layouts of existing home delivery vehicles are not necessarily optimised for maximum volumetric capacity, which is why the maximum number of totes does not match the maximum that might be predicted from the external dimensions. It was recognised that more radical solutions such as rearranging the layout of totes in the vehicle, or eliminating totes entirely might have a positive impact on capacity, but these design decisions are typically made for operational or cost reasons (for example the use of totes simplifies the picking operation at the store), and so were considered beyond the scope of this project.

The baseline vehicle carries a maximum of 95 totes, as shown in Figure 6.10. The first row of 15 totes are stacked perpendicular to the vehicle, in three stacks of five, and used for frozen goods. Behind this are four rows of totes stacked parallel to the vehicle, each row comprising four stacks of five. These are divided into two compartments, one chilled and one at ambient temperature. A small amount of space is left at the rear of the load space for a trolley and to provide a surface to assist the driver with loading. Given the limits of 95 totes and 1 t of payload, the maximum expected tote mass was calculated to be 10.5 kg, when averaged across the whole vehicle.

Since the majority of the totes are stacked parallel to the vehicle, any increase in length must be added in multiples of 0.6 m to match discrete numbers of totes. With the current loading pattern, every additional 0.6 m allows space for an additional 20 totes. Additional totes could be arranged perpendicular to the vehicle instead of parallel, such that an additional row only requires an additional 0.4 m of length (although the row only consists of 15 totes). Two scenarios will be considered: adding totes parallel (which fits with the current design) or perpendicular (which would require some redesign of the interior).

6.3.1.2 Manoeuvrability Performance

A library of 20 manoeuvres applicable to this operation was identified by a combination of interviews with drivers of home delivery vehicles, and analysing in-service GPS data

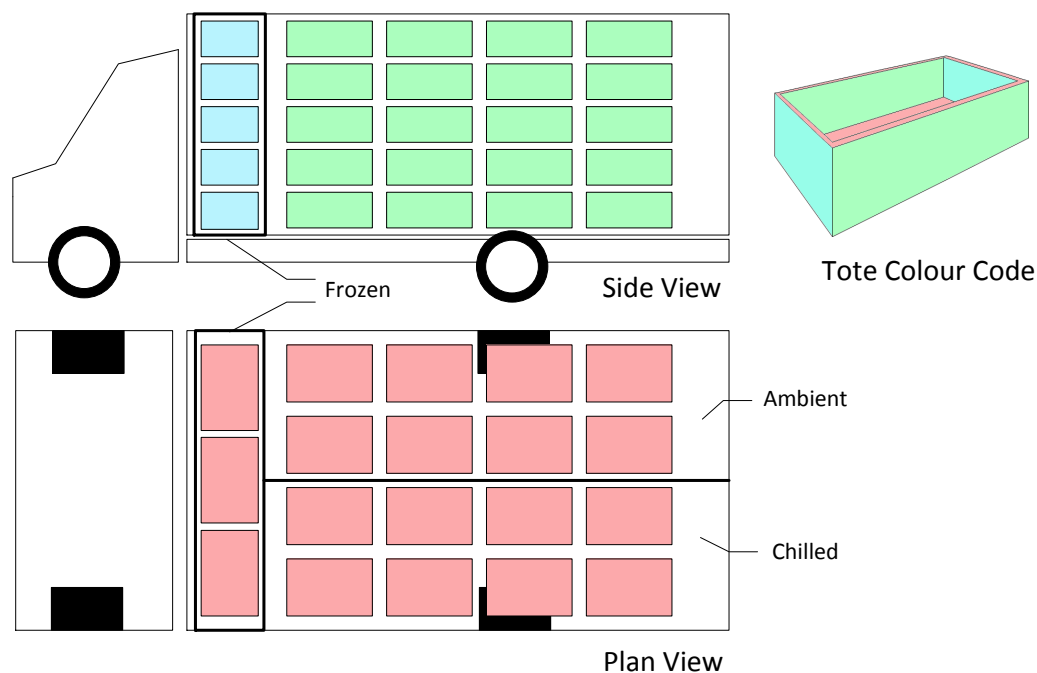


Fig. 6.10 Arrangement of totes in the baseline vehicle

from the existing vehicles. The manoeuvres were all in residential areas of Cambridge, UK. Figure 6.11 shows contours of constant success rate for vehicles attempting the library of manoeuvres. The location of the baseline vehicle is marked, as is the contour for 90% success rate, which corresponds to the success rate of the baseline vehicle. The use of only 20 manoeuvres generated some artefacts in the results. For example the distance between the 90% and 95% contours was much greater than between the 95% and 100% contours. This could be improved by using more manoeuvres, and was not considered detrimental to the conclusions drawn. Additionally, some of the contours displayed jagged edge effects due to the path optimisation algorithm hitting a local minimum. These were corrected by attempting the manoeuvres manually (by directly controlling steering angle).

Figure 6.11 shows that the baseline vehicle has some scope for improvement in the length and therefore capacity, without reducing the percentage of manoeuvres passed. However, Figure 6.12 shows additional constraints on the design of the vehicle which limit the options. These constraints are the UK limit on Gross Vehicle Weight without requiring a higher category license, and the rear axle load.

First, the UK limit on Gross Vehicle Weight (without requiring additional licensing) is 3.5 t. This was related to vehicle length, L , by the load model described in Chapter 4, and the contour shown on the graph as a vertical line at $L = 6.3$ m. While this is not a hard constraint,

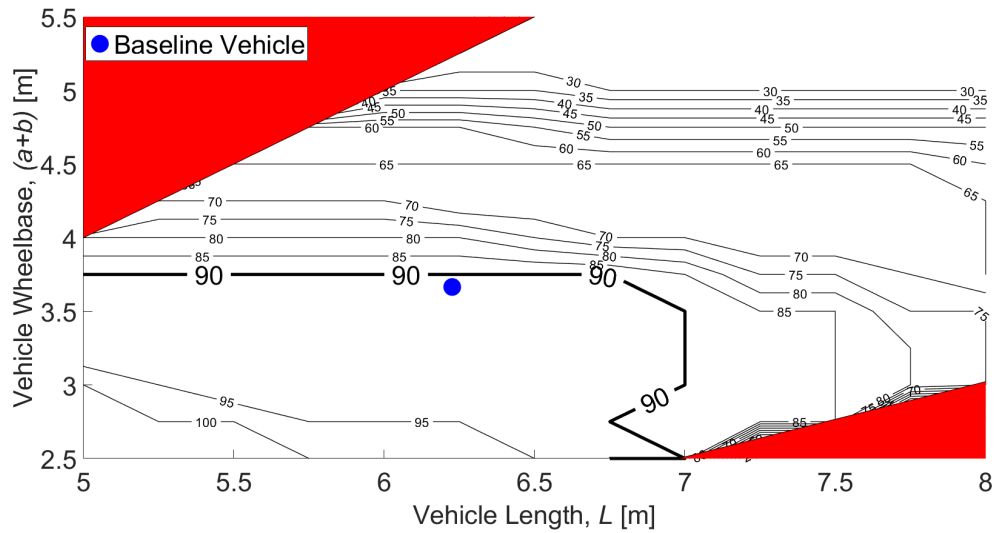


Fig. 6.11 Baseline grocery delivery vehicle. Contours show constant success rate across all residential manoeuvres for a rigid vehicle with fixed rear axle

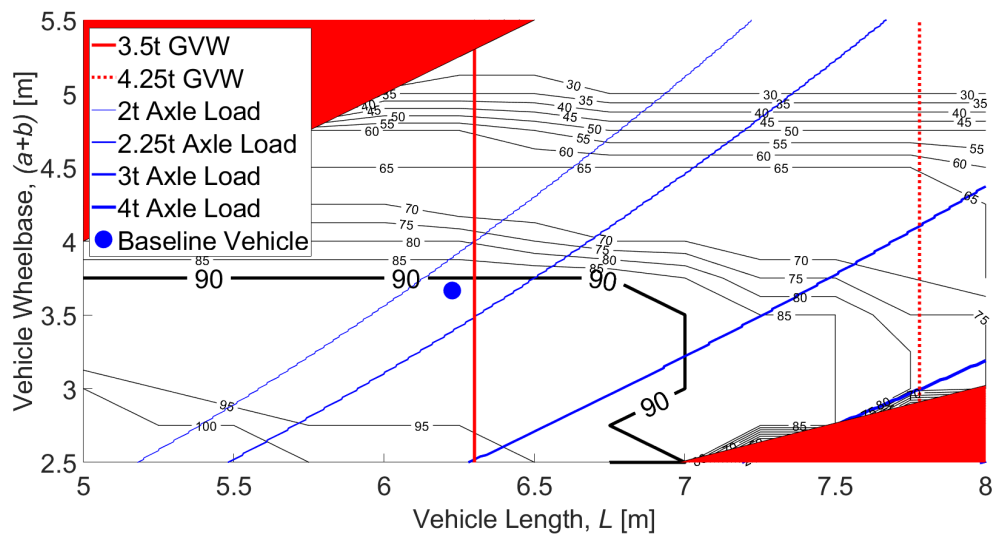


Fig. 6.12 Axle load and GVW constraints for a home grocery delivery vehicle. Contours show constant success rate across all residential manoeuvres for a rigid vehicle with fixed rear axle

the expense of paying a more highly trained driver and fitting the vehicle with the required additional monitoring equipment (tachograph) makes it desirable to remain below the limit. Also shown is the contour corresponding to a Gross Vehicle Weight of 4.25 t, which is set to become the new limit under forthcoming legislation [84]. The figure shows that the baseline vehicle is well optimised towards the current limit of 3.5 t, with little scope for improvement. However, the increase to 4.25 t would allow a significant addition to the length of up to 1.5 m (although only some of this is available without moving to a lower manoeuvrability contour).

Secondly, Figure 6.12 shows contours of constant rear axle load. The load on the rear axle increases whenever the vehicle either increases in length (and therefore total mass) or decreases in wheelbase (thereby moving the balance point further back). As with the GVW limit, this is not a hard constraint, since axles can be designed to bear more or less load. However, a higher rear axle load increases the likelihood of exceeding the rear axle load limit before the vehicle reaches full capacity, therefore the rear axle rated load would ideally be kept below 2.25 t, which is the designed maximum axle load for the baseline vehicle (although this is not a legal limit). The combination of this constraint and the 90% manoeuvrability contour limits the design almost exactly to the baseline vehicle, even with the relaxation of the GVW constraint.

6.3.2 Rear Axle Steering: Command Steer

A potential method for realising the available length benefits without violating the axle load constraint, is to steer the rear axle of the vehicle. Given an appropriate strategy, this allows the real wheelbase of the vehicle to move, without having any impact on the effective wheelbase, as described in Chapter 4. This has the effect of allowing the rear axle to be placed close to the rear of the vehicle (thus keeping the load balance between axles in the centre and minimising the rear axle load) while keeping the effective wheelbase close to the centre of the vehicle, thus providing the manoeuvrability of a shorter vehicle.

6.3.2.1 Manoeuvrability Performance

Figure 6.2 confirms the description in the previous paragraph, showing that the vehicle with a fixed rear axle typically has a maximum wheelbase for a given length, whereas the vehicle with a steered rear axle can usually achieve its maximum length at almost any wheelbase. Similar patterns are seen across the majority of the other manoeuvres.

Figure 6.13 shows the contours of constant manoeuvre success rate for the vehicle if fitted with a Command-Steered rear axle. Unlike the Rear Unsteered vehicle from Figure 6.11, the maximum length can now be achieved at almost any wheelbase. This effectively allows the

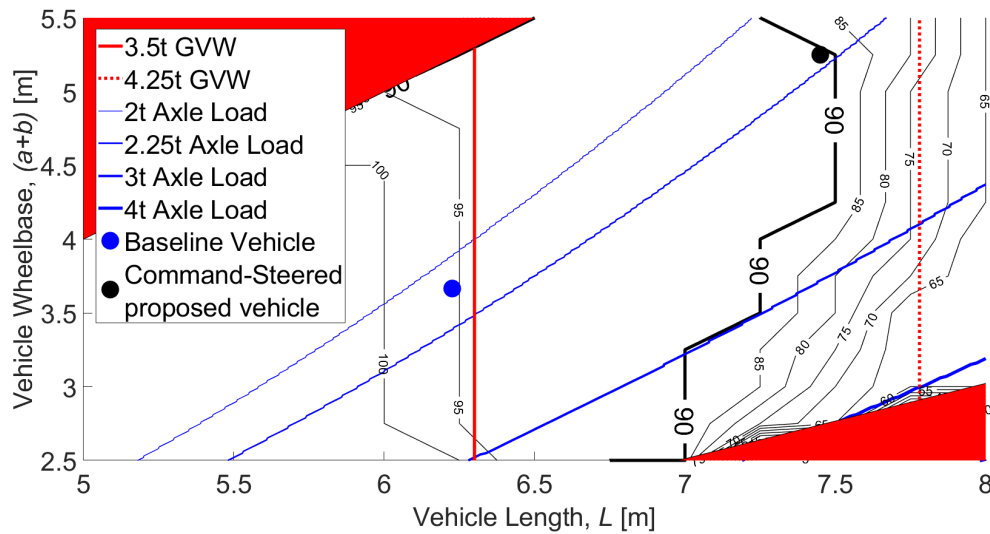


Fig. 6.13 Proposed Command-Steered alternative to the baseline grocery delivery vehicle. Contours show constant success rate across all residential manoeuvres for a rigid vehicle with Command-Steer strategy

design to follow the contours of constant rear axle load upwards along the 2.25 t contour, to greater wheelbases, but without violating the 90% manoeuvrability success rate. The figure shows the design point for a suggested vehicle, equipped with a Command-Steered rear axle, with a length of 7.45 m and a wheelbase of 5.25 m.

6.3.2.2 Gross Vehicle Weight and Rear Axle Loads

This Command-Steered vehicle remains under the 4.25 t GVW limit and the 2.25 t rear axle load guideline, maintains the baseline vehicle's manoeuvre success rate of 90%, and increases the length of the vehicle by 1.2 m. This corresponds to 40 additional totes in two rows of 20 totes.

Analysis of the baseline vehicle suggested an expected maximum tote mass of 10.5 kg, which across 40 additional totes corresponds to a total payload increase of 0.42 t. The vehicle mass distribution model described in Chapter 4 assumes a chassis mass of 208 kg m^{-1} . Over the 1.2 m vehicle length increase, this equals an increase in mass of 0.25 t. Thus the total increase in mass of the vehicle would be 0.67 t. This leads to a GVW of 4.17 t which does not violate the new 4.25 t limit, permitting the vehicle to be operated without HGV licensing (provided the rear axle steering technology can be provided with minimal weight increase).

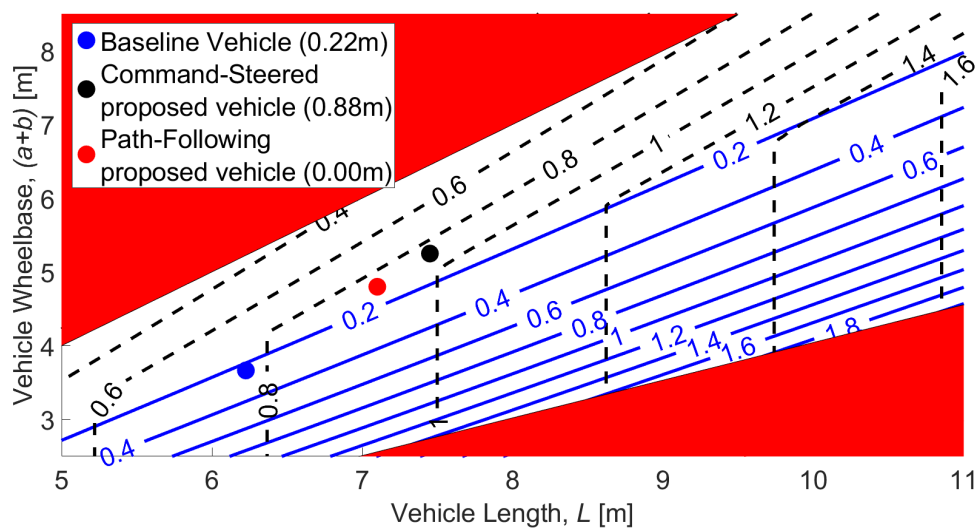


Fig. 6.14 Contours of constant tailswing for different rear axle steering strategies. Solid blue contours represent an unsteered vehicle, dashed black contours represent a Command-Steered vehicle

6.3.2.3 Tailswing

It is commonly accepted that the Command-Steer algorithm increases the tailswing of a vehicle compared to the case of the unsteered rear axle. This effect was quantified for different values of L and $(a+b)$ by evaluating the maximum possible tailswing by simulating the vehicle applying full front steering lock, and measuring the deviation of the rear outside corner from the straight line during the transient part of the manoeuvre. This allowed contours of constant tailswing to be plotted, as shown in Figure 6.14. This figure shows the design points for the Rear Unsteered, Command-Steered and Path-Following vehicles (presented below). The Rear Unsteered vehicle generates 0.22 m of tailswing, compared to 0.88 m for the Command-Steered vehicle.

In the absence of steering saturation, the Command-Steer contours would be purely vertical. This is because the effective wheelbase is always in the same position, so the real wheelbase has no effect on the tailswing. The diagonal region of the contour plot is the region where the rear steering angle demand is higher than the rear steering lock angle, thus the steering saturates. This pattern is also seen in the contours of constant manoeuvre success rate.

The selection of an acceptable limit for tailswing is difficult. For design of articulated Heavy Goods Vehicles the UK limit is 0.8 m. However, this assumes the standard roundabout test which would generate less tailswing than the maximum steering lock approach used here, since these vehicles are much smaller than those usually tested using the standard roundabout.

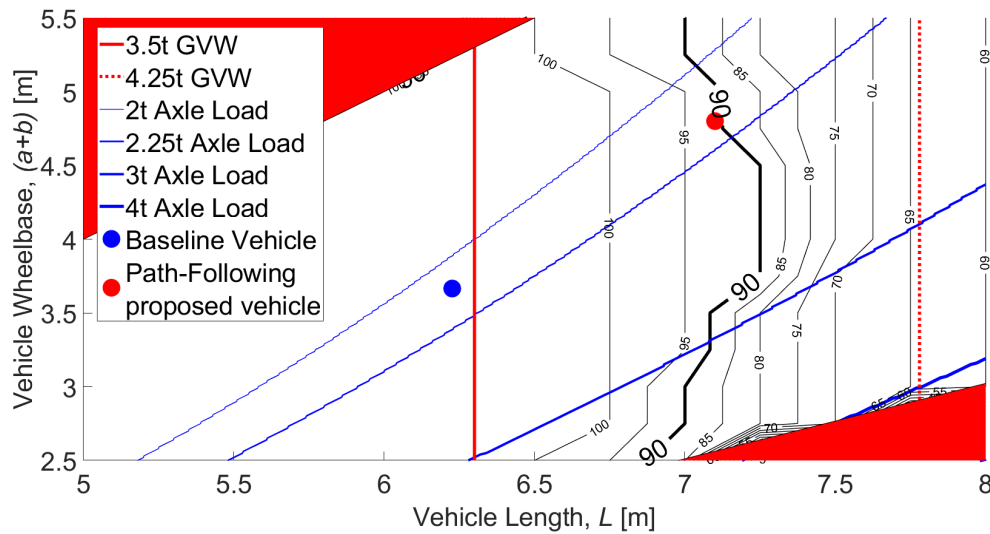


Fig. 6.15 Proposed Path-Following alternative to the baseline home delivery vehicle. Contours show constant success rate across all residential manoeuvres for a rigid vehicle with Path-Following strategy

This being the case, 0.8 m could be considered a generous upper bound on the tailswing limit. Alternatively, the vehicle could be designed to match the maximum tailswing of the baseline vehicle. It is clear from Figure 6.14 that either of these limits would be difficult to achieve using the Command-Steer strategy.

6.3.3 Rear Axle Steering: Path Following

The analysis above assumed the Command-Steer strategy commonly used in industry for the rear axle control strategy. Figure 6.15 shows the potential improvement available through implementing a Path-Following rear axle, compared to the Rear Unsteered vehicle. The increase in length is enough to allow a single additional row of 20 totes if the current tote layout is maintained, or an additional total of 30 totes if the totes can be rotated to accommodate two smaller rows. The Path-Following strategy is believed to provide greater drive-ability than Command-Steer, since it eliminates tailswing during the transient part of the manoeuvre (unlike Command-Steer which exaggerates it) and is easily predictable, as the rear of the vehicle follows the front. However, it is not as optimised for minimisation of Swept Path Width as the Command-Steer strategy. This means that Path-Following steering has less of a positive impact on the 90% success rate contour than Command-Steer, as can be seen from the optimised Path-Following and Command-Steer vehicles on Figure 6.16.

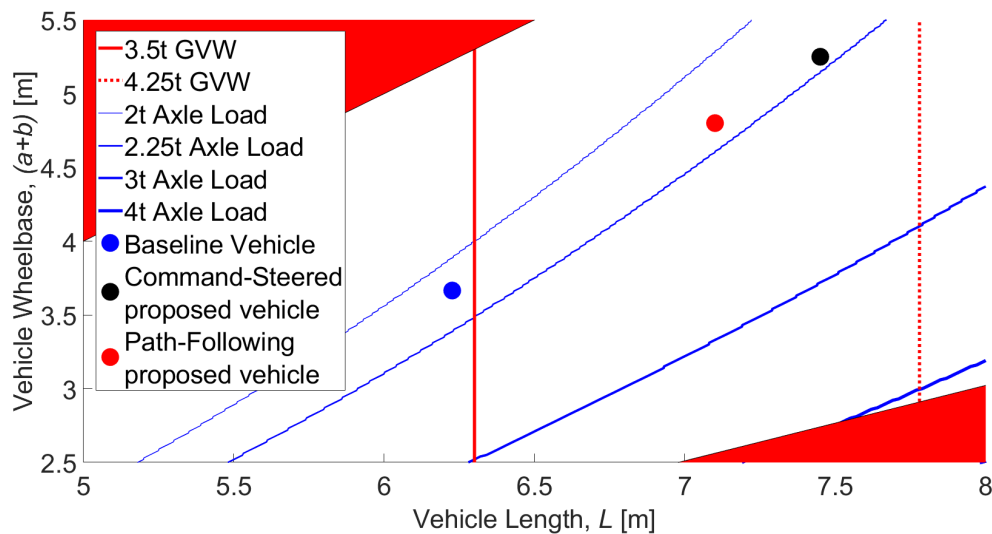


Fig. 6.16 Proposed design options for increasing capacity of a home grocery delivery vehicle

6.3.4 Comparison of Potential Designs

There is a need for consideration of steering strategy when designing vehicles with rear axle steering. Fixed strategies such as Command-Steer and Path-Following may be less optimal than a hybrid strategy, where the driver (or the vehicle) can select the optimal strategy. For example, turning from a small street into a main road requires minimisation of tailswing, thus Path-Following would be optimal. Conversely turning from a main road into a narrow street requires minimisation of cut-in, whereas there is plenty of room for tailswing, hence Command-Steer would be preferable. More complex options, such as the driver steering the front and the rear having an independent obstacle avoidance strategy could be considered. This work will be carried out as part of a future project.

It should be noted that these simulations assume ‘perfect knowledge’ of the road—i.e. driver blindspots are not considered. This assumption benefits the Command-Steer algorithm, because it overlooks the fact that tailswing can cause the rear of the vehicle to move dangerously in the driver’s blind spot. Conversely, the Path-Following algorithm does not cause tailswing and the rear of the vehicle always follows the path traversed by the front, which is much easier for the driver to understand.

The analysis presented here yields two potential alternatives to the baseline vehicle, if the GVW limit is increased to 4.25 t. These designs are shown in Figure 6.16 and summarised in Tables 6.1. The rear axle steering strategies have been abbreviated to CS (Command-Steer) and PF(Path-Following). All designs were volume limited, according to the average

Table 6.1 Comparison between potential designs of Grocery Delivery Vehicle

	Baseline	Design 1	Design 2
Rear Axle Steering Strategy	Fixed	CS	PF
Length, L (m)	6.23	7.45	7.10
Length Increase from Baseline (m)	0	1.22	0.87
Wheelbase, $a + b$ (m)	3.67	5.25	4.8
Manoeuvre Percentage Success Rate	90	90	90
Gross Vehicle Weight (t)	≤ 3.5	≤ 4.25	≤ 4.25
Rear Axle Load (t)	≤ 2.25	≤ 2.25	≤ 2.25
Maximum Tailswing (m)	0.22	0.88	0
Volumetric Capacity Increase (m ³)	0	4.88	3.48
Load Capacity Increase (t)	0	0.50	0.57
Additional Tote Capacity (stacked parallel)	0	40	20
Percentage Increase in Totes	0	42	21
Additional Tote Capacity (stacked perpendicular)	0	45	30
Percentage Increase in Totes	0	47	32

maximum tote mass described above, although this does not take into account any additional mass of a steered rear axle.

A typical day for the baseline vehicle when fully loaded consists of between 20 and 25 deliveries, suggesting an average delivery size of three to four totes. By this measure the Path-Following vehicle described above could complete up to an additional 8 deliveries per day, and the Command-Steered vehicle an additional 12 deliveries.

6.3.5 Summary

- i The home delivery vehicle used as a baseline is well optimised for a GVW limit of 3.5 t.
- ii Increasing the allowable GVW from 3.5 t to 4.25 t allows an increase of up to 1.5 m in the length of the vehicle without reducing the locations accessible to the vehicle. However without rear axle steering this requires shorter wheelbases, and thus increased rear axle loads.
- iii Rear axle steering removes this limitation and allows up to a 1.2 m increase in the length of the vehicle, without violating any constraints. Current technology for steering of rear axles either cannot be used with a single rear axle (in the case of mechanical Command-Steer) or is heavy and expensive. This would increase the mass of the vehicle beyond 4.25 t if fitted, so an alternative method of steering the rear axle would be required.

- iv The rear axle can be controlled by the Command-Steer algorithm. This leads to the maximum possible increase in tote capacity of 47%, but does this by generating unacceptably high tailswing.
- v An alternative steering strategy is the Path-Following algorithm, which removes the tailswing, at the expense of some additional cut-in, slightly reducing the possible length increase. However this still yields a potential 32% increase in tote carrying capacity.

6.4 Case Study B: Refuse Collection Vehicle

The role of a refuse collection vehicle is to collect domestic waste from residences and transport that waste to landfill sites (or recycling centres). The challenge in the design of these vehicles is that the sites to which the refuse is delivered are usually located far from towns and cities. This means that the vehicle must travel a significant distance every time it is full, in order to be emptied. The fuel and time cost of this distance makes it desirable to limit the amount of times the vehicle has to be emptied, and therefore to increase the capacity of the vehicle. While increasing the capacity of the vehicle would reduce the number of journeys to and from landfill sites or recycling centres, it would also limit the residential areas the vehicle can access, which would require bins to be walked to the vehicle, slowing down the process and increasing costs and driver workload.

An additional challenge is the weight of the bin lifting equipment, which is typically mounted at the back (although side-loading refuse vehicles do exist). This increases rear axle loads relative to the front axle.

6.4.1 Current Vehicle

The baseline vehicle used for this analysis was based on a Mercedes Econic 26 t 6x2 chassis, fitted with a Dennis Eagle Olympus body. The tandem rear axles of the Mercedes vehicle were combined in the simulation into a single heavier rear axle, at the position of the effective wheelbase of the original group. The performance of this vehicle is shown in Figure 6.17, on the plot showing manoeuvrability contours for a rigid vehicle on the same library of 'residential' manoeuvres as was used for Case Study A.

The success rate of the baseline vehicle was 30%. Note that this does not mean the vehicle can only access 30% of houses. There are several reasons why the percentage is so low. First, human error in extraction of the boundary constraints from the satellite imagery may have made them more difficult to complete. Second, it was assumed that all constraints were hard constraints, thus no part of the vehicle could cross them. In practise, a constraint such as a

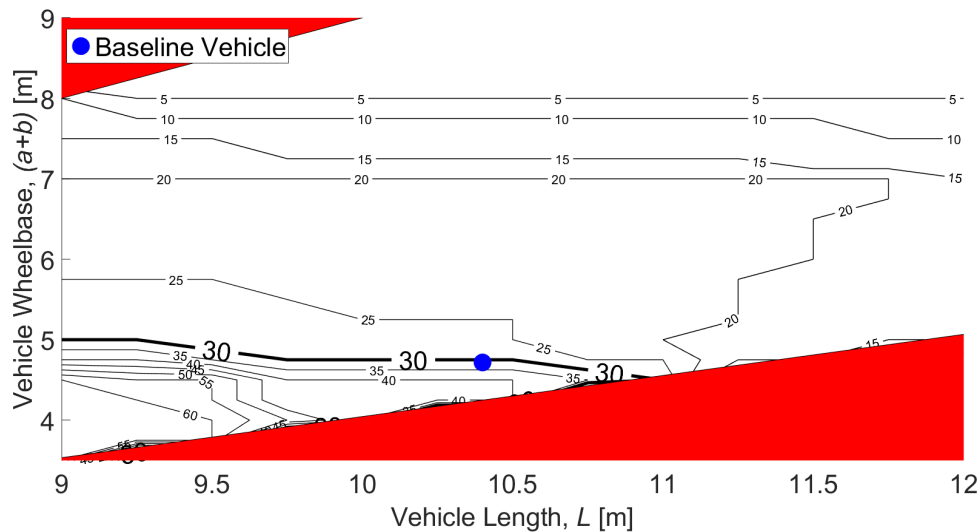


Fig. 6.17 Baseline refuse collection vehicle. Contours show constant success rate across all residential manoeuvres for a rigid vehicle with fixed rear axle

kerb will be crossed by the front and rear overhangs, and will only limit the positions of the wheels. Differentiating between these types of constraint would increase the apparent success rate. Third, several of the manoeuvres were chosen by inspection of satellite imagery, thus there is no guarantee that they are used by refuse vehicles. Although all manoeuvres were from residential areas, some may be bypassed by taking longer routes in practice. Finally, in service, the vehicle may be reversed one or more times for particularly difficult manoeuvres, which was not allowed by the simulation. None of these sources of error was considered critical, provided all vehicles were considered relative to the baseline vehicle.

The capacity of the baseline vehicle was 21.4 m^3 , and the vehicle was analysed using a standard density of compacted household refuse of 540 kg m^{-3} , for a total payload of 11.6 t. These values were taken from the vehicle specification sheet. The height and width were assumed constant along the length of the cargo section at 2 m each. This gives a volumetric capacity of $4 \text{ m}^3 \text{ m}^{-1}$, or 2.16 t m^{-1} . The length of the cargo section of the vehicle, without the bin lift was 5.2 m. The total length of the bin lift and compacting equipment was 3 m.

Several potential manoeuvrability interventions were considered for improving the capacity of the baseline vehicle: applying the three rear axle steering strategies described in Chapter 4; use of an articulated vehicle instead of a rigid vehicle; and use of an articulated vehicle with the Path-Following steering strategy.

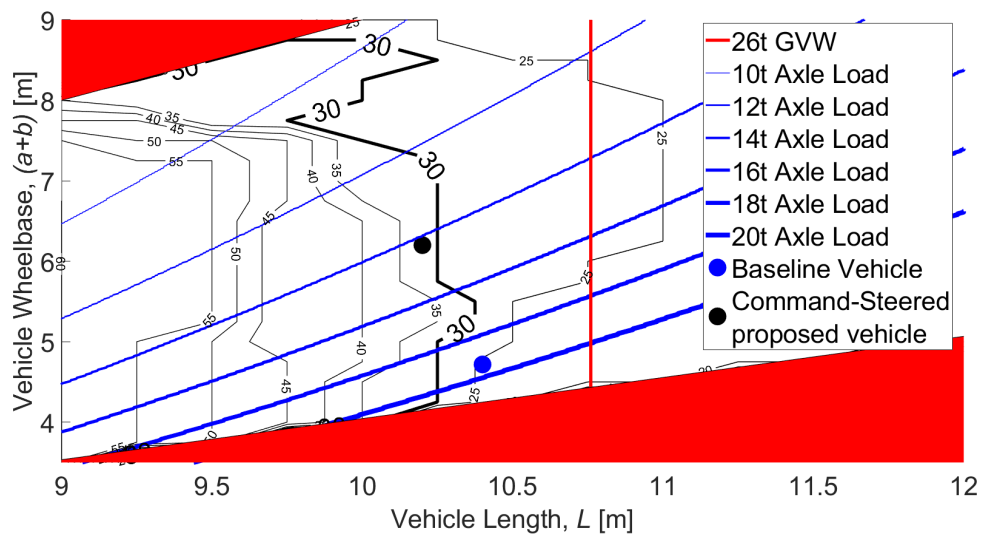


Fig. 6.18 Proposed Command-Steered alternative to the baseline refuse collection vehicle. Contours show constant success rate across all residential manoeuvres for a rigid vehicle with Command-Steer strategy

6.4.2 Rear Axle Steering: Command-Steer

The Command-Steer algorithm was used to generate a set of success rate contours, shown in Figure 6.18. The figure clearly shows that a rear axle steering vehicle cannot improve on the overall length of the baseline vehicle without reducing the manoeuvre success rate below 30%. The reasons for this are discussed in Section 6.2. The figure also shows the constant GVW contour at 26 t. This is the legal limit for a three-axle rigid vehicle (assuming certain axle specifications are met). This was considered a ‘soft’ constraint, as it could be exceeded by changing the configuration of the vehicle, or in the case of legislative changes.

The use of rear axle steering permits the wheelbase to be increased significantly for only a small penalty in length, to the operating point shown at 6.2 m wheelbase. Figure 6.18 shows that this would reduce the load on the rear axle group from 19 t to just 14 t. Alternatively, this would enable a higher density of payload without increasing the rear axle load. This could be achieved by using a stronger compactor.

Although there are equally manoeuvrable designs at even higher wheelbases, above the proposed design point indicated on Figure 6.18 the load on the front axle exceeds that on the rear. This design point reduces the vehicle length compared to the baseline vehicle by 0.25 m leading to a reduction in payload of 0.54 t.

The contours from Figure 6.14 can also be used to show that the tailswing for this vehicle is almost 1.5 m which is unacceptably large. In order to reduce the tailswing below the legal limit of 0.8 m, the vehicle must be reduced in length by approximately 2 m, thus reducing

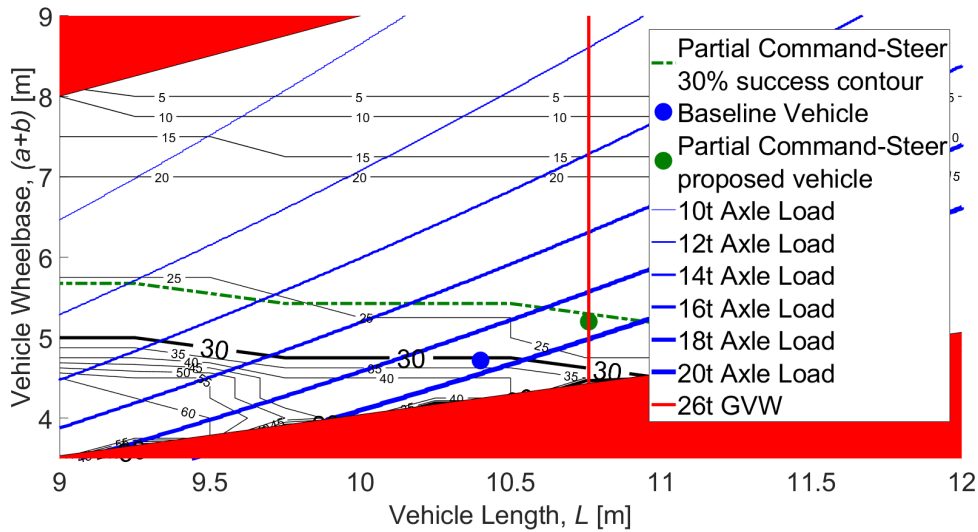


Fig. 6.19 Proposed Partial Command-Steered alternative to the baseline refuse collection vehicle. Contours show constant success rate across all residential manoeuvres for a rigid vehicle with fixed rear axle, and the 30% success rate contour for a rigid vehicle with Partial Command-Steer strategy

capacity significantly. Therefore, Partial Command-Steer was investigated as an alternative rear axle steering strategy to reduce tailswing.

6.4.3 Rear Axle Steering: Partial Command-Steer

Chapter 4 describes an alternative to the Command-Steer strategy, which is to steer only the axles of a group which are furthest from the centre of the vehicle. This positions the effective rear axle at the position of the front axle of the axle group, rather than at the centre of the group. This causes the vehicle to behave like a vehicle with shorter wheelbase. This strategy also has the effect of reducing tyre wear, by eliminating the scrubbing generated by multi-axle groups.

The wheelbase of the rear axle group of the baseline vehicle is 1.35 m. Therefore, moving the effective rear axle from the centre of the group to the front reduces the wheelbase by 0.675 m. This can be simulated by moving all the success contours upwards by 0.675 m. However, this analysis is not valid for wheelbases originally shorter than the current limit of half the vehicle length. Figure 6.19 shows the effect on the 30% success rate contour of applying this increase in wheelbase. The potential increase in capacity is 0.36 m or 0.78 t. This does not have any impact on the rear axle load (except a share of the additional 0.78 t plus the additional mass of the chassis) because the real rear axle position is unchanged.

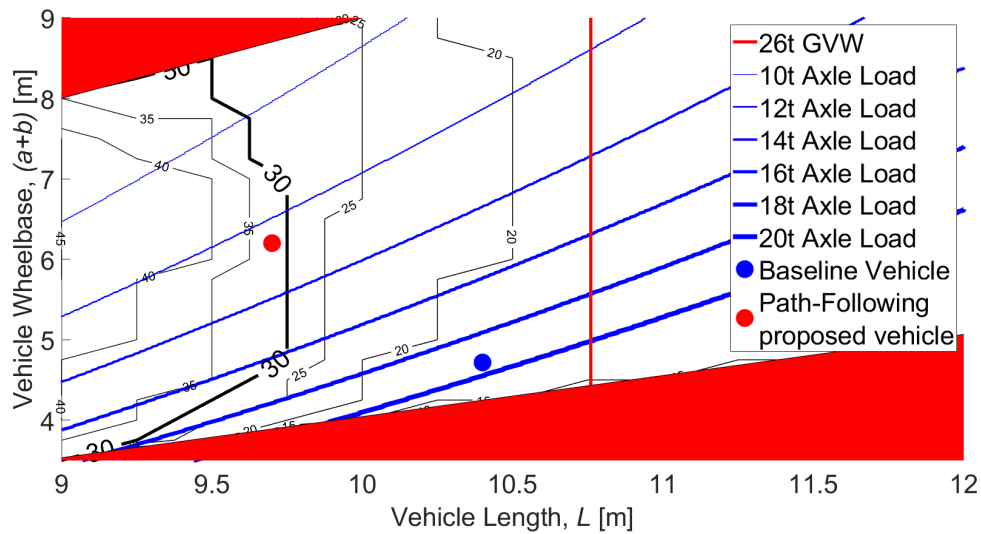


Fig. 6.20 Proposed Path-Following alternative to the baseline refuse collection vehicle. Contours show constant success rate across all residential manoeuvres for a rigid vehicle with Path-Following strategy

This strategy reduces tailswing compared to the full Command-Steer strategy, but still increases it relative to the baseline vehicle, above the legal limit of 0.8 m. Therefore, Path-Following rear axle steering was investigated as a method for eliminating tailswing completely.

6.4.4 Rear Axle Steering: Path-Following

Using the Path-Following algorithm instead of Command-Steer removes the tailswing entirely, but reduces the capacity even further. Figure 6.20 shows the contours of success rate for the Path-Following rigid vehicle.

The loss of length is 0.7 m which corresponds to a reduction in payload of 1.5 t. However, the wheelbase can be increased as for the Command-Steered vehicle, which reduces the rear axle loads down to similar levels.

6.4.5 Articulation

Figure 6.21 shows the contours of constant success rate for an articulated refuse vehicle. The tractor unit was described in Chapter 4. The axes of the figure represent different parameters for the articulated vehicle compared to the rigid vehicle, so direct comparison of the x-axis is not relevant, but Figure 6.21 shows that the trailer length, L_2 can be set to 11.45 m without reducing the manoeuvre success rate compared to the baseline vehicle.

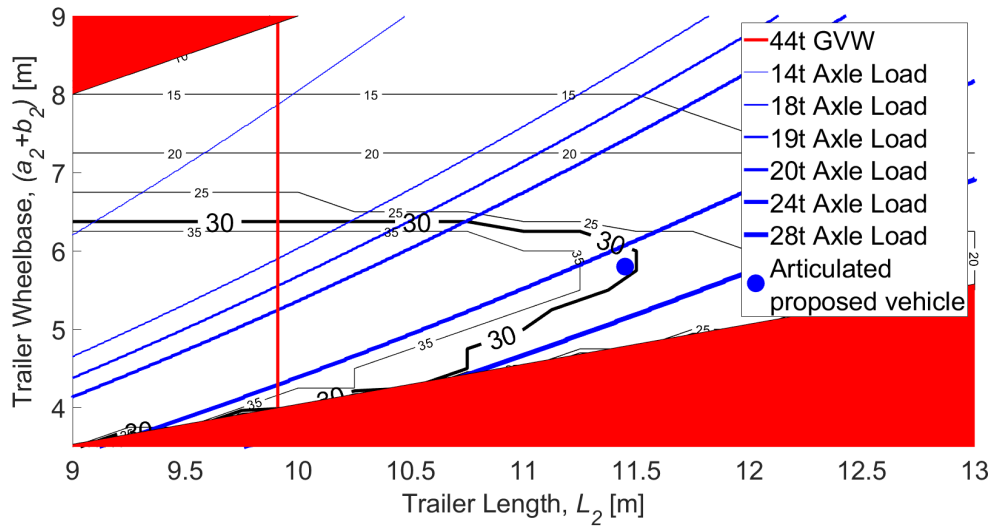


Fig. 6.21 Proposed articulated alternative to the baseline refuse collection vehicle. Contours show constant success rate across all residential manoeuvres for an articulated vehicle with fixed rear axle

Assuming the length of bin lift and compacting equipment is the same as for the baseline vehicle, this gives a cargo length of 8.45 m, thus the volumetric capacity of the articulated vehicle can be calculated as 33.8 m^3 and the payload as 18.3 t, which is an increase of 58% over the baseline vehicle.

The load models from Chapter 4 can be used to calculate the Gross Vehicle Weight of the articulated vehicle, and the load on the rear axle (or rear axles combined). These models give a rear axle load of 25 t. The limit in the UK for a tri-axle group is 25.5 t so this vehicle would just be acceptable. However, the proposed vehicle does exceed the current UK GVW limit of 44 t for Heavy Goods Vehicles, therefore some legislative change would be required to make this vehicle feasible. Alternatively, a trailer of this length would enable a 44 t vehicle with a lower compaction factor for the payload, thus reducing the cost of the vehicle. In the absence of changes to the 44 t GVW limit for Heavy Goods Vehicles, the optimum design point for an articulated vehicle would be at $L_2 = 9.8 \text{ m}$, $(a_2 + b_2) = 6 \text{ m}$.

6.4.6 Articulation and Rear Axle Steering

An articulated vehicle with trailer axle steering was also investigated. For this analysis the Path-Following algorithm was used, as the Command-Steer algorithm was expected to give unacceptable tailswing. Figure 6.22 shows the maximum possible trailer length for this vehicle without reducing the manoeuvre percentage success rate below 30%.

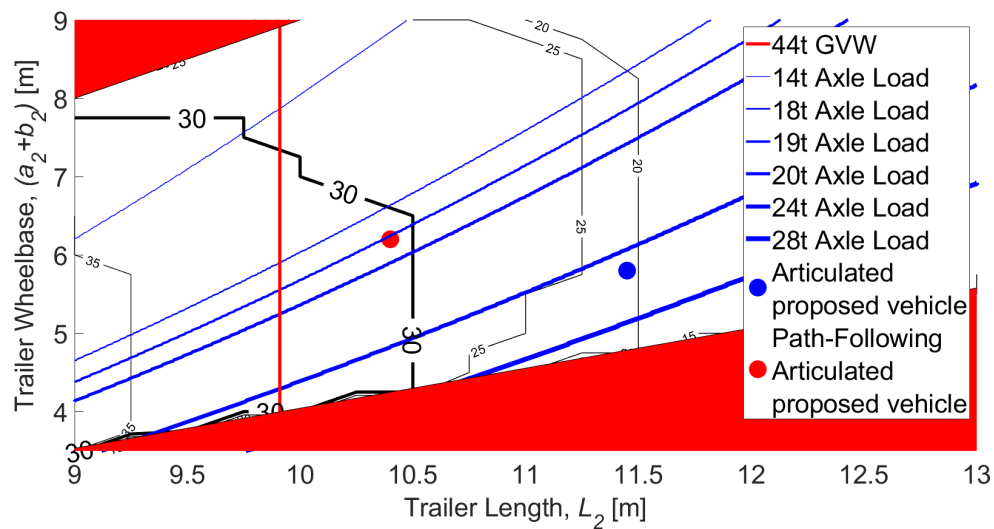


Fig. 6.22 Proposed Path-Following articulated alternative to the baseline refuse collection vehicle. Contours show constant success rate across all residential manoeuvres for an articulated vehicle with Path-Following strategy

The figure shows that the trailer length is more limited than the unsteered trailer. However, the maximum steered trailer length of 10.45 m still improves capacity from the baseline vehicle, from 11.6 t to 16.1 t. As for the rigid vehicle, this reduction in length caused by the addition of trailer steering is small, and is offset by the benefit of being able to increase the wheelbase, and thus use axles with a lower load rating, or to load the vehicle with a higher density payload without overloading the rear axles before the vehicle is full.

The contours of constant trailer axle load for the trailer axle group are shown in Figure 6.22. This figure shows that the axle load for this combination is reduced below 20 t.

6.4.7 Comparison of Potential Designs

The potential designs described above are summarised in the Table 6.2. The rear axle steering strategies have been abbreviated to CS (Command-Steer), PCS (Partial Command-Steer), and PF(Path-Following).

Table 6.2 Comparison between potential designs of Refuse Collection Vehicles

	Baseline	Design 1	Design 2	Design 3	Design 4	Design 5
Vehicle Type	Rigid	Rigid	Rigid	Rigid	Articulated	Articulated
Rear Axle Steering Strategy	Fixed	CS	PCS	PF	Fixed	PF
Length, L or L_2 (m)	10.4	10.2	10.7	9.7	11.45	10.4
Wheelbase, $a + b$ or $a_2 + b_2$ (m)	4.72	6.2	5.2	6.2	5.8	6.2
Manoeuvre Percentage Success Rate	30	30	30	30	30	30
Gross Vehicle Weight (t)	≤ 26	≤ 26	≤ 26	≤ 26	≥ 44	≥ 44
Rear Axle Group Load (t)	≤ 19	≤ 15	≤ 19	≤ 13	≤ 25	≤ 20
Total Vehicle Length (m)	10.4	10.2	10.7	9.7	14.1	13.05
Cargo Space Length (m)	5.2	5.0	5.5	4.5	8.5	7.5
Volumetric Capacity (m^3)	20.8	20	22	18	34	30
Load Capacity (t)	11.2	10.8	11.9	9.7	18.4	16.2
Percentage Load Capacity Increase	0	-3.6	6.25	-13.4	64.3	44.6

6.4.8 Summary

- i The refuse collection vehicle behaves very differently to the home delivery vehicle, largely due to the very large rear-overhang caused by the bin-lifting and compacting equipment.
- ii This vehicle already exhibits considerable tailswing. The addition of Command-Steer exacerbates this.
- iii The use of the Partial Command-Steer strategy gives a small increase in load capacity, along with a potentially large reduction in tyre wear.
- iv Using the Path-Following algorithm reduces the tailswing to zero, but generates large cut-in values to do so. Thus the length and therefore load capacity of the Path-Following vehicle is reduced. As for Case Study A, the use of any rear axle steering strategy permits the rear axles to be further back and therefore reduces the rear axle load.
- v The greatest gain in load carrying capacity can be found by creating an articulated vehicle, with a small urban tractor unit. However, this vehicle would likely have a Gross Vehicle Weight above 44 t when fully loaded and therefore could not be completely filled under current legislation. This vehicle could be suitable for collections with a lighter compactor and therefore lower payload density, if there was a suitable business case based on the cost of the compactor.
- vi Applying Path-Following steering to the articulated vehicle's trailer unit reduces the potential capacity relative to the vehicle with fixed rear axle, but still provides an increase in load carry capacity compared to the existing vehicle, and at lower rear axle load than the fixed rear axle vehicle. This vehicle still exceeds the 44 t GVW limit, and so would in practice need to be shorter, unless current legislation was relaxed.

6.5 Case Study C: Urban Store Vehicle

The third case study was an investigation of the vehicles used for restocking stores in city centres. Many of these stores are so-called 'convenience stores', with relatively low shelf space, and little storage space for excess stock. This means they have to receive multiple deliveries per day. Distributors often provide transport for multiple stores in the same city, so the ability to increase the capacity of the vehicle (and thus restock more stores without returning to a distribution centre) would be an advantage.

Table 6.3 Example vehicles typically used in city centres

Vehicle	Length (m)	Wheelbase (m)	Roll cage capacity	GVW (t)
10 t Rigid	8	5	18	10
18 t Rigid	11	7	30	18
Urban trailer	8.5	5.8	30	32
Standard trailer	13.6	8.5	51	44

A wide variety of vehicles are used to restock city centre stores. Choice of vehicle is dependent on a number of factors, including size of store, temperature (chilled, frozen, ambient) of products stocked, number of stores in the city to be visited by the same operator, and accessibility of the stores in terms of road dimensions. A logistics provider with a range of different trucks in its fleet was identified for the study, and four vehicles are summarised in Table 6.3. The length of the vehicle was given by the operator, the wheelbase was estimated from images of the vehicles, and the roll cage capacity was calculated using the load models from Chapter 4.

The load model for this case study was adapted for discrete numbers of roll cages (as opposed to a load density, which was used for the previous case studies). This generated ‘steps’ in the contours of constant axle load. Roll cages are used by the majority of grocery providers, and come in a variety of sizes. For this analysis, a roll cage was taken to have a footprint of 0.8 m by 0.7 m, which could be arranged in rows of three across the width of the vehicle, and a full laden mass of 450 kg (50 kg empty). Thus for every 0.8 m of additional length to the vehicle, three additional roll cages could be carried, with an additional payload of 400 kg each.

All simulated vehicles were considered single-deck vehicles, and it was assumed that any suitably manoeuvrable single-deck vehicle could also be designed as a double-deck. The disadvantage of conversion to double-deck is the reduced rollover stability, but this was not considered as part of this work.

Most stores tend to be on larger roads than the residential manoeuvre library used for the previous two case studies, thus a second library of ‘urban’ manoeuvres was collected. Observations in Cambridge were used to identify the most common routes from the surrounding trunk network into the city centre, and the library contains a combination of manoeuvres from these routes, and exits from some yards recognised as being particularly constrained.

Case Study C did not define a particular research question as clearly as the previous case studies, therefore a slightly different approach was used. Because such a wide range of vehicles are used for very similar tasks, the selection of vehicle is largely driven by operator

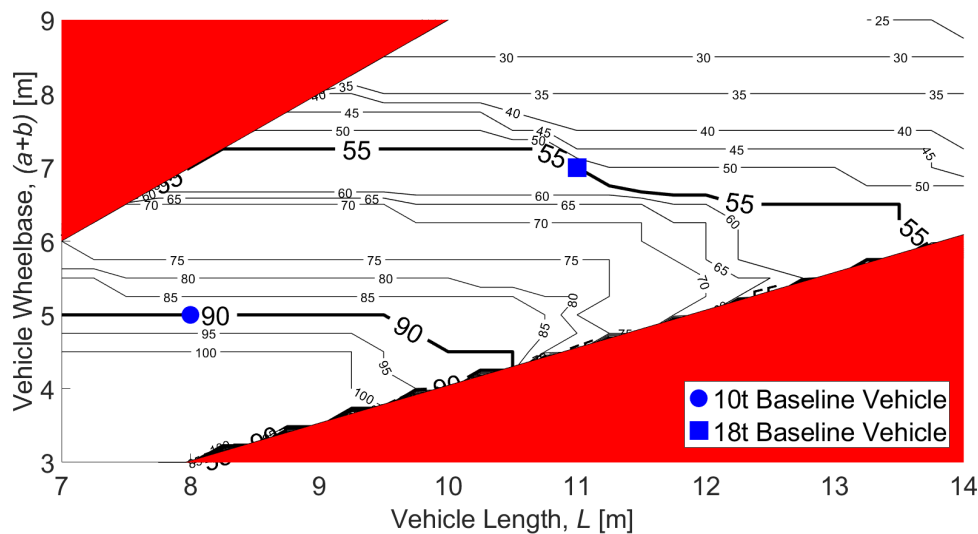


Fig. 6.23 Baseline 10 t and 18 t rigid vehicles. Contours show constant success rate across all urban manoeuvres for a rigid vehicle with fixed rear axle

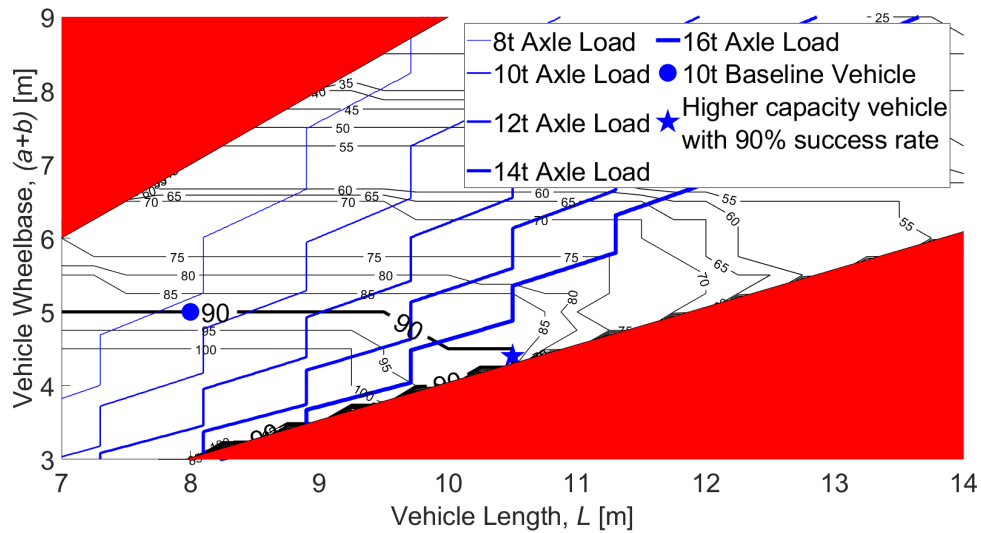
preference (partly guided by historical choices). However, some possible alternative vehicles were defined using the vehicles from Table 6.3 as baseline cases.

6.5.1 Rigid Vehicle

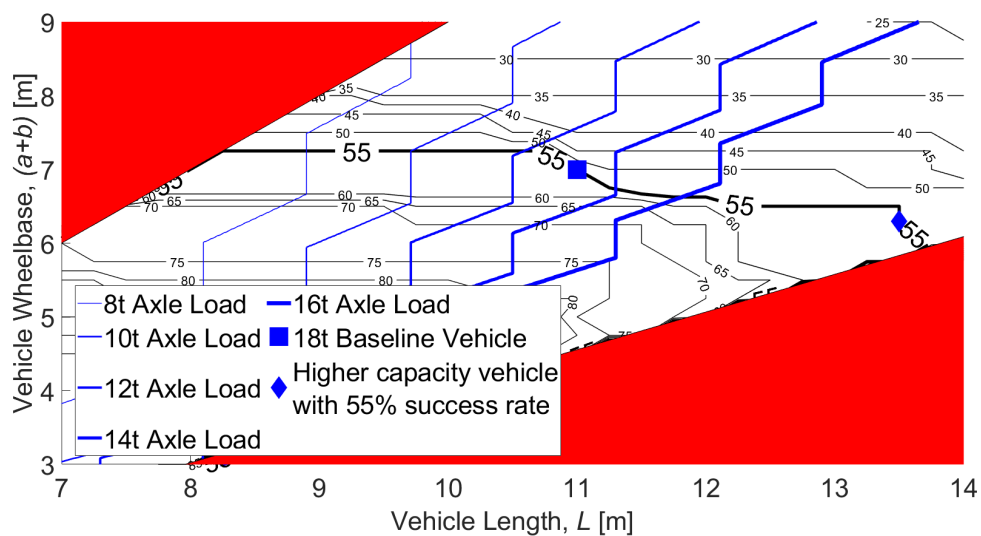
Figure 6.23 shows the contours of constant manoeuvre pass rate for rigid vehicles attempting manoeuvres from the urban library. The smallest vehicle (10 t) passed 90% of the manoeuvres, and the larger, 18 t vehicle passed 55%.

Figure 6.24 shows significant potential for increased length of both vehicles (of up to 2.5 m) without use of rear axle steering. This increases the number of roll cages carried by 12 for the smaller vehicle, up to a total of 30 (a 67% increase), and by 9 for the larger vehicle, up to a total of 39 (a 30% increase). However, this will increase rear axle loads, as described for the previous case studies, as the wheelbase must be reduced to maintain manoeuvrability. In some cases this may be acceptable, depending on the particular operation. However, the red shaded area in the bottom right-hand corner of the plot represents the region where the rear axle is forward of the centre of the vehicle. The two potential designs shown in Figure 6.24 are both close to the shaded region. This suggests the majority of the vehicle mass is carried by the rear axle, and the weight over the steering front axle is dangerously low for manoeuvrability.

Figure 6.25 shows the effect on the contour plot of applying rear axle steering, with the Path-Following algorithm. Both vehicles can be increased in size relative to the vehicle with



(a) 10 t vehicle and higher capacity alternative



(b) 18 t vehicle and higher capacity alternative

Fig. 6.24 Proposed higher capacity alternatives to the 10 t and 18 t rigid vehicles. Contours show constant success rate across all urban manoeuvres for a rigid vehicle with fixed rear axle

fixed rear axle without reducing the percentage pass rate (labelled ‘maximised capacity’). Alternatively, in applications where the total volume is relatively unimportant, but mass is a concern, Path-Following can be used to reduce the rear axle loads by increasing the wheelbase, without affecting the manoeuvrability (labelled ‘minimised axle load’). This gives a more modest gain in capacity. Both of these possible transformations are shown in Figure 6.25 for each of the rigid vehicle sizes being considered. All four of these design changes allow between 0.5 and 1.5 additional rows of 3 cages. This is unlikely to be economically viable given the increased cost of the steering axles in both cases.

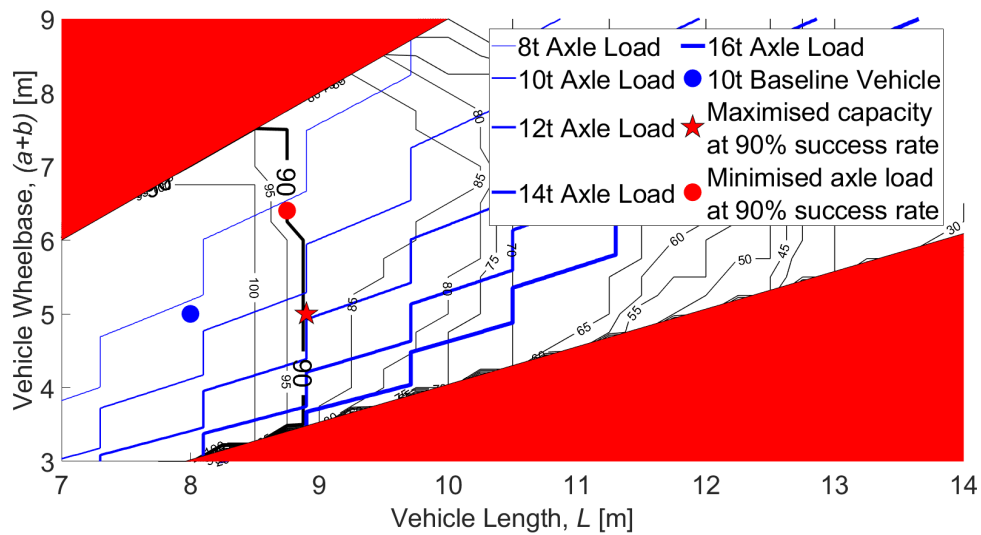
6.5.2 Articulated Vehicle

An additional question to answer is whether converting the rigid vehicles to articulated vehicles would allow increased capacity. The tractor unit from the previous case study was used to model articulated vehicles attempting the same manoeuvres, and the plots of constant success rate are shown in Figure 6.26. The maximum sizes of trailer which can achieve the same percentage success rates as each of the conventional rigid vehicles are shown.

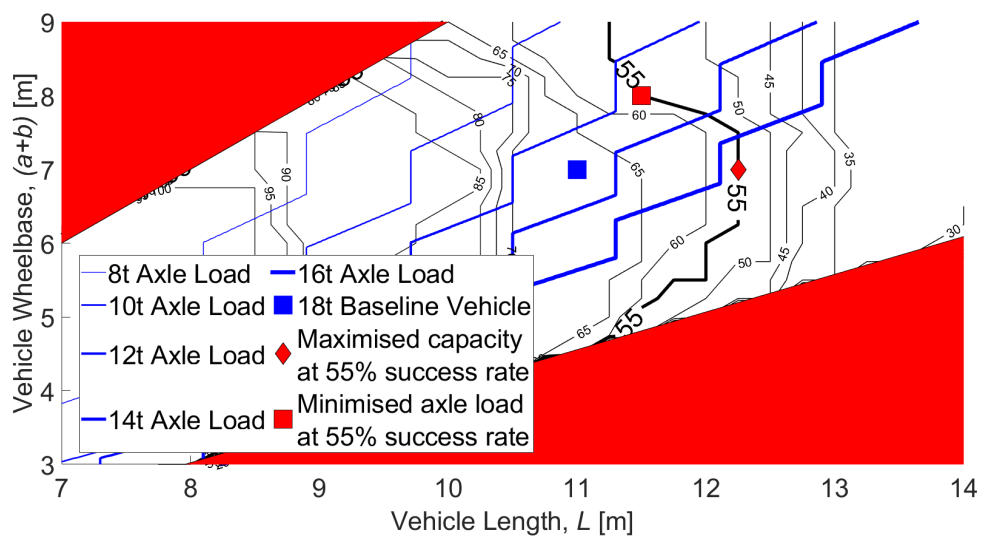
The smaller and larger trailers have rear axle loads of 12.5 t and 24.5 t, giving gross vehicle weights of 32 t and 43 t, and roll cage capacities of 30 and 51 cages respectively. This compares to 18 and 30 cages for the original vehicles, increases of 67 and 70%. These two vehicles are very similar to the baseline articulated vehicles from Table 6.3, in both length and capacity. The baseline articulated vehicles have slightly longer wheelbases, and thus lower rear axle loads, but at the expense of reduced manoeuvre pass rates.

Finally, the effect of rear axle steering on the articulated vehicles was considered. Both the two articulated baseline vehicles, and the two vehicles designed to have equivalent manoeuvrability to the rigid vehicles were considered. These four vehicles are shown in Figure 6.27, and the potential new design points in Figure 6.28. The new design points were chosen so as not to increase the rear axle loads.

The two vehicles designed to have equivalent manoeuvrability to the rigid vehicles have short wheelbases, and so sit in the region of the graph where applying rear axle steering has been shown to have only a small benefit (or negative benefit in the case of the larger vehicle). No full rows of cages can be gained for the smaller vehicle, and the larger vehicle requires a loss of 6 cages to provide equivalent manoeuvrability to the articulated vehicle with unsteered rear axle. However, compared to the existing 10 t rigid vehicle, the Path-Following articulated vehicle still gains 12 cages (67%), and compared to the 18 t rigid vehicle, the equivalent Path-Following articulated vehicle gains 15 cages (15%), with equivalent manoeuvrability.



(a) 10t vehicle and Path-Following alternative



(b) 18 t vehicle and Path-Following alternative

Fig. 6.25 Proposed Path-Following alternatives to the 10t and 18t rigid vehicles. Contours show constant success rate across all urban manoeuvres for a rigid vehicle with Path-Following strategy

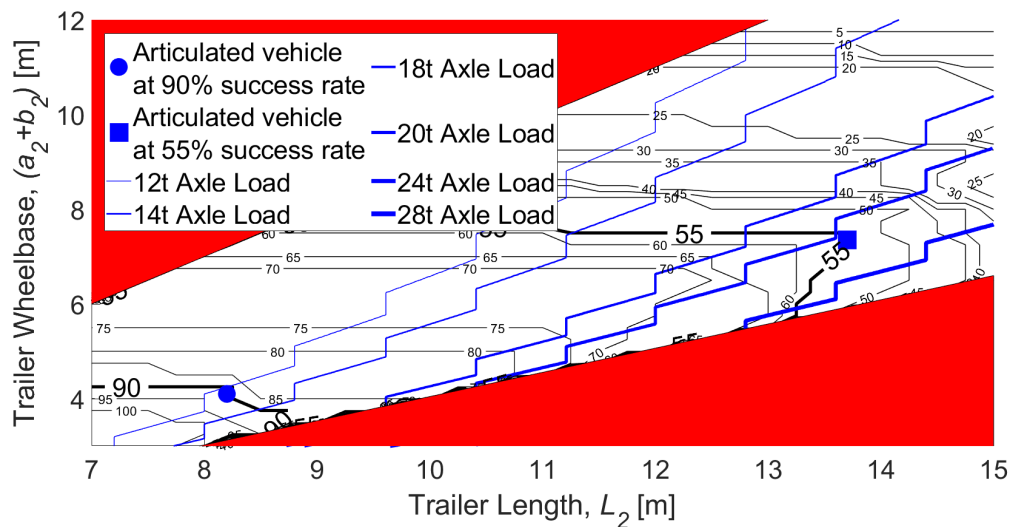
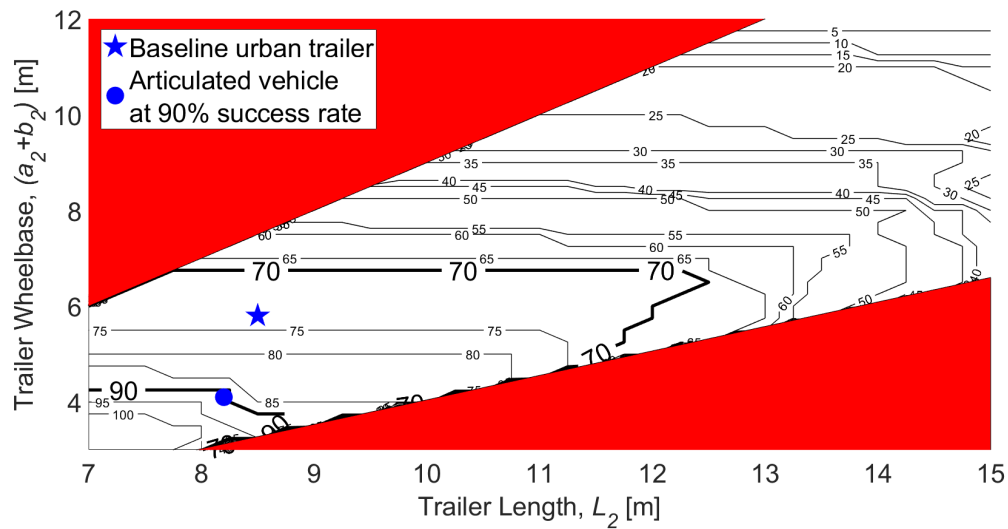


Fig. 6.26 Proposed articulated alternatives to the 10 t and 18 t rigid vehicles. Contours show constant success rate across all urban manoeuvres for an articulated vehicle with fixed rear axle

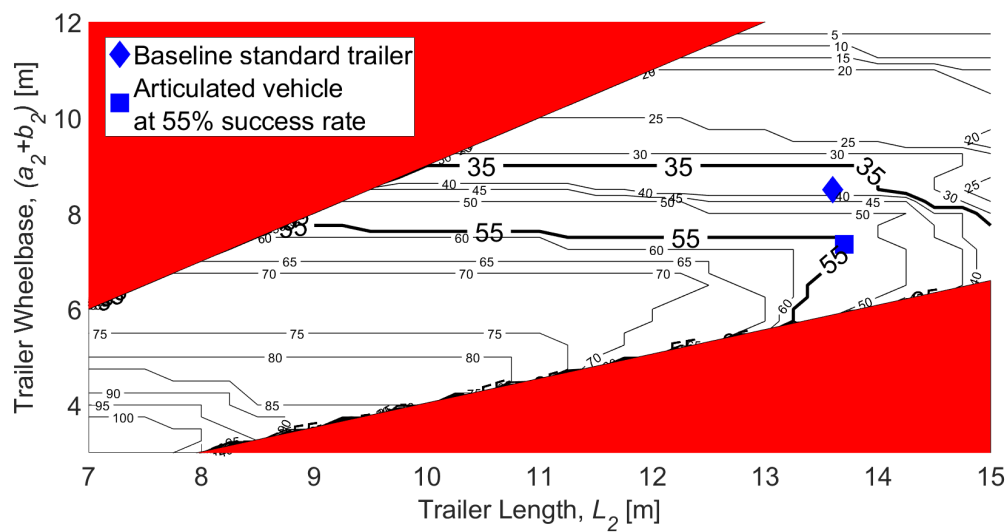
Converting the two baseline rigid vehicles to fixed rear axle articulated vehicles increases the rear axle load, from 8.5 t to 12.5 t for the smaller vehicle and from 13 t to 24.5 t for the larger vehicle. However, as shown in Figure 6.28, the use of rear axle steering reduces the rear axle loads to 10 t for the smaller vehicle and 14 t for the larger vehicle.

In other words, in terms of rear axle load required for every additional roll cage, the conversion from 10 t rigid to articulated vehicle costs 0.3 t/cage (4 t for 12 cages), whereas with the rear axle steered, the cost is only 0.1 t/cage (1.5 t for 12 cages). For the larger vehicle, despite the reduction in cages carried caused by the use of rear axle steering, the added rear axle load is only 0.01 t/cage (1 t for 15 cages) with the steered rear axle, compared to 0.5 t/cage (11.5 t for 21 cages) without steering.

For the baseline trailer units, the effect of adding rear axle steering was clearer. These vehicles had lower manoeuvrability percentages than the rigid vehicles, and thus had longer wheelbases than the articulated vehicles equivalent in manoeuvrability to the rigid vehicles. Therefore they sat in the region of the graph where application of rear axle steering allows longer vehicles to be used at the same manoeuvrability. The capacity of the urban trailer could be increased by 9 roll cages to 39 (30%) by the use of rear axle steering, and the capacity of the standard trailer could be increased by 3 roll cages to 54 (6%). Although this figure appears low, the value has been affected by the discrete nature of the roll cages (the existing vehicle fits 17 rows precisely, and the operating point shown in Figure 6.28 is just 40 cm short of a 19th row). The percentage increase in volume is 17%.

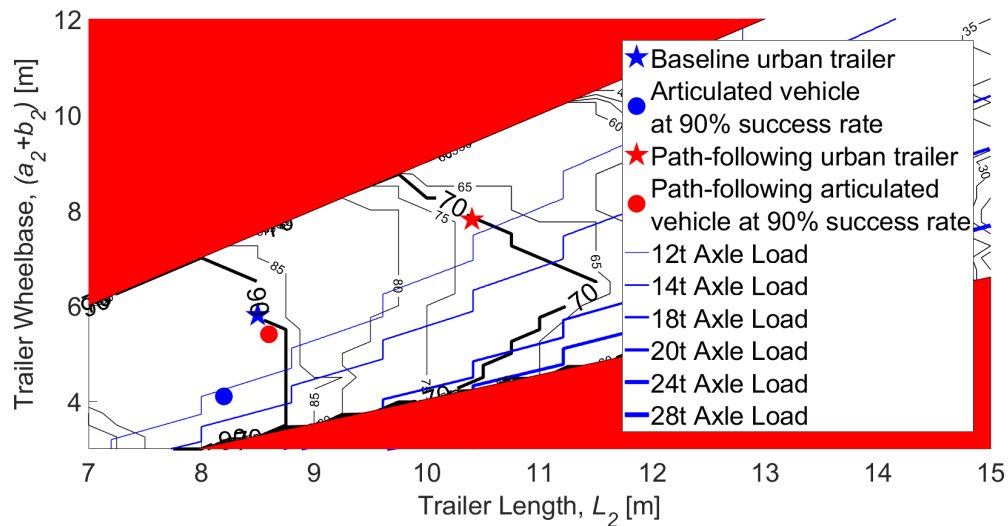


(a) Articulated alternative to 10 t vehicle and urban semi-trailer

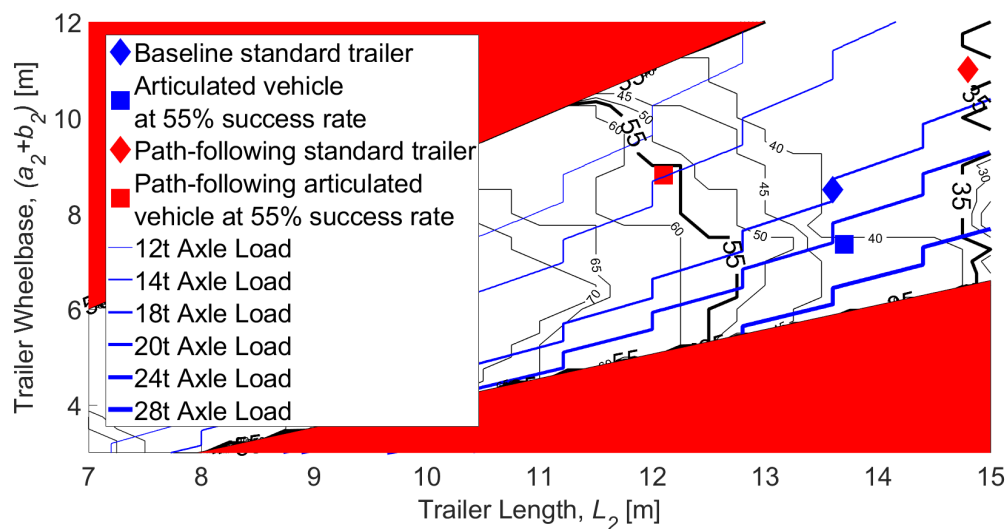


(b) Articulated alternative to 18 t vehicle and standard semi-trailer

Fig. 6.27 Baseline articulated vehicles and proposed articulated alternatives to the baseline rigid vehicles. Contours show constant success rate across all urban manoeuvres for an articulated vehicle with fixed rear axle



(a) Path-Following alternatives to baseline urban trailer and articulated alternative to the 10 t rigid vehicle



(b) Path-Following alternatives to baseline standard trailer and articulated alternative to the 18 t rigid vehicle

Fig. 6.28 Path-following alternatives to baseline and proposed articulated vehicles from Figure 6.27. Contours show constant success rate across all urban manoeuvres for an articulated vehicle with Path-Following strategy

6.5.3 Summary

- (i) The choice of freight vehicle for use in city centres is dependent on a large number of variables, and thus many different vehicles are used by different operators.
- (ii) Two commonly used rigid vehicles (10 t and 18 t) were identified. These vehicles could be increased in volumetric capacity by 67% and 30% respectively without penalty to manoeuvrability, but at the cost of very significantly increased rear axle loads.
- (iii) The use of rear axle steering to reduce the rear axle loads was investigated. This allowed the rear axle loads to be kept constant relative to the baseline vehicles, but allowed only small increases in capacity.
- (iv) Articulated vehicles could be designed with equivalent manoeuvrability to the existing rigid vehicles, yielding increased volumetric capacity of 67-70%, again resulting in high rear axle loads.
- (v) Rear axle steering for articulated vehicles can reduce those rear axle loads significantly, but slightly reduces the available volumetric capacity. However, this still gives an improvement on the existing rigid vehicles of 50-67%.
- (vi) Two commonly-used articulated vehicles were considered. A standard urban trailer could be increased in volume by 30% without penalty to either manoeuvrability or rear axle load, by the use of rear axle steering. A standard 13.6 m trailer could be increased in volume by 17%, although because of the discrete nature of the roll cages, according to the particular model used in this work, this only corresponds to an additional 6% in terms of roll cages.

6.6 Overview

The motivation for Chapters 4 to 6 was to build a tool which could be used by fleet operators to select the optimum vehicle configuration for their operations. The operator could select their own library of manoeuvres, and control parameters such as the width of their vehicles, steering lock angles, and the density of their freight, in order to increase the applicability.

This information could be used to generate a plot such as Figure 6.29. This figure shows a set of potential vehicles, and could be used to select alternative options.

As an example, an operator currently using 18 t rigid vehicles for restocking a city centre store wants to increase their efficiency. Several options are available:

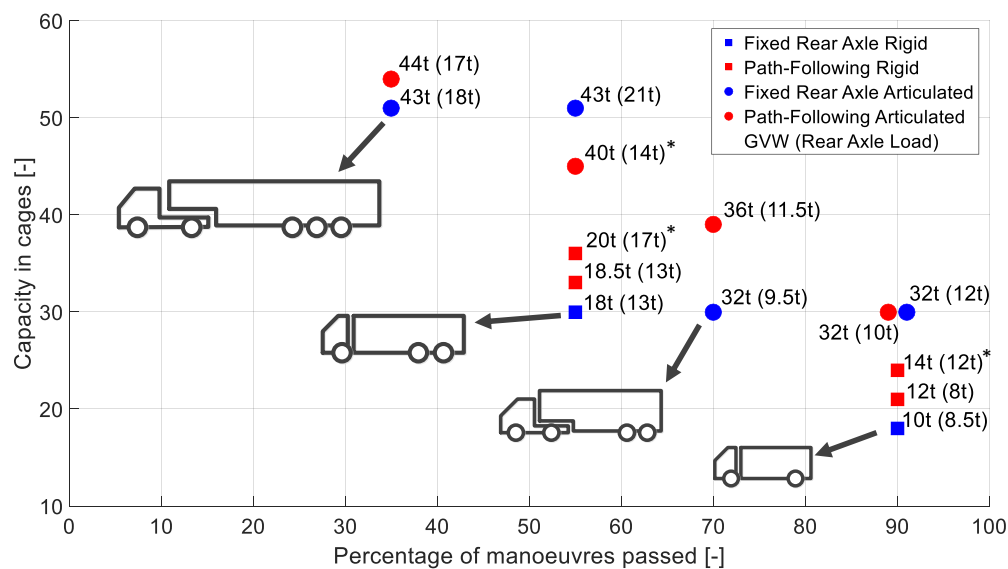


Fig. 6.29 Summary of all vehicles considered as part of Case Study C (*Some vehicles with apparently unrealistic axle loads are included as they may be applicable for some specific load cases)

- (i) Any of the 32 t articulated vehicles will increase the manoeuvrability of the vehicle while maintaining the same roll cage capacity. Although the vehicles are likely to be more expensive, this increased manoeuvrability could be used to find shorter routes into the centre, or possibly to apply for subsidies based on improved safety performance.
- (ii) The 43 t articulated vehicle increases capacity by 67% relative to the baseline vehicle. Although the vehicle will be significantly more expensive, the capacity increase is significant. It might be possible to consolidate multiple trips into one, which would reduce operating costs.
- (iii) The 36 t Path-Following articulated vehicle is an alternative to the conventional 32 t urban articulated vehicle, using rear axle steering to increase capacity. This vehicle increases capacity by 25%, and also increases the manoeuvrability. This could be key for operations with different sized outlets. For example, in addition to the duties of the original 18 t rigid, this vehicle could carry stock for a smaller store, and have the manoeuvrability to reach it, in the same trip.

6.7 Conclusions

A method has been developed for analysing the manoeuvrability of Heavy Goods Vehicles by simulating the vehicles attempting a library of real-world manoeuvres. The method allows proposed vehicle designs to be compared to the manoeuvrability of a baseline vehicle, and for the rear axle load and the GVW to be calculated. The method was used to evaluate three case studies, and increased capacity vehicles were proposed for each.

It was shown that the use of rear axle steering was sometimes detrimental to the maximum length of vehicle which could complete a given percentage of the manoeuvre library. This is because whereas a conventional vehicle compromises between tailswing and cut-in, a rear-steered vehicle is designed to minimise one of these (the Command-Steer strategy is designed to minimise cut-in, and the Path-Following algorithm is designed to eliminate tailswing). The loss of this compromise reduces the ability of certain vehicles to complete certain manoeuvres.

However, the use of rear axle steering reduces rear axle loads for a given manoeuvrability, as the rear axle can be placed further back on the vehicle while leaving the effective rear axle position unchanged. This reduces the likelihood of exceeding rear axle load limits before the vehicle is completely filled. For higher freight densities, the reduced rear axle loads would be key for successfully filling the vehicle.

Chapter 7

Performance-Based Standards Approach to Manoeuvrability

7.1 Introduction

7.1.1 Overview

The aim of the Performance-Based Standards approach to heavy vehicle regulation is to allow operators to maximise the productivity of HGVs by innovation in vehicle design, subject to a strict set of standards [81]. In Australia, an operator can apply for PBS certification of a given vehicle configuration. The vehicle configuration is simulated by a PBS assessor and awarded a score for each of 20 safety criteria, categorised into 5 groups: powertrain standards, low-speed performance, stability, high speed performance, and infrastructure protection. The level of PBS certification (1, 2, 3 or 4) then dictates what roads that vehicle configuration can be used on. This allows operators to optimise capacity for a given route or task. The use of simulation instead of direct testing facilitates the use of different or novel vehicles, as compared to countries without a PBS scheme, where operators must generally use standardised vehicles, with prescribed maximum weights and dimensions, to conform with regulations.

Roads are given a certification level which vehicles must meet. For example, the main trunk network is primarily Level 4. This means that any vehicle with a PBS Level of 4 or below can use the roads. Smaller roads have lower levels, requiring vehicles to meet more difficult targets on the assessment criteria to be permitted.

The Australian National Heavy Vehicle Regulator (NHVR) introduced the Performance-Based Standards (PBS) scheme in October 2007. Nearly 9000 PBS combinations have since been approved, and more than 1 in 5 new relevant heavy vehicles are PBS approved [208, 81].

The NHVR claims that PBS vehicles cause 46% fewer serious accidents per kilometre travelled, increase productivity by up to 30%, and were responsible for saving 173 million litres of fuel in 2018 [81]. The model has also been implemented in different forms in New Zealand [209], Canada [210], and South Africa [211]. In Europe, High-Capacity vehicles up to 25.25 m in length are permitted to operate under the European Modular System (EMS), but only within a single country, and not across borders [212]. The Freight and Logistics in a Multimodal Context project (Falcon) has made recommendations for a cross-border framework similar to a PBS scheme allowing Higher Productivity Vehicles in Europe [213].

7.1.2 Urban Performance-Based Standards

The Australian PBS scheme is not suitable for implementation in the UK in its exact form, because the largest vehicles used in Australia are impractical anywhere in the more densely populated UK. There are almost no routes in the UK where the multiply-articulated road trains seen on rural roads in Australia are considered appropriate. Work is in progress assessing how best to implement a PBS-style scheme in Europe, including the UK [213].

One potential application of the PBS concept, which would be particularly relevant to the UK would be the inclusion of a ‘Level 0’ categorisation for urban routes. In the Australian implementation, any vehicle achieving Level 1 certification can run on any route. In order to optimise capacity, it would be useful to have a further category for assessment of urban transport. Work carried out by Isted et al. investigated the potential assessment criteria and category thresholds which would be most suitable for a set of urban standards [5]. Isted et al. proposed a suitable set of standard manoeuvres and limits on performance metrics for two urban PBS levels, labelled in this work as ‘Level 0b’ and ‘Level 0’: Level 0b was intended to limit vehicle access to typical urban areas. Level 0 was developed to cater for urban areas with greater constraints, such as historic city centres, or narrow alleys.

7.1.3 Motivation

Chapters 4 to 6 presented a novel method for assessing the maximum size of higher capacity freight vehicles, based on the assumption that a higher capacity vehicle for a given task should be able to access the same areas as the lower capacity vehicle currently being used. This required some measure of the manoeuvrability of the vehicle to be assessed. The aim of these chapters was to use real-world manoeuvres to create a measurement of manoeuvrability which is more realistic than standard measurements from ‘idealised’ manoeuvres such as 90° turns or roundabouts. This method is suitable for any application, but particularly for urban freight vehicles, where manoeuvrability constraints tend to be more critical. On the other

Table 7.1 Recommendations for an Urban PBS framework by Isted et al. [5]

Level	Manoeuvre	Metric	Pass level
0	6.5 m Left Turn	Tailswing	< 0.25 m
0	6.5 m Left Turn	Front Swing	< 0.12 m
0	6.5 m Left Turn	Swept Path	< 5.5 m
0	6.5 m U-Turn	Required Track Width	< 4.5 m
0b	9 m Left Turn	Tailswing	< 0.4 m
0b	9 m Left Turn	Front Swing	< 1.2 m
0b	9 m Left Turn	Swept Path	< 5.75 m
0b	9 m U-Turn	Required Track Width	< 4 m
0 and 0b	3.5 m Lane Change at 18 m s^{-1}	High-Speed Transient Off-tracking	< 0.6 m
0 and 0b	3.5 m Lane Change at 18 m s^{-1}	Rearward Amplification Ratio	< 4
0 and 0b	Steering Impulse at 18 m s^{-1}	Yaw Damping Coefficient	> 0.15

hand, the Performance-Based Standards approach is simpler and requires less computation time than the method from the previous chapters, but may not lead to capacity of vehicles being completely maximised.

The primary aim of this chapter is to compare the results in Chapters 4 to 6 to the results generated by Isted et al. [5]. This is achieved by simulating the vehicles proposed in Chapter 6 over the set of standard manoeuvres described by Isted et al., and evaluating the performance metrics. This will assess whether the proposed vehicles would be permitted to operate in city centres under a PBS scheme as defined by Isted et al., and therefore whether the two methods agree on the maximum vehicle capacity for the case studies considered. The second aim of the chapter was to further investigate the effectiveness of rear axle steering on manoeuvrability.

7.2 Urban PBS Proposal

7.2.1 Proposed Framework

Table 7.1 lists the metrics and pass levels recommended by Isted et al., and the manoeuvres on which to measure those metrics. Isted et al. demonstrated that the roads of interest could be represented by turns of radius 6.5 m for Level 0 and turns of radius 9 m for Level 0b [5].

7.2.2 High Speed Analysis

Existing PBS frameworks for highway vehicles test for stability at high speeds. These frameworks do not impose any speed limiting on the vehicles being assessed, because all routes of levels 1 to 4 can involve driving at highway speeds. However, it was proposed by Isted et al. that vehicles used exclusively on urban roads could be allowed to have lower level high-speed stability as long as they had their maximum speed limited. This could permit the use of a group of higher capacity vehicles with excellent low-speed manoeuvrability, but limited high-speed stability, such as multiply-articulated vehicles with centre-axle trailer units. Isted et al. proposed that high-speed stability tests for Level 0 should be carried out at 40 mph instead of the 56 mph proposed by De Saxe et al. [213].

This approach would require a small change to the PBS framework. Under the Australian system, any vehicle that passes a given level automatically passes all higher levels (e.g. a level 1 vehicle is also permitted to operate on level 2, 3, and 4 roads). Under the recommendations by Isted et al., any vehicle passing Level 0 automatically passes the low speed requirements for higher levels, but is not guaranteed to pass the high speed tests. Therefore, Level 0 vehicles would either have to be speed limited, or tested separately against higher level high speed criteria.

The analysis from Chapters 4 to 6 considered only low-speed manoeuvrability, thus the proposed vehicles were not simulated using the high speed manoeuvres proposed by Isted et al. It was, however, recognised that vehicles which could achieve Level 0 status were not necessarily suitable for highway speeds.

7.2.3 Proposed Manoeuvres

At low speed, Isted et al. used two manoeuvres to assess vehicles. These were a 90° left turn, and a U-Turn. Each test was constructed with two outer radii: the first (6.5 m) to assess Level 0 vehicles, and the second (9 m) to assess Level 0b vehicles. Isted et al. assumed a speed of 0.5 m s^{-1} for all low-speed manoeuvres, also used for this work. The left turn manoeuvres were used to measure Tailswing (TS), Front Swing (FS), and Swept Path Width (SPW). The U-Turn manoeuvres were used to measure Required Track Width (RTW).

7.2.4 Proposed Metrics

This section defines the PBS metrics used by Isted et al. [5]. Some of the definitions are slightly different to those used earlier in this thesis.

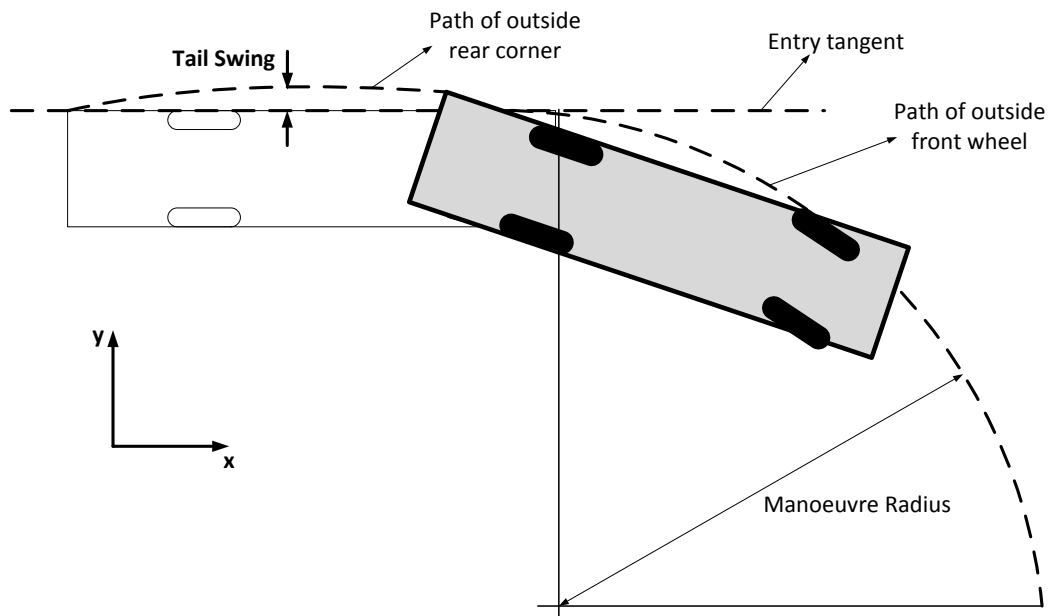


Fig. 7.1 Measurement of Tail Swing

7.2.4.1 Tail Swing (TS)

Tail Swing is defined as the maximum lateral displacement of the rear of the vehicle during the entry tangent to the 90° turn [5], shown diagrammatically in Figure 7.1. This can be measured by taking the maximum 'y-coordinate' in the position of the rear corner of the vehicle.

7.2.4.2 Front Swing (FS)

Front Swing is the maximum displacement between the path travelled by the outside front corner of a vehicle and the outside front wheel during the 90° turn [5], illustrated in Figure 7.2. This is measured by calculating the perpendicular to the path of the outside front corner at every point, and locating the intersection between this perpendicular and the path of the outside front wheel. The maximum of all distances between these intersections and the points on the path of the front corner is the Front Swing.

7.2.4.3 Swept Path Width (SPW)

Swept Path Width is described as the maximum perpendicular distance between the outer and innermost paths traced by the extremities of the vehicle during a 90° turn [5]. The metric is presented in Figure 7.3. For rigid, two-axle vehicles with only one steered axle this

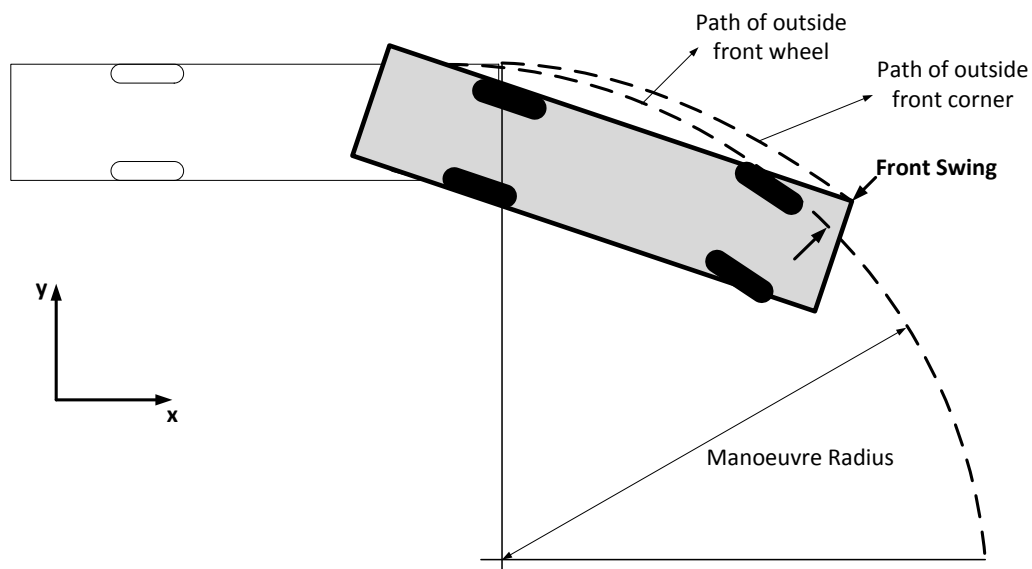


Fig. 7.2 Measurement of Front Swing

can be measured by taking the perpendicular distance between the path of the inside rear wheel and the path of either the outside front or outside rear corner. Which corner to use depends on whether the front or rear of the vehicle is swinging out more, which is governed by the relative sizes of the front and rear overhang. However, for vehicles with multiple axle steering, the innermost extremity of the vehicle changes according to the rear steer angle, and thus the path of the inside rear wheel cannot be used. Additionally, the outermost extremity can switch between the front and rear corners. To calculate Swept Path Width in this case, the paths of every point on the inside edge of the vehicle and every point on the outside edge of the vehicle must be traced, and the perpendicular distance from every point on every outside path to every inside path must be calculated. The Swept Path Width is the maximum of all of these perpendicular distances.

7.2.4.4 Required Track Width (RTW)

Required Track Width is described as the equivalent to Swept Path Width, but considering only the paths of the tyres rather than the edges of the body of the vehicle [5]. Note that this is not the same as the width of road required to make a U-Turn. This metric is shown diagrammatically in Figure 7.4, measured in the same way as Swept Path Width, but instead the innermost and outermost points are taken as the wheels, as opposed to any point on the body.

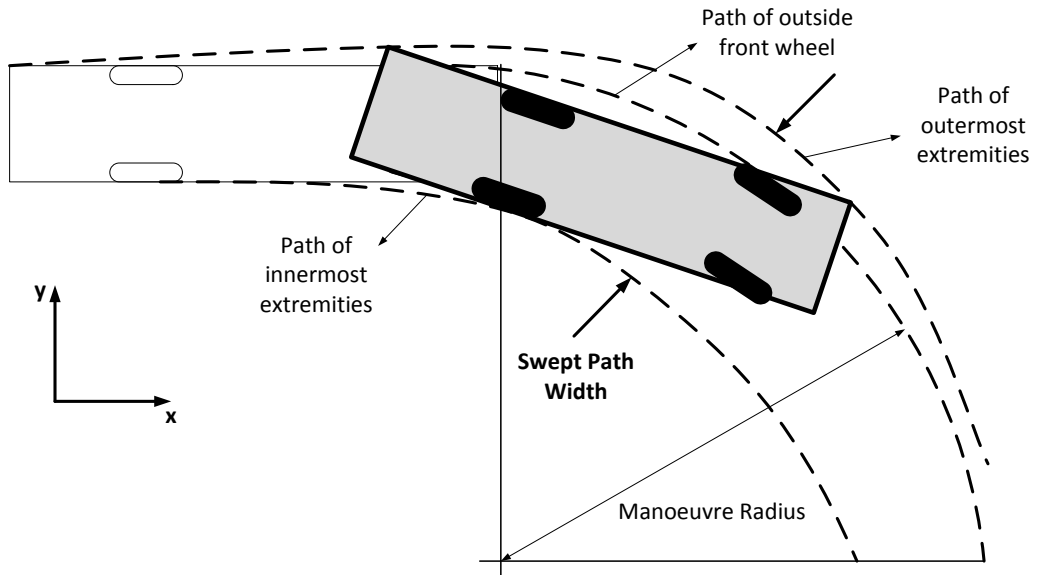


Fig. 7.3 Measurement of Swept Path Width

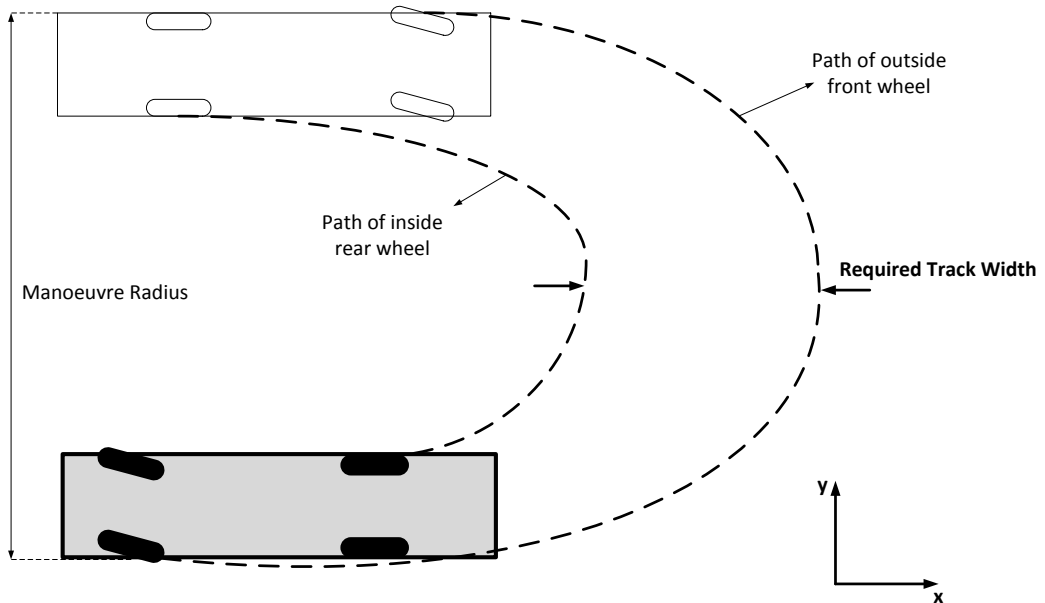


Fig. 7.4 Measurement of Required Track Width

7.3 Simulation Results and Analysis

The proposed vehicles in Chapter 6 were simulated performing the manoeuvres described. The metrics from Table 7.1 were calculated and compared to the required pass values for Level 0 and Level 0b. Some vehicles were unable to complete some manoeuvres, because the required steer angle to complete the manoeuvre at the given radius exceeded the steering lock angle. The method from Chapters 4 to 6 will from here on be known as the ‘real-world’ approach, as opposed to the Performance-Based Standards (PBS) approach.

7.3.1 Case Study A: Grocery Delivery Vehicle

Chapter 6 proposed increasing the size of grocery delivery vehicles from 3.5 t to 4.25 t. It was shown that the 4.25 t vehicle had significantly reduced manoeuvrability compared to the 3.5 t vehicle, and thus was not suitable for grocery delivery. It was shown, however, that the addition of rear axle steering could sufficiently improve the manoeuvrability to make the larger vehicle viable for such operations.

This agreed with the results generated using the PBS approach, as given in Table 7.2, with the performance metrics from Table 7.1. The 3.5 t vehicle ($L = 6.23$ m, $(a + b) = 3.67$ m) successfully met the criteria for all four low-speed metrics on the Level 0 manoeuvres (6.5 m radius). When the vehicle size was increased to 4.25 t ($L = 7.10$ m, $(a + b) = 4.80$ m) the vehicle failed the PBS tests, by being unable to complete the manoeuvres, due to exceeding the steering lock angle. However, the addition of Path-Following rear axle steering permitted the vehicle to complete the manoeuvres, and again all four criteria for achieving Level 0 status were met.

All three of the vehicles simulated (3.5 t, 4.25 t Rear Unsteered, and 4.25 t with Path-Following steering) achieved the criteria for Level 0b roads (9 m radius manoeuvres). This matches expectations for the larger set of manoeuvres.

For this case study, the results from the PBS assessment in this chapter, and the results from the ‘real-world’ method described in previous chapters agree well. Both suggest that any of the proposed grocery delivery vehicles should be capable of accessing the larger roads in city centres (Level 0b roads), but that to allow the higher capacity vehicle on the smallest roads (Level 0) requires the addition of rear axle steering.

7.3.2 Case Study B: Refuse Collection Vehicle

Three alternatives to the 26 t refuse collection vehicle ($L = 10.40$ m, $(a + b) = 4.72$ m) which were proposed in Chapter 6 were selected. These were 1) the addition of Path-

Table 7.2 Simulation results for vehicles proposed in Case Study A

			Level 0 manoeuvres (6.5 m)				
GVW (t)	Articulated	Rear Steering	SPW (m)	FS (m)	TS (m)	RTW (m)	Pass
			<5.50	<1.20	<0.25	<4.50	
3.5	No	No	3.72	0.57	0.08	3.15	Yes
4.25	No	No	-	-	-	-	No
4.25	No	Yes (PF)	3.29	0.53	0.00	2.76	Yes
			Level 0b manoeuvres (9 m)				
GVW (t)	Articulated	Rear Steering	SPW (m)	FS (m)	TS (m)	RTW (m)	Pass
			<5.75	<1.20	<0.30	<4.00	
3.5	No	No	3.23	0.44	0.06	2.79	Yes
4.25	No	No	3.94	0.53	0.03	0.62	Yes
4.25	No	Yes (PF)	2.92	0.39	0.00	2.53	Yes

Table 7.3 Simulation results for vehicles proposed in Case Study B

			Level 0 manoeuvres (6.5 m)				
GVW (t)	Articulated	Rear Steering	SPW (m)	FS (m)	TS (m)	RTW (m)	Pass
			<5.50	<1.20	<0.25	<4.50	
26	No	No	-	-	-	-	No
26	No	Yes (PF)	-	-	-	-	No
44	Yes	No	5.33	0.72	0.76	4.62	No
44	Yes	Yes (PF)	5.49	0.73	0.02	4.76	No
			Level 0b manoeuvres (9 m)				
GVW (t)	Articulated	Rear Steering	SPW (m)	FS (m)	TS (m)	RTW (m)	Pass
			<5.75	<1.20	<0.30	<4.00	
26	No	No	3.88	0.53	0.81	3.35	No
26	No	Yes (PF)	3.87	0.56	0.01	3.30	Yes
44	Yes	No	4.70	0.55	0.47	4.18	No
44	Yes	Yes (PF)	4.60	0.55	0.01	4.00	Yes

Following steering ($L = 9.70$ m, $(a + b) = 6.20$ m), 2) an articulated vehicle ($L_2 = 11.45$ m, $(a_2 + b_2) = 5.80$ m), and 3) an articulated vehicle with Path-Following steering ($L_2 = 10.40$ m, $(a_2 + b_2) = 6.20$ m). According to the analysis presented in Chapter 6, all three of these vehicles have equivalent manoeuvrability, (i.e. all were able to complete the same percentage of manoeuvres as the standard 26 t vehicle).

Table 7.3 gives the simulation results for these four vehicles attempting the Level 0 and Level 0b manoeuvres. At Level 0, none of the vehicles passed the criteria. The two rigid vehicles cannot complete the manoeuvres, and the articulated vehicles fail on Required Track Width (although by less than 0.3 m). For the Level 0b manoeuvres, both the 26 t rigid and the 44 t articulated vehicles require Path-Following steering to pass the Tail Swing criterion.

The real-world analysis from Chapter 6 uses the manoeuvrability of the existing vehicle as a baseline. This explains why the 26 t rigid vehicle passed by that method, but failed according to the PBS manoeuvres. The PBS analysis suggests that the addition of rear axle steering to the rigid vehicle is not sufficient to pass (whether it increases manoeuvrability is unknown, as neither vehicle could complete the manoeuvre). The real-world approach demonstrated that the use of rear axle steering reduced capacity for the same manoeuvrability (or conversely reduced manoeuvrability for a given capacity).

The real-world approach suggested that a 44 t articulated vehicle could have equivalent manoeuvrability to the 26 t rigid vehicle. The PBS approach agrees with this, suggesting that the manoeuvrability of the articulated vehicle is better than the rigid, since it can complete the manoeuvres whereas the rigid cannot. However, the articulated vehicle still fails the Level 0 criteria for Tail Swing and Required Track Width. The real-world approach again suggests that the addition of trailer steering to the articulated vehicle reduces manoeuvrability. This was supported by the PBS analysis, which showed an increase in both the Required Track Width and Swept Path Width due to the use of rear axle steering. The primary advantage of rear axle steering is that it reduces the Tail Swing almost to zero.

On the larger manoeuvres, the existing refuse vehicle's large rear overhang caused it to fail the Level 0b criterion for Tail Swing. However, the use of rear axle steering reduced the Tail Swing sufficiently for the vehicle to pass. The same observations were made for the articulated vehicle.

The pass values for the PBS Level 0 criteria are set such that all the vehicles fail, whereas the manoeuvrability of these vehicles was taken as the baseline value using the real-world method, therefore defining that all the vehicles pass.

Table 7.4 Simulation results for vehicles proposed in Case Study C

'Urban' Library Score: 90%			Level 0b manoeuvres (9 m)				
GVW (t)	Articulated	Rear Steering	SPW (m)	FS (m)	TS (m)	RTW (m)	Pass
			<5.75	<1.20	<0.30	<4.00	
10	No	No	4.08	0.55	0.09	3.53	Yes
10	No	Yes (PF)	3.34	0.47	0.00	2.87	Yes
32	Yes	No	3.87	0.55	0.16	3.32	Yes

'Urban' Library Score: 70%			Level 0b manoeuvres (9 m)				
GVW (t)	Articulated	Rear Steering	SPW (m)	FS (m)	TS (m)	RTW (m)	Pass
			<5.75	<1.20	<0.30	<4.00	
32	Yes	No	4.55	0.55	0.01	4.00	Yes
36	Yes	Yes (PF)	4.26	0.55	0.01	3.70	Yes

'Urban' Library Score: 55%			Level 0b manoeuvres (9 m)				
GVW (t)	Articulated	Rear Steering	SPW (m)	FS (m)	TS (m)	RTW (m)	Pass
			<5.75	<1.20	<0.30	<4.00	
18	No	No	-	-	-	-	No
18.5	No	Yes (PF)	4.01	0.59	0.00	3.50	Yes
43	Yes	No	5.03	0.55	2.60	4.49	No

'Urban' Library Score: 35%			Level 0b manoeuvres (9 m)				
GVW (t)	Articulated	Rear Steering	SPW (m)	FS (m)	TS (m)	RTW (m)	Pass
			<5.75	<1.20	<0.30	<4.00	
43	Yes	No	6.13	0.55	0.27	5.58	No
44	Yes	Yes (PF)	6.05	0.55	0.03	5.50	No

7.3.3 Case Study C: Urban Store Vehicle

Whereas the previous two case studies have a particular existing vehicle to use as a baseline, there are many different vehicles used for urban store delivery. In order to compare the PBS approach to the real-world approach, a set of the vehicles shown in Figure 6.29 was simulated attempting the proposed PBS manoeuvres. The results are presented in Table 7.4.

Three vehicles scored a 90% manoeuvre pass rate on the ‘urban’ manoeuvre library using the real-world approach. These were a standard 10 t truck ($L = 8.00$ m, $(a + b) = 5.00$ m), a lengthened 10 t truck with Path-Following steering ($L = 8.75$ m, $(a + b) = 5.00$ m), and a 32 t tractor semi-trailer ($L_2 = 8.20$ m, $(a_2 + b_2) = 4.00$ m) designed to have equivalent manoeuvrability to the 10 t truck. All three vehicles were able to complete the 9 m proposed PBS manoeuvres. Similarly, the two vehicles which scored 70% manoeuvre pass rate on the ‘urban’ manoeuvre library were able to pass the 9 m proposed PBS manoeuvres. These were the baseline Urban Trailer ($L_2 = 8.50$ m, $(a_2 + b_2) = 5.80$ m) and a lengthened Urban Trailer with Path-Following steering ($L_2 = 10.40$ m, $(a_2 + b_2) = 7.80$ m), designed to increase the capacity of the baseline Urban Trailer.

The three vehicles which successfully completed 55% of the ‘urban’ manoeuvre library using the real-world approach were a standard 18 t truck ($L = 11.00$ m, $(a + b) = 7.00$ m), a lengthened 18 t truck with path-following rear axle steering ($L = 11.50$ m, $(a + b) = 7.00$ m), and a 43 t tractor semi-trailer ($L_2 = 13.70$ m, $(a_2 + b_2) = 4.10$ m) designed to have equivalent manoeuvrability to the 18 t truck. The 18 t truck was only able to complete the PBS manoeuvres with the addition of rear axle steering. The articulated vehicle which was shown by the real-world approach to have equivalent manoeuvrability also failed the manoeuvres, because the Tail Swing was too high.

The vehicles which scored 35% on the real-world manoeuvres were a standard semi-trailer ($L_2 = 13.60$ m, $(a_2 + b_2) = 8.50$ m) and a Path-Following semi-trailer ($L_2 = 14.80$ m, $(a_2 + b_2) = 11.00$ m). Neither were able to pass the PBS manoeuvres. Both failed because of Swept Path Width and Required Track Width. Both vehicles achieved similar scores across all four assessment criteria.

Table 7.4 indicates that the two approaches to modelling manoeuvrability give similar results. Vehicles achieving a given percentage manoeuvre pass rate for the real-world simulations consistently passed or failed the PBS manoeuvres, with the exception of the 18.5 t rigid vehicle, which passed while the rest of the vehicles in the 55% category failed. This suggests that the PBS Level 0b standard is equivalent to a manoeuvre pass percentage on the ‘urban’ manoeuvre library of between 55-70%.

7.4 Conclusions

There were two aims to this chapter: to further investigate the effectiveness of rear axle steering on vehicle manoeuvrability with the goal of increasing capacity, and to compare the two methods for assessing manoeuvrability.

7.4.1 Effectiveness of Rear Axle Steering

Path-following rear axle steering was shown to be effective at removing Tail Swing and allowing vehicles which, without rear axle steering could not achieve a high enough yaw rate for success, to complete the required manoeuvres. However, it increases Swept Path Width and Required Track Width, and therefore was penalised in a number of cases by both manoeuvrability modelling methods. This corresponds to conclusions drawn in Chapter 6.

It is apparent that the impact that rear axle steering has on the balance between Tail Swing and Swept Path Width is highly dependent on the manoeuvre being simulated and the dimensions of the vehicle. Application of Path-Following rear axle steering always reduces Tail Swing, but only reduces Swept Path Width in some cases. In cases where it instead increases Swept Path Width, this is sometimes enough to cause the vehicle to fail the PBS manoeuvres. This is supported by the real-world analysis which showed that Path-Following steering sometimes increased the maximum achievable length of the vehicle, but sometimes decreased it.

One description of this effect, is that a given size of vehicle attempting a given manoeuvre must sweep an approximately constant area of road through the entire manoeuvre. In the case of a conventional vehicle, with fixed rear axle, the swept area is comprised of a compromise between cut-in and tailswing. The application of rear axle steering removes this compromise; for the case of the Command-Steer strategy, cut-in is converted to tailswing, and for the case of the Path-Following strategy, tailswing is eliminated, but cut-in is increased. It was shown in Chapter 6 that different manoeuvres penalise different aspects of the manoeuvrability (cut-in or tailswing).

This analysis effectively considers tailswing and cut-in to be equally disadvantageous, which may not be the case. Cut-in is a predictable response, expected by drivers, and generally occurring in a visible area of the road. Tailswing on the other hand is less predictable, and for articulated vehicles occurs in an area of the road which is hidden from the driver's mirrors, and which the front of the vehicle has not passed through. For this reason, the PBS analysis measures Tail Swing as a separate metric, and a vehicle can fail due to excessive Tail Swing, even if other metrics are passed.

Table 7.5 Approximate equivalence between PBS pass levels and real-world pass levels

	Equivalent 'Residential' Library Pass Rate	Equivalent 'Urban' Library Pass Rate
Level 0	90%	-
Level 0b	30%	55%

Irrespective of the impact on manoeuvrability, it has been shown that the use of rear axle steering always reduces rear axle loads by allowing the rear axle to be located further back on the vehicle. This reduces the likelihood that the rear axle load will be exceeded before the vehicle is filled, thus allowing a higher load density. Additionally, the high tyre wear experienced by vehicles with multi-axle groups on small-radius turns will be reduced, reducing the environmental and financial costs of replacing tyres.

7.4.2 Comparison of Methods

The two approaches used for modelling manoeuvrability cannot be definitively said to have yielded equivalent results, but have not been shown to contradict each other, for the vehicles considered in this chapter. Some data points are missing, because some vehicles could not complete the PBS manoeuvres due to exceeding the steering lock angle.

Table 7.2 suggests that the proposed PBS Level 0 standards are approximately equivalent to achieving a 90% manoeuvre success rate on the 'residential' manoeuvre library (the more tightly bounded library) since the largest vehicle which can achieve that 90% score can pass the Level 0 manoeuvres, but requires rear axle steering to do so, implying that any larger vehicles would be unsuccessful.

Similarly, Table 7.3 indicates that the proposed PBS Level 0b standards are approximately equivalent to a 30% manoeuvre success rate on the 'residential' library, given that both the 26 t rigid vehicle and the 44 t articulated vehicle again require rear axle steering to pass the manoeuvres. By the same argument, Table 7.4 suggests that the Level 0b standards are equivalent to a success rate of 55% on the 'urban' library. Therefore it can be reasoned that the 30% 'residential' manoeuvre success rate and the 55% 'urban' manoeuvre success rate are approximately equivalent. This is summarised in Table 7.5.

This equivalence negates the requirement for different manoeuvre libraries for different applications, provided the equivalent success rate can be found, however it presents a stronger argument to fleet operators for the validity of the results if the simulations are application specific. Vehicle manufacturers, on the other hand, typically prefer not to design to specific

applications, since this limits their market. Therefore further work is needed to understand the business case associated with vehicles designed by the real-world method.

In summary, both methods can provide an assessment of manoeuvrability, and equivalent pass levels between the two methods can be found. The real-world method has the advantage of allowing application-specific consideration of the roads which the vehicle will be operating on, thus finding the absolute maximum achievable capacity. However, it does not penalise tailswing, which can be dangerous, and over-specifying to a given application is considered by some to be a disadvantage. Further work is required to investigate the business case, in order to assess which method is most suitable.

Chapter 8

Conclusions and Further Work

8.1 Introduction (Chapter 1)

Chapter 1 reviewed the literature related to the road freight industry. The challenges associated with decarbonisation of road freight were discussed, and a number of interventions to help achieve decarbonisation were presented, with their respective advantages and disadvantages. Increasing vehicle capacity was identified as an important component of decarbonisation strategy.

Urban road freight was identified as a key target for decarbonisation efforts due to the increasing urbanisation of the world population. The negative externalities (impacts of road freight not directly factored into costs to fleet operators) associated with urban freight vehicles were assessed, with a focus on the context of higher capacity urban vehicles. Some barriers to increasing capacity were presented, including legislative limits, decreased manoeuvrability, increased driver workload, and safety of vulnerable road users. It was proposed that this project investigate methods for enabling higher capacity urban freight vehicles.

Three applications of urban freight vehicles were presented as case studies, to be investigated using the methods in the following chapters. The applications were home delivery of groceries, domestic refuse collection, and convenience store stock vehicles. Reviews of current approaches to these applications were carried out, and the case for selecting these applications was presented.

8.2 Cyclist Detection (Chapter 2)

A camera system was developed to observe and predict the motion of cyclists close to the side of Heavy Goods Vehicles, and compared to an ultrasonic system developed by Jia [108].

The system used two downward-facing cameras mounted high on the side of the vehicle. Bicycle wheels were detected using boosted classifiers. The point of contact between the wheel and the ground was converted into world coordinates using a coordinate mapping generated from a calibration grid.

The system was generally able to track the position of the cyclist to within 10 cm at distances of 1 m or greater from the HGV. At lateral distances of less than 1 m the system was found to be significantly less accurate due to occlusion and distortion of the image features. The system was slightly less accurate than Jia's ultrasonic system, most significantly when the cyclist was close to the HGV.

The system described in the chapter is promising but not sufficiently robust for all conditions, due to the loss of accuracy at close range, and the impracticality in low-light conditions. It is likely that the most suitable solution would be a hybrid system fusing image and ultrasonic data. This would combine the accuracy and robustness of the ultrasonic system with the ability of image processing to discern a single cyclist from the background or from a group of cyclists. The development of this system will be completed by other researchers.

8.3 Analysis of Urban Delivery Systems (Chapter 3)

In-service data were collected for two home delivery vehicles from different supermarkets, using the SRF logger. Comparisons between the two sets of data showed differences between the operations of the two supermarkets. It was shown that Supermarket B's vehicles regularly drove further than those of Supermarket A, and it was hypothesised that this was due to the profiles of the customers of the supermarkets.

A statistical model was constructed of the time spent on tasks by the delivery driver during a typical shift. The input parameters to this model were varied to investigate the effect of increasing number of deliveries on the driver's ability to complete the shift in under eight hours. It was shown that the number of deliveries could be increased by 30% without exceeding an eight hour shift, if the distance between deliveries could be decreased by half. If the time spent doing paperwork and packing and repacking the van could be eliminated, then the potential increase in the number of deliveries is 80%, assuming the same reduction in driving distance. These reductions in distance could be achieved by increasing the attractiveness of home delivery to consumers so that there is greater uptake in a given area, or by collaboration between supermarkets.

Analysis of in-service data logged for Refuse Collection Vehicles by Nicolaidis showed that in order for the vehicle to always be able to complete its collections in a single round trip, instead of requiring two trips, the vehicle capacity would need to be increased by 40%.

Current vehicles in Cambridge can complete all collections in a single trip on only 17% of days.

It was shown that in order to assess the operational impact of higher capacity vehicles used to restock city centre stores, modelling of an entire logistics network would be required. This was considered beyond the scope of this project.

8.4 Manoeuvrability Modelling: Methodology (Chapter 4)

A method was proposed for assessing the manoeuvrability of Heavy Goods Vehicles, taking into account the complexity of real-world manoeuvres. The steps of the method were as follows:

1. Collect in-service GPS data from the class of vehicle to be considered.
2. Identify from the GPS data a library of the most difficult manoeuvres.
3. Use satellite images to convert each manoeuvre into a set of boundary constraints on the vehicle motion.
4. Simulate a vehicle attempting each manoeuvre and determine whether or not it is physically able to pass.
5. Vary the vehicle design parameters, and generate a chart that shows the percentage of manoeuvres which can be completed as vehicle dimensions vary.
6. Plot additional constraints on the chart such as axle load limits and infeasible vehicle configurations.
7. Select the optimum vehicle design: the set of dimensions which maximises capacity without violating any constraints, and can complete at least the same percentage of manoeuvres as the existing vehicle.

To support this, kinematic vehicle models were developed for both rigid and articulated vehicles, and several rear axle steering strategies.

Mass distribution models of both rigid and articulated vehicles were developed and validated, to allow calculation of axle loads and Gross Vehicle Weight for any given vehicle.

A parameter space was defined, where the vehicle overall length, L , and vehicle wheelbase, $(a + b)$, varied. The design space was constrained by a GVW limit, the rear axle load limit, and the manoeuvrability performance envelope of the vehicle, which was calculated by simple geometric arguments for steady-state turning.

It was demonstrated that the capacity of existing home delivery vehicles could not be increased, because of the 3.5 t limit on GVW. Increasing this limit to 4.25 t was shown to be essential for any increase in capacity.

The vehicles were also constrained by their manoeuvrability, but it was proposed that applying rear axle steering to change the position of the manoeuvrability envelope would allow for longer vehicles, without increasing the rear axle loads. Similar results were presented for a standard articulated vehicle.

8.5 Manoeuvrability Modelling: Algorithm Selection (Chapter 5)

The method proposed in the previous chapter required an accurate calculation of the shape and position of the manoeuvrability envelope. It was proposed that simulating vehicles attempting manoeuvres and assigning a pass or fail result would be a suitable way to determine the envelope, thus a route planning method was required, to allow automatic simulation of many vehicles.

Four path-planning algorithms were tested. These were: Rapidly-exploring Random Trees (RRT), Model Predictive Control (MPC), Single- and Multi-segment Splines (SMS) and N Control Point Splines (NCPS).

The algorithms were tested on two simple manoeuvres. Scores were calculated for each algorithm, by taking the percentage difference between the area of success discovered by the algorithm and the 'true' area of success, as discovered by all the algorithms combined, with some manual checks.

None of the algorithms achieved a perfect score on either of the two manoeuvres. However, a combination of the MPC and NCPS methods discovered at least 96% of the true area for both of the simple manoeuvres, which was considered sufficient.

8.6 Manoeuvrability Modelling: Case Studies (Chapter 6)

This Chapter applied the results of the vehicle capacity optimisation method described in the previous chapters, in the context of three case studies: home delivery of groceries, refuse collection, and convenience store restocking vehicles.

First, an investigation was carried out into the shape of the manoeuvrability envelope, to understand the effect of rear axle steering on vehicle manoeuvrability. It was shown that while in some cases rear axle steering can increase the dimensions of the vehicle that can get

round a given manoeuvre, in other cases it can reduce it. However, the position of the steered rear axle generally reduces rear axle loads, allowing a heavier payload to be carried without exceeding the rear axle load limits.

8.6.1 Case Study A: Grocery Delivery Vehicle

The home delivery vehicles typically used by supermarkets usually run very close to the 3.5 t GVW limit. Therefore, no increase in vehicle length is useful, unless the GVW limit for Light Goods Vehicles can be increased.

Assuming this increase is permitted, the vehicles could be increased in length by 1.5 m without penalty to manoeuvrability. This would require either the rear axle to be moved forwards, thus increasing the rear axle load, or for rear axle steering technology to be used.

Capacity could be increased by nearly 50% by using the Command-Steer algorithm to control the rear axle steering angle. However, this would generate unacceptably high tailswing. Using the Path-Following algorithm instead would limit tailswing to near zero, and would permit a 30% increase in capacity.

8.6.2 Case Study B: Refuse Collection Vehicle

The rear axle or axles of the refuse collection vehicle carry an unusually high proportion of the load, due to the heavy bin lifting equipment on the rear of the vehicle. This also leads to a large rear overhang, and high risk of tailswing. Because of the naturally high tailswing, the use of the Command-Steer algorithm was inappropriate. Using the Partial Command-Steer algorithm does not add additional tailswing, but has only a small effect on manoeuvrability (although it might still be economically worthwhile for some business cases due to the reduction in tyre wear).

The use of the Path-Following steering algorithm removes the tailswing, but requires a small reduction in capacity due to the increased cut-in.

It was demonstrated that an articulated vehicle provides the best capacity increase for this application. A 44 t articulated vehicle using steered trailer axles and Path-Following control was shown to have equivalent manoeuvrability to the existing refuse collection vehicle.

8.6.3 Case Study C: Urban Store Vehicle

Due to the large number of variables involved in operator decision making, a wide variety of different vehicles are used for urban operations. Four commonly used vehicles were identified: 10 t and 18 t rigid trucks, an urban semi-trailer, and a standard semi-trailer.

All four vehicles could be increased in capacity without penalty to manoeuvrability by increasing the length and reducing the wheelbase slightly. However, this would lead to increased rear axle loads. These could be reduced by increasing the wheelbase, and applying rear axle steering to maintain the position of the effective wheelbase.

Replacing the rigid vehicles with articulated vehicles with equivalent manoeuvrability could increase capacity by more than 50%.

8.7 Performance-Based Standards Approach to Manoeuvrability (Chapter 7)

Vehicles proposed as viable alternatives to existing vehicles for the case studies were evaluated using a PBS approach. It was shown that an approximate equivalent manoeuvre pass rate could be found for a given PBS standard.

The effectiveness of Path-Following rear axle steering on vehicle manoeuvrability was investigated further. The PBS simulations revealed that while Path-Following steering reduces Tail Swing, in some configurations it increases Swept Path Width and Required Track Width. For some manoeuvres this caused vehicles to fail.

The advantage of the 'real-world' method was summarised as allowing application-specific consideration of the roads which the vehicle will be operating on, which allows the maximum achievable length and therefore capacity to be found. However, this is seen by some to be a disadvantage, since it limits the potential market for the vehicle. Further work is required to understand this business case.

8.8 Further Work

- (i) There is a requirement for further development of the camera system proposed in Chapter 2. This work should investigate possible sensor fusion approaches combining the differentiation of a camera-based system to distinguish between multiple cyclists and other entities, and the accuracy of an ultrasonic system.
- (ii) The realism of the manoeuvrability modelling should be considered. This work did not allow for the case where a driver chooses to reverse to complete a manoeuvre, nor for the case where the driver turns the wheel while stationary, causing a discontinuity in gradient of path. These were considered necessary simplifications in order to limit the complexity of the problem, but could be relaxed in further work.

- (iii) This work considered only the length and wheelbase of the vehicle as design parameters. The vehicle width plays a crucial role in manoeuvrability and could be included in future analysis. Other parameters may be important, such as the steering lock angle.
- (iv) Similarly, the scope of the manoeuvre libraries used in Chapter 6 should be improved. The limited number of manoeuvres used did not allow for any statistical smoothing effects, creating artefacts in the resulting contour plots. These could be removed by using libraries with more manoeuvres.
- (v) More work is needed to take forward the various proposals for increasing vehicle capacity: developing business cases and prototype vehicles to test their benefits in practice.
- (vi) Work by Isted et al. demonstrated the differences between the profiles of required manoeuvrability for different cities [5]. Further investigation is needed to assess whether proposed manoeuvrability standards should be tailored to different cities. Similarly, from the perspective of vehicle design, investigation is needed to determine whether vehicles in modern cities could be made larger and more productive than those operating in historic cities.
- (vii) Further work is needed to understand the business case associated with the ‘real-world’ method, as compared to the PBS method. It is not yet understood whether the ability to provide an application specific assessment of how to maximise capacity is considered an advantage by fleet operators or vehicle manufacturers.

References

- [1] Department for Business Energy and Industrial Strategy, “2017 UK Greenhouse Gas Emissions,” 2019. [Online]. Available: https://assets.publishing.service.gov.uk/government/uploads/system/uploads/attachment_data/file/776083/2017_Final_emissions_statistics_one_page_summary.pdf (Accessed 2019-04-20).
- [2] Department for Transport, “Freight Carbon Review 2017,” 2017. [Online]. Available: https://assets.publishing.service.gov.uk/government/uploads/system/uploads/attachment_data/file/590922/freight-carbon-review-2017.pdf (Accessed 2018-10-12).
- [3] T. L. Robinson and W. Chislett, “Commercial vehicle safety priorities - ranking of future priorities in the UK - based on detailed analysis of data from 2006-2008,” TRL Published Project Report, Tech. Rep., 2010.
- [4] Y. Jia, “An automated cyclist collision avoidance system for Heavy Goods Vehicles,” PhD Thesis, Cambridge, 2014.
- [5] C. Isted, C. Eddy, and D. Cebon, “Selection of tests and success levels for an Urban Performance Based Standards scheme,” Paper in preparation, University of Cambridge, 2019.
- [6] Act of Parliament, “Climate Change Act 2008 (2050 Target Amendment) Order 2019,” London, 2019. [Online]. Available: <http://www.legislation.gov.uk/ukxi/2019/1056/made> (Accessed 2019-07-20).
- [7] International Transport Forum, *ITF Transport Outlook 2017*. OECD Publishing Paris, Jan 2017.
- [8] A. Litschke and G. Knitschky, “Future development in road freight transport regarding more environmentally friendly vehicle technologies,” *Procedia - Social and Behavioral Sciences*, vol. 48, pp. 1557–1567, Jan 2012.
- [9] S. Chu and A. Majumdar, “Opportunities and challenges for a sustainable energy future,” *Nature*, vol. 488, no. 7411, pp. 294–303, Aug 2012.
- [10] M. I. Khan, T. Yasmin, and A. Shakoor, “Technical overview of compressed natural gas (CNG) as a transportation fuel,” *Renewable and Sustainable Energy Reviews*, vol. 51, pp. 785–797, Nov 2015.
- [11] M. Stettler, M. Woo, D. Ainalis, P. Achurra-Gonzalez, and J. Speirs, “Natural Gas as a Fuel for Heavy Goods Vehicles,” Imperial College London, Tech. Rep.

- [12] Business Energy, “Biogas Facts and Information,” 2019. [Online]. Available: <https://www.businessenergy.com/blog/biogas/> (Accessed 2019-05-15).
- [13] S. J. Curran, R. M. Wagner, R. L. Graves, M. Keller, and J. B. Green, “Well-to-wheel analysis of direct and indirect use of natural gas in passenger vehicles,” *Energy*, vol. 75, pp. 194–203, Oct 2014.
- [14] T. F. Stocker, D. Qin, G.-K. Plattner, M. M. B. Tignor, S. K. Allen, J. Boschung, A. Nauels, Y. Xia, V. Bex, and P. M. Midgley, *IPCC 5th assessment report: Climate Change 2013 The Physical Science Basis*. Cambridge University Press, 2013.
- [15] M. Odenberger and F. Johnsson, “Achieving 60% CO₂ reductions within the UK energy system—Implications for the electricity generation sector,” *Energy Policy*, vol. 35, no. 4, pp. 2433–2452, 2007.
- [16] D. Nicolaides, D. Cebon, and J. Miles, “Prospects for Electrification of Road Freight,” *IEEE Systems Journal*, vol. 12, no. 2, pp. 1838–1849, Jun 2018.
- [17] Transport for London, “Ultra Low Emission Zone,” 2016. [Online]. Available: <https://tfl.gov.uk/modes/driving/ultra-low-emission-zone#on-this-page-4> (Accessed 2016-08-26).
- [18] Transport for London, “Out-of-hours deliveries to be encouraged during London 2012 Olympic and Paralympic Games,” 2012. [Online]. Available: <https://tfl.gov.uk/info-for/media/press-releases/2012/april/outofhours-deliveries-to-be-encouraged-during-london-2012-olympic-games> (Accessed 2016-08-26).
- [19] A. McKinnon, J. Allen, and A. Woodburn, “Development of Greener Vehicles, Aircraft and Ships,” in *Green Logistics: Improving the Environmental Sustainability of Logistics*, 3rd ed. London: Kogan Page Publishers, 2015, pp. 165–193.
- [20] D. Nicolaides and J. Miles, “Wireless Electric Charge-On-The-Move: A Sustainability Appraisal of the Potential for the UK Transport Application,” *JMEST*, vol. 2, no. 8, pp. 53–59, 2015.
- [21] G. A. Covic and J. T. Boys, “Modern Trends in Inductive Power Transfer for Transportation Applications,” *IEEE Journal of Emerging and Selected Topics in Power Electronics*, vol. 1, no. 1, pp. 28–41, Mar 2013.
- [22] A. Thomson, “Wireless Charging: The Future of Electric Vehicles.” Heidelberg: Springer International Publishing, 2013, pp. 199–203.
- [23] ERoadArlanda, “The Technology,” 2017. [Online]. Available: <https://eroadarlanda.com/the-technology/> (Accessed 2019-07-21).
- [24] M. Browne, J. Allen, and J. Leonardi, “Evaluating the use of an urban consolidation centre and electric vehicles in central London,” *IATSS Research*, vol. 35, no. 1, pp. 1–6, Jul 2011.

- [25] J. Leonardi, M. Browne, and J. Allen, "Before-After Assessment of a Logistics Trial with Clean Urban Freight Vehicles: A Case Study in London," *Procedia - Social and Behavioral Sciences*, vol. 39, pp. 146–157, 2012.
- [26] E. Taniguchi, S. Kawakatsu, and H. Tsuji, "New Co-Operative System using Electric Vans for Urban Freight Transport," *Urban Transport and the Environment for the 21st Century VI (2000)*, vol. 49, no. 10, pp. 201–210, 2000.
- [27] J. P. Trovao, P. G. Pereirinha, and H. M. Jorge, "Simulation model and road tests comparative results of a small urban electric vehicle," in *2009 35th Annual Conference of IEEE Industrial Electronics*, Porto, Nov 2009, pp. 836–841.
- [28] A. M. C. Odhams, R. L. Roebuck, Y. J. Lee, S. W. Hunt, and D. Cebon, "Factors influencing the energy consumption of road freight transport," *Proceedings of the Institution of Mechanical Engineers, Part C: Journal of Mechanical Engineering Science*, vol. 224, no. 9, pp. 1995–2010, Sep 2010.
- [29] J. Galos and D. Cebon, "Design of a lightweight Heavy Goods Vehicle trailer," in *European Transport Conference 2014*, Frankfurt, 2014.
- [30] B. Beusen, S. Broekx, T. Denys, C. Beckx, B. Degraeuwe, M. Gijssbers, K. Scheepers, L. Govaerts, R. Torfs, and L. I. Panis, "Using on-board logging devices to study the longer-term impact of an eco-driving course," *Transportation Research Part D: Transport and Environment*, vol. 14, no. 7, pp. 514–520, Oct 2009.
- [31] M. Bedinger, G. Walker, M. Piecyk, and P. Greening, "21st century trucking: A trajectory for ergonomics and road freight," *Applied Ergonomics*, vol. 53, pp. 343–356, Mar 2016.
- [32] B. Öz, T. Özkan, and T. Lajunen, "Professional and non-professional drivers' stress reactions and risky driving," *Transportation Research Part F: Traffic Psychology and Behaviour*, vol. 13, no. 1, pp. 32–40, Jan 2010.
- [33] L. Schweitzer, C.-J. Brodrick, and S. E. Spivey, "Truck driver environmental and energy attitudes – an exploratory analysis," *Transportation Research Part D: Transport and Environment*, vol. 13, no. 3, pp. 141–150, May 2008.
- [34] W. Schade, C. Doll, M. Maibach, M. Peter, and D. Sutter, "Analysis of the contribution of transport policies to the competitiveness of the EU economy and com-parison with the United States," Fraunhofer Institute, Tech. Rep., 2006.
- [35] A. Eugensson, M. Brännström, D. Frasher, M. Rothoff, S. Solyom, and A. Robertsson, "Environmental, safety, legal and societal implications of autonomous driving systems," in *International Technical Conference on the Enhanced Safety of Vehicles (ESV)*, Seoul, 2013.
- [36] A. A. Alam, A. Gattami, and K. H. Johansson, "An experimental study on the fuel reduction potential of heavy duty vehicle platooning," in *13th International IEEE Conference on Intelligent Transportation Systems*, Funchal, Sep 2010, pp. 306–311.

- [37] P. Kavathekar and Y. Chen, "Vehicle platooning: A brief survey and categorization," in *Proceedings of The ASME 2011 International Design Engineering Technical Conference*, Washington, 2011, pp. 829–845.
- [38] A. C. McKinnon, M. Browne, A. E. Whiteing, and M. Piecyk, *Green logistics : improving the environmental sustainability of logistics*, 3rd ed. London: Kogan Page Publishers, 2015.
- [39] A. C. McKinnon, "Freight Transport Deceleration: Its Possible Contribution to the Decarbonisation of Logistics," *Transport Reviews*, vol. 36, no. 4, pp. 418–436, Jul 2016.
- [40] A. M. Campbell and M. Savelsbergh, "Decision support for consumer direct grocery initiatives," *Transportation Science*, vol. 39, no. 3, pp. 313–327, 2005.
- [41] M. Punakivi and J. Saranen, "Identifying the success factors in e-grocery home delivery," *Journal of Retail and Distribution Management*, vol. 29, no. 4, pp. 156–163, 2001.
- [42] T. M. Simatupang and R. Sridharan, "The Collaborative Supply Chain," *The International Journal of Logistics Management*, vol. 13, no. 1, pp. 15–30, Jan 2002.
- [43] A. Palmer, P. Mortimer, P. Greening, M. Piecyk, and P. Dadhich, "A cost and CO2 comparison of using trains and higher capacity trucks when UK FMCG companies collaborate," *Transportation Research Part D: Transport and Environment*, vol. 58, pp. 94–107, Jan 2018.
- [44] P. Dadhich, P. Greening, and C. Rutherford, "Allocating Cost In Horizontal Collaboration: An Analysis Of The UK FMCG Road Freight Transport Sector," in *EurOMA 2017*, Edinburgh, Jul 2017.
- [45] J. Allen, M. Browne, A. Woodburn, and J. Leonardi, "The Role of Urban Consolidation Centres in Sustainable Freight Transport," *Transport Reviews*, vol. 34, no. 2, pp. 473–490, 2012.
- [46] M. Browne, M. Sweet, A. Woodburn, J. Allen, and M. Browne, "Urban Freight Consolidation Centres Final Report," Transport Studies Group, University of Westminster, Tech. Rep., 2005.
- [47] M. K. Triantafyllou, T. J. Cherrett, and M. Browne, "Urban Freight Consolidation Centers," *Transportation Research Record: Journal of the Transportation Research Board*, vol. 2411, no. 1, pp. 34–44, Jan 2014.
- [48] D. Paddeu, "The Bristol-Bath urban freight consolidation centre from the perspective of its users," *Case Studies on Transport Policy*, vol. 5, no. 3, pp. 483–491, 2017.
- [49] A. Lewis, M. Fell, D. Palmer, and C. Douglas, "Freight Consolidation Centre Study Main Report," Transport and Travel Research Ltd., London, Tech. Rep., 2010.
- [50] E. Marcucci and R. Danielis, "The potential demand for a urban freight consolidation centre," *Transportation*, vol. 35, no. 2, pp. 269–284, Mar 2008.

- [51] T. G. Crainic, N. Ricciardi, and G. Storchi, “Advanced freight transportation systems for congested urban areas,” *Transportation Research Part C: Emerging Technologies*, vol. 12, no. 2, pp. 119–137, Apr 2004.
- [52] B. Montreuil, “Toward a Physical Internet: meeting the global logistics sustainability grand challenge,” *Logistics Research*, vol. 3, no. 2-3, pp. 71–87, May 2011.
- [53] B. Lenz and E. Riehle, “Bikes for Urban Freight?” *Transportation Research Record: Journal of the Transportation Research Board*, vol. 2379, no. 1, pp. 39–45, 2013.
- [54] J. Gruber, A. Kihm, and B. Lenz, “A new vehicle for urban freight? An ex-ante evaluation of electric cargo bikes in courier services,” *Research in Transportation Business & Management*, vol. 11, pp. 53–62, 2014.
- [55] CycleLogistics, “Final Public Report,” CycleLogistics Consortium, Tech. Rep., 2014.
- [56] G. Schliwa, R. Armitage, S. Aziz, J. Evans, and J. Rhoades, “Sustainable city logistics — Making cargo cycles viable for urban freight transport,” *Research in Transportation Business & Management*, vol. 15, pp. 50–57, 2015.
- [57] R. Schrub, “How UPS Sees Electric Cargo Bikes Fitting Into Global Logistics,” 2019. [Online]. Available: <https://electricbikereport.com/how-ups-sees-electric-cargo-bikes-fitting-into-global-logistics-video/> (Accessed 2019-07-21).
- [58] Outspoken Delivery, “Vision,” 2016. [Online]. Available: <http://www.outspokendelivery.co.uk/> (Accessed 2016-07-21).
- [59] P. Lebeau, C. Macharis, J. van Mierlo, and K. Lebeau, “Electrifying light commercial vehicles for city logistics? A total cost of ownership analysis,” *European Journal of Transport and Infrastructure Research*, vol. 15, no. 4, pp. 551–569, Sep 2015.
- [60] I. Knight, W. Newton, A. Mckinnon, A. Palmer, T. Barlow, I. Mccrae, M. Dodd, G. Couper, H. Davies, A. Daly, W. McMahan, E. Cook, V. Ramdas, and N. Taylor, “Longer and/or Longer and Heavier Goods Vehicles (LHVs)-a Study of the Likely Effects if Permitted in the UK: Final Report,” Transport Research Laboratory, Tech. Rep., 2008.
- [61] D. Leach and C. Savage, “Impact Assessment: High Capacity Vehicles,” University of Huddersfield, Tech. Rep., 2012.
- [62] J. Holguín-Veras, C. A. T. Cruz, and X. J. Ban, “On the comparative performance of urban delivery vehicle classes,” *Transportmetrica A: Transport Science*, vol. 9, no. 1, pp. 50–73, Jan 2013.
- [63] Act of Parliament, “Road Vehicles (Construction and Use) Regulations 1986 No. 1078,” London, 1986. [Online]. Available: <https://www.legislation.gov.uk/ukSI/1986/1078/contents/made> (Accessed 2019-06-15).
- [64] G. McGranahan and D. Satterthwaite, *Urbanisation Concepts and Trends*, 1st ed. IIED, 2014.

- [65] United Nations Department of Economic and Social Affairs: Population Division, "World Urbanization Prospects, 2014 Revision (Highlights)," pp. 1–16, 2014. [Online]. Available: <https://esa.un.org/unpd/wup/publications/files/wup2014-highlights.pdf> (Accessed 2018-11-02).
- [66] OECD, "Delivering the Goods: 21st Century Challenges to Urban Goods Transport," Organisation for Economic Co-operation and Development, Tech. Rep., 2003.
- [67] Office for National Statistics, "2011 Census Analysis - Comparing Rural and Urban Areas of England and Wales," 2013.
- [68] J. G. V. Vieira, J. C. Fransoo, and C. D. Carvalho, "Freight distribution in megacities: Perspectives of shippers, logistics service providers and carriers," *Journal of Transport Geography*, vol. 46, pp. 46–54, Jun 2015.
- [69] T. Cherrett, J. Allen, F. McLeod, S. Maynard, A. Hickford, and M. Browne, "Understanding urban freight activity – key issues for freight planning," *Journal of Transport Geography*, vol. 24, pp. 22–32, 2012.
- [70] A. Stathopoulos, E. Valeri, and E. Marcucci, "Stakeholder reactions to urban freight policy innovation," *Journal of Transport Geography*, vol. 22, pp. 34–45, 2012.
- [71] S. Yusoff and A. Ishak, "Evaluation of Urban Highway Environmental Noise Pollution," *Sains Malaysiana*, vol. 34, no. 2, pp. 81–87, 2005.
- [72] J. Fenger, "Urban air quality," *Atmospheric Environment*, vol. 33, no. 29, pp. 4877–4900, Dec 1999.
- [73] P. Pokorny, J. Drescher, K. Pitera, and T. Jonsson, "Accidents between freight vehicles and bicycles, with a focus on urban areas," *Transportation Research Procedia*, vol. 25, pp. 999–1007, Jan 2017.
- [74] Y. Jia and D. Cebon, "Measuring the Motion of Vulnerable Road Users Relative to Moving HGVs," *IEEE Transactions on Intelligent Transportation Systems*, vol. 20, no. 4, pp. 1404–1415, Apr 2019.
- [75] G. Zamboni, M. André, A. Roveda, and M. Capobianco, "Experimental evaluation of Heavy Duty Vehicle speed patterns in urban and port areas and estimation of their fuel consumption and exhaust emissions," *Transportation Research Part D: Transport and Environment*, vol. 35, pp. 1–10, Mar 2015.
- [76] M. Treiber, A. Kesting, C. Thiemann, M. Treiber, A. Kesting, and C. Thiemann, "How Much does Traffic Congestion Increase Fuel Consumption and Emissions? Applying a Fuel Consumption Model to the NGSIM Trajectory Data," 2008.
- [77] P. Edmunds, "Report on demonstration of longer semi-trailers and risks to vulnerable road users," Campaign for Better Transport, Tech. Rep., 2013.
- [78] J. Woodrooffe, D. Anderson, and L. Ash, "The influence of policy on crash rate of long combination vehicles," in *8th International Symposium on Heavy Vehicle Weights & Dimensions*, Johannesburg, 2004.

- [79] Risk Solutions, "Evaluation of the Longer Semi-Trailer Trial: Annual Report 2016," Department for Transport, Tech. Rep., 2016.
- [80] Road Transport Management System, "Success Stories RTMS - South Africa," 2019. [Online]. Available: <http://www.rtms-sa.org/successstories> (Accessed 2019-07-21).
- [81] National Heavy Vehicle Regulator and Australian Road Transport Suppliers Association, "Performance Based Standards: An introduction for road managers," 2019. [Online]. Available: <https://www.nhvr.gov.au/files/201810-0924-pbs-a-guide-for-road-managers.pdf>
- [82] G. Morrison, R. L. Roebuck, and D. Cebon, "Effects of longer heavy vehicles on traffic congestion," *Proceedings of the Institution of Mechanical Engineers, Part C: Journal of Mechanical Engineering Science*, vol. 228, no. 6, pp. 970–988, Aug 2013.
- [83] Act of Parliament, "Goods Vehicles (Licensing of Operators) Act 1995," London, 1995. [Online]. Available: <https://www.legislation.gov.uk/ukpga/1995/23/contents> (Accessed 2019-05-16).
- [84] Department for Transport, "Goods vehicle operator licensing exemptions and related regulatory changes Government Response to Consultation," 2017. [Online]. Available: https://assets.publishing.service.gov.uk/government/uploads/system/uploads/attachment_data/file/667467/hgv-roadworthiness-testing-and-operator-licensing-proposals-gov-response.pdf (Accessed 2019-05-16).
- [85] Department for Transport, "Domestic Road Freight Statistics, United Kingdom 2014," p. 12. [Online]. Available: https://www.gov.uk/government/uploads/system/uploads/attachment_data/file/480115/domestic-road-freight-statistics-2014.pdf (Accessed 2019-04-07).
- [86] Office for National Statistics, "Compendium: Family Spending," 2014. [Online]. Available: <http://www.ons.gov.uk/peoplepopulationandcommunity/personalandhouseholdfinances/incomeandwealth/compendium/familyspending/2015/chapter1overview> (Accessed 2018-10-22).
- [87] M. Browne, J. Allen, and C. Rizet, "Assessing transport energy consumption in two product supply chains," *International Journal of Logistics*, vol. 9, no. 3, pp. 237–252, 2011.
- [88] M. Browne, C. Rizet, J. Leonardi, and J. Allen, "Analysing energy use in supply chains: the case of fruits and vegetables and furniture," in *Proceedings of the Logistics Research Network Conference*, Liverpool, 2008, pp. 1–6.
- [89] P. H. Jespersen, "The transport content of products," *World Transport Policy & Practice*, vol. 10, no. 3, pp. 28–35, 2004.
- [90] C. Weber, C. Hendrickson, P. Jaramillo, S. Matthews, A. Nagengast, and R. Nealer, "Life Cycle Comparison of Traditional Retail and E-commerce Logistics for Electronic Products: A Case Study of buy.com," Green Design Institute - Carnegie Mellon University, Tech. Rep., 2008.

- [91] J. Edwards, A. McKinnon, and S. Cullinane, "Carbon Auditing the 'Last Mile': Modelling the Environmental Impacts of Conventional and Online Non-food Shopping," in *Green Logistics Report*. Heriot-Watt University, 2009.
- [92] H. Siikavirta, M. Punakivi, M. Kärkkäinen, and L. Linnanen, "Effects of E-Commerce on Greenhouse Gas Emissions: A Case Study of Grocery Home Delivery in Finland," *Journal of Industrial Ecology*, vol. 6, no. 2, pp. 83–97, Feb 2008.
- [93] M. A. Maimoun, D. R. Reinhart, F. T. Gammoh, and P. McCauley Bush, "Emissions from US waste collection vehicles," *Waste Management*, vol. 33, no. 5, pp. 1079–1089, May 2013.
- [94] S. Burnley, "The impact of the European landfill directive on waste management in the United Kingdom," *Resources, Conservation and Recycling*, vol. 32, no. 3-4, pp. 349–358, Jul 2001.
- [95] M. Hands, R. Burton, C. M. K. Birring, and I. Fieldling, "Recent growth trends in quantities of municipal waste," in *Proceedings of the IWM*, 1999, pp. 26–30.
- [96] O. M. Johansson, "The effect of dynamic scheduling and routing in a solid waste management system," *Waste Management*, vol. 26, no. 8, pp. 875–885, Jan 2006.
- [97] L. Rose, M. Hussain, S. Ahmed, K. Malek, R. Costanzo, and E. Kjeang, "A comparative life cycle assessment of diesel and compressed natural gas powered refuse collection vehicles in a Canadian city," *Energy Policy*, vol. 52, pp. 453–461, Jan 2013.
- [98] F. A. Bender, T. Bosse, and O. Sawodny, "An investigation on the fuel savings potential of hybrid hydraulic refuse collection vehicles," *Waste Management*, vol. 34, no. 9, pp. 1577–1583, Sep 2014.
- [99] S. Vonolfen, M. Affenzeller, A. Beham, S. Wagner, and E. Lengauer, "Simulation-based evolution of municipal glass-waste collection strategies utilizing electric trucks," in *3rd IEEE International Symposium on Logistics and Industrial Informatics*. Budapest: IEEE, Aug 2011, pp. 177–182.
- [100] R. M. Bodner, E. A. Cassell, and P. J. Andros, "Optimal Routing of Refuse Collection Vehicles," *Journal of the Sanitary Engineering Division*, vol. 96, no. 4, pp. 893–904, 1970.
- [101] V. N. Bhat, "A model for the optimal allocation of trucks for solid waste management," *Waste Management & Research*, vol. 14, no. 1, pp. 87–96, Feb 1996.
- [102] S. Baptista, R. C. Oliveira, and E. Zúquete, "A period vehicle routing case study," *European Journal of Operational Research*, vol. 139, no. 2, pp. 220–229, Jun 2002.
- [103] D. V. Tung and A. Pinnoi, "Vehicle routing–scheduling for waste collection in Hanoi," *European Journal of Operational Research*, vol. 125, no. 3, pp. 449–468, Sep 2000.
- [104] J. Smaros, "Best Practices for Managing Grocery Retail Supply Chains." [Online]. Available: <https://www.relexsolutions.com/managing-grocery-retail-supply-chains/>

- [105] C. Eddy, "Cyclist Detection," Master's Thesis, University of Cambridge, 2015.
- [106] C. Eddy, C. de Saxe, and D. Cebon, "Camera-based measurement of cyclist motion," *Proceedings of the Institution of Mechanical Engineers, Part D: Journal of Automobile Engineering*, vol. 233, no. 7, pp. 1793–1805, Jun 2019.
- [107] Department for Transport, "Road accidents and safety: statistical tables index - Statistical data sets," 2013. [Online]. Available: <https://www.gov.uk/government/statistical-data-sets/road-accidents-and-safety-statistical-tables-index> (Accessed 2014-10-05).
- [108] Y. Jia and D. Cebon, "A strategy for avoiding collisions between heavy goods vehicles and cyclists," *Proceedings of the Institution of Mechanical Engineers, Part D: Journal of Automobile Engineering*, vol. 233, no. 6, pp. 1367–1379, May 2018.
- [109] Safety Shield Systems, "Cycle Safety Shield - Safety Shield Systems," 2015. [Online]. Available: <http://safetyshieldsystems.com/cycle-safety-shield/> (Accessed 2015-05-19).
- [110] Fusion Processing, "CycleEye® | Fusion Processing," 2015. [Online]. Available: <http://www.fusionproc.com/products/> (Accessed 2015-05-19).
- [111] Y. Jia and D. Cebon, "Field Testing of a Cyclist Collision Avoidance System for Heavy Goods Vehicles," *IEEE Transactions on Vehicular Technology*, vol. 65, no. 6, pp. 4359–4367, Jun 2016.
- [112] T. Ardeshiri, F. Larsson, F. Gustafsson, T. Schon, and M. Felsberg, "Bicycle tracking using ellipse extraction," in *Information Fusion (FUSION), 2011 Proceedings of the 14th International Conference on*, Chicago, 2011, pp. 1–8.
- [113] J. Illingworth and J. Kittler, "A survey of the hough transform," *Computer Vision, Graphics, and Image Processing*, vol. 44, no. 1, pp. 87–116, Oct 1988.
- [114] H. Yuen, J. Princen, J. Illingworth, and J. Kittler, "Comparative study of Hough Transform methods for circle finding," *Image and Vision Computing*, vol. 8, no. 1, pp. 71–77, Feb 1990.
- [115] L. Xu, E. Oja, and P. Kultanen, "A new curve detection method: Randomized Hough transform (RHT)," *Pattern Recognition Letters*, vol. 11, no. 5, pp. 331–338, May 1990.
- [116] R. A. McLaughlin, "Randomized Hough Transform: Improved ellipse detection with comparison," *Pattern Recognition Letters*, vol. 19, no. 3-4, pp. 299–305, Mar 1998.
- [117] Yonghong Xie and Qiang Ji, "A new efficient ellipse detection method," in *Object recognition supported by user interaction for service robots*, vol. 2. IEEE Comput. Soc, 2002, pp. 957–960.
- [118] C. Lai and W. Tsai, "Estimation of moving vehicle locations using wheel shape information in single 2-D lateral vehicle images by 3-D computer vision techniques," *Robotics and Computer-Integrated Manufacturing*, vol. 15, no. 2, pp. 111–120, Apr 1999.

- [119] P. Viola and M. Jones, "Rapid object detection using a boosted cascade of simple features," in *Proceedings of the 2001 IEEE Computer Society Conference on Computer Vision and Pattern Recognition. (CVPR '01)*, vol. 1. Kauai, Hawaii: IEEE Comput. Soc, 2001, pp. I-511-I-518.
- [120] Y. Freund and R. E. Schapire, "A Decision-Theoretic Generalization of On-Line Learning and an Application to Boosting," *Journal of Computer and System Sciences*, vol. 55, no. 1, pp. 119-139, Aug 1997.
- [121] Y. Freund and R. E. Schapire, "A Short Introduction to Boosting," *Journal of Japanese Society for Artificial Intelligence*, vol. 14, no. 5, pp. 771-780, 1999.
- [122] G. Bradski, "The OpenCV Library," *Dr Dobb's Journal of Software Tools*, 2000.
- [123] A. Chavez-Aragon, R. Laganier, and P. Payeur, "Vision-based detection and labelling of multiple vehicle parts," in *2011 14th International IEEE Conference on Intelligent Transportation Systems (ITSC)*. Washington: IEEE, Oct 2011, pp. 1273-1278.
- [124] P. F. Felzenszwalb, R. B. Girshick, D. McAllester, and D. Ramanan, "Object Detection with Discriminatively Trained Part-Based Models," *IEEE Transactions on Pattern Analysis and Machine Intelligence*, vol. 32, no. 9, pp. 1627-1645, Sep 2010.
- [125] M. Bertozzi, A. Boggi, P. Medici, P. Porta, and A. Sjogren, "Stereo Vision-Based Start-Inhibit for Heavy Goods Vehicles," in *2006 IEEE Intelligent Vehicles Symposium*. Meguro-Ku, Japan: IEEE, 2006, pp. 350-355.
- [126] Point Grey Research Inc., "Flea 3 specifications sheet." 2012. [Online]. Available: https://www.kycom.co.jp/dcms_media/other/Flea3_U3.pdf (Accessed 2015-07-07).
- [127] Fujinon, "YV2.8x2.8SA02 CCTV lens specifications sheet." 2014. [Online]. Available: https://www.fujifilm.com/products/optical_devices/cctv/pdf/fujinon_cctv_lens_catalog.pdf (Accessed 2015-07-07).
- [128] D. Claus and A. Fitzgibbon, "A Rational Function Lens Distortion Model for General Cameras," in *2005 IEEE Computer Society Conference on Computer Vision and Pattern Recognition (CVPR'05)*, vol. 1, San Diego, 2005, pp. 213-219.
- [129] G. H. Silva, R. L. Riche, J. Molimard, and A. Vautrin, "Exact and efficient interpolation using finite elements shape functions," *European Journal of Computational Mechanics/Revue Européenne de Mécanique Numérique*, vol. 18, no. 3-4, pp. 307-331, May 2012.
- [130] P. Rosin and G. West, "Nonparametric Segmentation of Curves into Various Representations," *Pattern Analysis and Machine Intelligence, IEEE Transactions on.*, vol. 17, no. 12, pp. 1140-1153, 1995.
- [131] F. Mai, Y. Hung, H. Zhong, and W. Sze, "A hierarchical approach for fast and robust ellipse extraction," *Pattern Recognition*, vol. 41, no. 8, pp. 2512-2524, Aug 2008.
- [132] T. Mainzer, "Genetic Algorithm for Shape Detection," University of West Bohemia, Pilsen, Tech. Rep., 2002.

- [133] J. Xiao, J. Hays, K. A. Ehinger, A. Oliva, and A. Torralba, "SUN database: Large-scale scene recognition from abbey to zoo," in *2010 IEEE Computer Society Conference on Computer Vision and Pattern Recognition (CVPR'10)*, San Francisco, Jun 2010, pp. 3485–3492.
- [134] A. Geiger, P. Lenz, and R. Urtasun, "Are we ready for Autonomous Driving? The KITTI Vision Benchmark Suite," in *2012 IEEE Conference on Computer Vision and Pattern Recognition*, Providence, 2012, pp. 3354–3361.
- [135] M. Lowther, "Identifying Cyclists Using Vision Data," Master's Thesis, University of Cambridge, 2017.
- [136] A. Fitzgibbon, M. Pilu, and R. Fisher, "Direct least square fitting of ellipses," *IEEE Transactions on Pattern Analysis and Machine Intelligence*, vol. 21, no. 5, pp. 476–480, May 1999.
- [137] M. A. Fischler and R. C. Bolles, "Random sample consensus: a paradigm for model fitting with applications to image analysis and automated cartography," *Communications of the ACM*, vol. 24, no. 6, pp. 381–395, Jun 1981.
- [138] D. Winfield and D. Parkhurst, "Starburst: A hybrid algorithm for video-based eye tracking combining feature-based and model-based approaches," in *2005 IEEE Computer Society Conference on Computer Vision and Pattern Recognition (CVPR'05) - Workshops*, vol. 3, San Diego, 2005, pp. 79–79.
- [139] J. Canny, "A Computational Approach to Edge Detection," *IEEE Transactions on Pattern Analysis and Machine Intelligence*, vol. PAMI-8, no. 6, pp. 679–698, Nov 1986.
- [140] N. H. Ali and G. M. Hassan, "Kalman Filter Tracking," *International Journal of Computer Applications*, vol. 89, no. 9, pp. 15–18, 2014.
- [141] A. Chowdhury, T. Chakravarty, and P. Balamuralidhar, "Estimating true speed of moving vehicle using smartphone-based GPS measurement," in *2014 IEEE International Conference on Systems, Man, and Cybernetics (SMC)*. San Diego: IEEE, Oct 2014, pp. 3348–3353.
- [142] T. Markel, A. Brooker, T. Hendricks, V. Johnson, K. Kelly, B. Kramer, M. O'Keefe, S. Sprik, and K. Wipke, "ADVISOR: a systems analysis tool for advanced vehicle modeling," *Journal of Power Sources*, vol. 110, no. 2, pp. 255–266, Aug 2002.
- [143] J. D. Bishop, M. E. Stettler, N. Molden, and A. M. Boies, "Engine maps of fuel use and emissions from transient driving cycles," *Applied Energy*, vol. 183, pp. 202–217, Dec 2016.
- [144] K. Wipke, M. Cuddy, and S. Burch, "ADVISOR 2.1: a user-friendly advanced powertrain simulation using a combined backward/forward approach," *IEEE Transactions on Vehicular Technology*, vol. 48, no. 6, pp. 1751–1761, 1999.
- [145] MathWorks UK, "Gamma Distribution - MATLAB & Simulink," 2015. [Online]. Available: <https://uk.mathworks.com/help/stats/gamma-distribution.html> (Accessed 2019-06-04).

- [146] European Council, “Directive 97/27/EC of the European Parliament and of the Council of 22 July 1997 relating to the masses and dimensions of certain categories of motor vehicles and their trailers and amending Directive 70/156/EEC,” 1997. [Online]. Available: <https://eur-lex.europa.eu/legal-content/en/ALL/?uri=CELEX%3A31997L0027> (Accessed 2019-07-10).
- [147] Gillespie, T. and Sayers, M. and Fancher, P., *Mechanics of Heavy-Duty Truck Systems: Lecture Notes*. University of Michigan Transort Research Institute, 2004.
- [148] J. C. Dixon, “Linear and Non-Linear Steady State Vehicle Handling,” *Proceedings of the Institution of Mechanical Engineers, Part D: Journal of Automobile Engineering*, vol. 202, no. 3, pp. 173–186, 1988.
- [149] S. Lukowski, M. Momot, D. Kraemer, and D. Kunz, “Basic linear theory of handling and stability of automobiles,” *Proceedings of the Institution of Mechanical Engineers, Part D: Journal of Automobile Engineering*, vol. 223, no. 1, pp. 1–10, Jan 2009.
- [150] H. Pacejka, “Simplified Analysis of Steady-state Turning Behaviour of Motor Vehicles. Part 1. Handling Diagrams of Simple Systems.” *Vehicle System Dynamics*, vol. 2, no. 3, pp. 161–172, Jul 1973.
- [151] H. Pacejka, “Simplified Analysis of Steady-State Turning Behaviour of Motor Vehicles Part 2: Stability of the Steady-State Turn,” *Vehicle System Dynamics*, vol. 2, no. 4, pp. 173–183, 1973.
- [152] H. Pacejka, “Simplified Analysis of Steady-State Turning Behaviour of Motor Vehicles Part 3: More Elaborate Systems,” *Vehicle System Dynamics*, vol. 2, no. 4, pp. 185–204, 1973.
- [153] W. C. Mitchell, A. Staniforth, and I. Scott, “Analysis of Ackermann Steering Geometry,” in *Proceedings of the 2006 Motorsports Engineering Conference and Exhibition*. Dearborn, Michigan: SAE International, Dec 2006.
- [154] P. Fancher, J. Bernard, C. Clover, and C. Winkler, “Representing truck tire characteristics in simulations of braking and braking-in-a-turn maeuvers,” *Vehicle System Dynamics*, vol. 27, no. 1, pp. 207–220, Jan 1997.
- [155] H. B. Pacejka and E. Bakker, “The Magic Formula Tyre Model,” *Vehicle System Dynamics*, vol. 21, no. S1, pp. 1–18, Aug 1992.
- [156] A. Eichberger and M. Schittenhelm, “Implementations, applications and limits of tyre models in multibody simulation,” *Vehicle System Dynamics*, vol. 43, no. sup1, pp. 18–29, Jan 2005.
- [157] G. Morrison, “Combined Emergency Braking and Cornering of Articulated Heavy Vehicles,” PhD Thesis, University of Cambridge, 2015.
- [158] C. Cheng, “Enhancing Safety of Actively-Steered Articulated Vehicles,” PhD Thesis, University of Cambridge, 2009.
- [159] M. Blundell and D. Harty, *Multibody Systems Approach to Vehicle Dynamics*, 2nd ed. Elsevier, 2015.

- [160] A. Rimmer, "Autonomous Reversing of Multiply-Articulated Vehicles," PhD Thesis, University of Cambridge, 2014.
- [161] B. Jujnovich, "Active Steering of Articulated Vehicles," PhD Thesis, University of Cambridge, 2005.
- [162] S. Lukowski and R. Fiedler, "Manoeuvrability analysis of articulated vehicle combinations with multi-wheel steering systems," in *XXIV Fisita Congress*. London: Mechanical Engineering Publications Ltd., 1992, pp. 256–259.
- [163] P. Sweatman, M. Coleman, and R. Di Cristoforo, "Evaluation of an active-steering triaxle group (Trackaxle)," Roaduser Systems, Tech. Rep., 2003.
- [164] B. Jujnovich and D. Cebon, "Comparative performance of semi-trailer steering systems," in *Proc. 7th Inter. Symposium on Heavy Vehicle Transport Technology*, Delft, 2002, pp. 195–214.
- [165] B. A. Jujnovich and D. Cebon, "Path-Following Steering Control for Articulated Vehicles," *Journal of Dynamic Systems, Measurement, and Control*, vol. 135, no. 3, Mar 2013.
- [166] N. Hata, S. Hasegawa, S. Takahashi, K. Ito, and T. Fujishiro, "A Control Method For 4WS Truck To Suppress Excursion of a Body Rear Overhang," vol. 98, no. 2, pp. 754–760, Nov 1989.
- [167] J. Aurell and S. Edlund, "The Influence of Steered Axles on the Dynamic Stability of Heavy Vehicles," vol. 98, no. 2, pp. 612–629, Nov 1989.
- [168] J. Pentzer, S. Brennan, and K. Reichard, "Model-based Prediction of Skid-steer Robot Kinematics Using Online Estimation of Track Instantaneous Centers of Rotation," *Journal of Field Robotics*, vol. 31, no. 3, pp. 455–476, May 2014.
- [169] J. Jingang Yi, H. Hongpeng Wang, J. Junjie Zhang, D. Dezhen Song, S. Jayasuriya, and J. Jingtai Liu, "Kinematic Modeling and Analysis of Skid-Steered Mobile Robots With Applications to Low-Cost Inertial-Measurement-Unit-Based Motion Estimation," *IEEE Transactions on Robotics*, vol. 25, no. 5, pp. 1087–1097, Oct 2009.
- [170] Y. Zhang, J. Hu, and X. Li, "Steady-state characteristics of skid steering for wheeled vehicles," *Proceedings of the Institution of Mechanical Engineers, Part D: Journal of Automobile Engineering*, vol. 228, no. 9, pp. 1095–1104, Aug 2014.
- [171] A. Mandow, J. L. Martinez, J. Morales, J. L. Blanco, A. Garcia-Cerezo, and J. Gonzalez, "Experimental kinematics for wheeled skid-steer mobile robots," in *2007 IEEE/RSJ International Conference on Intelligent Robots and Systems*. San Diego: IEEE, Oct 2007, pp. 1222–1227.
- [172] J. Yi, X.-L. Wang, Y.-J. Hu, and C.-G. Li, "Modelling and simulation of a fuzzy controller of automatic transmission of a tracked vehicle in complicated driving conditions," *Proceedings of the Institution of Mechanical Engineers, Part D: Journal of Automobile Engineering*, vol. 221, no. 10, pp. 1259–1272, Jan 2007.

- [173] B. Maclaurin, “Comparing the steering performances of skid- and Ackermann-steered vehicles,” *Proceedings of the Institution of Mechanical Engineers, Part D: Journal of Automobile Engineering*, vol. 222, no. 5, pp. 739–756, May 2008.
- [174] J. Morales, J. Martinez, A. Mandow, A. Garcia-Cerezo, and S. Pedraza, “Power Consumption Modeling of Skid-Steer Tracked Mobile Robots on Rigid Terrain,” *IEEE Transactions on Robotics*, vol. 25, no. 5, pp. 1098–1108, Oct 2009.
- [175] J. Morales, J. L. Martinez, A. Mandow, A. Pequeno-Boyer, and A. Garcia-Cerezo, “Simplified power consumption modeling and identification for wheeled skid-steer robotic vehicles on hard horizontal ground,” in *2010 IEEE/RSJ International Conference on Intelligent Robots and Systems*. IEEE, Oct 2010, pp. 4769–4774.
- [176] K. Grosch and A. Schallamach, “Tyre wear at controlled slip,” *Wear*, vol. 4, no. 5, pp. 356–371, Sep 1961.
- [177] A. Schallamach and D. Turner, “The wear of slipping wheels,” *Wear*, vol. 3, no. 1, pp. 1–25, Jan 1960.
- [178] M. J. L. Boada, B. L. Boada, A. Muñoz, and V. Díaz, “Integrated control of front-wheel steering and front braking forces on the basis of fuzzy logic,” *Proceedings of the Institution of Mechanical Engineers, Part D: Journal of Automobile Engineering*, vol. 220, no. 3, pp. 253–267, Apr 2006.
- [179] R. Pusca, Y. Ait-Amirat, A. Berthon, and J. Kauffmann, “Modeling and simulation of a traction control algorithm for an electric vehicle with four separate wheel drives,” in *Proceedings IEEE 56th Vehicular Technology Conference*, vol. 3. Vancouver: IEEE, 2002, pp. 1671–1675.
- [180] C. Eddy, “Maximising Home Delivery,” First Year PhD Report, University of Cambridge, 2016.
- [181] J. Wang, Q. Wang, L. Jin, and C. Song, “Independent wheel torque control of 4WD electric vehicle for differential drive assisted steering,” *Mechatronics*, vol. 21, no. 1, pp. 63–76, Feb 2011.
- [182] U-Sok Chong, Eok Namgoong, and Seung-Ki Sul, “Torque steering control of 4-wheel drive electric vehicle,” in *Power Electronics in Transportation*, Dearborn, 1996, pp. 159–164.
- [183] Department for Transport, “Regulatory changes to support the take-up of alternatively-fuelled light commercial vehicles,” 2016. [Online]. Available: https://assets.publishing.service.gov.uk/government/uploads/system/uploads/attachment_data/file/695984/cat-b-driving-licence-derog-gov-response.pdf (Accessed 2019-07-03).
- [184] D. Gonzalez, J. Perez, V. Milanés, and F. Nashashibi, “A Review of Motion Planning Techniques for Automated Vehicles,” *IEEE Transactions on Intelligent Transportation Systems*, vol. 17, no. 4, pp. 1135–1145, Apr 2016.

- [185] M. Idris, Y. Leng, E. Tamil, N. Noor, and Z. Razak, "Car Park System: A review of smart parking system and its technology," *Information Technology Journal*, vol. 8, no. 2, pp. 101–113, 2009.
- [186] P. Raja and S. Pugazhenth, "Optimal path planning of mobile robots: A review," *International Journal of Physical Sciences*, vol. 7, no. 9, pp. 1314–1320, 2012.
- [187] A. A. Ata, "Optimal trajectory planning of manipulators: a review," vol. 2, no. 1, pp. 32–54, 2007.
- [188] S. LaValle, *Planning Algorithms*, 1st ed. Cambridge University Press, 2006.
- [189] C. Urmson and R. Simmons, "Approaches for heuristically biasing RRT growth," in *Proceedings 2003 IEEE/RSJ International Conference on Intelligent Robots and Systems (IROS 2003) (Cat. No.03CH37453)*, vol. 2. Las Vegas: IEEE, 2003, pp. 1178–1183.
- [190] J. Barraquand and J.-C. Latombe, "On nonholonomic mobile robots and optimal maneuvering," in *Proceedings. IEEE International Symposium on Intelligent Control 1989*. Albany: IEEE Comput. Soc. Press, 1989, pp. 340–347.
- [191] Y. Kuwata, G. Fiore, J. Teo, E. Frazzoli, and J. How, "Motion planning for urban driving using RRT," in *2008 IEEE/RSJ International Conference on Intelligent Robots and Systems*. Nice: IEEE, Sep 2008, pp. 1681–1686.
- [192] R. Pepy, A. Lambert, and H. Mounier, "Path Planning using a Dynamic Vehicle Model," in *2006 2nd International Conference on Information & Communication Technologies*, Damascus, 2006, pp. 781–786.
- [193] J. B. Rawlings, "Tutorial overview of model predictive control," *IEEE Control Systems*, vol. 20, no. 3, pp. 38–52, Jun 2000.
- [194] S. J. Qin and T. A. Badgwell, "An Overview off Industrial Model Predictive Control Technology," *AIChE Symposium Series*, vol. 93, no. 316, pp. 232–256, 1997.
- [195] S. J. Qin and T. A. Badgwell, "An Overview of Nonlinear Model Predictive Control Applications," in *Nonlinear Model Predictive Control*. Basel: Birkhäuser Basel, 2000, pp. 369–392.
- [196] C. E. Beal and J. C. Gerdes, "Model Predictive Control for Vehicle Stabilization at the Limits of Handling," *IEEE Transactions on Control Systems Technology*, vol. 21, no. 4, pp. 1258–1269, Jul 2013.
- [197] H. A. Borhan, A. Vahidi, A. M. Phillips, M. L. Kuang, and I. V. Kolmanovsky, "Predictive energy management of a power-split hybrid electric vehicle," in *2009 American Control Conference*. St Louis: IEEE, 2009, pp. 3970–3976.
- [198] J. Ji, A. Khajepour, W. W. Melek, and Y. Huang, "Path Planning and Tracking for Vehicle Collision Avoidance Based on Model Predictive Control With Multiconstraints," *IEEE Transactions on Vehicular Technology*, vol. 66, no. 2, pp. 952–964, Feb 2017.

- [199] L. E. Dubins, "On Curves of Minimal Length with a Constraint on Average Curvature, and with Prescribed Initial and Terminal Positions and Tangents," *American Journal of Mathematics*, vol. 79, no. 3, p. 497, Jul 1957.
- [200] B. Lau, C. Sprunk, and W. Burgard, "Kinodynamic motion planning for mobile robots using splines," in *2009 IEEE/RSJ International Conference on Intelligent Robots and Systems*. St Louis: IEEE, Oct 2009, pp. 2427–2433.
- [201] Z. Shiller and Y.-R. Gwo, "Dynamic motion planning of autonomous vehicles," *IEEE Transactions on Robotics and Automation*, vol. 7, no. 2, pp. 241–249, Apr 1991.
- [202] M. Likhachev and D. Ferguson, "Planning Long Dynamically Feasible Maneuvers for Autonomous Vehicles," *The International Journal of Robotics Research*, vol. 28, no. 8, pp. 933–945, Aug 2009.
- [203] R. Cipolla, "Lecture Notes: Computer Vision and Robotics, Cambridge University Engineering Department 4F12," 2015.
- [204] J. T. Schwartz and M. Sharir, "On the "piano movers"" problem I. The case of a two-dimensional rigid polygonal body moving amidst polygonal barriers," *Communications on Pure and Applied Mathematics*, vol. 36, no. 3, pp. 345–398, May 1983.
- [205] J. Canny, "A Voronoi method for the piano-movers problem," in *Proceedings. 1985 IEEE International Conference on Robotics and Automation*, vol. 2. St Louis: Institute of Electrical and Electronics Engineers, 1985, pp. 530–535.
- [206] J. Basch, L. Guibas, D. Hsu, and An Thai Nguyen, "Disconnection proofs for motion planning," in *Proceedings 2001 ICRA. IEEE International Conference on Robotics and Automation*, vol. 2. Seoul: IEEE, 2001, pp. 1765–1772.
- [207] H. A. Vasseur, F. G. Pin, and J. R. Taylor, "Navigation of car-like mobile robots in obstructed environments using convex polygonal cells," *Robotics and Autonomous Systems*, vol. 10, pp. 133–146, 1992.
- [208] National Heavy Vehicle Regulator and Australian Road Transport Suppliers Association, "Australia's PBS fleet," 2019. [Online]. Available: <https://www.nhvr.gov.au/files/201905-1047-nhvr-artsa-pbs-report-may-2019.pdf> (Accessed 2019-05-21).
- [209] New Zealand Transport Agency, "High Productivity Motor Vehicles (HPMV)," 2019. [Online]. Available: <https://www.nzta.govt.nz/vehicles/vehicle-types/vehicle-classes-and-standards/vehicle-dimensions-and-mass/high-productivity-motor-vehicles/> (Accessed 2019-05-22).
- [210] J. Woodrooffe, *Review of Canadian Experience with the Regulation of Large Commercial Motor Vehicles*. Transportation Research Board, 2010, vol. 671.
- [211] P. Nordengen, C. De Saxe, and F. Kienhöfer, "Vehicle safety performance improvements using a performance-based standards approach: four case studies," in *Proc. 13th Inter. Symposium on Heavy Vehicle Transport Technology*, San Luis, 2014.

-
- [212] European Council, “Council Directive 96/53/EC of 25 July 1996 laying down for certain road vehicles circulating within the community the maximum authorized dimensions in national and international traffic and the maximum authorized weights in international traffic,” pp. 59–75, 1996. [Online]. Available: <https://eur-lex.europa.eu/legal-content/en/TXT/?uri=CELEX%3A31996L0053> (Accessed 2019-07-10).
- [213] C. C. De Saxe, “FALCON III: Defining a Performance-Based Standards Framework for High Capacity Vehicles in Europe,” in *Proc. 15th Inter. Symposium on Heavy Vehicle Transport Technology*, Rotterdam, 2018.

